学位論文

Supernovae Interacting with Circumstellar Media

(星周物質と相互作用する超新星)

平成２５年５月博士（理学）申請

東京大学大学院理学系研究科
天文学専攻

守屋 尭

Supernovae Interacting with Circumstellar Media

星周物質と相互作用する超新星

A dissertation submitted in partial satisfaction of
the requirement for the degree of

Doctor of Philosophy

in

Astronomy

by

Takashi José Moriya

守屋 尭

Department of Astronomy, Graduate School of Science
University of Tokyo

May 2013

Abstract

Core-collapse supernovae are explosions of massive stars. Massive stars lose their mass during their evolution in many ways and core-collapse supernovae always occur within circumstellar media created by their progenitors. We study signatures of circumstellar media which appear in supernovae due to the interaction between supernova ejecta and circumstellar media. Our study reveals mass loss of supernova progenitors immediately prior to their explosions. We especially focus on supernovae whose main radiation energy source is kinetic energy of supernova ejecta. If circumstellar media of supernovae are dense enough, supernova ejecta is decelerated by the interaction and the kinetic energy of the supernova ejecta is eventually released as radiation. The efficient conversion from kinetic energy to radiation energy can make supernovae bright.

We develop theoretical formalisms to study the light curves of such interacting supernovae at first. We derive an analytical bolometric light curve model under the assumption that circumstellar media are optically thin. When circumstellar media are optically thick, we need to model light curves numerically. However, if the optical depth of a circumstellar medium is sufficiently high and the shock breakout occurs within the circumstellar medium, we find that the rising time of the light curve and the shock propagation timescale in the circumstellar medium can be estimated analytically. These timescales can be used to infer the properties of circumstellar media in which the shock breakout occurs.

We apply our analytic light curve model to observed Type IIn supernova light curves. Type IIn supernovae are supernovae which show clear signatures of the interaction in their spectra and they are presumed to be mainly powered by the interaction. By fitting the observed light curves by our analytic model, the properties of the circumstellar media of several Type IIn supernova progenitors are estimated. We find that the density structures of them are likely to deviate slightly from the density structures expected from the steady mass loss and Type IIn supernova progenitors generally experience non-steady mass loss shortly before their explosions. Especially, we find that Type IIn supernova progenitors may tend to increase their mass-loss rates as they get closer to the time of their explosions. In addition, the mass-loss rates estimated are found to be more than 0.001 solar mass per year. No supernova progenitors are predicted to have such high mass-loss rates shortly before thieir explosions by the current stellar evolution theories and our results clearly challenge our understanding of mass loss from massive stars.

Superluminous supernovae are a new kind of supernovae whose existence is recently recognized. Their peak luminosities are brighter than -21 magnitude in optical. Most of them are Type IIn supernovae and they are suggested to become superluminous because of the interaction between supernova ejecta and circumstellar media. To explain the huge luminosities of superluminous supernovae, their circumstellar media need to be very dense and the shock breakout is presumed to occur within the circumstellar media. By modeling the light curve numerically, we find that the observed properties of the best observed superluminous supernova 2006gy (Type IIn) can be actually explained by the shock breakout model we developed. Our results indicate that the progenitor of supernova 2006gy underwent non-steady mass loss with the rate exceeding 0.1 solar mass per year in a few decades before the explosion. No current stellar evolution models can explain the estimated mass loss. There also exist super-

luminous supernovae whose spectral type is not Type IIn and their huge luminosities are not necessarily from the interaction. However, we find that the lack of the Type IIn features in their spectra can be explained by our shock breakout model and they likely get bright due to the interaction as well. Especially, the existence of the two spectral types (Type IIn and Type IIL) in hydrogen-rich superluminous supernovae and a short-term luminosity decline observed between the precursor and the main light curve of hydrogen-poor superluminous supernova 2006oz are naturally expected from the shock breakout model.

So far, we have discussed the mass-loss properties of the observed supernovae which show the signatures of the interaction and found that their mass-loss rates are much higher than those predicted by the current stellar evolution theories. However, there do exist some theoretical supernova progenitor models whose mass-loss rates are enhanced shortly before their explosions, namely, super-asymptotic-giant-branch stars, massive red supergiants, and luminous blue variables. We discuss the expected observational signatures of these theoretical supernova progenitors with the mass-loss enhancement. We obtain light curves from the explosions of electron-capture supernovae theoretically suggested to explode within super-asymptotic-giant-branch winds. Some observed supernovae are suggested to come from super-asymptotic-giant-branch stars but we find that their light curves are inconsistent with the light curves obtained by the super-asymptotic-giant-branch star model from the current stellar evolution theories. Massive red supergiants are suggested to have enhanced mass loss shortly before their explosions and supernovae from them are found to have a long ultraviolet-bright phase and possible spectral transition from Type IIn to Type II. Supernovae with these features exist (2009kf, 1987C, and 2007pk) and they are likely from massive red supergiants. The mass-loss rates of recently reported luminous blue variable supernova progenitors are found to be too low to affect optical supernova light curves but their episodic mass-loss enhancement due to the bistability can explain episodic modulations observed in some supernova radio light curves.

Finally, we investigate supernova remnants of supernovae interacting with dense circumstellar media. We suggest that recombining supernova remnants whose existence is recently confirmed are from supernovae interacting with dense circumstellar media. We find that the progenitors of recombining supernova remnants should be mostly massive red supergiants and Type IIn supernova progenitors.

Committee in Charge

Professor Izumi Hachisu, Chair
Professor Mamoru Doi
Professor Yasushi Suto
Professor Masuo Tanaka
Professor Tomonori Totani
Professor Hideyuki Umeda

Acknowledgments

First of all, I would like to thank Ken'ichi Nomoto for leading me to the interesting fields in astronomy, supernovae and stellar evolution, and initiating my researches in these fields. In addition, his international connections enabled me to have discussion with researchers all over the world which stimulated my research activities. Having interactions with international researchers also made my life enjoyable. Moreover, he allowed me to perform my research as I like and I was able to gratify my curiosity as I wanted. I would also like to thank Toshikazu Shigeyama for his continuous support for my research. My first research was led by him and I learned the basics of astrophysics and research from him. I would like to thank him for allowing me to be at Kavli Institute for the Physics and Mathematics of the Universe and doing many paper works for me as my official supervisor.

Many results obtained in this dissertation were never obtained without the support from Sergei I. Blinnikov, who provided me with `STELLA` code which enabled me to study phenomena involving radiation hydrodynamics. He also taught me the basics of the radiation hydrodynamics. He helped me during my stays at Max Planck Institute for Astrophysics and I enjoyed my stays very much. I would like to express my gratitude to him. I would like to thank Keiichi Maeda, with whom I had many discussions which pushed my research forward. His wide range of interest led me to think about radio and X-ray properties of supernovae. He also gave me fruitful chances to visit *Subaru* telescope and Stockholm University. Nozomu Tominaga and Masaomi Tanaka also led my research and I had many stimulating discussions with them. I would like to thank them for their continuous support to me. I would also like to thank Naoki Yoshida for advising me to start to think about observations of high-redshift supernovae and having useful discussions. I also had many fruitful seminars and discussions with Takaya Nozawa, Melina C. Bersten, Gastón Folatelli, Robert M. Quimby, Yasuomi Kamiya, Jun Okumura, Masayuki Yamanaka, Kohki Konishi, Tomoki Morokuma, Hanindyo Kuncarayakti, and Koh Takahashi. I would like to thank them as well.

I am also grateful to the researchers all over the world who kindly allowed me to visit them and hosted me with warm hospitality. I would like to thank Jesper Sollerman and Trancesco Taddia at Stockholm University, Daniel Kasen, Naotaka Suzuki, and Hitoshi Murayama at University of California, Berkeley, Georges Meynet and José H. Groh at Geneva University, Norbert Langer at University of Bonn, and Mario Hamuy and Joseph P. Anderson at University of Chile.

I spent most of my graduate school days at Kavli Institute for the Physics and Mathematics of the Universe. I enjoyed talking with people in other research fields at the tea time of the institute. I would like to thank all researchers, visitors, and administrative stuff in the institute for making my daily life enjoyable and supporting my research activities. I would like to especially thank students with whom I shared my office, namely, Takeshi Kobayashi, Hironao Miyatake, Ryoichi Nishio, Sourav Mandal, William L. Klemm, Xu-Feng Wang, Kimihiko Nakajima, Tomonori Ugajin, Kohsaku Tobioka, Ayuki Kamada, Tomohiro Fujita, Keisuke Harigaya, Masato Shirasaki, Gen Chiaki, Wen Yin, Hidemasa Oda, Yuuki Nakaguchi, Yusuke Ono, Noriaki Watanabe, Ryo Matsuda and many visitors from all over the world. I would also like to express my gratitude to Mieko Minamisawa and Sayuri Nagano for their crucial support to my research activities. I spent one year in the Hongo campus of

University of Tokyo and I would like to thank Masaomi Tanaka, Daisuke Kato, Ho-Gu Lee, Yusei Koyama, Yoshiaki Ono, Takashi Shimonishi, Yasuomi Kamiya, Natsuko Izutani, Ryou Ohsawa, Kimihiko Nakajima, Takafumi Sonoi, and Kazunori Komai, who made my daily life enjoyable when I was there. Especially, I would like to thank a Chinese restaurant near the campus, *Oishii-ya* (Koyama 2010), where we had great time with great dishes and drinks.

I originally made an ambition to be a researcher studying the Universe at *Tateyama-juku* when I was a high school student. I would like to thank teachers there, especially Yuji Miwa, Hideyuki Matsuyama, Toshihide Ebisu, Masaru Harada, Mikio Kumakura, and Ken Uomizu. They taught me not only knowledge but also the joy of learning which is a main driver of my research activities. We also need physical and mental strength to continue research activities and I would like to thank Hiroyuki Tanaka, who trained me both physically and mentally as a coach of the rugby club at Hibiya high school. I would also like to thank my friends from *Tateyama-juku* and the rugby team, especially Yuki Ogishima, Daisuke Harada, Yosuke Kondo, Tsutomu Saito, Satoshi Mori, Yuhei Nozoe, Taisuke Namiki, Keisuke Tada and Hitomi Iwamoto for continuous friendship. I would like to thank my friends in 36R of Hibiya high school for the continuous friendship as well.

I would like to express my sincere gratitude to my parents, Sakae Moriya and Felisa Moriya. My interest in the Universe was originated from my young days with my parents. They also gave me a healthy body which is important to continue my research activities. Moreover, I could not continue my research in astronomy without their support and I really thank them for allowing me to be a student for more than 20 years. ¡Muchas gracias!

Finally, I would like to thank Mei Sasaki for being with me throughout my tough years in the graduate school. She has always been cheering me up in spite of her being in Heidelberg for more than two years. This dissertation has never been accomplished without her support and smile.

This research is supported by the Japan Society for the Promotion of Science Research Fellowship for Young Scientists (23·5929), World Premier International Research Center Initiative (WPI Initiative), MEXT, Japan, and a grant from the Hayakawa Satio Fund awarded by the Astronomical Society of Japan. Numerical calculations were carried out on the general-purpose PC farm at Center for Computational Astrophysics, CfCA, of National Astronomical Observatory of Japan.

Contents

Supernovae Interacting with Circumstellar Media

When I had satisfied myself that no star of that kind had ever shone before, I was led into such perplexity by the unbelievability of the thing that I began to doubt the faith of my own eyes.

Tycho Brahe (1546 - 1601)

1 Introduction

1.1 Supernovae

Supernovae (SNe) are stars which suddenly appear in the sky and fade away gradually. As is first suggested by Baade & Zwicky 1934, SNe are now known to be dramatic explosions of stars. In this chapter, we briefly summarize the current knowledge and mysteries of SNe and introduce the aim of this dissertation. SNe are explosions of stars which happen mainly at two critical stages of stars: one is core collapse of massive stars (Section 1.3.1) and the other is thermonuclear runaway of stars (Section 1.3.2). In either case, a SN typically has the kinetic energy of the order of 10^{51} erg and emits the radiation energy of the order of 10^{49} erg in the first ~ 1 year after the explosion. SNe are observationally divided into several types (Section 1.2) The observational types are related to their progenitor stars and how they explode (Section 1.3).

SNe are an essential ingredient in understanding the history of the Universe. The standard big bang nucleosynthesis predicts that H and He are dominant elements created at the beginning of the Universe. Heavy elements in the Universe, especially the elements heavier than C, are mainly created in stars. For the heavy elements to spread out in the Universe, explosions of stars, i.e., SNe, which eject the heavy elements synthesized in stars are required. In addition, SNe themselves are considered to be important sites for nucleosynthesis because they make strong shock waves and neutron-rich environments. What is more, SNe release huge energy into the Universe. They are considered to be an energy source of some high energetic events in the Universe, like cosmic-ray accelerations. The released energy can also trigger the next generation star formation. The history of the Universe cannot be described without the detailed understanding of SNe. The SN research leads us to the better understanding of not only SNe and stellar evolution but also the evolution of the Universe.

SNe are also regarded as an important tool to probe the distant Universe because of their high luminosities. SNe provided an observational evidence for the accelerating expansion

of the Universe, i.e., the existence of dark energy (Perlmutter et al. 1999, Riess et al. 1998). It is also a potential probe to reveal the star formation history of the Universe as will be discussed in Chapter 4. Better understanding of SNe is required when we try to use them as a tool and get information of the Universe from them.

1.2 Observational Classification of Supernovae

SNe are observationally classified into several types. Figure 1.1 summarizes the current classification scheme of SNe with major SN types. The classification is mainly based on their spectra (Figures 1.2 and 1.3; see also Filippenko 1997 for a review). Only Type IIP and Type IIL are divided based on light curves (LCs) (Figure 1.3). SN types are related to explosion mechanisms of SNe in the next section.

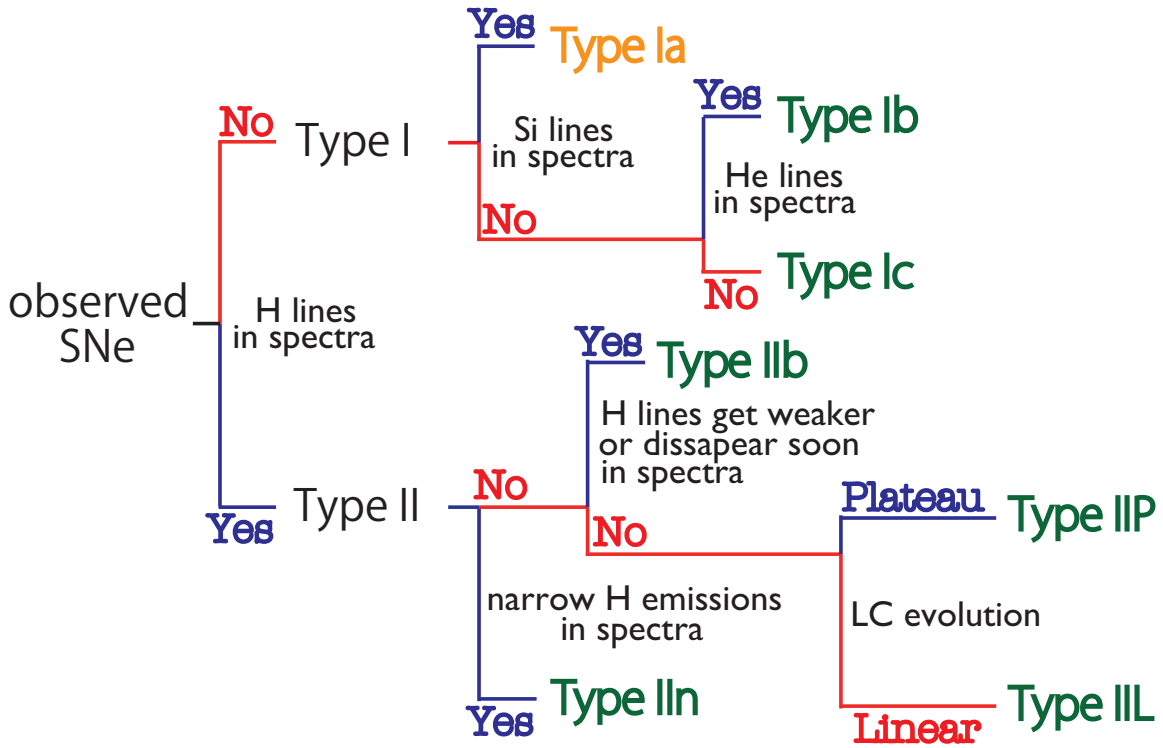

Figure 1.1: Observational classification scheme of SNe. The classification is basically done by spectra of SNe. SNe Ia (orange) are thermonuclear explosions of white dwarfs and SNe of the other types (green) are explosions of massive stars (see Section 1.3). 'Linear' LC evolution used in Type IIL means the linear evolution in time-magnitude plane (Figure 1.3).

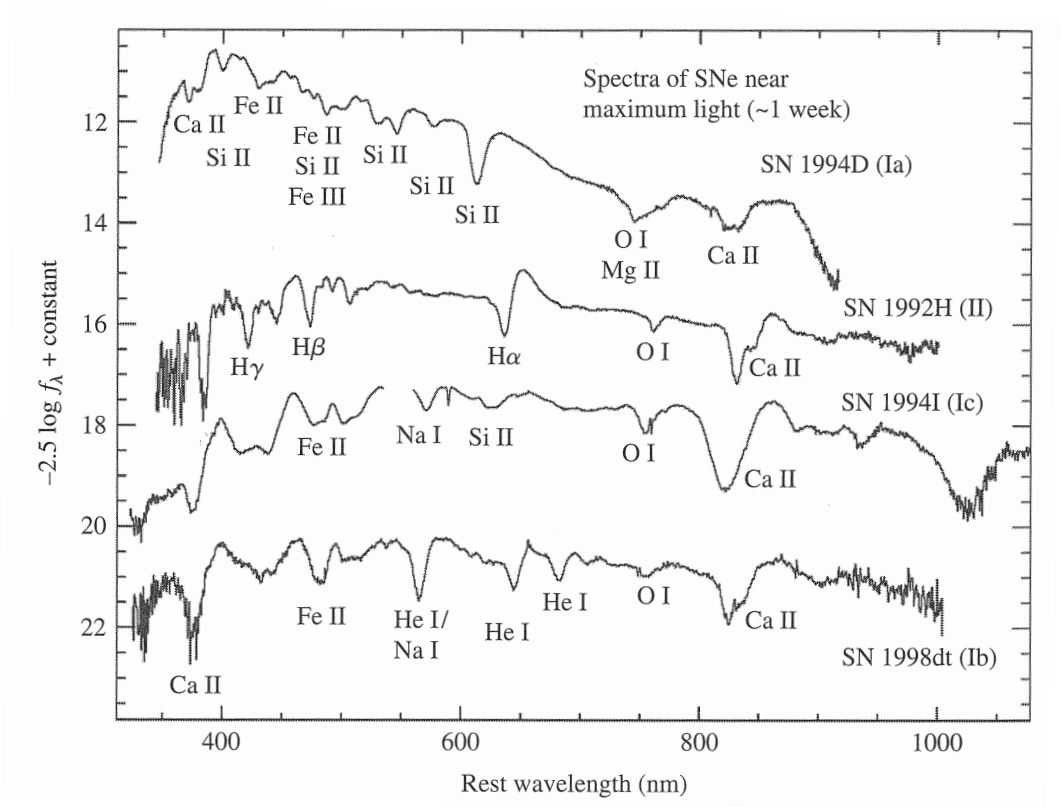

Figure 1.2: Spectra of SNe near the maximum luminosities (Ostlie & Carroll 2006).

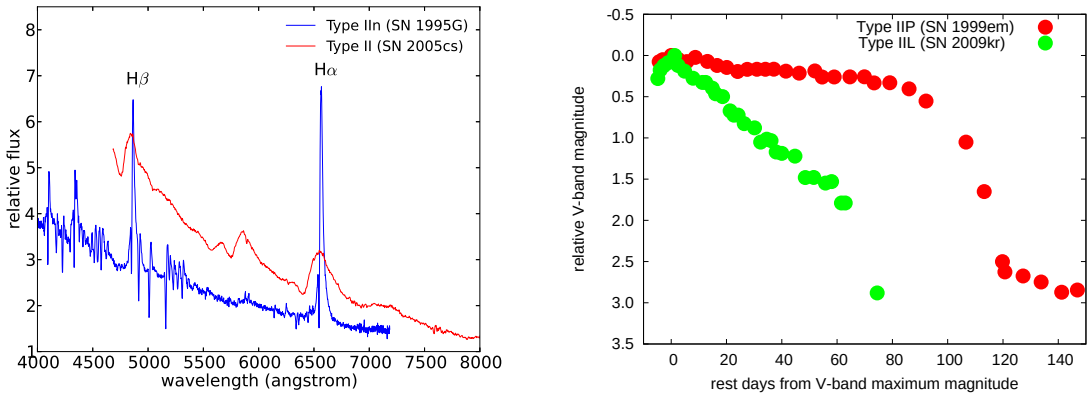

Figure 1.3: *Left:* Spectra of SN IIn 1995G (Barbon et al. 1999) and SN IIP 2005cs (Pastorello et al. 2006). *Right:* LCs of SN IIP 1999em (Hamuy et al. 2001) and SN IIL 2009kr (Elias-Rosa et al. 2010).

1.3 Explosion Mechanisms of Supernovae

1.3.1 Core-Collapse Supernovae

SNe Ib, Ic, IIb, IIn, IIP and IIL are related to deaths of massive stars. They are called core-collapse SNe because the explosions are triggered by the gravitational collapses of the cores of massive stars.

1.3.1.1 From Collapse to Explosion

When a star is formed, the entire star is basically made of materials of the same composition. After H at the center of the star is ignited, H at the center is converted to He, then He to C and O, and so on. Hence, as the star evolves, its chemical structure gets stratified as is shown in Figure 1.4. Whether nuclear burning of the core can synthesize Fe is determined by the stellar mass. If the mass is small, the core can be supported only by the electron degeneracy pressure. In other words, the core no longer need to release energy by nuclear burning to support itself and the nuclear burning stops at that point. The cores of the stars below the zero-age main-sequence (ZAMS) mass $M_{\rm ZAMS} \simeq 8\ M_\odot$ are thought to end their lives as the degenerated cores and become white dwarfs. White dwarfs usually just cool down and do not explode. However, if one is in a binary system, it can explode as a SN Ia (Section 1.3.2).

The stars with ZAMS mass between $\simeq 8\ M_\odot$ and $\simeq 10\ M_\odot$ are still not massive enough to make an Fe core at the center. However, at this mass range, it is suggested that the O+Ne+Mg core becomes so dense that the electron capture reactions occur in the degenerated core. Due to the electron capture reactions, the electron degeneracy pressure which supports the core from inside is suddenly reduced and the core collapses. SNe induced by this mechanism is called electron-capture SNe (ECSNe, e.g., Miyaji et al. 1980). The stars with $M_{\rm ZAMS} \gtrsim 10\ M_\odot$ are massive enough to continue the nuclear burning up to Fe. As Fe is the most stable nuclei, Fe cannot produce energy to support the core by nuclear burning. Thus, the Fe core continues to contract and eventually becomes so hot that the photodisintegration of Fe which absorbs, not releases, energy starts. As the internal energy of the Fe core is suddenly reduced, the core suddenly loses the pressure support and collapses catastrophically. These collapses lead to core-collapse SNe.

How a collapse of a core ends up with a SN explosion? Nobody knows. However, there is a rough picture for the answer. If the center of the collapsing core becomes as dense as the density of nuclei ($\sim 10^{14}$ g cm^{-3}), the strong force becomes the major force to unite the center of the core and it suddenly gets stiff. This central part eventually becomes a neutron star or a black hole and is called a proto-neutron star. Even after the sudden stiffening of the central part, materials continue to fall onto the proto-neutron star. The falling materials bounce at the surface of the proto-neutron star, start to go outward, and make a shock wave. The energy gained by the shock wave is mostly used for the nuclear reactions. Hence, the ram pressure of the shock wave cannot overcome that of the falling materials and the shock wave eventually stalls before going out of the surface of the star. The shock wave must be revived for the collapsing star to explode but we still do not have a decisive picture of the shock wave revival. Somehow, the shock wave is revived and goes out of the star and we can observe a SN.

There are several suggested mechanisms to revive the shock wave and make a collapsing star explode:

- Neutrino explosion mechanism
  (e.g., Colgate & White 1966; discussed below)
- Magnetic explosion mechanism
  (e.g., Bisnovatyi-Kogan et al. 1976, Akiyama et al. 2003; see also Kotake et al. 2006)
- Acoustic explosion mechanism
  (e.g., Burrows et al. 2006)
- Phase transition induced explosion mechanism
  (e.g., Takahara & Sato 1986, Fischer et al. 2010)

Here, we briefly look into the neutrino explosion mechanism which is the most studied mechanism among all. When a core collapses, protons in the proto-neutron stars are neutronized and neutrinos appear. This is confirmed by the observation of neutrinos from SN 1987A (Hirata et al. 1987). If 1% of the total energy of the neutrinos emerged from the proto-neutron star ($\simeq 3 \times 10^{53}$ erg) can be transferred to the stalled shock wave, the shock wave gains enough energy to explain the kinetic energy of observed SNe ($\sim 10^{51}$ erg). However, despite of the great efforts by a bunch of scientists, the computer simulations of this neutrino mechanism still have not succeeded in reproducing observed SNe. For a long time, the neutrino mechanism is simulated in one dimension, i.e., assuming the spherical symmetry, but, except for ECSNe (e.g., Kitaura et al. 2006), the neutrino mechanism is turned out to fail in reviving the shock wave in the spherical symmetry (e.g., Liebendörfer et al. 2005). Recently, after the emergence of multidimensional codes for SN simulations, it is found that multidimensional motions of materials during the core collapse are important to revive the shock wave (e.g., Herant et al. 1994). This is because convection can efficiently transfer materials heated by neutrinos and materials are easily heated up in multidimensional simulations. Thus, it is suggested that the shock revival should be easier as the dimension increases (e.g., Nordhaus et al. 2010). What is more, the stalled shock wave is unstable in multidimension and an instability called Standing Accretion Shock Instability (SASI) evolves (Blondin et al. 2003). The existence of SASI is confirmed by an experiment with water flow (Foglizzo et al. 2012) and SASI is not an artificial instability caused numerically. Because of SASI, materials move back and forth and get more chance to interact with neutrinos. However, the evolution of SASI which was found in two-dimensional simulations may not be so efficient in three dimensions as in two dimensions so the importance of the effect is still under discussion (e.g., Iwakami et al. 2008, Hanke et al. 2013). Nonetheless, several efforts have succeeded in obtaining SN explosions in multidimensional simulations but they still do not have enough explosion energy to explain observed SNe (e.g., Janka et al. 2012, Janka et al. 2007, Bruenn et al. 2013, Suwa et al. 2010, Takiwaki et al. 2012).

1.3.1.2 Difference in Observed Core-Collapse Supernovae

The difference in several observational types of core-collapse SNe comes from the difference in the stellar structures at the time of their explosions. SNe IIP and IIL which show H

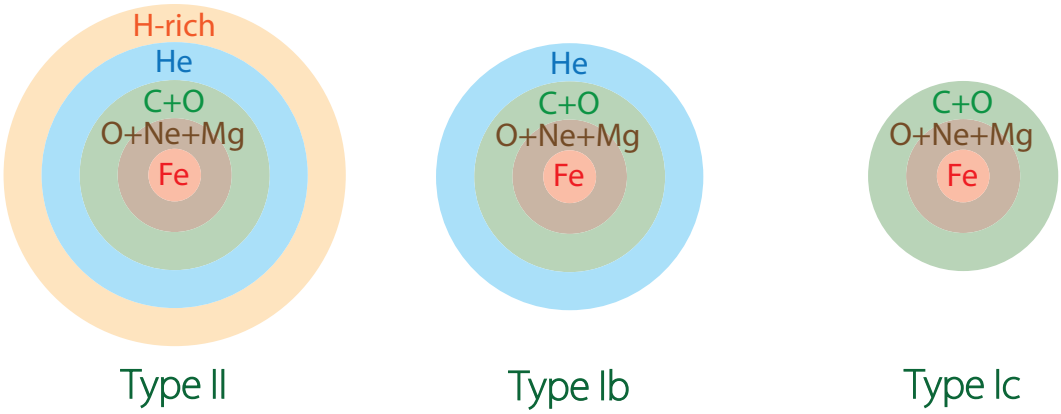

Figure 1.4: Presumed structures of progenitors of SNe II, Ib, and Ic at the time of their explosions.

lines are explosions of stars with a H-rich layer (Figure 1.4). The difference between SNe IIP and IIL are generally presumed to be the remaining amount of H but there is still no clear picture about what makes the two H-rich SN classes (e.g., Blinnikov & Bartunov 1993, Swartz et al. 1991). SNe Ib are explosions of He stars which do not have a H-rich layer and SNe Ic are explosions of stars without both H-rich and He layers (Figure 1.4). SNe IIb are considered to be between Type IIL and Type Ib. Roughly speaking, as the ZAMS mass of a star increases, the luminosity of the star becomes larger and the star undergoes more mass loss. Thus, if we only take a single star evolution into account, the types of SNe are expected to change as IIP $\rightarrow$ IIL $\rightarrow$ IIb $\rightarrow$ Ib $\rightarrow$ Ic as the ZAMS mass increases. Binary evolution also plays an important role in the determination of the structure of the pre-SN stage of massive stars. For example, it is suggested that the majority of SNe Ib may come from binary systems (e.g., Yoon et al. 2010, see also Benvenuto et al. 2013). Spiral-in of stars may also cause mass loss and makes less massive stars explode as SNe Ib or Ic (e.g., Nomoto et al. 1995). In addition, about 70% of nearby massive stars are observationally suggested to be in a close binary system in which they are affected by their companion during their evolution (Sana et al. 2012).

Type IIn is a relatively new type of SNe which is first suggested by Schlegel 1990. SNe IIn show narrow H emission lines in their spectra and 'n' in 'IIn' stands for narrow. The narrow emission lines are considered to be emitted due to the existence of circumstellar media (CSM) around SNe. SNe IIn are one of the main subject of this dissertation and discussed in detail in Section 1.4.1.

1.3.2 Thermonuclear Supernovae

Nuclear burning inside stars is usually stable and the energy released by nuclear burning is balanced with the gravitational potential of stars. However, there exist some conditions in which the nuclear burning occurs explosively and the nuclear energy enough to unbind a whole star is released. Two representative SNe of this kind are SNe Ia and pair-instability SNe.

SNe Ia are explosions of C+O white dwarfs (Nugent et al. 2011). White dwarfs are supported by the degeneracy pressure of electrons. There are the maximum mass which can be supported by the electron degeneracy and it is called the Chandrasekhar mass limit (Chandrasekhar 1931). Typical mass of white dwarfs is about 0.6 $M_{\odot}$ (e.g., Kepler et al. 2007) while the Chandrasekhar mass limit for them is about 1.4 $M_{\odot}$. If the mass of a white dwarf somehow approaches to the Chandrasekhar mass limit, the white dwarf collapses and the center of the white dwarf gets dense and hot enough to ignite the explosive C and O burning. This ignition ends up with an explosion of the white dwarf. Because of the large amount of Si produced by the nuclear burning, the deep Si lines appear in the spectra and thus it is categorized as a SN Ia.

How a white dwarf grows its mass to the Chandrasekhar mass limit is still under discussion. If a white dwarf is in a close binary system and the companion star is a main-sequence star, materials from the companion star can accrete the white dwarf and it can reach the limit under a certain condition (e.g., Nomoto 1982, Nomoto et al. 1984). This scenario is called the single-degenerate (SD) model. Some SNe Ia are observed with dense CSM and support the SD model (e.g., SN 2002ic in Hamuy et al. 2003, PTF11kx in Dilday et al. 2012). However, there are many observational properties of SNe Ia which seem in contradict with the SD scenario. For example, no companion stars are observed in many SNe Ia and their remnants (e.g., Li et al. 2011a, Schaefer & Pagnotta 2012, but see also Hachisu et al. 2012).

Another way to make a Chandrasekhar mass white dwarf is to make two white dwarfs collide. If two white dwarfs are in a binary system, they will eventually collide because of the energy loss by the gravitational wave. This scenario is called the double-degenerate (DD) model (e.g., Iben & Tutukov 1984). This scenario can explain the lack of the companion stars in observed SNe Ia. Moreover, the delay-time distribution, the time difference between the formation of SN Ia progenitors and their actual explosions as SNe Ia, matches what is predicted from the energy loss by the gravitational waves (Totani et al. 2008). Currently, SD and DD models have both 'pros and cons'. It is also probable that SNe Ia are coming from the two formation channels. We finally note that there are also suggestions that SNe Ia may not come from the Chandrasekhar mass white dwarf in the DD scenario (e.g., Woosley & Weaver 1994, Kromer et al. 2010).

Pair-instability SNe (PISNe) are SNe whose existence is theoretically predicted in 1960s (Rakavy et al. 1967; Barkat et al. 1967). If a star is as massive as $M_{\rm ZAMS} \simeq 140 - 300\ M_{\odot}$, the O-rich core becomes dynamically unstable owing to the electron-positron pair creation. As the internal energy is spent by the pair creation, the core loses the stability and starts to collapse. When the central temperature exceeds $\simeq 5 \times 10^9$ K, the core gets stable again but the temperature is so high that O burning becomes explosive and releases enough energy to unbind the entire star. A large amount of ^{56}Ni can be synthesized by the explosive nucleosynthesis and the subsequent radioactive decays power their LCs (Heger & Woosley 2002, Umeda & Nomoto 2002, Scannapieco et al. 2005, Kasen et al. 2011, Dessart et al. 2013). For a massive star to have the pair unstable condition, the star should not lose much mass during its evolution as the core should be very massive to be pair-unstable (above $\simeq 50\ M_{\odot}$). However, massive stars can easily lose mass because of their high luminosities. Thus, PISNe are considered to be able to exist only in metal-poor environments (e.g., Heger & Woosley 2002, Langer et al. 2007).

PISNe have interesting features from the nucleosynthesis point of view. As little neutron excess is expected, there are strong contrast in the amount of odd elements and even elements produced (Heger & Woosley 2002, Umeda & Nomoto 2002). In addition, a large amount of ^{56}Ni which can be produced by PISNe can make them very bright. As will be discussed in Section 1.5, some very bright SNe are suggested to be PISNe.

1.4 Supernovae in Circumstellar Media

Massive stars lose their mass during their evolution. Accreting materials may exist around the progenitors of SNe Ia. SNe always explode within some surrounding materials, i.e., CSM. Our focus in this dissertation is on the effect of the CSM on core-collapse SNe. Massive stars can easily lose their mass thanks to their large luminosities which make the radiation pressure in their envelope high. This means that there must be the CSM originated from the evolution of their progenitors around core-collapse SNe. CSM are usually so thin that they do not affect LCs and spectra of SNe so much (e.g., Chevalier et al. 2006, Chevalier & Fransson 2006). However, in some cases, CSM are expected to be dense enough to affect LCs and spectra of SNe much and there are actually some SNe which show the features which are considered to come from the dense CSM around the SN progenitors. Such kind of SNe showing the features of the dense CSM is one of the main subjects of this dissertation. In this section, we introduce SNe IIn which show the features of the surrounding dense CSM in their spectra.

1.4.1 Type IIn Supernovae

1.4.1.1 Properties

SNe IIn have narrow H emission lines in their spectra. They are considered to be emitted from the dense CSM surrounding their progenitors. The dense CSM are presumed to be ejected from the progenitors during their evolution[1]. If there is a dense CSM surrounding SN ejecta, SN ejecta collides to the dense CSM, making a shock wave in between (Figure 1.5). At the shock wave, kinetic energy of the SN ejecta is converted to thermal energy. The thermal energy is released as radiation, making the SN bright. In other words, kinetic energy of SN ejecta which is usually converted to thermal energy in a timescale of $\sim 10^6$ years (a typical lifetime of supernova remnants) is efficiently converted to thermal energy in the timescale of years to decades because of the dense CSM. This efficient conversion makes the SN bright when it is very young. The main energy source powering SNe IIn is considered to be this interaction between SN ejecta and dense CSM. Actually, SNe IIn are known to have diversities in their peak luminosities and LC shapes (e.g., Kiewe et al. 2012, Taddia et al. 2013, Li et al. 2011b). The observed heterogeneousness of their LCs is what is naturally expected from the diversities in the dense CSM which are linked to the diversities in stellar mass loss. In addition, thanks to the additional energy source, SNe IIn are likely to be brighter than other types of SNe on average (Richardson et al. 2002, but see also Li et al. 2011b). The mass-loss rates of SN IIn progenitors have been roughly estimated

[1] There is also a suggestion that a relic of the proto-stellar disk may remain at the time of the explosion and make SNe IIn (Metzger 2010).

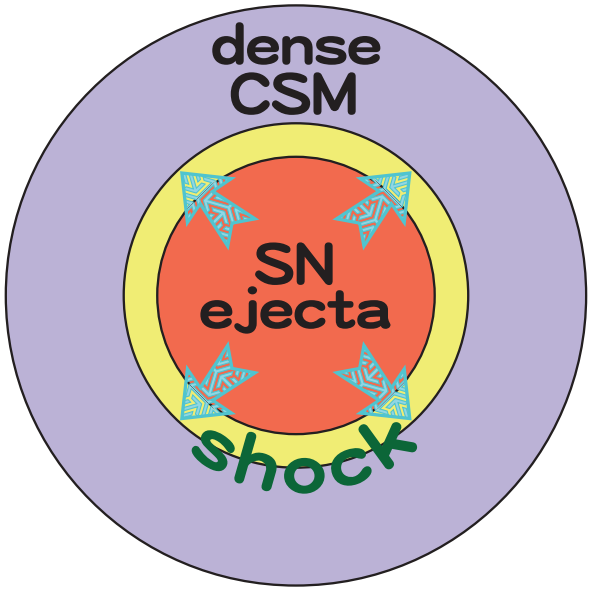

Figure 1.5: Schematic illustration of a SN in a dense CSM.

from Hα luminosities and known to range from $\sim 10^{-4}\ M_\odot\ \mathrm{yr}^{-1}$ to $\sim 10^{-2}\ M_\odot\ \mathrm{yr}^{-1}$, which are much higher than those of typical SN progenitors (Kiewe et al. 2012, Taddia et al. 2013).

Thanks to the fact that some SNe IIn can be very bright and their color tends to be blue (Figure 1.6), they can be observed even if they appear at very high redshifts. A SN IIn at $z = 2.36$ is currently confirmed (Cooke et al. 2009). SNe IIn may also be able to be used as a distance ladder (Blinnikov et al. 2012, Potashov et al. 2013).

1.4.1.2 Progenitors of Type IIn Supernovae

The estimated mass-loss rates of SN IIn progenitors are much higher than those of usual massive stars ($\lesssim 10^{-5}\ M_\odot\ \mathrm{yr}^{-1}$) and SN IIn progenitors must have enhanced mass loss shortly before their explosions. There are several possible ZAMS mass ranges in which stars are suggested to experience such enhanced mass loss shortly before their explosions (Figure 1.7). The first range is in $M_{\mathrm{ZAMS}} \simeq 8 - 10\ M_\odot$ where ECSNe occur in the dense CSM created by super-asymptotic-giant-branch (AGB) stars (e.g., Poelarends et al. 2008). Indeed, the progenitor of SN IIn 2008S, which is discovered in the archival near-infrared (NIR) image of *Spitzer* telescope but the corresponding star is not found in *Hubble Space Telescope (HST)* optical image (Prieto et al. 2008), is consistent with a super-AGB star (Botticella et al. 2009, Pumo et al. 2009, Thompson et al. 2009). The statistical study of the association between SN IIn sites and Hα emitting regions in their host galaxies prefers this relatively low mass progenitors as the main channel for SNe IIn (Anderson et al. 2012).

The second possible ZAMS mass range of SN IIn progenitors is between the maximum ZAMS mass of SN IIP progenitors ($M_{\mathrm{IIP}}^{\mathrm{up}}$) and the lowest ZAMS mass for SN IIL progenitors. Recent SN progenitor searches in archival images of SN sites reveal that there is a significant discrepancy between the predicted SN progenitor ZAMS rage from stellar evolution

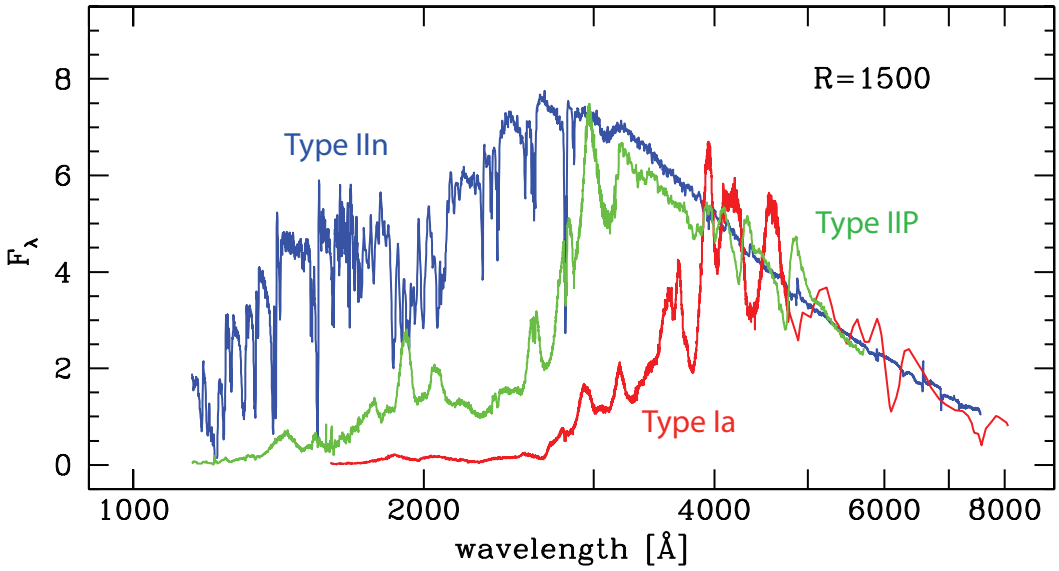

Figure 1.6: Spectra of SN IIn 1998S compared with those of SN Ia 1992A and SN IIP 1999em (Riess et al. 2004).

theories and the mass actually observed (see Smartt 2009 for a review). Especially, $M_{\rm IIP}^{\rm up}$ estimated from observation is $\simeq 17\ M_\odot$ (Smartt et al. 2009) while stellar evolution modeling predicts much higher mass which is $\simeq 25\ M_\odot$ (e.g., Heger et al. 2003, Georgy et al. 2009). There are several suggested reasons to account for this discrepancy. One of them is the enhancement of mass loss in massive red supergiants (RSGs). The progenitors of SNe IIP are RSGs and $M_{\rm IIP}^{\rm up}$ corresponds to the maximum RSG mass. Recently, the observations of RSGs are revealing the very high mass-loss rates of massive RSGs (e.g., Smith et al. 2009a, Boyer et al. 2010). In addition, massive RSGs are theoretically suggested to be unstable because their radii are so large that the temperature of the outer H-rich layers reaches the H ionization temperature and the κ-mechanism can be activated (e.g., Li & Gong 1994, Heger et al. 1997, Yoon & Cantiello 2010, Paxton et al. 2013). The g-mode oscillations of the core (Quataert & Shiode 2012, see also Arnett & Meakin 2011) and dust formation in the RSG surface (van Loon et al. 2005) may also enhance the mass-loss rates of massive RSGs. If the mass-loss enhancement occurs shortly before their explosions, massive RSGs can be SNe IIn.

The third possible mass range is in very massive ZAMS mass in which stars can become luminous blue variables (LBVs) during their evolution (see Humphreys & Davidson 1994 for a review of LBVs). LBVs are known to experience extensive mass loss. The most famous example of LBVs is η Carinae whose ZAMS mass is estimated to be more than 120 $M_\odot$ (Figure 1.8). It has a dense CSM whose mass is $\simeq 10\ M_\odot$ (Smith 2006). The progenitor of SN IIn 2005gl in the *HST* archival image is found to be very luminous ($M_V \simeq -10$ mag) and consistent with a LBV (Gal-Yam & Leonard 2009, Gal-Yam et al. 2007). SN 2009ip provides another example of the LBV explosions. SN 2009ip was given a SN name in 2009 because of its sudden brightening but it was found to be caused by the surface eruption of a

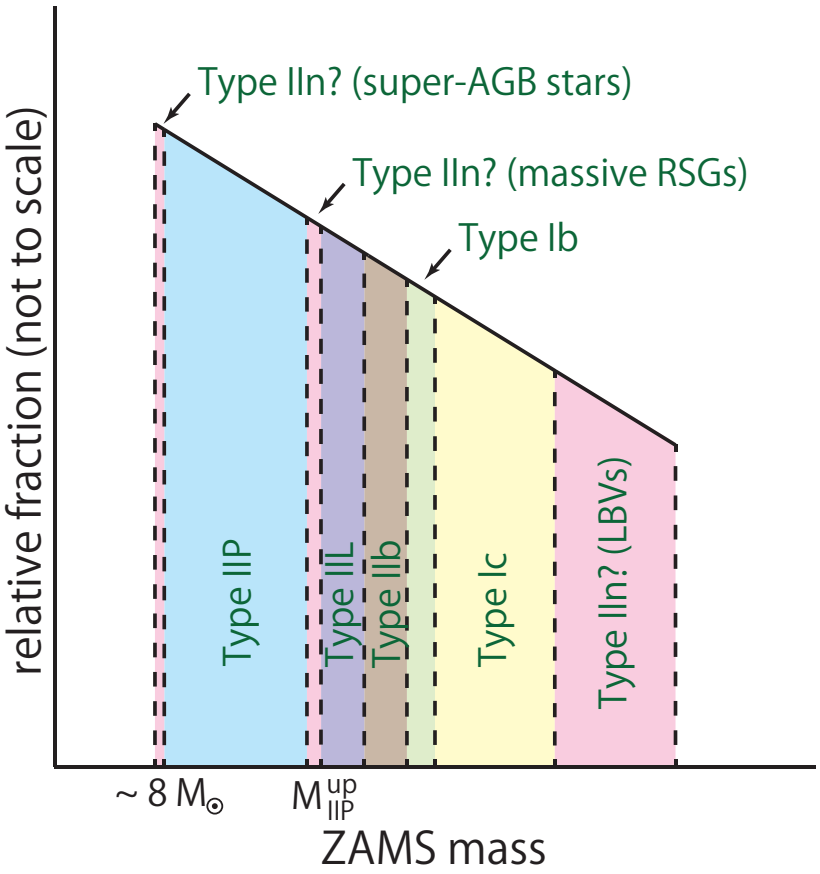

Figure 1.7: One possible relation between SN types and their ZAMS mass. y-axis is a relative fraction of SNe (number density of SNe) which is determined by an initial mass function. $M_{\rm IIP}^{\rm up}$ is the maximum ZAMS mass of the progenitor of SNe IIP.

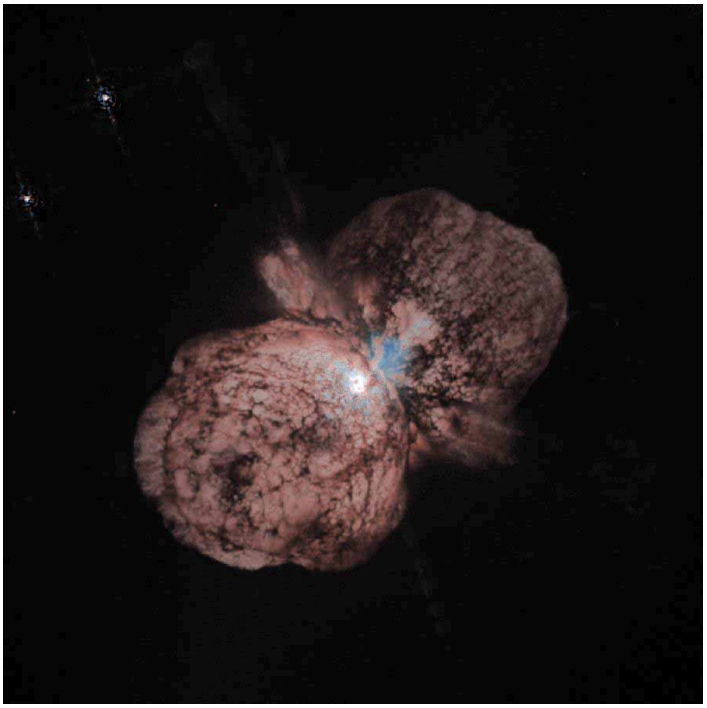

Figure 1.8: *HST* image of η Carinae. It is classified as a LBV and known to have experienced extensive mass loss in the 19th century during the Great Eruption (Davidson & Humphreys 1997).

LBV and it was not a SN (Foley et al. 2011, Smith et al. 2010b). A LBV with $M_R \simeq -10$ mag remained at the position. However, in 2012, the star got suddenly bright again. The luminosity in 2012 was much brighter than in 2009 and the spectra were those of SNe IIn. The star is likely to have exploded as a SN this time (Mauerhan et al. 2013, Prieto et al. 2013), although other interpretations also exist (Pastorello et al. 2013, Fraser et al. 2013). Another SN IIn 2010jl whose explosion site is found in the *HST* archive image is suggested to have a very massive progenitor, possibly a LBV (Smith et al. 2011). Also, some features of LBVs are suggested to be discovered in LCs and spectra of some SNe with other spectral types (e.g., Kotak & Vink 2006, Trundle et al. 2008).

However, despite many evidences suggesting the explosions of LBVs, LBVs are theoretically not considered to be the final stage of massive stars (e.g., Maeder & Meynet 2000b, but see also Langer 2012). LBVs are considered to evolve to Wolf-Rayet (WR) stars as is shown in Figure 1.9. Groh et al. 2013 found for the first time that rotating 20 $M_\odot$ and 25 $M_\odot$ pre-SN models of Ekström et al. 2012 are actually LBVs at the time of their core collapse but their luminosities are not as high as those of the stars observed in the archival images of SNe IIn.

So far, we assume that a SN explodes in a dense CSM to explain SNe IIn. However, what is colliding from inside to the dense CSM does not have to be SN ejecta. Even if ejecta whose kinetic energy is much lower than that of SN ejecta, the system can be very

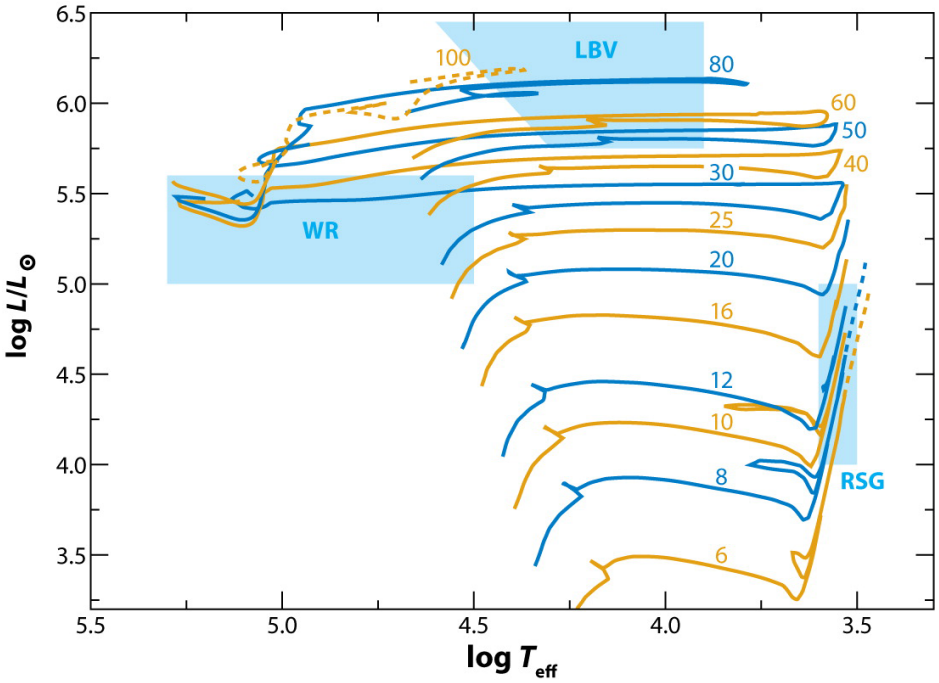

Figure 1.9: Hertzsprung-Russell (HR) diagram from the STARS stellar evolution code (Eldridge & Tout 2004) presented in Smartt 2009. Typical temperatures and luminosities of RSGs, WR stars, and LBVs are shaded.

bright because of the efficient conversion from kinetic energy to radiation energy at the shock wave. Several studies show that such a collision can explain the high luminosities of SNe IIn and their spectra (e.g., Woosley et al. 2007, Dessart et al. 2009). There are transients called SN impostors which get bright and show spectra which are similar to those of SNe IIn (see Davidson & Humphreys 2012 for reviews). They are suggested to be caused by the continuous eruptions of LBVs, as was observed for SN 2009ip in 2009.

We finally note that some SNe IIn may even come from SNe Ia and may not be related to massive stars at all. As SNe Ia explode within the accretiong materials from their companion stars in the SD scenario, it predicts that some SNe Ia show features coming from the CSM (e.g., Hachisu et al. 2008, Hachisu et al. 1999). There are some SNe Ia which show narrow Hα profiles coming from their CSM (Silverman et al. 2013 and references therein). PTF11kx (Dilday et al. 2012) and SN 2002ic (Hamuy et al. 2003) are the typical SNe Ia of this kind.

1.5 Superluminous Supernovae

Superluminous supernovae (SLSNe) are a new class of SNe with huge luminosities whose existence is revealed by the recent untargeted transient surveys (see Gal-Yam 2012 for a review). SNe which are brighter than $\simeq -21$ mag are canonically called SLSNe (Figure 1.10). This means that their luminosities are more than 10 times larger than typical SNe Ia

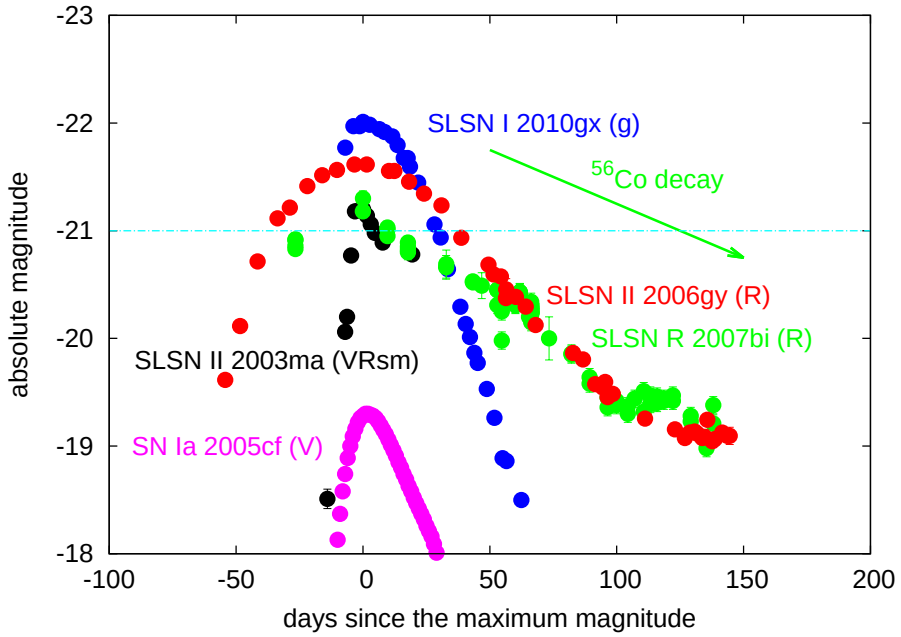

Figure 1.10: Optical LCs of SLSNe. LCs are from Smith et al. 2007 (SN 2006gy), Rest et al. 2011 (SN 2003ma), Gal-Yam et al. 2009 (SN 2007bi), and Pastorello et al. 2010 (SN 2010gx). The LC of SN Ia 2005cf (Wang et al. 2009) and the ^{56}Co decay timescale are also plotted for comparison.

which have been used for cosmology. Total radiation energies emitted in ~ 1 years after their explosions exceed 10^{51} erg while a typical SN emit 10^{49} erg by radiation (Gal-Yam 2012). 10^{51} erg is a typical kinetic energy of core-collapse SNe and SLSNe have this amount of energy just by the form of radiation.

SLSNe are a very rare kind of SNe whose nearby rate at $z \simeq 0.2$ is similar to that of gamma-ray bursts ($\sim 0.1\%$ of all core-collapse SNe, Quimby et al. 2013b) and traditional SN surveys performed by following the nearby galaxies missed these very rare objects. The first observed SN of this kind was SN 1999as (Knop et al. 1999) but its nature had been unclear. After the discovery of SN 2006gy by Quimby 2006, many SLSNe have been discovered and information about them has been accumulated. However, the reasons for the huge luminosities of SLSNe and their progenitors are not understood well. If they are revealed, SLSNe can be used as a probe of the early Universe as their huge luminosities allow us to observe them at very high redshifts. The most distant SLSN currently discovered is at $z = 3.90$ (Cooke et al. 2012). They are also able to be used as a light source to probe the interstellar media of distant galaxies (Berger et al. 2012).

1.5.1 Observational Diversities of Superluminous Supernovae

SLSNe are known to have some diversities in their spectra and LC evolution. Gal-Yam 2012 classified SLSNe into three types and called them SLSN II, SLSN I, and SLSN R. We follow

this nomenclature in this dissertation. Here, we summarize the observational features of the three types of SLSNe.

SLSN II is the most common kind of SLSNe (Quimby et al. 2013b). They show H lines in their spectra. All of them, expect for SN 2008es, show narrow H lines in their spectra and they are SNe IIn. They have a wide range of the peak luminosities, reaching to $M_V \simeq -23$ mag in the most luminous case (CSS100217:102913+404220, Drake et al. 2011). Their LCs typically have long durations but there are several exceptions (e.g., SN 2003ma in Figure 1.10, Rest et al. 2011). From the fact that they are SNe IIn, they are likely to become SLSNe because of the existence of the dense CSM around the progenitors. SN IIL 2008es (Miller et al. 2009, Gezari et al. 2009) is the only SLSN II without narrow H components and we cannot directly attribute its huge luminosity to the existence of the dense CSM. SLSN II typically appears in metal-poor galaxies but the best observed SLSN, i.e., SN 2006gy, appeared in a metal-rich galaxy (Neill et al. 2011).

SLSN R and SLSN I do not show H in their spectra. The two types are divided based on their LC evolution. SLSN R, in which R stands for the Radioactive decay, has LCs whose decline rates are consistent with the radioactive decay time of ^{56}Co (Figure 1.10, Gal-Yam et al. 2009). The natural interpretation is that their huge luminosities are due to the huge amount of ^{56}Ni produced at the time of their explosions. The required amount of ^{56}Ni to explain their luminosities are more than 5 $M_\odot$.

SLSN I is, in a sense, the most mysterious SLSN among the three types. It does not show any signatures of their power source. It does not show any signatures of dense CSM in their spectra. Its LCs decline very quickly and they are inconsistent with the ^{56}Ni heating scenario (Quimby et al. 2011). The upper ^{56}Ni mass limit constrained from its LCs is ~ 0.1 $M_\odot$ (Chen et al. 2013). The spectra of SLSN I 2010gx are followed for a long time and their spectra are found to get similar to those of energetic core-collapse SNe which are often associated with gamma-ray bursts (Pastorello et al. 2010). Leloudas et al. 2012 reported the observation of the precursor before the main LC of SLSN I 2006oz. Both SLSN R and SLSN I are known to appear in metal-poor galaxies (Neill et al. 2011, Quimby et al. 2011). The nearby rate of SLSN I is about 10% of SLSN II (Quimby et al. 2013b).

Finally, Chornock et al. 2013 reported the discovery of a SLSN (PS1-10afx) whose properties, especially colors, are completely different from currently known SLSNe. However, it turned out to be a SN Ia whose luminosity is 30 times amplified by the gravitational lens because of its striking similarity to SNe Ia except for its luminosity (Quimby et al. 2013a).

1.5.2 Suggested Origins and Progenitors of Superluminous Supernovae

There are several suggested models to explain SLSNe's huge luminosities and their progenitors but they are still far from being matured. The mechanism to power SLSN II is likely to be the deceleration of SN ejecta due to dense CSM because of their spectral type (Type IIn). However, the required amount of the dense CSM should be very large to account for the huge luminosities. Even if we can explain their luminosities by the interaction, we are still not sure if such dense CSM are expected from the stellar evolution and stellar mass loss points of view as we discussed with SNe IIn in the previous section. In addition, it is not clear whether we can explain SN IIL 2008es in the context of the interaction.

The very large required mass of ^{56}Ni to explain the LCs of SLSN R is naturally expected from PISNe. However, whether PISNe can appear in the local Universe is unclear. In addition, there are other suggested mechanisms to explain the LCs declining with the ^{56}Co decay timescale. For example, if a magnetar is born at the core collapse, the rotational energy can be released in a short timescale, depending on its rotational period and magnetic field, and they can reproduce the SLSN R LCs as well (e.g., Kasen & Bildsten 2010, Dessart et al. 2012).

Finally, SLSN I has many possible mechanisms to explain its properties because of little observational constraint. A natural extension of the idea of SLSN II is that the interaction between SN ejecta and C+O dense CSM makes them superluminous (e.g., Blinnikov & Sorokina 2010). Actually, WR stars seem to have a path to experience a LBV-like mass eruption shortly before their explosions. An evidence is provided by SN Ib 2006jc whose progenitor is found to have had a LBV-like eruption two years before its explosion (Nakano et al. 2006, Pastorello et al. 2007, Foley et al. 2007) and its progenitor is found to be a WR star of $M_{\rm ZAMS} \simeq 40\ M_\odot$ (Tominaga et al. 2008). Although SN 2006jc was not a SLSN, similar mechanisms may play a role to make an explosion of a WR star superluminous. As is suggested for SLSN R, magnetars can also explain the LCs of SLSN I (e.g., Kasen & Bildsten 2010, Inserra et al. 2013). Other exotic mechanisms, like the heating by the latent heat which is released when the central neutron star makes a phase transition to a quark star (e.g., Ouyed & Leahy 2012), are also suggested.

To summarize, although we are starting to catch hints for the nature of SLSNe, there remain many unanswered questions which require theoretical interpretations. In addition, little is know about their progenitors and we need to connect the observational information to their progenitors.

1.6 Goals and Structures of this Dissertation

We have seen that there are a class of SNe, namely, SNe IIn and SLSNe, which are influenced by the CSM created by their progenitors shortly before their explosions. To understand the SNe interacting with CSM and reveal their progenitors and related mass-loss mechanisms, we need to approach this problem from both observational side and theoretical side. From the observational side, we need to interpret the observed SN properties like LCs to estimate the state of the CSM involved in the SNe ((i) in Figure 1.11). For this purpose, we need a theoretical framework to interpret the observations. Given the CSM properties obtained by interpreting the observations, we can connect the CSM properties to the predictions of the stellar evolution and the mass-loss theories (ii). We can also follow this path starting from the opposite side. There are theoretical progenitor models which are predicted to have large mass-loss rates. We can construct the CSM properties form the models (iii) and see what happens if a SN explode within the CSM (iv). The whole processes (i)-(iv) are required to reveal the mysteries involved in these SNe and progenitors. In this dissertation, by following the both ways from (i) to (ii) and from (iii) to (iv) in Figure 1.11, we will revise the current understanding of SNe interacting with CSM and show what is missing there and what should be considered.

From the observational side, we first develop an analytic LC model which can be used for interpret SN IIn LCs (Chapter 2). We will show that CSM properties of SNe IIn which

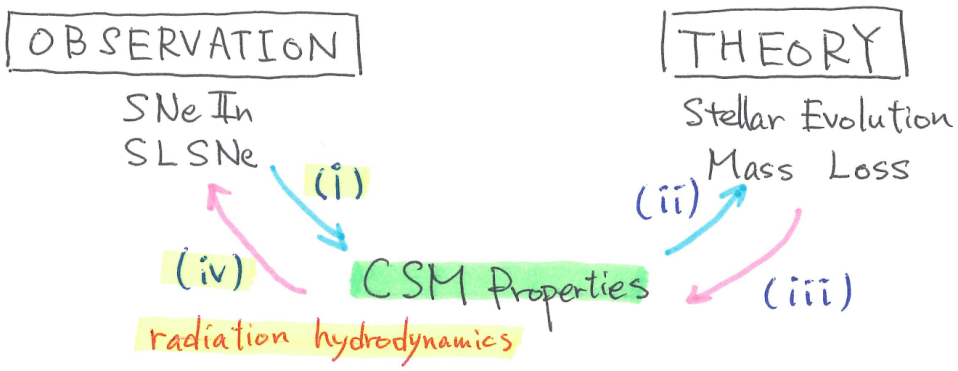

Figure 1.11: We study SNe interacting with CSM starting from both observations and theories in this dissertation. From observations, we need to interpret the observed quantities to obtain the CSM properties involved (i). Then, we need to see if there are theories which predicts the obtained CSM properties (ii). Theories predict that some SNe can have large mass-loss rates shortly before their explosions. We need to construct CSM properties from the model (iii) and predict the observational properties of them (iv). To bridge the CSM properties and the observational properties ((i) and (iv)), radiation hydrodynamics is a must because the main radiation energy source of the system we are interested in is the kinetic energy of SN ejecta.

are currently estimated by using crude spectral interpretations can be obtained by using our analytic LC model ((i), Chapter 3). The obtained CSM properties should be compared to the current theoretical models to see such mass loss can be achieved by SN progenitor models (ii).

The analytic model we developed for modeling some SNe IIn cannot be applied for every SN IIn, especially for SLSNe. As kinetic energy of SN ejecta is the main power source of radiation in the system we are interested in, we essentially need to treat radiation hydrodynamics to model LCs of such SNe (in (i) and (iv)). In Chapter 2, we also summarize the essence of radiation hydrodynamics and a way to treat it numerically. We focus on a numerical one-dimensional radiation hydrodynamics code `STELLA` which we use in this dissertation.

SLSNe are a typical system in which we cannot use the analytic approach to model LCs. However, we will show that we can crudely estimate the CSM properties of them analytically from observed properties and show that the analytic way works well by numerically modeling their LCs (Chapter 4). Combining both analytic and numerical approaches to interpret the observational properties of SLSNe, we try to reveal the nature of SLSNe and their progenitors in Chapter 4.

Next, we follow the opposite way (from (iii) to (iv)) in Chapter 5. We start from the SN progenitors which are theoretically suggested to have extensive mass loss shortly before their explosions. We construct the predicted CSM properties form the models and obtain the LC evolution assuming a SN exploded inside. We find that no current theoretical models of

the stellar evolution can explain the LC properties of SNe IIn and SLSNe. However, some observational properties of peculiar SNe are found to be explained by current theoretical stellar evolutionary models.

Finally, in Chapter 6, we consider possible signatures of the interaction between SN ejecta and CSM remaining in their remnants. SNe showing the clear signatures of the CSM interaction are rare. If there are SN remnants (SNRs) showing such signatures, they will also add valuable information about the progenitors of such SNe.

Light can be gentle, dangerous, dreamlike, bare, living, dead, misty, clear, hot, dark, violet, springlike, falling, straight, sensual, limited, poisonous, calm and soft.

Sven Nykvist (1922 - 2006)

2

Emission from Supernovae Interacting with Circumstellar Media

2.1 Overview

Almost all the observational signatures we obtain from SNe are in the form of electromagnetic waves. We need to interpret radiation observed to understand properties of SNe. We need to show expected radiative signatures from a theory and compare them to observations to prove it. Hence, understanding the radiative processes of SNe is the first step for the SN research.

SNe interacting with CSM have some special emission mechanisms which are usually not taken into account when we model emission from SNe. Especially, kinetic energy of SN ejecta can be the major source of radiation energy due to the deceleration of SN ejecta by CSM. Thus, we need to treat radiational and hydrodynamical variables at the same time to model the emission from the SNe we are interested in. Radiation hydrodynamics, therefore, is essential in this dissertation.

In this chapter, we briefly summarize the emission mechanism from SNe interacting with CSM. Our special focus is on the system in which kinetic energy of SN ejecta is the main radiation source. As we will find, we can develop an analytic bolometric LC model for SNe interacting with CSM in some cases. However, in general, we need to treat radiation hydrodynamics numerically. We are going to use a numerical one-dimensional radiation hydrodynamics code `STELLA` in this dissertation and we will review how the code treats radiation hydrodynamics numerically.

2.2 Emission from SNe with Normal CSM

2.2.1 Synchrotron

Synchrotron emission is typical emission caused by the interaction between SN ejecta and CSM. Electrons are accelerated by the so-called Fermi mechanism at the forward shock where the weak magnetic field in the CSM is amplified and gets strong. These accelerated electrons are presumed to be the cause of the synchrotron emission observed from SNe, especially in radio wavelengths, and the radio observations are extensively used to estimate the CSM properties shortly before the explosions. However, the detailed processes of the electron acceleration and the magnetic field amplification are not known well (e.g., Maeda 2012, Maeda 2013). To estimate the CSM properties, we usually assume a fraction ε_B of the SN kinetic energy is converted to the magnetic energy and a fraction ε_e is used for the electron acceleration. In other words,

$$\frac{B^2}{8\pi} = \frac{\varepsilon_B}{2}\rho_{\rm csm}v_{\rm sh}^2, \tag{2.1}$$

$$\int_{\gamma_{\rm min}}^{\gamma_{\rm max}} m_e c^2 \gamma n_{\rm rel}(\gamma) d\gamma = \frac{\varepsilon_e}{2}\rho_{\rm csm}v_{\rm sh}^2, \tag{2.2}$$

where B is the magnetic field strength, m_e is the electron mass, γ is the Lorentz factor of a electron, $\gamma_{\rm max}$ and $\gamma_{\rm min}$ are the maximum and the minimum Lorentz factors of the accelerated electrons, respectively, and $n_{\rm rel}(\gamma)$ is the accelerated electron number density. In the electron acceleration at the SN forward shock, $\gamma_{\rm min} \sim 1$ is usually assumed. The number density of the accelerated electrons is assumed to follow the power-law distribution

$$\frac{dn_{\rm rel}}{d\gamma} = n_0 \gamma^{-p}. \tag{2.3}$$

The canonical values in SN studies are $\varepsilon_B = 0.1$, $\varepsilon_e = 0.1$, and $p = 3$ (e.g., Chevalier et al. 2006, Chevalier & Fransson 2006). We assume $\gamma_{\rm min} \ll \gamma_{\rm max}$ in the following discussion. Fransson & Björnsson 1998, Björnsson & Fransson 2004 derive a simple formalism for the synchrotron emission luminosity L_ν from SNe,

$$\nu L_\nu \simeq \pi r_{\rm sh}^2 v_{\rm sh} n_{\rm rel} \left(\frac{\gamma_\nu}{\gamma_{\rm min}}\right)^{1-p} \gamma_\nu m_e c^2 \left[1 + \frac{t_{\rm sync}(\nu)}{t} + \frac{t_{\rm sync}(\nu)}{t_{\rm other}(\nu)}\right]^{-1}, \tag{2.4}$$

where

$$\gamma_\nu = \left(\frac{2\pi m_e c \nu}{eB}\right)^{\frac{1}{2}}, \tag{2.5}$$

is the Lorentz factor of electrons emitting at the characteristic frequency ν and e is the electron charge. $t_{\rm sync}$ is the synchrotron cooling timescale

$$t_{\rm sync}(\nu) = \frac{6\pi m_e c}{\sigma_T(\gamma_\nu - 1/\gamma_\nu)B^2} \simeq \frac{6\pi m_e c}{\sigma_T \gamma_\nu B^2} \quad (\gamma_\nu \gg 1), \tag{2.6}$$

where σ_T is the Thomson scattering cross section. $t_{\rm other}(\nu)$ is the cooling timescale for other cooling mechanisms. Other possible cooling mechanisms include, for instance, the inverse

Compton cooling

$$t_{\rm IC}(\nu) = \frac{3\pi r_{\rm sh}^2 m_e c^2}{\sigma_T(\gamma_\nu - 1/\gamma_\nu)L_{\rm bol}} \simeq \frac{3\pi r_{\rm sh}^2 m_e c^2}{\sigma_T \gamma_\nu L_{\rm bol}} \quad (\gamma_\nu \gg 1), \tag{2.7}$$

where $L_{\rm bol}$ is the bolometric luminosity of the SN inside. The cooling due to the Coulomb interaction can also be important when the CSM density is very high (Fransson & Björnsson 1998).

2.2.1.1 Absorption Processes

The synchrotron radiation from the forward shock is not directly observed. There are absorption mechanisms involved. The important absorption mechanisms in the synchrotron radiation from the SN forward shock are the synchrotron self-absorption (SSA) at the emitting region and the free-free absorption in the unshocked CSM. For typical SNe, the CSM density is not high enough for the free-free absorption to be significant and we can usually consider the effect of the SSA only. However, when the CSM density is high, the free-free absorption becomes the dominant absorption process. Here, we review the two absorption processes.

Synchrotron Self-Absorption

The synchrotron emission from relativistic electrons can be absorbed by the relativistic electrons themselves. This absorption by the electrons which are emitting the synchrotron radiation is called the SSA. The SSA coefficient $\alpha_{\rm SSA}(\nu)$ for the power-law distribution of relativistic electrons is

$$\alpha_{\rm SSA}(\nu) \simeq \frac{n_0 e^2}{4\sqrt{3} m_e c}\left(\frac{3eB}{2\pi m_e c}\right)^{\frac{p+2}{2}} \Gamma\left(\frac{3p+2}{12}\right)\Gamma\left(\frac{3p+22}{12}\right)\nu^{-\frac{p+4}{2}}, \tag{2.8}$$

$$= \frac{e^2 \varepsilon_e (p-2) B^{\frac{p+6}{2}} \gamma_{\rm min}^{p-2}}{32\sqrt{3}\pi m_e^2 c^3 \varepsilon_B}\left(\frac{3e}{2\pi m_e c}\right)^{\frac{p+2}{2}} \Gamma\left(\frac{3p+2}{12}\right)\Gamma\left(\frac{3p+22}{12}\right)\nu^{-\frac{p+4}{2}}. \tag{2.9}$$

$\Gamma(x)$ is the Gamma function. We have assumed $\gamma_{\rm min} \ll \gamma_{\rm max}$ and $p \neq 2$ in Equation 2.9. We refer Rybicki & Lightman 1986, Shu 1991 for the detailed derivation of the SSA coefficient. Assuming that the emitting region is $\simeq 2r_{\rm sh}/3$ (Chevalier 1998), the SSA frequency $\nu_{\rm SSA}$ is

$$\nu_{\rm SSA} \simeq \left[\frac{e^2(p-2)}{48\sqrt{3}\pi m_e^2 c^3}\Gamma\left(\frac{3p+2}{12}\right)\Gamma\left(\frac{3p+22}{12}\right)\right]^{\frac{2}{p+4}}\left(\frac{3e}{2\pi m_e c}\right)^{\frac{p+2}{p+4}}\left(\frac{\varepsilon_e}{\varepsilon_B}\right)^{\frac{2}{p+4}} r_{\rm sh}^{\frac{2}{p+4}} B^{\frac{p+6}{p+4}} \gamma_{\rm min}^{\frac{p-2}{p+4}}. \tag{2.10}$$

From Equations 2.4 and 2.10, we can easily find that the spectral energy distributions (SEDs) of the synchrotron emission have two power-law components when the synchrotron cooling is the dominant cooling process,

$$L_\nu \propto \begin{cases} \nu^{\frac{5}{2}} & (\nu \ll \nu_{\rm SSA}), \\ \nu^{-\frac{p-1}{2}} & (\nu \gg \nu_{\rm SSA}). \end{cases} \tag{2.11}$$

Free-Free Absorption

When the CSM density is sufficiently high, the free-free absorption above the emitting region becomes more effective than the SSA. In the case of the SSA, the SEDs at the frequencies below the SED peak are strictly proportional to $\nu^{2.5}$ while the SEDs affected by the free-free absorption can have steeper spectral declines. As a result, the SN radio LC rise can be faster than that affected by the SSA if it is affected by the free-free absorption (e.g., Chevalier 1998). In a CSM with the blackbody temperature of T, the free-free absorption coefficient $\alpha_{\rm ff}(\nu)$ is

$$\alpha_{\rm ff}(\nu) = \frac{4e^6}{3m_e hc}\left(\frac{2\pi}{3k_B m_e}\right)^{\frac{1}{2}} T^{-\frac{1}{2}} Z^2 n_e n_i \nu^{-3}\left(1-e^{-h\nu/k_B T}\right)\overline{g}_{\rm ff}(T,\nu), \tag{2.12}$$

where h is the Planck constant, Z is an atomic number, n_e is electron number density, n_i is ion number density, and $\overline{g}_{\rm ff}(T,\nu)$ is a velocity averaged Gaunt factor. With typical radio frequencies and CSM temperatures, $h\nu \ll k_B T$ and the free-free absorption coefficient becomes

$$\alpha_{\rm ff}(\nu) = \frac{4e^6}{3m_e k_B c}\left(\frac{2\pi}{3k_B m_e}\right)^{\frac{1}{2}} T^{-\frac{3}{2}} Z^2 n_e n_i \nu^{-2}\overline{g}_{\rm ff}(T,\nu). \tag{2.13}$$

2.2.2 X-Ray

X-rays from SNe are mainly emitted from the shocked regions. Both CSM and SN ejecta are shocked by the forward shock and the reverse shock, respectively, and the electron temperatures of the shocked regions becomes $\sim 10^9$ K and $\sim 10^7$ K, respectively (e.g., Chevalier & Fransson 1994, Fransson et al. 1996, Chevalier et al. 2006, Nymark et al. 2006). The shocked hot gas is cooled mainly by the free-free radiation which can be observed in X-ray wavelengths. As the free-free cooling timescale is short in the high density region which is typically the SN ejecta shocked by the reverse shock, most of the X-rays observed from SNe at early epochs are presumed to come from the reverse shocked region. If the CSM is very dense, the shocked dense CSM can also be a strong X-ray emitter (e.g., Pan et al. 2013, Levan et al. 2013). The inverse Compton scattering of the optical and the synchrotron radiation can also be a cause of X-rays from SNe (e.g., Björnsson & Fransson 2004, Maeda 2012).

2.3 Emission from SNe Interacting with Optically Thin Dense CSM

In this section, we develop an analytic SN bolometric LC model under the assumption that its main power source is kinetic energy of SN ejecta colliding with a dense CSM. At first, we analytically investigate the evolution of the dense shell created by the interaction in Section 2.3.1. The analytic solution for the evolution of the dense shell before time t_t (see below) is essentially the same as obtained in previous works (e.g., Chevalier 1982b, Chevalier 1990, Chevalier & Fransson 1994, Chevalier & Fransson 2003) but our solution does not assume steady mass loss (see also Fransson et al. 1996).

After deriving the evolution of the dense shell, we provide an analytic expression for bolometric LCs. This method was introduced by Chugai & Danziger 1994 (see also

Wood-Vasey et al. 2004) to explain the luminoisity due to the interaction but their model assumes a CSM from steady mass loss. We generalize this method for the cases of non-steady mass loss and apply our model to entire bolometric LCs. Chatzopoulos et al. 2012 also follow a similar approach to obtain an analytic LC model from the interaction but they consider the case where the unshocked CSM is optically thick. Here, we consider the cases in which the unshocked CSM does not affect the bolometric LC so much or the dense CSM is optically thin. High energy photons like X-rays are expected to be emitted when the CSM is optically thin (e.g., Chevalier & Fransson 1994) but they can be absorbed by the CSM because of their high column density and re-emitted as optical photons (e.g., Wilms et al. 2000). Some SNe IIn are suggested to have very optically thick CSM to explain their huge luminosities (e.g., Chapter 4, Chevalier & Irwin 2011, Ginzburg & Balberg 2012). They are beyond the scope of this section and will be discussed in the next section.

2.3.1 Evolution of the Shocked Dense Shell

2.3.1.1 General Case

The shocked dense CSM and SN ejecta form a thin dense shell because of the efficient radiative cooling. We assume that the thickness of the shocked shell is much smaller than its radius and it can be denoted by a radius $r_{\rm sh}(t)$. The conservation of momentum requires

$$M_{\rm sh}\frac{dv_{\rm sh}}{dt} = 4\pi r_{\rm sh}^2\left[\rho_{\rm ej}(v_{\rm ej}-v_{\rm sh})^2 - \rho_{\rm csm}(v_{\rm sh}-v_{\rm w})^2\right], \tag{2.14}$$

where $M_{\rm sh}$ is the total mass of the shocked SN ejecta and CSM, $v_{\rm sh}$ is the velocity of the shell, $\rho_{\rm ej}$ is the SN ejecta density, $v_{\rm ej}$ is the SN ejecta velocity, $\rho_{\rm csm}$ is the CSM density, and $v_{\rm w}$ is the CSM velocity. We derive the evolution of $r_{\rm sh}$ based on this equation. We do not use the equation for the conservation of energy which is necessary to derive the self-similar solution including the reverse shock and the forward shock (Chevalier 1982a, Nadyozhin 1985). This is because of the radiative energy loss from the dense shell. When the radiative cooling is efficient, the shocked region does not extend as wide as the width expected from the self-similar solution due to the loss of the thermal pressure caused by the radiative energy loss. Thus, our approximation to neglect the shell width is presumed to be a good approximation to the shell evolution.

We further assume that the CSM density follows $\rho_{\rm csm} = Dr^{-s}$ and that the CSM velocity $v_{\rm w}$ is constant. We adopt a double power-law profile for the density of homologously ($v_{\rm ej} = r/t$) expanding SN ejecta ($\rho_{\rm ej} \propto r^{-n}$ outside and $\rho_{\rm ej} \propto r^{-\delta}$ inside) based on numerical simulations of SN explosions (e.g., Matzner & McKee 1999). With SN kinetic energy $E_{\rm ej}$ and SN ejecta mass $M_{\rm ej}$, the SN density structure is expressed as

$$\rho_{\rm ej}(v_{\rm ej},t) = \begin{cases} \frac{1}{4\pi(n-\delta)}\frac{[2(5-\delta)(n-5)E_{\rm ej}]^{(n-3)/2}}{[(3-\delta)(n-3)M_{\rm ej}]^{(n-5)/2}}t^{-3}v_{\rm ej}^{-n} & (v_{\rm ej} > v_t), \\ \frac{1}{4\pi(n-\delta)}\frac{[2(5-\delta)(n-5)E_{\rm ej}]^{(\delta-3)/2}}{[(3-\delta)(n-3)M_{\rm ej}]^{(\delta-5)/2}}t^{-3}v_{\rm ej}^{-\delta} & (v_{\rm ej} < v_t), \end{cases} \tag{2.15}$$

where v_t is obtained from the density continuity condition at the interface of the two density structures as well as $E_{\rm ej}$ and $M_{\rm ej}$ as follows,

$$v_t = \left[\frac{2(5-\delta)(n-5)E_{\rm ej}}{(3-\delta)(n-3)M_{\rm ej}}\right]^{\frac{1}{2}}. \tag{2.16}$$

The outer density slope n depends on the SN progenitor and $n \simeq 7$ ($n = 6.67$ exactly) is the lowest allowed n expected from the self-similar solution of Sakurai 1960 (e.g., Chevalier 1990). A value of $n \simeq 10$ is expected for SN Ib/Ic and SN Ia progenitors (Matzner & McKee 1999, Kasen 2010) and $n \simeq 12$ is expected for explosions of RSGs (Matzner & McKee 1999). The inner density slope δ is $\delta \simeq 0 - 1$.

At first, the outer SN ejecta with $\rho_{\rm ej} \propto r^{-n}$ starts to interact with the CSM. In this phase, $M_{\rm sh}$ becomes

$$M_{\rm sh} = \int_{R_{\rm p}}^{r_{\rm sh}} 4\pi r^2 \rho_{\rm csm} dr + \int_{v_{\rm ej}/t}^{v_{\rm ej,max}/t} 4\pi r^2 \rho_{\rm ej} dr, \tag{2.17}$$

$$= \frac{4\pi D}{3-s} r_{\rm sh}^{3-s} + \frac{t^{n-3}}{(n-\delta)(n-3) r_{\rm sh}^{n-3}} \frac{[2(5-\delta)(n-5)E_{\rm ej}]^{(n-3)/2}}{[(3-\delta)(n-3)M_{\rm ej}]^{(n-5)/2}}, \tag{2.18}$$

where $R_{\rm p}$ is the radius of the progenitor, $v_{\rm ej,max}$ is the velocity of the outermost layer of the SN ejecta before the interaction. In deriving Equation 2.18 from Equation 2.17, we have assumed $r_{\rm sh} \gg R_{\rm p}$, $v_{\rm ej,max} \gg v_{\rm ej}$, and $s < 3$.

With the above equations and $v_{\rm ej} = r_{\rm sh}/t$ (homologous expansion of the SN ejecta), the equation for the conservation of momentum becomes

$$\left[\frac{4\pi D}{3-s} r_{\rm sh}^{3-s} + \frac{t^{n-3}}{(n-\delta)(n-3) r_{\rm sh}^{n-3}} \frac{[2(5-\delta)(n-5)E_{\rm ej}]^{(n-3)/2}}{[(3-\delta)(n-3)M_{\rm ej}]^{(n-5)/2}} \right] \frac{d^2 r_{\rm sh}}{dt^2} =$$
$$\frac{1}{(n-\delta)} \frac{[2(5-\delta)(n-5)E_{\rm ej}]^{(n-3)/2} t^{n-3}}{[(3-\delta)(n-3)M_{\rm ej}]^{(n-5)/2} r_{\rm sh}^{n-2}} \left(\frac{r_{\rm sh}}{t} - \frac{dr_{\rm sh}}{dt} \right)^2 - 4\pi D r_{\rm sh}^{2-s} \left(\frac{dr_{\rm sh}}{dt} \right)^2 . \tag{2.19}$$

Here, we assume that the CSM velocity is much smaller than the shell velocity ($v_{\rm sh} \gg v_{\rm w}$). Solving the differential equation, we get a power-law solution

$$r_{\rm sh}(t) = \left[\frac{(3-s)(4-s)}{4\pi D(n-4)(n-3)(n-\delta)} \frac{[2(5-\delta)(n-5)E_{\rm ej}]^{(n-3)/2}}{[(3-\delta)(n-3)M_{\rm ej}]^{(n-5)/2}} \right]^{\frac{1}{n-s}} t^{\frac{n-3}{n-s}}. \tag{2.20}$$

Note that $r_{\rm sh}(t)$ obtained with this approach has the same time dependence as the self-similar solution [$t^{(n-3)/(n-s)}$] (Chevalier 1982b, Chevalier 1982a, Chevalier & Fransson 2003, Nadyozhin 1985).

Equation 2.20 holds until the time t_t when the interacting region reaches down to the inner ejecta, namely when the $v_{\rm ej}$ entering the shell becomes v_t or $r_{\rm sh}(t_t) = v_t t_t$ is satisfied, i.e.,

$$t_t = \left[\frac{(3-s)(4-s)}{4\pi D(n-4)(n-3)(n-\delta)} \frac{[(3-\delta)(n-3)M_{\rm ej}]^{(5-s)/2}}{[2(5-\delta)(n-5)E_{\rm ej}]^{(3-s)/2}} \right]^{\frac{1}{3-s}}. \tag{2.21}$$

After t_t, the density structure of the SN ejecta entering the shell starts to follow $\rho_{\rm ej} \propto r^{-\delta}$ and the equation of the momentum conservation becomes

$$\left[\frac{4\pi D}{3-s} r_{\rm sh}^{3-s} + M_{\rm ej} - \frac{r_{\rm sh}^{3-\delta}}{(n-\delta)(3-\delta) t^{3-\delta}} \frac{[2(5-\delta)(n-5)E_{\rm ej}]^{(\delta-3)/2}}{[(3-\delta)(n-3)M_{\rm ej}]^{(\delta-5)/2}} \right] \frac{d^2 r_{\rm sh}}{dt^2} =$$
$$\frac{1}{(n-\delta)} \frac{[2(5-\delta)(n-5)E_{\rm ej}]^{(\delta-3)/2} r_{\rm sh}^{2-\delta}}{[(3-\delta)(n-3)M_{\rm ej}]^{(\delta-5)/2} t^{3-\delta}} \left(\frac{r_{\rm sh}}{t} - \frac{dr_{\rm sh}}{dt} \right)^2 - 4\pi D r_{\rm sh}^{2-s} \left(\frac{dr_{\rm sh}}{dt} \right)^2 . \tag{2.22}$$

The solution of Equation 2.22 is expected to asymptotically approach the solution of the differential equations

$$M_{\rm sh}\frac{d^2r_{\rm sh}}{dt^2} = 4\pi r_{\rm sh}^2(-\rho_{\rm csm}v_{\rm sh}^2), \tag{2.23}$$

$$\left(\frac{4\pi D}{3-s}r_{\rm sh}^{3-s}+M_{\rm ej}\right)\frac{d^2r_{\rm sh}}{dt^2} = -4\pi D r_{\rm sh}^{2-s}\left(\frac{dr_{\rm sh}}{dt}\right)^2. \tag{2.24}$$

The asymptotic solution from Equation 2.24 satisfies the equation

$$\frac{4\pi D}{4-s}r_{\rm sh}(t)^{4-s}+(3-s)M_{\rm ej}r_{\rm sh}(t)-(3-s)M_{\rm ej}\left(\frac{2E_{\rm ej}}{M_{\rm ej}}\right)^{\frac{1}{2}}t=0. \tag{2.25}$$

The boundary conditions

$$r_{\rm sh}(t=0) = 0, \tag{2.26}$$

$$\frac{dr_{\rm sh}}{dt}(t=0) = \left(\frac{2E_{\rm ej}}{M_{\rm ej}}\right)^{\frac{1}{2}}, \tag{2.27}$$

are applied in deriving Equation 2.25. As the asymptotic solution is derived by assuming that most of the SN ejecta is in the dense shell, the dependence of $r_{\rm sh}(t)$ on the SN ejecta structure (n and δ) disappears.

2.3.1.2 Case of Steady Mass Loss (s=2)

Here, we write down $r_{\rm sh}(t)$ derived in the previous section for the special case of steady mass loss ($s=2$). The CSM density structure becomes

$$\dot{M}=4\pi r^2\rho_{\rm csm}v_{\rm w}, \tag{2.28}$$

where $\dot{M}$ is the mass-loss rate and D can be expressed as

$$D=\frac{\dot{M}}{4\pi v_{\rm w}}. \tag{2.29}$$

Then, $r_{\rm sh}(t)$ before $t=t_t$ is

$$r_{\rm sh}(t)=\left[\frac{2}{(n-4)(n-3)(n-\delta)}\frac{[2(5-\delta)(n-5)E_{\rm ej}]^{(n-3)/2}}{[(3-\delta)(n-3)M_{\rm ej}]^{(n-5)/2}}\frac{v_{\rm w}}{\dot{M}}\right]^{\frac{1}{n-2}}t^{\frac{n-3}{n-2}}\quad(t<t_t), \tag{2.30}$$

and

$$t_t=\frac{2}{(n-4)(n-3)(n-\delta)}\frac{[(3-\delta)(n-3)M_{\rm ej}]^{3/2}}{[2(5-\delta)(n-5)E_{\rm ej}]^{1/2}}\frac{v_{\rm w}}{\dot{M}}. \tag{2.31}$$

The asymptotic solution after t_t becomes

$$r_{\rm sh}(t)=\frac{v_{\rm w}}{\dot{M}}M_{\rm ej}\left[-1+\left(1+2\sqrt{\frac{2E_{\rm ej}}{M_{\rm ej}^3}}\frac{\dot{M}}{v_{\rm w}}t\right)^{\frac{1}{2}}\right]. \tag{2.32}$$

As noted in Section 2.3.1.1, the asymptotic solution is independent of the SN density structure (n and δ).

2.3.2 Bolometric Light Curve

2.3.2.1 General Case

We construct an analytic bolometric LC based on $r_{\rm sh}(t)$ obtained in the previous section. We assume that kinetic energy of the SN ejecta is the dominant source of the SN luminosity. The available kinetic energy is

$$dE_{\rm kin} = 4\pi r_{\rm sh}^2 \frac{1}{2}\rho_{\rm csm} v_{\rm sh}^2 dr_{\rm sh}, \tag{2.33}$$

and thus the bolometric luminosity will be

$$L = \varepsilon_k \frac{dE_{\rm kin}}{dt} = 2\pi\varepsilon_k \rho_{\rm csm} r_{\rm sh}^2 v_{\rm sh}^3, \tag{2.34}$$

where ε_k is the conversion efficiency from kinetic energy to radiation. Especially, the bolometric luminosity before t_t can be expressed as a power-law function

$$L = L_1 t^\alpha, \tag{2.35}$$

where

$$L_1 = \frac{\varepsilon_k}{2}(4\pi D)^{\frac{n-5}{n-s}} \left(\frac{n-3}{n-s}\right)^3 \left[\frac{(3-s)(4-s)}{(n-4)(n-3)(n-\delta)} \frac{[2(5-\delta)(n-5)E_{\rm ej}]^{(n-3)/2}}{[(3-\delta)(n-3)M_{\rm ej}]^{(n-5)/2}}\right]^{\frac{5-s}{n-s}}, \tag{2.36}$$

$$\alpha = \frac{6s-15+2n-ns}{n-s}. \tag{2.37}$$

In Figure 2.1, α is plotted as a function of s for $n = 12, 10, 7$.

After t_t, the asymptotic bolometric LC can be obtained based on the asymptotic radius evolution from Equation 2.25.

$$L = 2\pi\varepsilon_k \rho_{\rm csm} r_{\rm sh}^2 v_{\rm sh}^3, \tag{2.38}$$

$$= 2\pi\varepsilon_k D r_{\rm sh}^{2-s} \left[\frac{(3-s)M_{\rm ej}\left(\frac{2E_{\rm ej}}{M_{\rm ej}}\right)^{\frac{1}{2}}}{4\pi D r_{\rm sh}^{3-s} + (3-s)M_{\rm ej}}\right]^3. \tag{2.39}$$

2.3.2.2 Case of Steady Mass Loss (s=2)

In the case of steady mass loss ($s = 2$), we can use $4\pi D = \dot{M}/v_{\rm w}$ and express L before t_t as

$$L = \frac{\varepsilon_k}{2}\frac{\dot{M}}{v_{\rm w}} v_{\rm sh}^3, \tag{2.40}$$

$$= \frac{\varepsilon_k}{2}\left(\frac{\dot{M}}{v_{\rm w}}\right)^{\frac{n-5}{n-2}} \left(\frac{n-3}{n-2}\right)^3 \left[\frac{2}{(n-4)(n-3)(n-\delta)} \frac{[2(5-\delta)(n-5)E_{\rm ej}]^{(n-3)/2}}{[(3-\delta)(n-3)M_{\rm ej}]^{(n-5)/2}}\right]^{\frac{3}{n-2}} t^{-\frac{3}{n-2}}. \tag{2.41}$$

This equation is basically the same as the equations obtained in previous studies (e.g., Chugai & Danziger 1994, Wood-Vasey et al. 2004).

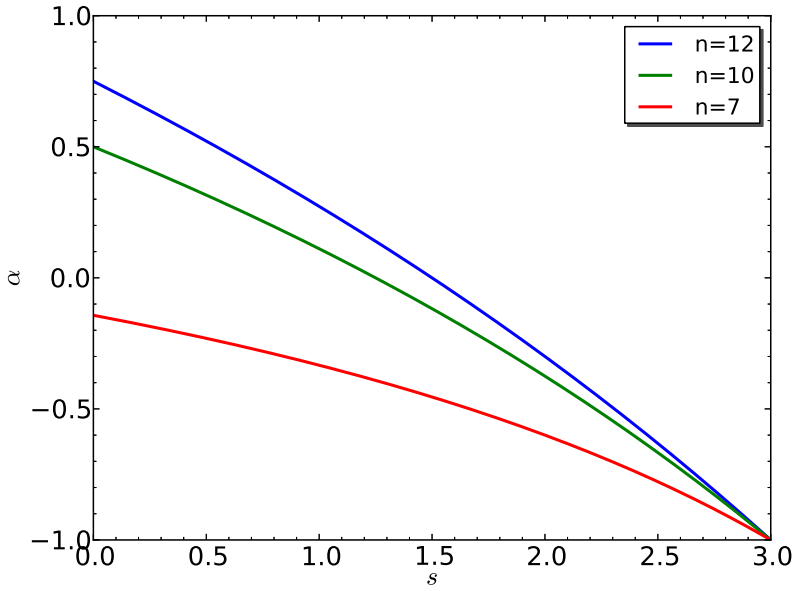

Figure 2.1: α ($L \propto t^{\alpha}$ before t_t) as a function of s for some n. $n \simeq 12$ represents RSG explosions and $n \simeq 10$ is for SN Ib/Ic and SN Ia progenitors. $n \simeq 7$ is the minimum possible n.

We can also express the asymptotic bolometric LC after t_t using Equation 2.32.

$$L = \frac{\varepsilon_k}{2}\frac{\dot{M}}{v_{\rm w}}\left(\frac{2E_{\rm ej}}{M_{\rm ej}}\right)^{\frac{3}{2}}\left[1+2\frac{\dot{M}}{v_w}\left(\frac{2E_{\rm ej}}{M_{\rm ej}^3}\right)^{\frac{1}{2}}t\right]^{-\frac{3}{2}}. \tag{2.42}$$

By defining two parameters a and b as

$$a = \frac{\varepsilon_k}{2}\frac{\dot{M}}{v_{\rm w}}\left(\frac{2E_{\rm ej}}{M_{\rm ej}}\right)^{\frac{3}{2}}, \tag{2.43}$$

$$b = 2\frac{\dot{M}}{v_{\rm w}}\left(\frac{2E_{\rm ej}}{M_{\rm ej}^3}\right)^{\frac{1}{2}}, \tag{2.44}$$

we can express L in a simple way. Namely,

$$L = 2^{-\frac{3(n-7)}{2(n-2)}}ab^{-\frac{3}{n-2}}\left(\frac{n-3}{n-2}\right)^3\frac{[2(5-\delta)(n-5)]^{\frac{3(n-3)}{2(n-2)}}}{[(n-4)(n-3)(n-\delta)]^{\frac{3}{n-2}}\,[(3-\delta)(n-3)]^{\frac{3(n-5)}{2(n-2)}}}t^{-\frac{3}{n-2}}, \tag{2.45}$$

before t_t and

$$L = a\,(1+bt)^{-\frac{3}{2}}, \tag{2.46}$$

long after t_t. Here, t_t is expressed as

$$t_t = \frac{4\left[(3-\delta)(n-3)\right]^{\frac{3}{2}}}{(n-4)(n-3)(n-\delta)\left[(5-\delta)(n-5)\right]^{\frac{1}{2}} b}. \tag{2.47}$$

The physical parameters of CSM and SN ejecta have the relations

$$E_{\rm ej} = \frac{2a}{\varepsilon_k b}, \tag{2.48}$$

$$\frac{\dot{M}}{v_{\rm w}} M_{\rm ej}^{-\frac{3}{2}} = \frac{1}{4}\left(\frac{\varepsilon_k b^3}{a}\right)^{\frac{1}{2}}. \tag{2.49}$$

In addition, for instance, if we express the shell velocity evolution at $t > t_t$ which can be estimated from spectral observations as

$$v_{\rm sh} = d(1+bt)^{-\frac{1}{2}}, \tag{2.50}$$

where

$$d = \frac{M_{\rm ej} b}{2}\frac{v_{\rm w}}{\dot{M}}, \tag{2.51}$$

we can obtain $M_{\rm ej}$ and $\dot{M}$ separately as

$$M_{\rm ej} = \frac{4a}{\varepsilon_k b d^2}, \tag{2.52}$$

$$\dot{M} = \frac{2a v_{\rm w}}{\varepsilon_k d^3}. \tag{2.53}$$

We will use the analytic bolometric LC model developed in this section in Chapter 3 to fit observed bolometric LCs. We will show that SN ejecta and CSM properties of SNe IIn can be constrained by the fitting.

2.4 Emission from SNe Interacting with Optically Thick Dense CSM

In the previous section, we consider the case in which the CSM is optically thin and the emission from the shocked shell is directly observed. This assumption breaks when the CSM is optically thick and photons emitted from the shocked region can be scattered and absorbed in the CSM. In principle, we need to treat the system numerically in such cases. However, when the CSM is so optically thick that the shock breakout occurs in it, we can analytically estimate some timescales which can be constrained observationally.

2.4.1 Shock Breakout

Shock breakout is a phenomenon which is predicted to be observed when a shock wave emerges from the surface of an exploding star. Before the shock wave approaches the surface of the star, the diffusion timescale of photons is much longer than the dynamical timescale of the shock wave because of the high optical depth of the stellar interior and

photons cannot go out of the shock wave. At the stellar surface, the optical depth above the shock wave suddenly becomes low enough for photons to diffuse out from the shock wave and photons start to travel away from the star. This sudden release of photons is predicted to be observed as a flash of X-rays or ultraviolet (UV) photons (e.g., Ohyama 1963, Colgate 1974, Klein & Chevalier 1978, Ensman & Burrows 1992, Blinnikov et al. 1998, Blinnikov et al. 2000, Matzner & McKee 1999, Calzavara & Matzner 2004, Nakar & Sari 2010, Tominaga et al. 2011) and it is actually observed for several times, e.g., XRO 080109/SN 2008D (e.g., Soderberg et al. 2008) and SNLS-04D2dc (Schawinski et al. 2008, Gezari et al. 2009).

2.4.1.1 Shock Breakout Condition in Dense CSM

If a CSM around a SN progenitor is dense and optically thick, the shock breakout signal is altered by the CSM. If the CSM is much denser, the shock breakout itself can take place in the CSM. In this section, we investigate the shock breakout in the dense CSM. As we will find, to explain the huge luminosities of SLSNe by the interaction between SN ejecta and dense CSM, the CSM must be so dense that we cannot neglect the effect of the shock breakout, as is first suggested by Chevalier & Irwin 2011. Also, the shock breakout in the dense CSM is related to many other astrophysical phenomena, e.g., PTF 09uj (Ofek et al. 2010), XRO 080109 (Balberg & Loeb 2011), and production of high energy particles (Murase et al. 2011, Katz et al. 2011).

Let us consider a spherically symmetric dense CSM extending from $r = R_i$ to $r = R_o$. The CSM density $\rho_{\rm csm}$ is assumed to follow $\rho_{\rm csm}(r) = Dr^{-s}$ with a constant D. The opacity $\kappa_{\rm csm}$ of the CSM is assumed to be constant and we only consider H-rich CSM in this section. Let us set the radius of the forward shock at the time of the shock breakout $r = xR_o$. We also introduce a radius $y_{\tau_{\rm csm}} R_o$ where the optical depth evaluated from the CSM surface becomes $\tau_{\rm csm}$, i.e.,

$$\tau_{\rm csm} = \int_{y_{\tau_{\rm csm}} R_o}^{Ro} \kappa_{\rm csm} \rho_{\rm csm} dr. \tag{2.54}$$

The shock breakout occurs when the diffusion timescale in the CSM and the timescale for the shock propagation get similar

$$\frac{c}{\tau_{\rm csm}} \simeq v_s, \tag{2.55}$$

(see, e.g., Weaver 1976, Nakar & Sari 2010 for the details of the shock breakout condition). In previous works, the shock breakout condition in a CSM had been simply defined to occur when the diffusion timescale of the *entire* CSM is comparable to the shock propagation timescale of the *entire* CSM, i.e.,

$$\int_{xR_o}^{R_o} \kappa_{\rm csm} \rho_{\rm csm} dr \simeq \frac{c}{v_s}. \tag{2.56}$$

However, the CSM can contain a large optically thin region even if the entire CSM is optically thick. Figure 2.2 is a simplified illustration of the effect of s in the dense CSM. Two dense CSM with the different s but the same R_o and xR_o are compared in the figure: (a) a CSM

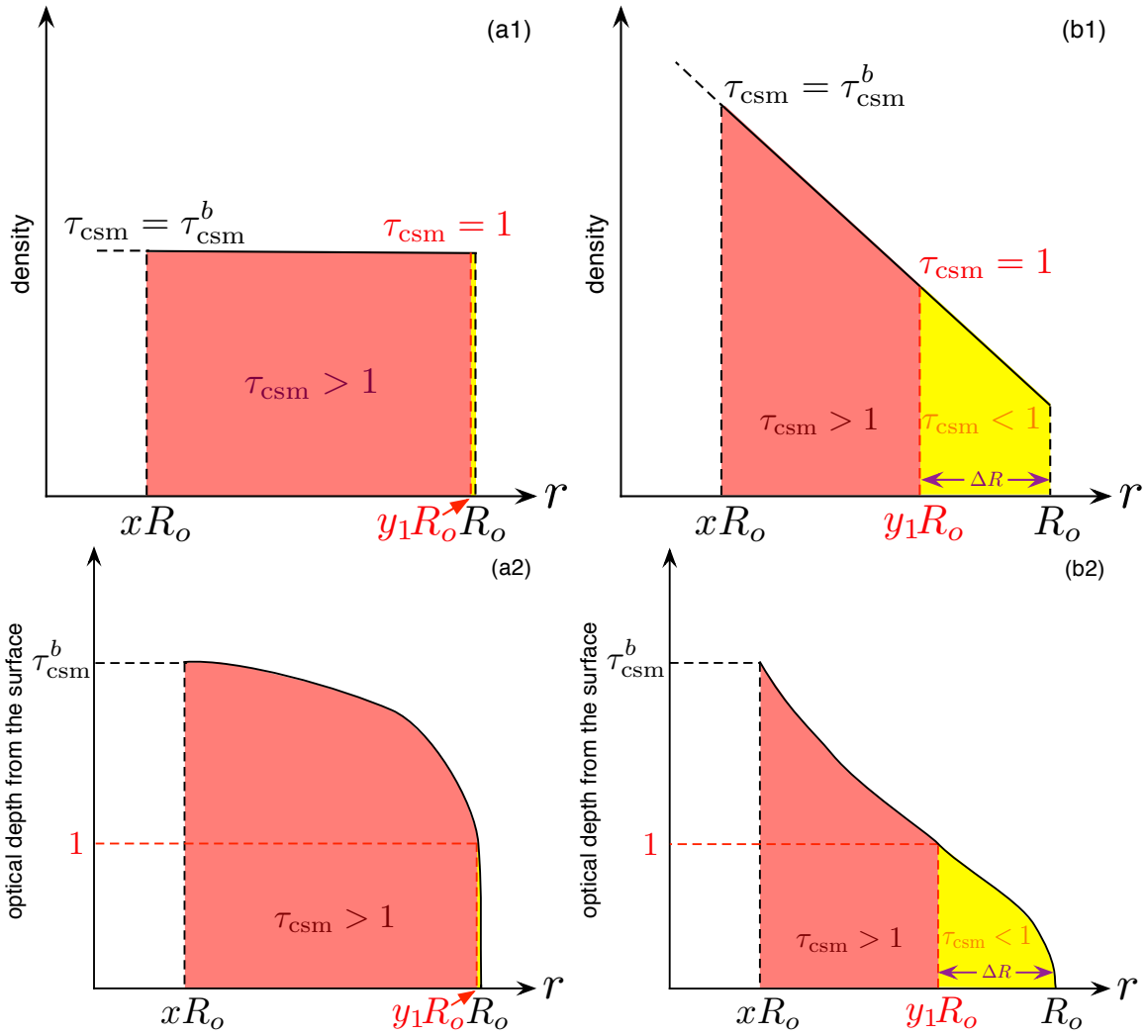

Figure 2.2: Illustration of the density and the optical depth distributions for the CSM with different density slopes: (a) a flat density slope and (b) a steep density slope. The corresponding (1) density structures and (2) optical depth distributions are shown. The shock breakout is assumed to occur at the same $r = xR_o$ with $x < 1$ where the opacity $\tau_{\rm csm}$ from R_o becomes $\tau^b_{\rm csm}$. All the opacities shown in the figure is evaluated from R_o. Large $\tau_{\rm csm} < 1$ region appears in the outer part of the CSM in (b).

with a constant density and (b) a CSM with a steep density gradient. In both cases, the shock breakout is assumed to occur in the CSM at the same radius $r = xR_o$ ($x < 1$) with the same forward shock velocity v_s and thus the optical depth between xR_o and R_o is exactly the same in both cases ($\tau^b_{\rm csm}$). One of the important differences in the two CSM are in the radius of the last scattering surface $y_1 R_o$, where $\tau_{\rm csm} = 1$ (see Figure 2.3 in the following for the value of y_1). Even if the entire CSM is optically thick in both cases, the region where $\tau_{\rm csm}$ becomes larger than 1 ($r < y_1 R_o$) is more concentrated to the central region and the CSM contains larger optically thin outside region whose size is $\Delta R = R_o - y_1 R_o$ in the case of large s.

If the CSM contains an extended optically thin region, Equation 2.56 is no longer an appropriate condition for the shock breakout because it postulates that the entire CSM at $r \leq R_o$ is optically thick enough for photons to be diffusive. The shock breakout condition should be evaluated only at the optically thick region where photons are diffusive. Hence, the shock breakout condition should be

$$\tau^x_{\rm csm} \equiv \int_{xR_o}^{y_1 R_o} \kappa_{\rm csm}\rho_{\rm csm} dr \simeq \frac{c}{v_s}, \tag{2.57}$$

where $\tau^x_{\rm csm} = \tau^b_{\rm csm} - 1$. In Equation 2.57, we presume that photons diffuse in the region where the optical depth evaluated from the CSM surface exceeds 1 for simplicity. In other words, photons are assumed to diffuse at $R_i < r < y_1 R_o$ and freely stream at $y_1 R_o < r < R_o$. In this sense, Equation 2.57 may also be interpreted as Equation 2.56 combined with a kind of flux limited diffusion approximation. For the case of the shock breakout at the surface of the CSM ($x \simeq 1$), the conditions of Equations 2.56 and 2.57 are similar.

In the following discussion, we assume that v_s is constant for simplicity. This assumption can be inappropriate if the shocked CSM mass becomes comparable to the SN ejecta mass. Equations 2.54 and 2.57 lead us to

$$D \simeq \begin{cases} \frac{(1-s)(1+c/v_s)}{\kappa_{\rm csm}(1-x^{1-s})R_o^{1-s}} & (s \neq 1), \\ \\ \frac{1+c/v_s}{\kappa_{\rm csm}(-\ln x)} & (s = 1). \end{cases} \tag{2.58}$$

In addition, using Equation 2.58, we can express $y_{\tau_{\rm csm}}$ as

$$y_{\tau_{\rm csm}} \simeq \begin{cases} \left(\frac{c/v_s + \tau_{\rm csm} x^{1-s}}{c/v_s + \tau_{\rm csm}}\right)^{\frac{1}{1-s}} & (s \neq 1), \\ \\ x^{\frac{\tau_{\rm csm}}{c/v_s + \tau_{\rm csm}}} & (s = 1). \end{cases} \tag{2.59}$$

Figure 2.3 shows a plot of y_1 as a function of x for several s. Larger s leads to smaller y_1 for a given x, as is discussed qualitatively above.

2.4.1.2 Timescales of Photon Diffusion and Shock Propagation in Dense CSM

Based on the shock breakout condition derived above, we estimate the timescale of photon diffusion (t_d) in the dense CSM after the shock breakout and the timescale of the shock propagation (t_s). t_d corresponds to the timescale for a SN LC to reach the peak after the shock

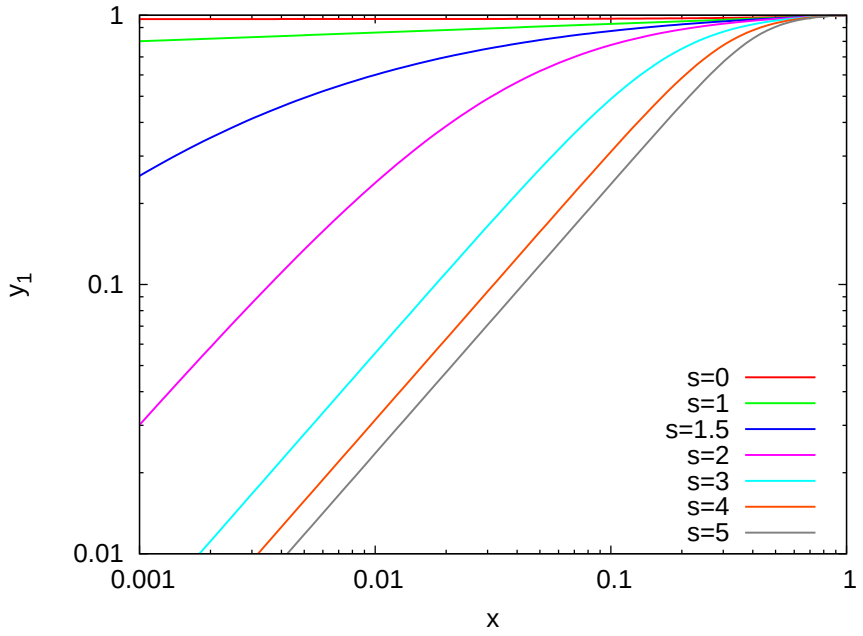

Figure 2.3: Location of the last scattering surface in CSM within which the shock breakout occurs. The region $r > y_1 R_o$ is optically thin and photons do not diffuse in the region.

breakout (e.g., Arnett 1980, Arnett 1982) and t_s represents the timescale for the forward shock to go through the entire CSM after the shock breakout. t_d can be expressed as

$$t_d \simeq \frac{\tau^x_{\rm csm}(R_o - xR_o - \Delta R)}{c}, \tag{2.60}$$

$$= \frac{\tau^x_{\rm csm}(y_1 R_o - xR_o)}{c}, \tag{2.61}$$

$$= \begin{cases} \frac{R_o}{v_s}\left[\left(\frac{c/v_s + x^{1-s}}{c/v_s+1}\right)^{\frac{1}{1-s}} - x\right] & (s \neq 1), \\ \frac{R_o}{v_s}\left(x^{\frac{1}{1+c/v_s}} - x\right) & (s = 1). \end{cases} \tag{2.62}$$

t_s is defined as the time required for the forward shock to go through the entire CSM including the optically thin region after the shock breakout,

$$t_s = \frac{R_o - xR_o}{v_s}. \tag{2.63}$$

Hence, we can derive the ratio of the two timescales as

$$\frac{t_d}{t_s} \simeq \begin{cases} \frac{1}{1-x}\left[\left(\frac{c/v_s + x^{1-s}}{c/v_s+1}\right)^{\frac{1}{1-s}} - x\right] & (s \neq 1), \\ \frac{1}{1-x}\left(x^{\frac{1}{1+c/v_s}} - x\right) & (s = 1). \end{cases} \tag{2.64}$$

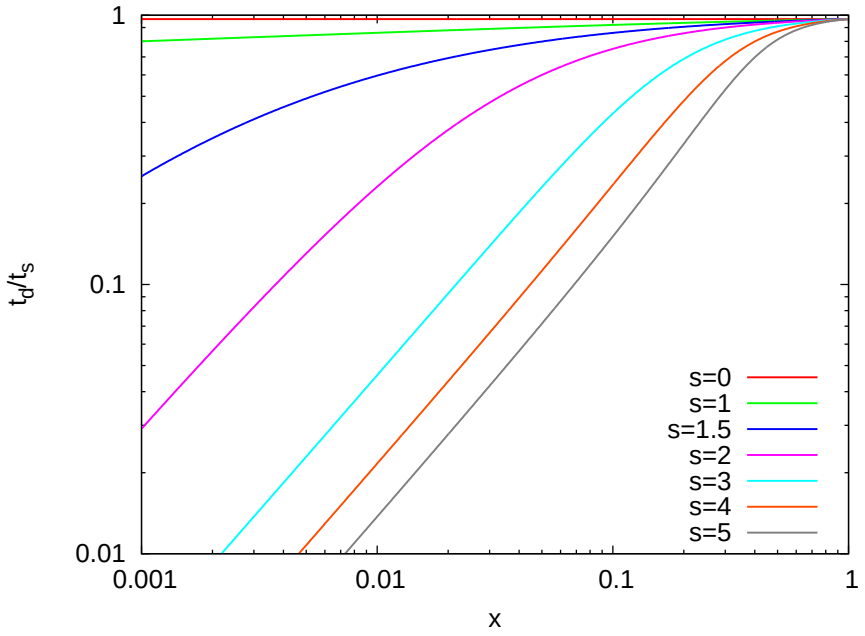

Figure 2.4: Ratio of the diffusion timescale (t_d) and the shock propagation timescale (t_s) as a function of the location of the shock breakout (x).

Figure 2.4 shows the ratio as a function of x for several s, in which v_s is set to a typical value for SNe ($10,000$ km s^{-1}). Every line reaches $t_d/t_s \simeq c/\left(v_s + c\right) = 0.97$ at $x \simeq 1$. In this case, the shock breakout occurs at the surface of the CSM. When the shock breakout occurs inside the CSM ($x < 1$), the ratio t_d/t_s varies depending on the density slope of the CSM. For a given x, t_d/t_s gets smaller as the density slope of the CSM gets steeper (i.e., larger s). This is because the last scattering surface of the CSM locates farther away from the surface as the density slope gets steeper, i.e., y_1 gets smaller as s gets larger for a given x (see Figure 2.3 for values of y_1). In other words, the optically thin region in the CSM is spatially larger for the CSM with steeper density gradient. Note that when the shock breakout occurs in the CSM, the forward shock reaches the last scattering surface ($r = y_1 R_o$) with the diffusion timescale t_d, i.e., the shock locates at $r \simeq y_1 R_o$ at the LC peak.

The difference in the ratio of the two timescales which is determined by the CSM density slope can explain the existence of the two spectral types in SLSN II. We discuss this in Chapter 4 in detail.

2.5 Radiation Hydrodynamics

In the previous section, we only considered the special case that the dense CSM is optically thick enough to cause the shock breakout. We find that we can derive two timescales analytically in this case. However, for the detail modeling of SN LCs powered by the interaction, especially in the case of the optically thick CSM for which we cannot use the analytic solution derived in Section 2.3, we need to rely on the numerical apporach. We need to take account

of not only hydrodynamical variables but also radiation numerically at the same time because the source of photons is kinetic energy in the system we consider. Radiation hydrodynamics, therefore, is essential for modeling SN LCs powered by the interaction. In this section, we briefly summarize the basics of radiation hydrodynamics and how to treat it numerically. We focus on a numerical one-dimensional multigroup radiation hydrodynamics code `STELLA` which is mainly used in this dissertation.

2.5.1 Basic Equations

2.5.1.1 Equations of Hydrodynamics

First of all, we briefly summarize the equations of hydrodynamics. As is shown below, the equations of hydrodynamics, i.e., the Euler equations, are derived from the Boltzmann transport equation by taking the velocity moments of a distribution function. Ideally, the evolution of hydrodynamical quantities are better to be obtained by solving the Boltzmann equation but, practically, it takes literally forever with the current available computational resources and we need to treat it in a simplified way, i.e., by using the Euler equations. The Boltzmann transport equation

$$\frac{\partial}{\partial t}f(\boldsymbol{x},\boldsymbol{\xi},t)+\xi_i\frac{\partial}{\partial x_i}f(\boldsymbol{x},\boldsymbol{\xi},t)+\frac{\partial}{\partial \xi_i}\mathcal{F}_i(\boldsymbol{x},\boldsymbol{\xi},t)f(\boldsymbol{x},\boldsymbol{\xi},t)=C(f) \tag{2.65}$$

describes the evolution of the non-relativistic particle distribution function in the phase space. Here, $\boldsymbol{x}$ is a position of a particle, $\boldsymbol{\xi}$ is its velocity, $f(\boldsymbol{x},\boldsymbol{\xi},t)$ is a distribution function of particles (number density in the phase space), $\mathcal{F}(\boldsymbol{x},\boldsymbol{\xi},t)$ is a specific external force, and $C(f)$ is a collision integral. Multiplying the Boltzmann transport equation by an arbitrary function $\psi(\boldsymbol{x},\boldsymbol{\xi},t)$ and taking the integral of the velocity component $\boldsymbol{\xi}$ lead us to the following equation

$$\frac{\partial}{\partial t}\int\psi f d\boldsymbol{\xi}+\frac{\partial}{\partial x_i}\int\psi\xi_i f d\boldsymbol{\xi}-\int\left[\frac{\partial\psi}{\partial t}+\xi_i\frac{\partial\psi}{\partial x_i}+\mathcal{F}_i\frac{\partial\psi}{\partial\xi_i}\right]f d\boldsymbol{\xi}=\int\psi C d\boldsymbol{\xi}. \tag{2.66}$$

Let m the mass of a particle. The zeroth, the first, and the second $\boldsymbol{\xi}$ moments of $mf(\boldsymbol{x},\boldsymbol{\xi},t)$ correspond to macroscopic thermodynamical variables we are interested in, i.e., mass density $\rho(\boldsymbol{x},t)$, momentum density $\rho v_i(\boldsymbol{x},t)$, and energy density $\rho u(\boldsymbol{x},t)$, respectively:

$$\rho(\boldsymbol{x},t) = \int mf(\boldsymbol{x},\boldsymbol{\xi},t)d\boldsymbol{\xi}, \tag{2.67}$$

$$\rho v_i(\boldsymbol{x},t) = \int m\xi_i f(\boldsymbol{x},\boldsymbol{\xi},t)d\boldsymbol{\xi}, \tag{2.68}$$

$$\rho u(\boldsymbol{x},t) = \frac{1}{2}\int m\boldsymbol{\xi}^2 f(\boldsymbol{x},\boldsymbol{\xi},t)d\boldsymbol{\xi}. \tag{2.69}$$

We also introduce the moments of $mf(\boldsymbol{x},\boldsymbol{\xi},t)$ taken by a peculiar velocity $\Xi_i=\xi_i-v_i$:

$$p_{ij}(\boldsymbol{x},t) = \int m\Xi_i\Xi_j f(\boldsymbol{x},\boldsymbol{\xi},t)d\boldsymbol{\xi}=\frac{1}{3}p(\boldsymbol{x},t)\delta_{ij}, \tag{2.70}$$

$$\rho\varepsilon(\boldsymbol{x},t) = \frac{1}{2}\int m\boldsymbol{\Xi}^2 f(\boldsymbol{x},\boldsymbol{\xi},t)d\boldsymbol{\xi}, \tag{2.71}$$

$$q_i(\boldsymbol{x},t) = \frac{1}{2}\int m\Xi_i\boldsymbol{\Xi}^2 f(\boldsymbol{x},\boldsymbol{\xi},t)d\boldsymbol{\xi}, \tag{2.72}$$

where $p(\boldsymbol{x},t)$ is gas pressure and δ_{ij} is the Kronecker's delta. $p_{ij}(\boldsymbol{x},t)$ and $q_i(\boldsymbol{x},t)$ are called a pressure tensor and a heat flux, respectively. $\rho\varepsilon(\boldsymbol{x},t)$ is internal energy density. We assume that $q_i(\boldsymbol{x},t)$ is known in the system. Note that the zeroth $\boldsymbol{\Xi}$ moment of $mf(\boldsymbol{x},\boldsymbol{\xi},t)$ is $\rho(\boldsymbol{x},t)$ and the first moment is 0.

The Euler equations are obtained by setting $\psi(\boldsymbol{x},\boldsymbol{\xi},t)$ in Equation 2.66 as $m, m\xi_i$, and $m\boldsymbol{\xi}^2/2$,

$$\frac{\partial}{\partial t}\rho + \frac{\partial}{\partial x_i}\rho v_i = 0, \tag{2.73}$$

$$\frac{\partial}{\partial t}\rho v_i + \frac{\partial}{\partial x_j}\left(\rho v_i v_j + p_{ij}\right) = \rho\mathcal{F}_i, \tag{2.74}$$

$$\frac{\partial}{\partial t}\rho u + \frac{\partial}{\partial x_i}\left(\rho u v_i + p_{ij} v_j\right) = \rho\mathcal{F}_i v_i - \frac{\partial q_i}{\partial x_i}. \tag{2.75}$$

Note that the total energy of the gas ρu is the sum of its kinetic energy density $\rho\boldsymbol{v}^2/2$ and its internal energy density $\rho\varepsilon$,

$$\rho u = \frac{1}{2}\rho\boldsymbol{v}^2 + \rho\varepsilon. \tag{2.76}$$

The Euler equations (Equations 2.73, 2.74, and 2.75) are still not closed. However, in the case of hydrodynamics, we have an equation which relates the second peculiar velocity moments of $f(\boldsymbol{x},\boldsymbol{\xi},t)$ (i.e., $\varepsilon(\boldsymbol{x},t)$ and $p(\boldsymbol{x},t)$) and the zeroth peculiar velocity moments of $f(\boldsymbol{x},\boldsymbol{\xi},t)$ (i.e., $\rho(\boldsymbol{x},t)$) which is called an *equation of state*,

$$p(\boldsymbol{x},t) = p(\varepsilon,\rho). \tag{2.77}$$

Given an *equation of state*, the equations of hydrodynamics are closed and become able to be solved with a certain initial condition.

2.5.1.2 Equations of Radiation

The equations followed by radiation can be derived by using a similar way as we used to derive the Euler equations. The equation for radiation which corresponds to the Boltzmann transport equation in the case of hydrodynamics is the radiative transfer equation

$$\frac{1}{c}\frac{\partial}{\partial t}I_\nu(\boldsymbol{x},\hat{\boldsymbol{k}},t) + \hat{k_i}\frac{\partial}{\partial x_i}I_\nu(\boldsymbol{x},\hat{\boldsymbol{k}},t) = j_\nu(\boldsymbol{x},\hat{\boldsymbol{k}},t) - \kappa_\nu(\boldsymbol{x},t)I_\nu(\boldsymbol{x},\hat{\boldsymbol{k}},t), \tag{2.78}$$

where c is the speed of light, $\hat{\boldsymbol{k}}$ is a normalized wave vector $\boldsymbol{k}$, ν is a frequency, $I_\nu(\boldsymbol{x},\hat{\boldsymbol{k}},t)$ is an intensiy of radiation, $j_\nu(\boldsymbol{x},\hat{\boldsymbol{k}},t)$ is an emissivity, and $\kappa_\nu(\boldsymbol{x},t)$ is total opacity. Just looking at the radiative transfer equation, it seems that the equation is for I_ν, not for a number distribution function $g(\boldsymbol{x},\boldsymbol{p},t)$[1] of photons in the phase space (where $\boldsymbol{p} = h\boldsymbol{k}/2\pi$ is a momentum of a photon) and that the radiative transfer equation does not correspond to the Boltzmann transport equation. However, as an intensity I_ν can be expressed as

$$I_\nu(\boldsymbol{x},\hat{\boldsymbol{k}},t) = \frac{2h^4\nu^3}{c^2}g(\boldsymbol{x},\boldsymbol{p},t), \tag{2.79}$$

[1] $g(\boldsymbol{x},\boldsymbol{p},t)$ is a number distribution function for one spin state. We assume that every spin state is equally occupied and the exact number density of photons is $2g(\boldsymbol{x},\boldsymbol{p},t)$ as a photon have two spin states.

I_ν can be regarded as a number distribution function and the radiative transfer equation actually corresponds to the Boltzmann transport equation. This means that conservation laws for radiation which correspond to the Euler equations of hydrodynamics can be found by using the $\hat{\boldsymbol{k}}$ moments of the intensity I_ν. We also define a photon occupation number $\mathcal{N}_\nu(\boldsymbol{x}, \hat{\boldsymbol{k}}, t)$ which is used in the following section,

$$\mathcal{N}_\nu(\boldsymbol{x}, \hat{\boldsymbol{k}}, t) = h^3 g(\boldsymbol{x}, \boldsymbol{p}, t). \tag{2.80}$$

The zeroth, the first, and the second $\hat{\boldsymbol{k}}$ moments of I_ν are

$$E_\nu(\boldsymbol{x}, t) = \frac{1}{c}\int I_\nu(\boldsymbol{x}, \hat{\boldsymbol{k}}, t) d\Omega, \tag{2.81}$$

$$F_{\nu,i}(\boldsymbol{x}, t) = \int \hat{k_i} I_\nu(\boldsymbol{x}, \hat{\boldsymbol{k}}, t) d\Omega, \tag{2.82}$$

$$P_{\nu,ij}(\boldsymbol{x}, t) = \frac{1}{c}\int \hat{k_i}\hat{k_j} I_\nu(\boldsymbol{x}, \hat{\boldsymbol{k}}, t) d\Omega, \tag{2.83}$$

respectively. Following the similar way to hydrodynamics, we get the conservation laws for radiation,

$$\frac{\partial}{\partial t}E_\nu + \frac{\partial}{\partial x_i}F_{\nu,i} = 4\pi j_\nu - \kappa_\nu c E_\nu, \tag{2.84}$$

$$\frac{1}{c}\frac{\partial}{\partial t}F_{\nu,i} + c\frac{\partial}{\partial x_j}P_{\nu,ij} = -\kappa_\nu F_{\nu,i}. \tag{2.85}$$

As was the case for hydrodynamics, the conservation equations (Equations 2.84 and 2.85) are not closed. The Euler equations are closed by introducing an *equation of state* but there is no corresponding equation for radiation. There are several ways to close the equations for radiation. The simplest way is to treat radiation always diffusive and introduce a flux limiter so that photons do not exceed the speed of light. The equations can also be closed in the first moment equation by introducing the so-called M_1 closer condition. A more precise scheme is to close the equations by introducing the variable Eddington tensor. This method is called the variable Eddington factor method. To close the conservation equations, we assume that there is a relation held by the zeroth and the second $\hat{\boldsymbol{k}}$ moments (E_ν and $P_{\nu,ij}$), as was the case for hydrodynamics,

$$P_{\nu.ij} = f_{\nu,ij} E_\nu, \tag{2.86}$$

where $\mathbf{f}(\boldsymbol{x}, t)$ is the *Eddington tensor*. Equation 2.86 corresponds to an *equation of state* in the case of hydrodynamics[2]. Thus, introducing the *Eddington tensor* for radiation is equivalent to introduce an *equation of state* for radiation. Now, the conservation equations for radiation are closed and the evolution of radiational variables can be evaluated.

2.5.1.3 Equations of Radiation Hydrodynamics

Radiation hydrodynamics treats hydrodynamics and radiation at the same time. The conservation equations for hydrodynamics and radiation are solved at the same time. Taking

[2] An *equation of state* does not include tensors because gas pressure is assumed to be homogenious.

account of the source terms due to the interaction of hydrodynamical particles and radiation, the conservation equations and the equation of state for hydrodynamical variables are expressed as follows.

$$\frac{\partial}{\partial t}\rho + \frac{\partial}{\partial x_i}\rho v_i = 0, \tag{2.87}$$

$$\frac{\partial}{\partial t}\rho v_i + \frac{\partial}{\partial x_j}\left(\rho v_i v_j + p_{ij}\right) = \rho\mathcal{F}_i + \frac{1}{c}\int \kappa_\nu F_{\nu,i} d\nu, \tag{2.88}$$

$$\frac{\partial}{\partial t}\rho u + \frac{\partial}{\partial x_i}\left(\rho u v_i + p_{ij} v_j\right) = \rho\mathcal{F}_i v_i - \frac{\partial q_i}{\partial x_i} + \int \left(-4\pi j_\nu + \kappa_\nu c E_\nu\right) d\nu, \tag{2.89}$$

$$p(\boldsymbol{x}, t) = p(\varepsilon, \rho). \tag{2.90}$$

To solve the conservation equations of radiation in a moving fluid, there are two different ways to treat them. One is to stay in a fixed frame of reference to describe the radiational variables and the other is to use a comoving frame. We choose the latter frame, a comoving frame, to treat radiation. This approach makes the equations rather complicated but we do not need to introduce complicated absorption and emission coefficients. Here, we omit the derivation of the conservation equations of radiation in a comoving frame. The detailed derivation of them can be found in, e.g., Castor 2004, Mihalas & Mihalas 1999. Following the work of Buchler 1983, we use the approximated conservation equations of radiation in a comoving frame which is valid up to $\mathcal{O}(v/c)$,

$$\frac{\partial}{\partial t}E_\nu + \frac{\partial}{\partial x_i}v_i E_\nu + \frac{\partial}{\partial x_i}F_{\nu,i} + \left(P_{\nu,ij} - \frac{\partial}{\partial \nu}\nu P_{\nu,ij}\right)\frac{\partial v_j}{\partial x_i} = 4\pi j_\nu - \kappa_\nu c E_\nu, \tag{2.91}$$

$$\frac{1}{c}\frac{\partial}{\partial t}F_{\nu,i} + \frac{1}{c}\left(v_i\frac{\partial F_{\nu,j}}{\partial x_j} + F_{\nu,i}\frac{\partial v_j}{\partial x_j}\right) + c\frac{\partial}{\partial x_j}P_{\nu,ij} = -\kappa_\nu F_{\nu,i}. \tag{2.92}$$

We close the equations by using the Eddington tensor $\boldsymbol{f}$ defined as

$$f_{\nu,ij} = \frac{P_{\nu.ij}}{E_\nu}, \tag{2.93}$$

which is estimated by using the radiative transfer equation.

2.5.2 One-Dimensional Numerical Radiation Hydrodynamics

In this section, we discuss how to numerically treat the equations of radiation hydrodynamics introduced in Section 2.5.1 in one dimension using the spherical coordinates. We focus on a one-dimensional multigroup radiation hydrodynamics code `STELLA` which is used in this dissertation. `STELLA` has been used in modeling SNe and details can also be found in, e.g., Blinnikov & Bartunov 1993, Blinnikov et al. 1998, Blinnikov et al. 2000, Blinnikov et al. 2006, Blinnikov & Tolstov 2011.

2.5.2.1 Equations of Radiation Hydrodynamics in One Dimension

When we assume the spherical symmetry in a system and take only the r coordinate in space, each photon moves in two dimensions in the phase space. We define $\mu = \cos\theta$, which expresses the direction of the photon transport as is shown in Figure 2.5, to describe photons

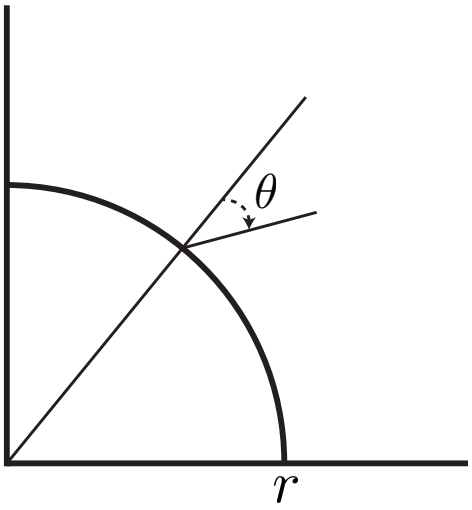

Figure 2.5: $(r, \mu = \cos\theta)$ coordinate used in one-dimensional radiation hydrodynamics.

in the phase space. Lagrangian coordinates are adopted in STELLA. The intensity $I_\nu(r, \mu, t)$ is expressed as

$$I_\nu(r, \mu, t) = \frac{2h^4\nu^3}{c^2} g\,(r, p, t) = \frac{2h\nu^3}{c^2}\mathcal{N}_\nu(r, \mu, t). \tag{2.94}$$

In STELLA, we use the angular moments of $\mathcal{N}_\nu$, instead of I_ν, to describe the conservation laws for radiation,

$$\mathcal{J}_\nu\,(r) = \frac{1}{2}\int_{-1}^{1} \mathcal{N}_\nu d\mu, \tag{2.95}$$

$$\mathcal{H}_\nu\,(r) = \frac{1}{2}\int_{-1}^{1} \mu\mathcal{N}_\nu d\mu, \tag{2.96}$$

$$\mathcal{K}_\nu\,(r) = \frac{1}{2}\int_{-1}^{1} \mu^2\mathcal{N}_\nu d\mu. \tag{2.97}$$

The derivations of the conservation equations for $\mathcal{J}_\nu$, $\mathcal{H}_\nu$, $\mathcal{K}_\nu$ in the comoving frame which corresponds to Equations 2.91 and 2.92 can be found in, e.g., Castor 1972. The results are

$$\begin{aligned}\frac{\partial}{\partial t}\mathcal{J}_\nu &= -\frac{c}{r^2}\frac{\partial}{\partial r}r^2\mathcal{H}_\nu + c\left(\kappa^s_\nu\rho\mathcal{B}_\nu - \kappa^a_\nu\rho\mathcal{J}_\nu\right) \\ &\quad + \frac{v}{r}\left(3\mathcal{K}_\nu - \mathcal{J}_\nu\right) - \frac{1}{r^2}\frac{\partial}{\partial r}\left[r^2 v\left(\mathcal{J}_\nu + \mathcal{K}_\nu\right)\right] \\ &\quad - \frac{1}{\nu^3}\frac{\partial}{\partial \nu}\left[\frac{\nu^4 v}{r}\left(3\mathcal{K}_\nu - \mathcal{J}_\nu\right) - \frac{\nu^4}{r^2}\frac{\partial}{\partial r}r^2 v\mathcal{K}_\nu\right],\end{aligned} \tag{2.98}$$

$$\begin{aligned}\frac{\partial}{\partial t}\mathcal{H}_\nu &= -c\frac{\partial}{\partial r}\mathcal{K}_\nu - \frac{c}{r}\left(3\mathcal{K}_\nu - \mathcal{J}_\nu\right) \\ &\quad - 2\left(\frac{v}{r} + \frac{\partial v}{\partial r}\right)\mathcal{H}_\nu - c\left(\kappa^a_\nu + \kappa^s_\nu\right)\rho\mathcal{H}_\nu + \dot{\mathcal{H}}_{\nu\mathrm{diff}},\end{aligned} \tag{2.99}$$

where

$$\mathcal{B}_\nu\,(T) = \frac{1}{\exp\left(h\nu/k_B T\right) - 1}, \tag{2.100}$$

T is a material temperature, k_B is the Boltzmann constant, κ^a_ν is an absorptive opacity, κ^s_ν is a scattering opacity, and $\dot{\mathcal{H}}_{\nu\mathrm{diff}}$ is an artificial diffusion to stabilize the equation which is described in Blinnikov et al. 1998. Note that $\mathcal{B}_\nu$ is a photon occupation number for the black body radiation $B_\nu(T)$ and the same as that of the Bose-Einstein distribution;

$$B_\nu(T) = \frac{2h\nu^3}{c^2}\mathcal{B}_\nu(T). \tag{2.101}$$

The equations of hydrodynamics in the one-dimensional Lagrangian coordinate are

$$\frac{\partial r}{\partial t} = v, \tag{2.102}$$

$$\frac{\partial v}{\partial t} = -4\pi r^2 \frac{\partial}{\partial m}(p+q) - \frac{Gm}{r^2} + \frac{4\pi}{c}\int (\kappa^a_\nu + \kappa^s_\nu)\frac{2h\nu^3}{c^2}\mathcal{H}_\nu d\nu + a_{\mathrm{mix}}, \tag{2.103}$$

$$\frac{\partial r}{\partial m} = \frac{1}{4\pi r^2 \rho}, \tag{2.104}$$

$$\left(\frac{\partial \varepsilon}{\partial T}\right)_\rho \frac{\partial T}{\partial t} = \phi + 4\pi\int \kappa^a_\nu \frac{2h\nu^3}{c^2}(\mathcal{J}_\nu - \mathcal{B}_\nu)\,d\nu - 4\pi\frac{\partial r^2 v}{\partial m}\left[T\left(\frac{\partial p}{\partial T}\right)_\rho + q\right], \tag{2.105}$$

where m is the mass coordinate, G is the gravitational constant, q is standard von Neumann artificial viscous pressure (von Neumann & Richtmyer 1950), ϕ is the local specific heating ($\phi > 0$) or cooling ($\phi < 0$), and a_{mix} is a term used to smear thin dense layers whose definition is provided in Blinnikov et al. 1998. We discuss the smearing in Section 2.5.2.3 as well.

In addition to the equations listed above, we add the equation of state $p = p(\rho, T)$ and $\varepsilon = \varepsilon(\rho, T)$ and the Eddington factor[3] $f_E(r,\nu) = \mathcal{K}_\nu/\mathcal{J}_\nu$. Although we assume the equation of state based on the properties of fluid we consider, the Eddington factor is derived by solving the time-independent radiative transfer equation (the variable Eddington factor method, Section 2.5.2.2). In `STELLA`, both hydrodynamics and radiation are solved implicitly.

2.5.2.2 Solving the Radiative Transfer Equation

The Eddington factor f_E which is required to close the equations of radiation hydrodynamics with the variable Eddington factor method is estimated by solving the time-independent radiative transfer equation. There are several ways to treat the radiative transfer equation. In `STELLA`, we introduce impact parameters and apply the Feautrier's method (Feautrier 1964) to solve the radiative transfer equation at every ray marked by the impact parameters.

Information we need to derive the Eddington factor $f_E(r) = \mathcal{K}_\nu(r)/\mathcal{J}_\nu(r)$ is the angular behavior of the radiation field at each r. In one-dimensional radiation hydrodynamics, we set a new coordinate system (p, z) to solve the radiative transfer equation, instead of (r, μ). Figure 2.6 shows the relation between (r, μ) and (p, z). p_i, traditionally called impact parameters, are chosen to be tangent to every radial shell r_i. z_{ij} are taken at all the intersection of p and r. We also add some p_i under the inner most radial mesh where we call a core. This is because the resolution for θ in (p, z) mesh become cruder at smaller r, since the number of intersections between r and p become smaller with smaller r (Figure 2.7). To get a sufficient angular resolution at the small r, we need to add some extra impact parameters in the core.

[3] The Eddington tensor is a factor in one dimension.

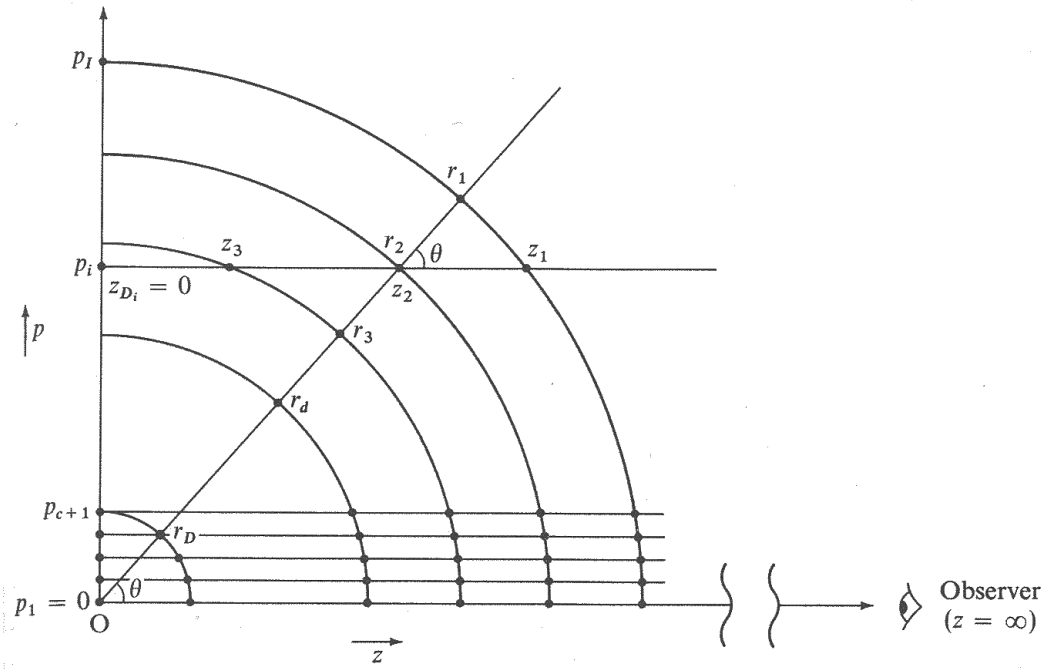

Figure 2.6: Relation between (p, z) and (r, θ). The number of the impact parameters in the core is defined as c. This figure is from Mihalas 1978.

There are one-to-one correspondence between (p, z) and (r, μ), i.e.,

$$r_i = p_{i+c}, \tag{2.106}$$

$$\mu_{ij} = \mu\,(p_{i+c}, r_j) = \frac{\sqrt{r_j^2 - p_{i+c}^2}}{r_j} = \frac{z_{i+c\ j}}{r_j}, \tag{2.107}$$

where c is the number of the impact parameters in the core. Hence, once we get $I_\nu(p_i, z_{ij})$, it can be converted to $I_\nu(r_i, \mu_{ij})$ which is required to obtain the Eddington factor.

$I_\nu(p_i, z_{ij})$ can be obtained by adopting the Feautrier's method at each ray labeled by the impact parameters. Note that the reason why we can use this approach is exactly in our assumption of the spherical symmetry. The solution obtained by tracing the ray cannot easily be converted to the angular information without the spherical symmetry. At each ray specified by p_i, the time-independent radiative transfer equations along the ray are

$$\frac{\partial}{\partial z} I_\nu^+(p_i, z_{ij}) = j_\nu(r) - \kappa_\nu(r) I_\nu^+(p_i, z_{ij}), \tag{2.108}$$

$$-\frac{\partial}{\partial z} I_\nu^-(p_i, z_{ij}) = j_\nu(r) - \kappa_\nu(r) I_\nu^-(p_i, z_{ij}), \tag{2.109}$$

where $I_\nu^+(p_i, z_{ij})$ and $I_\nu^-(p_i, z_{ij})$ are the radiation toward and away from the observer at $z = \infty$, respectively. Note that j_ν is assumed to be isotropic and $\kappa_\nu = \kappa_\nu^a + \kappa_\nu^s$.

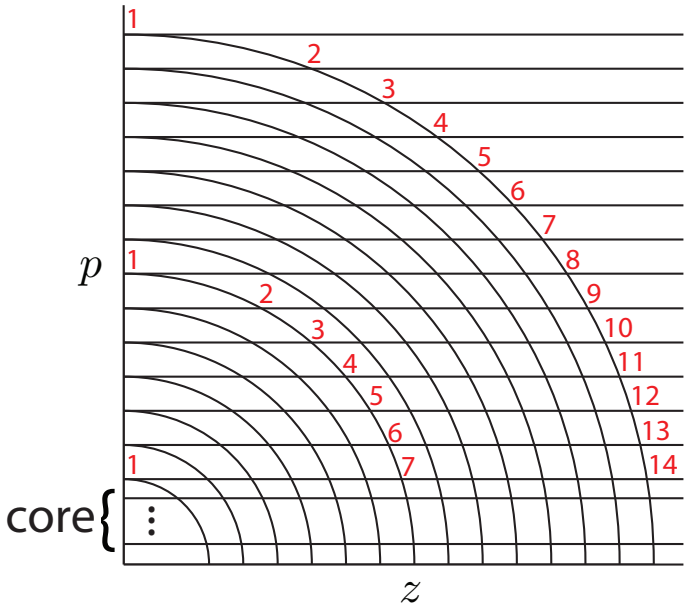

Figure 2.7: (p, z) mesh used to solve the radiative transfer equation in one-dimensional radiation hydrodynamics. For some radii, the number of the intersection between p and r are shown. Without the impact parameters in the core, we cannot get a sufficient angular resolution at small r.

Now, we define Ψ_ν and Φ_ν as

$$\Psi_\nu(p_i, z_{ij}) = \frac{1}{2}\left[I_\nu^+(p_i, z_{ij}) + I_\nu^-(p_i, z_{ij})\right], \tag{2.110}$$

$$\Phi_\nu(p_i, z_{ij}) = \frac{1}{2}\left[I_\nu^+(p_i, z_{ij}) - I_\nu^-(p_i, z_{ij})\right]. \tag{2.111}$$

We also define the optical depth along the ray as $d\tau_\nu(p_i, z_{ij}) = -\kappa_\nu(p_i, z_{ij})dz$. Then, the time-independent radiative transfer equations (Equations 2.108 and 2.109) become

$$\frac{\partial \Psi_\nu}{\partial \tau_\nu} = \Phi_\nu, \tag{2.112}$$

$$\frac{\partial \Phi_\nu}{\partial \tau_\nu} = \Psi_\nu - S_\nu, \tag{2.113}$$

where $S_\nu(p_i, z_{ij}) = j_\nu(r)/\kappa_\nu(r)$ is a source function. Equations 2.112 and 2.113 lead

$$\frac{\partial^2 \Psi_\nu}{\partial \tau_\nu^2} = \Psi_\nu - S_\nu, \tag{2.114}$$

which can be solved numerically at each ray. Given the solution, we can calculate the Eddington factor f_E. In `STELLA`, the Eddington factor is evaluated every 50 time steps, assuming that there is no dramatic change in radiation field in 50 time steps. This assumption is found to be valid based on our experiences.

2.5.2.3 Smearing

The interaction of SN ejecta and dense CSM results in a dense cool shell between the SN ejecta and the dense CSM. This is because of the radiative cooling of the shocked region. The shocked region becomes very dense and cools down efficiently by radiation. The cooling prevents the pressure from growing sufficiently enough to sustain the shell. Hence, the shell becomes thinner and denser and the cooling becomes more efficient. Thus, this cooling process is catastrophic. However, in reality, such a shell is unstable because of several instabilities like the Rayleigh-Taylor instability which require multidimensional calculations to treat (e.g., Chevalier & Blondin 1995). The multidimensional effect smears the shell and less kinetic energy is converted to radiation energy. In other words, the cooling by radiation is less efficient in three dimensions than in one dimension. In `STELLA` code, we take such multidimensional effects into account by introducing a smearing term in the equation of motion (Equation 2.103) so that the conversion efficiency from kinetic energy to radiation energy can be reduced (Blinnikov et al. 1998). This term is similar to artificial viscosity, although the smearing term has the opposite effect.

As is shown in Blinnikov et al. 1998, the smearing term is defined such that the total energy is manifestly conserved. Only the neighbouring zones are affected by the smearing term. The overall normalization factor $R_{\rm cut}(\tau)$ of the smearing is expressed as

$$R_{\rm cut}(\tau) = B_q f(\tau). \tag{2.115}$$

See Blinnikov et al. 1998 for the definitions of $R_{\rm cut}(\tau)$ and the smearing term. $f(\tau)$ is introduced so that the artificial smearing is reduced at optically thick regions where the effect of cooling is less efficient and the multidimensional instabilities due to the cooling grow less (e.g., Jiang et al. 2013). In `STELLA` code, $f(\tau)$ is an empirically obtained monotonically decreasing function which satisfies $f(\tau \to 0) = 1$. B_q determines the overall strength of the smearing effect. B_q is a parameter similar to ε_k we introduced in Section 2.3 during the analytical LC modeling. Ideally, B_q should be calibrated by comparing results obtained by our one-dimensional calculations to those of multidimensional calculations in which the effect of multidimensional instabilities in the shell is taken into account. However, such a multidimensional radiation hydrodynamical code with which we can compare our results is not available yet. We use $B_q = 1$ as our standard value. We also show the effect of B_q on model LCs (Section 4.3.3.2). The results of LC calculations of the interacting SNe strongly depend on B_q, as the smearing term directly affects the conversion efficiency from kinetic energy to radiation. We need a multidimensional radiation hydrodynamics code for the calibration of the parameter B_q.

2.5.2.4 Input Physics

Equation of State

The equation of state used in `STELLA` takes into account of ideal gas, electrons, degeneracy of electrons, and pressure ionization. The ionization level is derived by solving the Saha equation assuming the local thermodynamic equilibrium. The most abundant 15 elements are included in the equation of state, namely, H, He, C, O, Ne, Mg, Si, S, Ar, Ca, Ti, Cr, Fe,

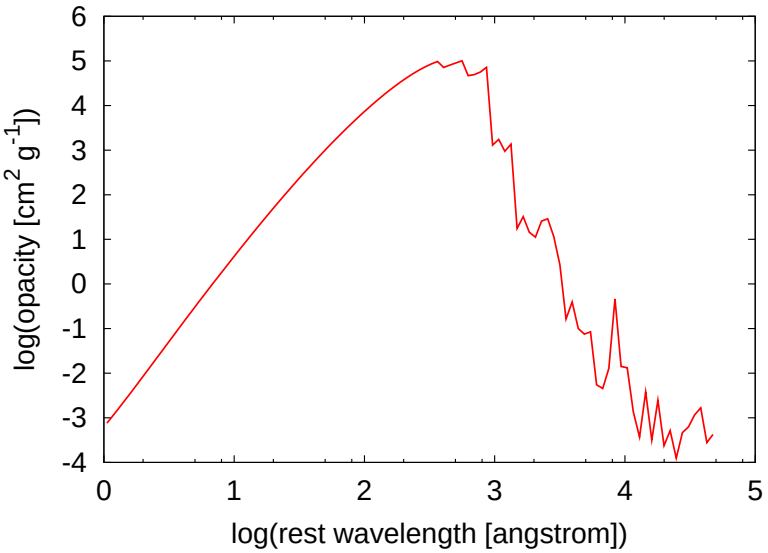

Figure 2.8: An example of opacity. The condition is 10^{-15} g cm^{-3} and 5000 K. The local thermodynamic equilibrium is assumed. The wavelengths from 1 Å to 5×10^4 Å are divided into 100 bins.

Co, and Ni. The Saha equation is treated by the fast Newton iteration technique introduced in Karp 1980. The degeneracy of electrons is treated with the method of Basko 1985 and the pressure ionization is included in an approximate way but they are not dominant source of pressure in our work.

Opacity

Opacity used in `STELLA` includes the contributions from photoionization, bremsstrahlung, lines, and electron scattering. We use 100 bins between 1 Å and 5×10^4 Å. An example of opacity used in the code is shown in Figure 2.8. The bound-free photoionization cross sections we adopt is the analytic fit obtained by Verner & Yakovlev 1995. Approximately 110,000 lines in the list of Kurucz 1991 is taken into account for line opacity and the line contribution to the total opacity is computed by using the approximation introduced in Eastman & Pinto 1993.

Heating from Radioactive Decay

The radioactive heating by the decay of ^{56}Ni $\rightarrow$ ^{56}Co $\rightarrow$ ^{56}Fe, which is one of the major energy source to power SNe, is taken into account. γ-rays emitted by the decay of ^{56}Ni $\rightarrow$ ^{56}Co and ^{56}Co $\rightarrow$ ^{56}Fe and positrons emitted by the decay of ^{56}Co $\rightarrow$ ^{56}Fe are absorbed by SN ejecta and heat them. The radiative transfer equations for γ-rays are solved by using one-group approximation (Swartz et al. 1995) with the effective opacity $\kappa_\gamma = 0.05 Y_e$ cm^2 g^{-1} where Y_e is the total electron number density over baryon density. All positrons are assumed to be absorbed in situ.

The timing of death, like the ending of a story, gives a changed meaning to what preceded it.

Mary Catherine Bateson (1939 -)

3 Type IIn Supernovae

3.1 Overview

SNe IIn show signatures of the interaction between SN ejecta and dense CSM. The main power source of SNe IIn is the kinetic energy of the SN ejecta as is indicated by the large variations in their LCs (e.g., Kiewe et al. 2012, Taddia et al. 2013). The dense CSM decelerate the SN ejecta and the kinetic energy is converted to radiation. The large variations in the LCs are likely from the variations in the dense CSM. To unveil the nature of the mysterious SN IIn progenitors and mass loss related to them, we need to know the properties of the SN ejecta and dense CSM related to them. In this chapter, we apply our analytic bolometric LC model developed in Section 2.3 to observed SN IIn LCs. The SN ejecta and dense CSM properties of SNe IIn are estimated based on the analytic model. This information can be eventually used to constrain the SN IIn progenitors and their mass-loss mechanisms.

In Section 3.2, we demonstrate example ways to apply our analytic LC model developed in Section 2.3 to observed bolometric LCs of SNe IIn. In Section 3.3, we apply our model to the three best observed SNe IIn, namely, SN 2005ip, SN 2006jd, and SN 2010jl. After giving caveat about the applicability of our analytic model in Section 3.4, we apply our model to larger SNe IIn samples provided by Taddia et al. 2013 to see statistical properties of the dense CSM around SNe IIn in Section 3.5. We discuss some issues in Section 3.6 and summarize this chapter in Section 3.7.

3.2 Example Procedures

We show examples of procedures to fit our analytic bolometric LC presented in Section 2.3 to bolometric LCs constructed from observations. The actual processes for the comparison depend on the available information from observations but the basic concepts will be essentially the same as the examples presented here.

Our bolometric LC model consists of two components. Before t_t, the model LC has a power-law dependence on time ($L = L_1 t^{\alpha}$). Thus, we can first use the function $L_1 t^{\alpha}$ to fit an early LC and obtain L_1 and α. Assuming n, the CSM density slope s can be constrained just by α through Equation 2.37 (Figure 2.1).

If there are spectral observations at these epochs and the shell velocity evolution can be estimated by them, we can use

$$v_{\rm sh}(t) = \frac{dr_{\rm sh}}{dt}, \tag{3.1}$$

$$= \frac{n-3}{n-s}\left[\frac{(3-s)(4-s)}{4\pi D(n-4)(n-3)(n-\delta)}\frac{[2(5-\delta)(n-5)E_{\rm ej}]^{(n-3)/2}}{[(3-\delta)(n-3)M_{\rm ej}]^{(n-5)/2}}\right]^{\frac{1}{n-s}} t^{-\frac{3-s}{n-s}}, \tag{3.2}$$

$$\equiv v_1 t^{-\frac{3-s}{n-s}}, \tag{3.3}$$

to fit the velocity evolution and obtain v_1. Just from the three values, L_1, α, and v_1, we can obtain the CSM density structure for given ε_k and n,

$$D = \frac{1}{2\pi\varepsilon_k}\left(\frac{n-3}{n-s}\right)^{2-s} L_1 v_1^{s-5}. \tag{3.4}$$

This means that we can estimate the mass-loss rate without assuming $M_{\rm ej}$ and $E_{\rm ej}$. As the time dependence of $v_{\rm sh}$ is small, the velocity information of just a single epoch can constrain D. So far, $M_{\rm ej}$ and $E_{\rm ej}$ are degenerated and we have to assume either $M_{\rm ej}$ or $E_{\rm ej}$ to constrain the other parameter.

The formulae $L = L_1 t^{\alpha}$ and $v_{\rm sh} = v_1 t^{-(3-s)/(n-s)}$ can only be applied before t_t. After obtaining the physical values, we have to check whether t_t is larger than the epochs used for the fitting. If there is an available bolometric LC after t_t, we can fit Equation 2.39 to the LC and obtain further constraints to break the degeneracy between $E_{\rm ej}$ and $M_{\rm ej}$.

We show how this procedure works in the next section by using actual bolometric LCs from observations.

3.3 Application to Some Observed Bolometric LCs

Here we compare our analytic bolometric LCs to observed LCs of SNe IIn 2005ip, 2006jd, and 2010jl, and estimate CSM and SN ejecta properties of them. We assume $\varepsilon_k = 0.1$ in this section. ε_k is affected by SN ejecta mass and CSM mass but it is typically of the order of 0.1 (Section 4.3.4.1). All the fitting procedures in this section are performed by using the least-squares method unless otherwise mentioned. Table 3.1 is a summary of the SN IIn properties derived in this section.

3.3.1 SN 2005ip

SN 2005ip was intensively observed by Stritzinger et al. 2012 from UV to NIR wavelengths. They derived a bolometric LC that we use for the comparison to our bolometric LC model. Optical photometric and spectroscopic observations are also reported by Smith et al. 2009b, whereas Fox et al. 2009, Fox et al. 2010, Fox et al. 2011, Fox et al. 2013 summarize the NIR

Table 3.1: SN IIn properties estimated in Section 3.3

SN	s ($\rho_{\rm csm} \propto r^{-s}$)		$\langle \dot{M} \rangle^a$	$E_{\rm ej}$
	$n = 10$	$n = 12$	($M_\odot$ yr^{-1})	(10^{51} erg)
2005ip	2.28	2.36	$1.2 - 1.4 \times 10^{-3}$	13-15^b
2006jd	1.40	1.62	$1.3 - 1.7 \times 10^{-3}$	12-13^b
2010jl	2.2^b		0.039^b	23^b

^{a}Average rate derived by the CSM mass within 10^{16} cm and the CSM velocity 100 km s^{-1}.
^{b}Derived assuming $M_{\rm ej} = 10\ M_\odot$.

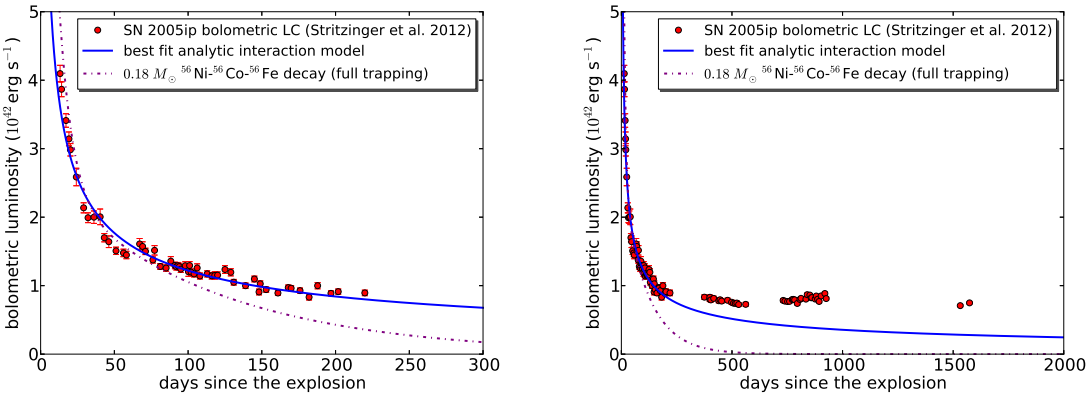

Figure 3.1: Bolometric LC of SN 2005ip (Stritzinger et al. 2012) and some LC models. The solid line is the best fit to $L = L_1 t^\alpha$ up to 220 days. The dot-dashed line is the available energy from the radioactive decay of 0.18 $M_\odot$ ^{56}Ni. The luminosity inputs from the two power souces resemble each other up to about 100 days and the later LC is required to distinguish between them.

observations of SN 2005ip. We assume that the explosion date of SN 2005ip was 9 days before its discovery and all the following dates are since the explosion.

At first, we fit the obtained bolometric LC up to 220 days by $L = L_1 t^\alpha$ and we get

$$L = (1.44 \pm 0.08) \times 10^{43} \left(\frac{t}{1\ \text{day}} \right)^{-0.536 \pm 0.013} \ \text{erg s}^{-1}. \tag{3.5}$$

The errors are the statistical error here and hereafter. In Figure 3.1 we show the result. $\alpha = -0.536 \pm 0.013$ corresponds to $s = 2.28 \pm 0.03$ and $s = 2.36 \pm 0.02$ for $n = 10$ and $n = 12$, respectively. Thus, the CSM around the progenitor of SN 2005ip likely had slightly steeper density structure than the expected density structure from steady mass loss.

One interesting feature in Figure 3.1 is the similarity of the analytic LC from the SN ejecta-CSM interaction to the available energy from the radioactive decay of 0.18 $M_\odot$ ^{56}Ni before around 100 days. The available energy from the radioactive decay ^{56}Ni $\rightarrow$^{56}Co $\rightarrow$^{56}Fe

is (Nadyozhin 1994)

$$\left[6.45\times10^{43}e^{-t/(8.8\text{ days})}+1.45\times10^{43}e^{-t/(111.3\text{ days})}\right]\frac{M_{^{56}\mathrm{Ni}}}{M_\odot}\text{ erg s}^{-1}, \tag{3.6}$$

where $M_{^{56}\mathrm{Ni}}$ is the initial ^{56}Ni mass. We cannot distinguish between the two power sources only from the bolometric LC before about 100 days. The two energy sources can only be distinguished by LCs at later epochs. The similarity, especially at around 50 days, is because of the decay time of ^{56}Co. At around 50 days, the radioactive energy from ^{56}Co is dominant and the available energy from the decay follows $\propto e^{-t/(111.3\text{ days})}$. The values and the decline rates (the first derivatives) of the functions following $\propto e^{-t/(111.3\text{ days})}$ and $\propto t^{-m}$ (m is a constant) can get similar at $t = 111.3m$ days. Looking at Figure 2.1, $m \simeq 0.5$ at around $s \simeq 2$, so the two functions can be similar at around $t \simeq 50$ days. For a LC from the interaction to have a similar decline rate to that from the ^{56}Co radioactive decay after $\simeq 100$ days, m should be close to unity and the CSM density slope should be steep ($s \simeq 3$).

The shell velocity of SN 2005ip around 100 days since the explosion is likely $\simeq 17,500$ km s^{-1} (Stritzinger et al. 2012). Then, based on Equation 3.4, we get

$$\rho_{\mathrm{csm}}(r) = \begin{cases} 8.4\times10^{-16}\left(\frac{r}{10^{15}\text{ cm}}\right)^{-2.28}\text{ g cm}^{-3} & (n=10),\\ 1.0\times10^{-15}\left(\frac{r}{10^{15}\text{ cm}}\right)^{-2.36}\text{ g cm}^{-3} & (n=12). \end{cases} \tag{3.7}$$

The Thomson optical depth τ_{sh} of the solar-metallicity unshocked CSM when the shock is at 10^{15} cm (the blackbody radii of SNe IIn are usually above 10^{15} cm) is

$$\tau_{\mathrm{sh}} = \begin{cases} 0.22 & (n=10),\\ 0.25 & (n=12), \end{cases} \tag{3.8}$$

and our assumption that the unshocked CSM does not affect the LC is justified. We estimate an average mass-loss rate $\langle\dot{M}\rangle$ by using the CSM mass within 10^{16} cm. Assuming $v_{\mathrm{w}} = 100$ km s^{-1}, the CSM mass within 10^{16} cm is lost from the progenitor in 32 years before the explosion. The average mass-loss rate in this period is

$$\langle\dot{M}\rangle = \begin{cases} 1.2\times10^{-3}\ M_\odot\text{ yr}^{-1} & (n=10),\\ 1.4\times10^{-3}\ M_\odot\text{ yr}^{-1} & (n=12). \end{cases} \tag{3.9}$$

The bolometric luminosity of SN 2005ip after 300 days is almost constant ($\simeq 8.2\times10^{41}$ erg s^{-1}). The asymptotic solution (Equation 2.39) can have a constant luminosity at a certain condition. For example, the asymptotic solution for $s = 2$ (Equation 2.46) can be constant if $bt \ll 1$. However, for the case of SN 2005ip, we could not find a constant asymptotic solution which is consistent with the early LC before 300 days. The constant luminosity may be due to, e.g., another CSM component or light echos.

To constrain the SN properties, we assume $M_{\mathrm{ej}} = 10\ M_\odot$. Then, from L_1 above, we obtain

$$E_{\mathrm{ej}} = \begin{cases} 1.3\times10^{52}\text{ erg s}^{-1} & (n=10),\\ 1.5\times10^{52}\text{ erg s}^{-1} & (n=12). \end{cases} \tag{3.10}$$

t_t becomes

$$t_t = \begin{cases} 4.2\times10^{3}\text{ days} & (n=10),\\ 5.0\times10^{3}\text{ days} & (n=12), \end{cases} \tag{3.11}$$

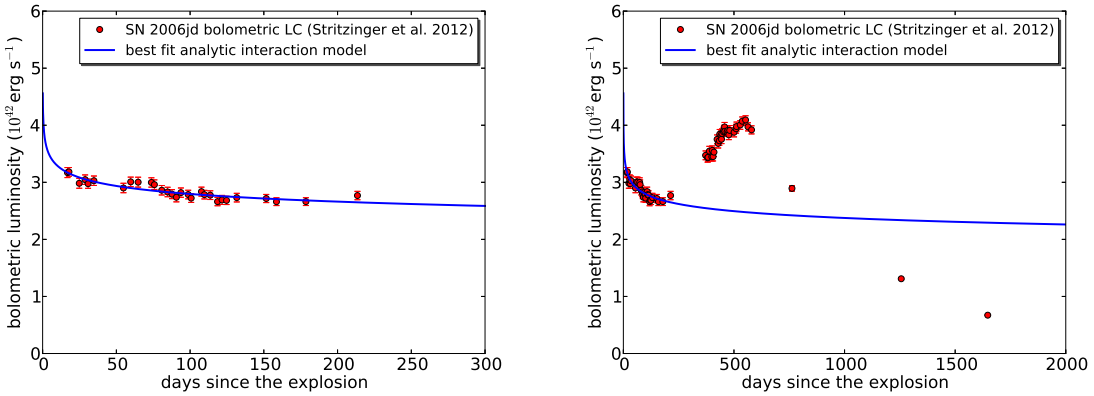

Figure 3.2: Bolometric LC of SN 2006jd (Stritzinger et al. 2012) and the best fit $L = L_1 t^{\alpha}$ model up to 250 days. The second rise starting around 400 days cannot be explained by our model and may be due to, e.g., another CSM component.

so the epochs we used for the fitting ($t < 220$ days) are justified.

The average mass-loss rate we obtained (10^{-3} $M_{\odot}$ yr^{-1}) is consistent with the rate estimated by Fox et al. 2011 (1.8×10^{-3} $M_{\odot}$ yr^{-1}) but larger than the rate suggested by Smith et al. 2009b (2×10^{-4} $M_{\odot}$ yr^{-1}). Based on these mass-loss rates, Smith et al. 2009b conclude that the progenitor of SN 2005ip is a massive RSG like VY CMa (e.g., Smith et al. 2009b), while Fox et al. 2011 prefer a more massive progenitor like a LBV. Our results seem to support the latter scenario but depend on the value of ε_k assumed in deriving D so we cannot constrain the progenitor strongly. In principle, we may be able to distinguish between the two progenitors with n, but our results are found not to depend much on n. Binary evolution may also be related to the large mass-loss rate (e.g., Chevalier 2012).

3.3.2 SN 2006jd

SN 2006jd was also observed in a wide spectral range by Stritzinger et al. 2012 and they obtained a bolometric LC. We use their bolometric LC for our modeling. We assume that the date of the explosion is 9 days before its discovery and the following dates are since the explosion. Chandra et al. 2012a estimate CSM properties of SN 2006jd based on the X-ray and radio observations after about 400 days since the explosion. They conclude that the CSM density profile is rather flat ($s \simeq 1.5 - 1.6$) and the CSM density is $\sim 10^6$ cm^{-3} at $\simeq 2 \times 10^{16}$ cm. Fox et al. 2011 estimate the mass-loss rate based on NIR observations (2.8×10^{-3} $M_{\odot}$ yr^{-1}).

By fitting the LC before 250 days with $L = L_1 t^{\alpha}$ (Figure 3.2), we obtain

$$L = (3.9 \pm 0.1) \times 10^{42} \left(\frac{t}{1 \text{ day}} \right)^{-0.0708 \pm 0.0064} \text{ erg s}^{-1}. \tag{3.12}$$

From $\alpha = -0.0708$ obtained by the bolometric LC fitting, we obtain $s = 1.40 \pm 0.01$ and $s = 1.62 \pm 0.01$ for $n = 10$ and $n = 12$, respectively. The shell velocity of SN 2006jd around

100 days since the explosion is likely $\simeq 15,000$ km s^{-1} (Stritzinger et al. 2012). Then, based on Equation 3.4, we get

$$\rho_{\rm csm}(r) = \begin{cases} 2.6\times10^{-16}\left(\frac{r}{10^{15}\ {\rm cm}}\right)^{-1.40}\ {\rm g\ cm^{-3}} & (n=10), \\ 4.8\times10^{-16}\left(\frac{r}{10^{15}\ {\rm cm}}\right)^{-1.62}\ {\rm g\ cm^{-3}} & (n=12). \end{cases} \tag{3.13}$$

The Thomson optical depth of the solar-metallicity unshocked CSM when the shock is at 10^{15} cm is

$$\tau_{\rm sh} = \begin{cases} 0.22 & (n=10), \\ 0.26 & (n=12). \end{cases} \tag{3.14}$$

We estimate an average mass-loss rate by using the CSM mass within 10^{16} cm and $v_{\rm w} = 100$ km s^{-1} as we did for SN 2005ip. The average mass-loss rate is

$$\langle \dot{M} \rangle = \begin{cases} 1.3\times10^{-3}\ M_\odot\ {\rm yr^{-1}} & (n=10), \\ 1.7\times10^{-3}\ M_\odot\ {\rm yr^{-1}} & (n=12). \end{cases} \tag{3.15}$$

The estimated average mass-loss rate is consistent with the rate derived by Fox et al. 2011 from dust emission ($2.8\times10^{-3}\ M_\odot$ yr^{-1}). Interestingly, the mass-loss rate is very close to those of SN 2005ip estimated in the previous section, although the density slopes are quite different ($s = 2.3-2.4$ for SN 2005ip and $s = 1.4-1.6$ for SN 2006jd).

The late phase LC of SN 2006jd shows an increase which is not expected in our model so we do not use the late time LC in the fit. This luminosity increase may be due to, e.g., another CSM component. Since we can only fit the early phases, we cannot constrain $M_{\rm ej}$ and $E_{\rm ej}$ independently. Here, we assume $M_{\rm ej} = 10\ M_\odot$ to estimate $E_{\rm ej}$. The estimated $E_{\rm ej}$ is

$$E_{\rm ej} = \begin{cases} 1.2\times10^{52}\ {\rm erg} & (n=10), \\ 1.3\times10^{52}\ {\rm erg} & (n=12). \end{cases} \tag{3.16}$$

Note again that we assume $\varepsilon_k = 0.1$ and $E_{\rm ej}$ is inversely proportional to ε_k. The time t_t obtained by these values are

$$t_t = \begin{cases} 4.1\times10^{2}\ {\rm days} & (n=10), \\ 1.8\times10^{2}\ {\rm days} & (n=12). \end{cases} \tag{3.17}$$

The epochs we used to fit $L = L_1 t^\alpha$ ($t < 250$ days) are justified for the $n = 10$ case. For the $n = 12$ case, t_t is smaller than 250 days. However, there are only two observational data points beyond 178 days and we find that the results of fitting by using $t < 178$ days are almost the same as the results we obtained with $t < 250$ days.

The CSM properties we derived are consistent with $s \simeq 1.5-1.6$ and the CSM density $\sim 10^6$ cm^{-3} at $\simeq 2\times10^{16}$ cm as obtained by Chandra et al. 2012a from X-ray and radio observations. However, the X-ray and radio observations were performed after the epochs when the bolometric LC starts to rise (after about 400 days since the explosion). Our model is not applicable at these epochs as is discussed above and this correspondence can be a coincidence.

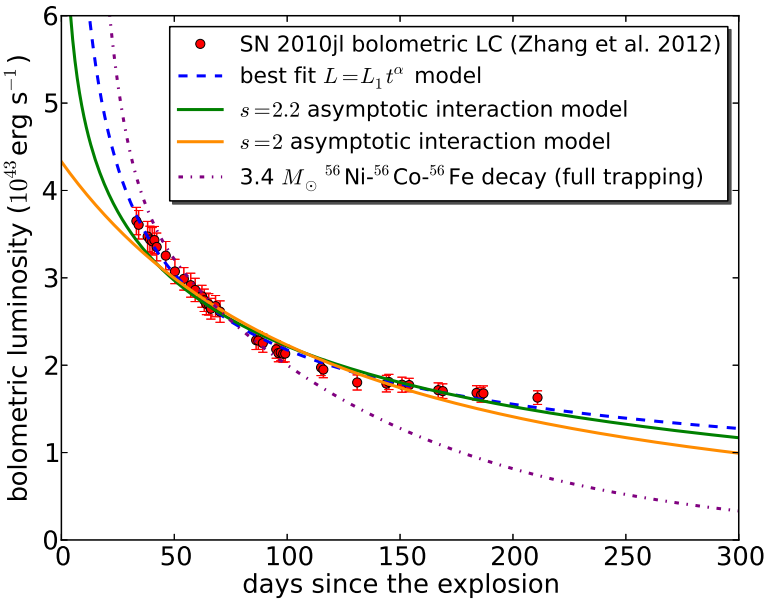

Figure 3.3: Bolometric LC of SN 2010jl (Zhang et al. 2012) and some model fits to it. The dashed line represents the best fit for $L = L_1 t^{\alpha}$. However, t_t expected from the result of the fit is too small to apply this model to the entire LC. Thus, we need to apply the asymptotic LC formula which is applicable after t_t. We get a good fit with $s = 2.2$ (green line). The orange line is the best fit from the $s = 2$ model. The dot-dashed line is the radioactive decay energy available from 3.4 $M_{\odot}$ ^{56}Ni. The radioactive decay model is suggested by Zhang et al. 2012 to explain the early bolometric LC but our interaction model can explain the entire LC with a single component.

3.3.3 SN 2010jl

SN 2010jl has been extensively observed in a wide range of wavelengths (Smith et al. 2011, Smith et al. 2012, Stoll et al. 2011, Andrews et al. 2011, Chandra et al. 2012b). Zhang et al. 2012 obtained a bolometric LC of SN 2010jl based on their optical observations and we use it for our model comparison. Note that they do not have NIR observations and the bolometric LC is constructed without them. The date of the explosion is set to 12 days before the V-band LC peak reported by Stoll et al. 2011. We apply our spherically symmetric bolometric LC model but the observation of polarization indicates an asymmetric nature of the CSM around SN 2010jl (Patat et al. 2011).

At first, we use $L = L_1 t^{\alpha}$ to fit the bolometric LC and get

$$L = (2.0 \pm 0.7) \times 10^{44} \left(\frac{t}{1 \text{ day}} \right)^{-0.486 \pm 0.001} \text{ erg s}^{-1} \tag{3.18}$$

$\alpha = -0.486 \pm 0.001$ corresponds to $s = 2.20 \pm 0.02$ and $s = 2.29 \pm 0.01$ for $n = 10$ and $n = 12$,

respectively. However, t_t become

$$t_t = \begin{cases} 9.5 \text{ days} & (n = 10), \\ 3.8 \text{ days} & (n = 12), \end{cases} \tag{3.19}$$

for $E_{\rm ej} = 10^{52}$ erg or

$$t_t = \begin{cases} 57 \text{ days} & (n = 10), \\ 23 \text{ days} & (n = 12), \end{cases} \tag{3.20}$$

for $E_{\rm ej} = 2.5 \times 10^{52}$ erg with the obtained L_1. This means that the $L = L_1 t^{\alpha}$ formula we used for the fitting is not applicable for most of the epochs we used for the fitting. Thus, we need to use the asymptotic formula (Equation 2.39) to fit the LC.

In Figure 3.3, we show some asymptotic LC models from Equation 2.39. We have searched for a good fit by changing s, D, and $E_{\rm ej}$. We assume $M_{\rm ej} = 10\ M_{\odot}$. The best model we found is shown in Figure 3.3 and it has

$$\rho_{\rm csm}(r) = 2.5 \times 10^{-14} \left(\frac{r}{10^{15} \text{ cm}} \right)^{-2.2} \text{ g cm}^{-3}, \tag{3.21}$$

and

$$E_{\rm ej} = 2.3 \times 10^{52} \text{ erg}. \tag{3.22}$$

The Thomson optical depth of the solar-metallicity unshocked CSM when the shock is at 10^{15} cm is $\tau_{\rm sh} = 7.1$. $\tau_{\rm sh}$ becomes $\simeq 1$ at $\simeq 5 \times 10^{15}$ cm and the shock is above $\simeq 5 \times 10^{15}$ cm at the epochs we apply our model (after $\simeq 30$ days since the explosion). The average mass-loss rate estimated by the CSM mass within 10^{16} cm for $v_{\rm w} = 100$ km s^{-1} is

$$\langle \dot{M} \rangle = 0.039\ M_{\odot} \text{ yr}^{-1}. \tag{3.23}$$

$t_t = 29$ days for $n = 10$ and $\delta = 1$ and $t_t = 15$ days for $n = 12$ and $\delta = 1$. Thus the usage of the asymptotic formula is justified.

Since s obtained above is close to the case of the steady mass loss ($s = 2$), we also try to fit the bolometric LC by the asymptotic formula $L = a(1 + bt)^{-3/2}$ for $s = 2$ (Equation 2.46). We obtain $a = 4.38 \times 10^{43}$ erg s^{-1} and $b = 6.44 \times 10^{-8}$ s^{-1} with $t_t = 22$ days ($n = 10$ and $\delta = 1$) or $t_t = 13$ days ($n = 12$ and $\delta = 1$). By using a, b, and $\varepsilon_k = 0.1$, we get

$$E_{\rm ej} = 1.4 \times 10^{52} \text{ erg}, \tag{3.24}$$

from Equation 2.48. Assuming $M_{\rm ej} = 10\ M_{\odot}$ and $v_{\rm w} = 100$ km s^{-1}, we obtain

$$\dot{M} = 0.087\ M_{\odot} \text{ yr}^{-1}, \tag{3.25}$$

from Equation 2.49. The rate is similar to the average rate from the $s = 2.2$ model derived above. We assign the statistical error of 0.05 for s when we use the asymptotic formula in this section.

Comparing the $s = 2.2$ and $s = 2$ models, we find that the $s = 2$ model has flatter LC than the $s = 2.2$ model. As we make s smaller, the model LC gets flatter and it gets harder to explain the bolometric LC of SN 2010jl. Thus, we presume that the CSM around the progenitor of SN 2010jl may be a bit steeper than the CSM expected from steady mass loss.

This conclusion contradicts that obtained by Chandra et al. 2012b from X-ray observations. Chandra et al. 2012b suggest $s = 1.6$ for SN 2010jl based on X-ray observations. However, their estimate is obtained by assuming $r_{\rm sh} \propto t^{(n-3)/(n-s)}$ which is not likely applicable at the epochs when they obtained X-ray data ($\simeq 60$ days and $\simeq 360$ days since the explosion). This is because of the small t_t mainly due to the high CSM density as is shown above.

So far, we fit the entire bolometric LC up to about 200 days by a single component. On the contrary, Zhang et al. 2012 suggested a two-componet model for the bolometric LC. They suggested that the LC before around 100 days is mainly powered by 3.4 $M_\odot$ of ^{56}Ni whose available radioactive energy is shown in Figure 3.3. They suggested that the SN ejecta-CSM interaction started playing a role at later epochs by using a model LC of the interaction developed by Wood-Vasey et al. 2004. However, the required ^{56}Ni mass is very large (3.4 $M_\odot$) and this amount of ^{56}Ni is rather difficult to be produced in a core-collapse SN explosion (e.g., Umeda & Nomoto 2008). In addition, no signatures of Fe elements are observed in the late phase spectra of SN 2010jl which are expected if there is large amount of ^{56}Ni production (e.g., Dessart et al. 2013). As noted in Section 3.3.1, the bolometric LC powered by the interaction resembles to the LC powered by the radioactive decay of ^{56}Ni at early epochs and we need to use additional late-phase LCs to distinguish between the two power sources. We have shown here that we need only one component from the interaction model to explain the whole LC of SN 2010jl.

3.4 Applicability

In deriving the evolution of the shocked-shell radius $r_{\rm sh}(t)$, we have assumed that s is smaller than 3. This condition is also required to derive a physical self-similar solution (e.g., Nadyozhin 1985). The allowed range of α for $s < 3$ is $\alpha > -1$ because $\alpha \to -1$ ($s \to 3$) and α is a monotonically-decreasing function at $n > 5$. Thus, if we obtain $\alpha < -1$ by fitting $L = L_1 t^\alpha$, this is beyond the applicability of our model and we need to consider other ways to explain the LC.

First, we need to check t_t. If t_t is smaller than the time used for the fitting, we need to use the asymptotic formula for the fitting. The asymptotic formula can have a rapid decline in the bolometric LC depending on parameters.

Another possibility is a CSM with $s > 3$. Most of the mass in the CSM with $s > 3$ exists near the inner edge of the CSM. In other words, for the case of $s > 3$,

$$M_{\rm csm} \equiv \int_{R_p}^{r_{\rm sh}} 4\pi r^2 \rho_{\rm csm} dr \tag{3.26}$$

$$= \frac{4\pi D}{s-3}\left(R_p^{3-s} - r_{\rm sh}^{3-s}\right) \tag{3.27}$$

$$\simeq \frac{4\pi D}{s-3} R_p^{3-s} = \text{constant} \quad (r_{\rm sh} \gg R_p). \tag{3.28}$$

Thus, most of the CSM is shocked soon after the explosion. If the CSM density is relatively low, the LCs will decline quickly soon after the explosion when most of the CSM component is swept up. If the shocked shell becomes optically thick, the LCs may resemble the 'shell-shocked diffusion' model LC suggested by Smith & McCray 2007 as a model for superluminous SNe based on the formalisms by Arnett 1980 (but see also Section 4.3.4.5). This is

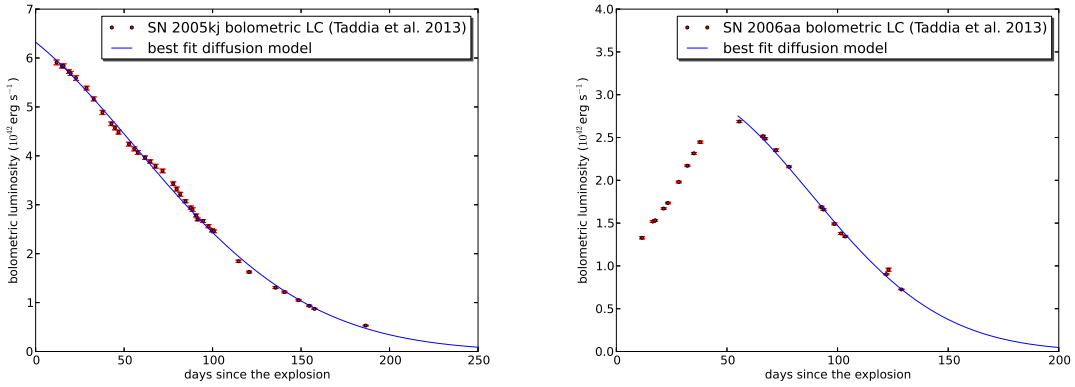

Figure 3.4: Two SNe IIn with the LC declines faster than $L \propto t^{-1}$ from the Taddia et al. 2013 SN IIn LC samples. We cannot apply the analytic SN IIn LC model developed in Section 2.3. However, the LCs can be well fitted by the so-called 'shell-shocked' diffusion model (Equation 3.29). The explosion dates of SN 2005kj and SN 2006aa are set to be 8 days before the discoveries.

a LC model for the declining part of the bolometric LC after the shock wave passes through a dense CSM. According to this model, the declining part of the bolometric LCs follows

$$L = L_0 \exp\left[-\frac{t}{\tau_{\rm diff}}\left(1+\frac{t}{2\tau_{\rm exp}}\right)\right], \tag{3.29}$$

where t is the time since the maximum luminosity, $\tau_{\rm diff}$ is the characteristic diffusion timescale in the shocked shell and $\tau_{\rm exp}$ is the expansion timescale of the shocked shell.

Bolometric LCs can also follow Equation 3.29 even if $s < 3$. This is the case when the high-density CSM is small in radius and the entire high-density CSM is shocked soon after the beginning of the interaction. Then, there is no continuous interaction and the bolometric LC should decline quickly, possibly following the shell-shocked diffusion model. However, in this case, there may be little remaining CSM to emit narrow emission lines in spectra and the SN may not continue to be of Type IIn.

So far, we have only considered possible ways to understand rapidly declining LCs in the context of SN ejecta-dense CSM interaction. For the case of SNe IIn, it is natural to consider in the context of the interaction model. However, it is possible that CSM around some SNe IIn are dense enough only to affect their spectra while their LCs are not much affected by the dense CSM. Then, rapidly declining LCs may be powered by other mechanisms like ^{56}Ni, magnetars (Maeda et al. 2007, Kasen & Bildsten 2010, Woosley 2010), or fallback (Dexter & Kasen 2012).

3.4.1 SN 2005kj and SN 2006aa

Taddia et al. 2013 recently published large SN IIn samples with bolometric LCs. We analyze the new samples in the next section. Here, we focus on the two SNe IIn, SN 2005kj and SN

2006aa, whose bolometric LCs are found to decline faster than $\alpha = -1$. As shown in Figure 3.4, the two bolometric LCs can be well fitted by the diffusion model (Equation 3.29). This result indicates that the CSM around the progenitors of these SNe may have had the density structure with $s > 3$.

The best fit model for SN 2005kj is $\tau_{\rm diff} = 221$ days and $\tau_{\rm exp} = 45$ days. SN 2005kj follows the diffusion model soon after the explosion and it is quite likely that the progenitor had a $s > 3$ CSM. For SN 2006aa, we fit the diffusion model after the LC peak and obtain $\tau_{\rm diff} = 133$ days and $\tau_{\rm exp} = 27$ days. In the case of SN 2006aa in which the rising time of the LC is relatively long, the CSM can be optically thick from the beginning and the photons from the shocked region may have been diffused in the CSM. Then, when the forward shock have gone through the dense CSM, the LC may have started to follow the diffusion model. This indicate that the CSM around SN 2006aa have large optically thick region. This fact is difficult to be explained by $s > 3$ CSM because of the steepness and the CSM around SN 2006aa seems to be explained better by the flatter CSM with extended optically thick region.

3.5 Statistical Properties of Dense CSM around SNe IIn

To apply the analytic bolometric LC model we developed in Section 2.3, bolometric LCs of SNe IIn are required. However, there are not many SN IIn bolometric LCs available. This is partly because SNe IIn are intrinsically rare type of SNe (e.g., Li et al. 2011b) and there are not many observations so far. In addition, to obtain bolometric LCs, observations with wide spectral range, from UV to infrared, are required and there are not many SNe IIn with such intensive observations. The largest SN IIn bolometric LC samples currently reported are those of Taddia et al. 2013. In addition to the bolometric LC analysis we have done in Section 3.3, we apply our bolometric LC model to the Taddia et al. 2013 samples and discuss the statistical properties of the CSM around SNe IIn.

In addition to the detailed SN IIn bolometric LCs we have discussed in Section 3.3, Taddia et al. 2013 report five additional SN IIn bolometric LCs. Two of them (SN 2005kj and SN 2006aa) have LCs which decline faster than $L \propto t^{-1}$ (see Section 3.4) and our analytic model cannot be applied. We have shown in Section 3.4 that the two SNe can be explained by the diffusion model. They may come from the dense CSM $s > 3$ (Section 3.4.1). At first, we show the results of the fitting of the analytic model to the remaining three, namely, SN 2006bo, SN 2006qq, and SN 2008fq.

Figure 3.5 shows the results of the fitting. The bolometric LC of SN 2006bo below 100 days can be fitted by the formula $L = L_1 t^{\alpha}$ self-consistently and we find

$$L = (1.03 \pm 0.06) \times 10^{43} \left(\frac{t}{1 \text{ day}} \right)^{-0.627 \pm 0.014} \text{ erg s}^{-1}. \tag{3.30}$$

From the obtained α, we find that $s = 2.44 \pm 0.03$ ($n = 10$) and $s = 2.49 \pm 0.03$ ($n = 12$). With the velocity evolution estimated by Taddia et al. 2013, the CSM density structure becomes

$$\rho_{\rm csm}(r) = \begin{cases} 2.8 \times 10^{-15} \left(\frac{r}{10^{15} \text{ cm}} \right)^{-2.44} & (n = 10), \\ 3.2 \times 10^{-15} \left(\frac{r}{10^{15} \text{ cm}} \right)^{-2.49} & (n = 12), \end{cases} \tag{3.31}$$

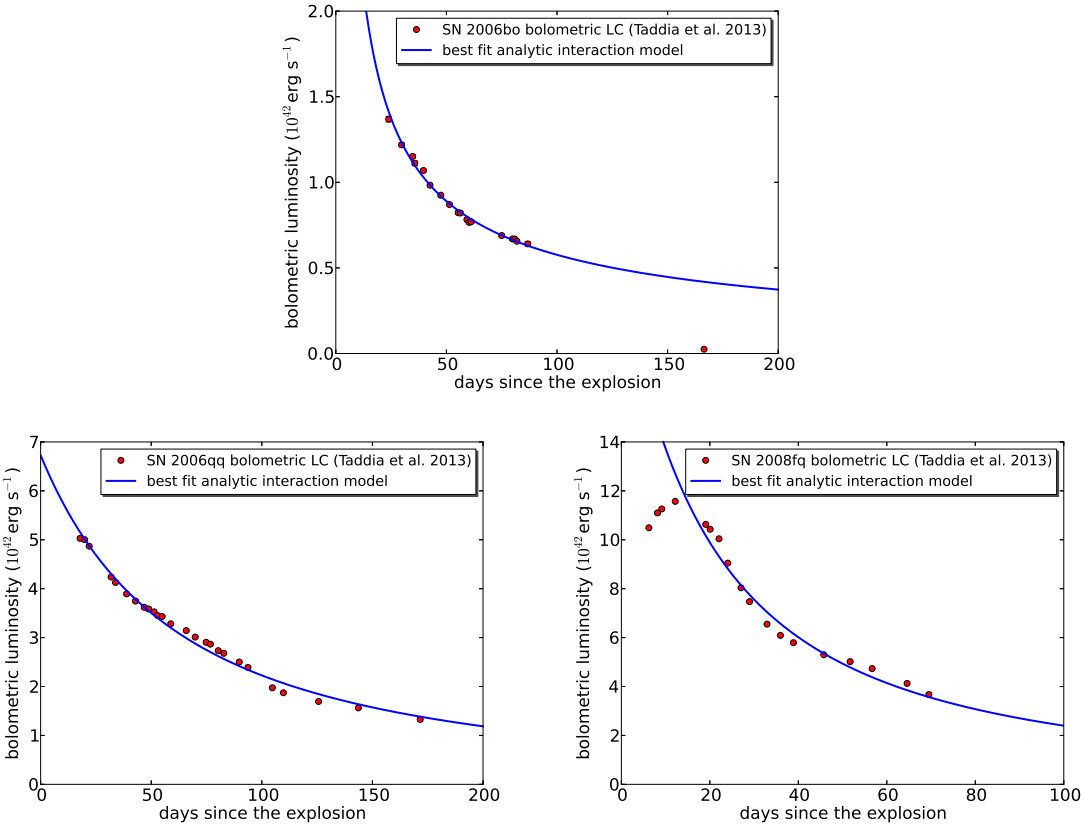

Figure 3.5: Bolometric LCs of SN 2006bo, SN 2006qq, and SN 2008fq from Taddia et al. 2013 and the results of the model fitting to them. The explosion dates of SN 2006bo, SN 2006qq, and SN 2008fq are set to 20 days, 16 days, and 5 days before the discovery, respectively.

with the Thomson optical depth

$$\tau_{\rm sh} = \begin{cases} 0.66 & (n=10), \\ 0.72 & (n=12), \end{cases} \tag{3.32}$$

and the average mass-loss rate is

$$\langle \dot{M} \rangle = \begin{cases} 3.6 \times 10^{-3}\ M_\odot\ {\rm yr}^{-1} & (n=10), \\ 4.0 \times 10^{-3}\ M_\odot\ {\rm yr}^{-1} & (n=12). \end{cases} \tag{3.33}$$

For SN 2006qq and SN 2008fq, t_t becomes too small to fit the $L = L_1 t^\alpha$ formula. We find that their bolometric LCs can be fitted well by the $L = a(1+bt)^{-3/2}$ formula (Equation 2.46) which is expected from the $s = 2$ CSM (Figure 3.5). The best fit parameters for SN 2006qq are

$$a = 6.73 \times 10^{42}\ {\rm erg\ s}^{-1}, \tag{3.34}$$

$$b = 0.0109\ {\rm day}^{-1}. \tag{3.35}$$

Table 3.2: CSM properties estimated in Chapter 3

SN	s ($\rho_{\rm csm} \propto r^{-s}$)		$\langle \dot{M} \rangle^a$
	$n = 10$	$n = 12$	($M_\odot$ yr^{-1})
2005ip	2.28	2.36	1.2×10^{-3}
2005kj	s>3?		-
2006aa	s>3?		-
2006bo	2.44	2.49	3.6×10^{-3}
2006jd	1.40	1.62	1.3×10^{-3}
2006qq	2.0[b]		0.021
2008fq	2.0[b]		0.13
2010jl	2.2[b]		0.039[b]

[a] Average rate derived by the CSM mass within 10^{16} cm and the CSM velocity 100 km s^{-1} for $n = 10$.

[b] Derived assuming $M_{\rm ej} = 10\ M_\odot$.

With Equation 2.48 and $\varepsilon_k = 0.1$, we can estimate

$$E_{\rm ej} = 1.1 \times 10^{51} \text{ erg}. \tag{3.36}$$

We can use the velocity information to additionally constrain the CSM and SN ejecta properties. From the spectral observation, the parameter d (Equation 2.51) can be constrained as

$$d \simeq 10,000 \text{ km s}^{-1}. \tag{3.37}$$

Assuming $v_{\rm w} = 100$ km s^{-1}, we find

$$M_{\rm ej} = 1.1\ M_\odot, \tag{3.38}$$
$$\dot{M} = 0.021\ M_\odot \text{ yr}^{-1}, \tag{3.39}$$

from Equations 2.52 and 2.53. t_t is 12 days ($n = 10$ and $\delta = 1$) or 7.1 days ($n = 12$ and $\delta = 1$) and our fitting is self-consistent. The Thomson optical depth above 10^{15} cm is $\tau_{\rm sh} = 3.6$ and it gets near unity at around 3×10^{15} cm. This does not contradict with our fitting.

SN 2008fq can be fitted by $L = a(1 + bt)^{-3/2}$ after 20 days since the explosion. Before 20 days, the LC rises and we discuss the rising part in the next section. From the fitting, we get

$$a = 2.09 \times 10^{43} \text{ erg s}^{-1}, \tag{3.40}$$
$$b = 0.0324 \text{ day}^{-1}. \tag{3.41}$$

With $\varepsilon_k = 0.1$, we find

$$E_{\rm ej} = 1.1 \times 10^{51} \text{ erg}. \tag{3.42}$$

From spectral information, we estimate

$$d \simeq 8,000 \text{ km s}^{-1}. \tag{3.43}$$

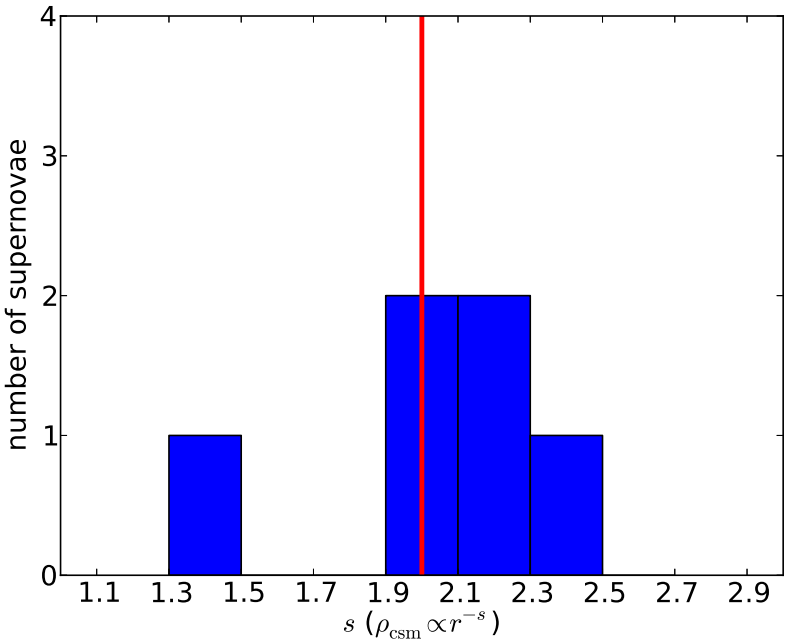

Figure 3.6: Distribution of the CSM density slope s ($\rho_{\rm csm} \propto r^{-s}$) for $n = 10$. The distribution does not change so much even if we use $n = 12$. Two SNe IIn which are not shown in this plot may have $s > 3$. The red line is at $s = 2$.

Given a, b, d, and $v_{\rm w} = 100$ km s^{-1}, we obtain

$$M_{\rm ej} = 1.7\ M_\odot, \tag{3.44}$$
$$\dot{M} = 0.13\ M_\odot\ {\rm yr}^{-1}, \tag{3.45}$$

from Equations 2.52 and 2.53. t_t becomes 3.7 days ($n = 10$ and $\delta = 1$) or 2.1 days ($n = 12$ and $\delta = 1$) and our fitting is, again, self-consistent. The Thomson optical depth above 10^{15} cm is $\tau_{\rm sh} = 22$. This is consistent with the existence of the early long rising time when the photons emitted from the shock is supposed to be scattered in the optically thick CSM. We applied our LC model after the peak when the optical depth of the CSM gets less. The optical depth becomes unity at around 2×10^{16} cm. Interestingly, both SN 2006qq and SN 2008fq have low $M_{\rm ej}$ and the standard $E_{\rm ej}$ for SNe ($\simeq 10^{51}$ erg). Both $M_{\rm ej}$ and $E_{\rm ej}$ are close to those of SNe Ia but the estimated mass-loss rates are far beyond what is expected from the SN Ia progenitor system.

Figure 3.6 and Table 3.2 summarize s obtained in this chapter. The results of SN 2005kj and SN 2006aa are not included but they can be from the CSM with $s > 3$ (Section 3.4). s in the figure is derived by assuming $n = 10$ but the distribution does not change much even if we adopt $n = 12$. Most of s are close to 2 and the mass loss of SN IIn progenitors is not likely to deviate much from what is expected from the steady mass loss. However, many s seem to slightly deviate from $s = 2$. The possible deviation from the steady mass loss in SN IIn

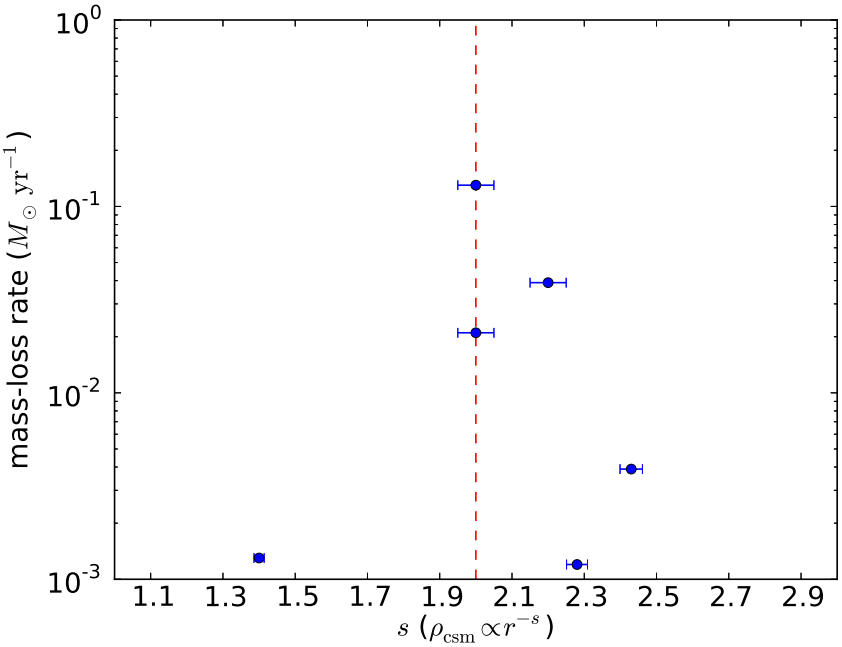

Figure 3.7: Distribution of the mass-loss rate as a function of s for $n = 10$. The distribution does not change so much even if we use $n = 12$. The red dashed line is at $s = 2$. Note that some assumptions, like $\varepsilon_k = 0.1$, are adopted to estimate the mass-loss rates (see text).

progenitors are also indicated by X-ray observations of SNe IIn (Dwarkadas & Gruszko 2012) and the deviation is likely to exist. In particular, what we newly discovered in this dissertation is that there is a possible preference to $s > 2$. If it is true, this means that the mass-loss rates of SN IIn progenitors increase as they get closer to the time of the core collapse, assuming the constant CSM velocity. This indicates that mass loss of SN IIn progenitors which occurs at the surface of them may be connected to the core growth of them. The surface behavior and the core growth are usually separated at the late stages of the stellar evolution and our results may support mass-loss mechanisms which somehow connect the two different parts of the progenitors shortly before their explosions. Some mass-loss mechanisms (e.g., Quataert & Shiode 2012) predict this possible connection but the number of samples in Figure 3.6 is small and we cannot make any strong statements at this time. There is one SN IIn, SN 2006jd, which clearly has a much flatter CSM structure than that expected from the steady mass loss.

The distribution of the estimated average mass-loss rates of SN IIn progenitors is presented in Figure 3.7. Again, the distribution is for the case of $n = 10$ but n does not affect the results much. The estimated mass-loss rates do not have clear trend in the figure. The mass-loss rates of SN IIn progenitors have been estimated from Hα line luminosities ($\sim 10^{-2}-10^{-4}\ M_\odot$ yr^{-1}, c.f. Taddia et al. 2013, Kiewe et al. 2012) and our results derived from the bolometric LCs are consistent with them.

3.6 Discussion

3.6.1 Initial Luminosity Increase

The analytic bolometric LC model applied in this section does not have a rising part at the beginning while the rising part is observed in some SNe IIn we fitted. There are several mechanisms to make the initial luminosity increase in LCs which are not taken into account in our model.

We have assumed that the radiation emitted from the dense shell is not affected by the unshocked CSM. However, especially at the early phases just after the explosion, the unshocked CSM surrounding the dense shell can be optically thick and the radiation from the shell can be scattered within the CSM. In this case, the diffusion timescale in the optically thick region determines the evolution of the initial luminosity increase and subsequent decline. Our model should only be applied to the epochs when the unshocked CSM surrounding the dense shell is optically thin and should not be applied at the epochs when the luminosity increases. When the CSM is optically thick, some signatures can be seen in spectra as well (e.g., Chugai 2001).

If the CSM is optically thin, the timescale of the initial luminosity increase is expected to be very small. Two mechanisms can affect the initial luminosity increase. One is the shock breakout at the surface of the progenitor and the other is the on-set of the SN ejecta-CSM interaction. Both are presumed to have a short timescale. If the dense part of the CSM and the progenitor are detached, we may see two luminosity peaks in the early phases: one from the shock breakout and the other from the on-set of the interaction.

3.6.2 Comparison with Numerical Bolometric Light Curves

To show the reliability of our analytic LC model, we also performed numerical LC calculations using a one-dimensional radiation hydrodynamics code `STELLA` (Section 2.5). We set the initial conditions following the physical parameters obtained in Section 3.3. The density structure of the homologously expanding SN ejecta has two power-law components as is assumed in the analytic model. The SN ejecta and CSM are initially connected at 10^{14} cm. The CSM outer radius of all the models is set to 10^{17} cm. The parameter B_q which controls the conversion efficiency from kinetic energy to radiation in the code (see Section 4.3.4.1 for the details) is adjusted to make $\varepsilon_k \simeq 0.1$. Both SN ejecta and CSM in the calculations have solar composition.

Figure 3.8 presents the results of our LC calculations. We performed the LC calculations of three models in Section 3.3, namely, SN 2005ip ($s = 2.28$, $n = 10$, $\delta = 1$, $E_{\rm ej} = 1.2 \times 10^{52}$ erg, and $M_{\rm ej} = 10\ M_\odot$), SN 2006jd ($s = 1.40$, $n = 10$, $\delta = 1$, $E_{\rm ej} = 1.3 \times 10^{52}$ erg, and $M_{\rm ej} = 10\ M_\odot$), and SN 2010jl ($s = 2.2$, $n = 10$, $\delta = 1$, $E_{\rm ej} = 2.3 \times 10^{52}$ erg, and $M_{\rm ej} = 10\ M_\odot$). The overall features of the analytic LCs are well reproduced by the numerical LCs and the analytic model used in this section is shown to provide a good prediction to the numerical results.

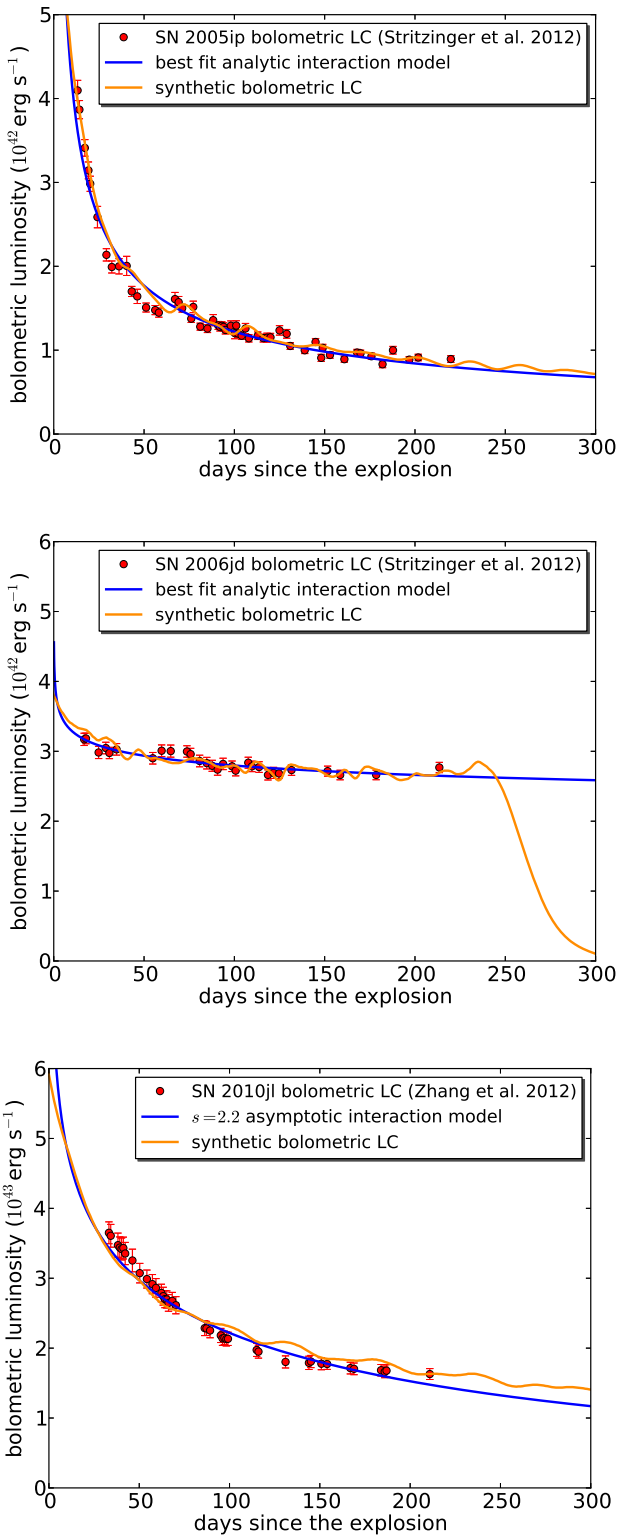

Figure 3.8: Comparisons between the numerical bolometric LCs and the analytic bolometric LCs based on which the initial conditions for the numerical LCs are constructed.

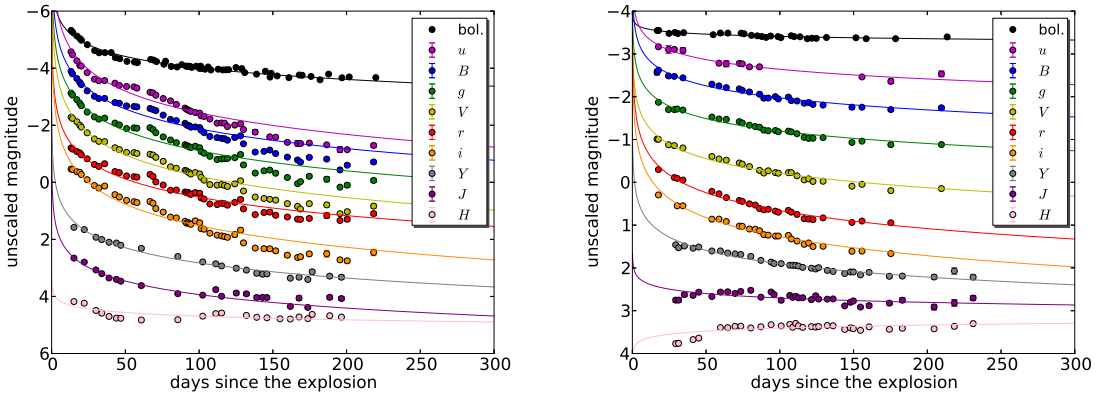

Figure 3.9: Multicolor LCs of SN 2005ip and SN 2006jd and the results of the fits to $L \propto t^{\alpha}$. α obtained by multicolor LCs are not consistent with α obtained from the bolometric LC. We need bolometric LCs to infer the CSM and SN ejecta properties from LCs properly.

3.6.3 Non-Bolometric Light Curves

As our LC model takes only the sum of the available energy into account, the LC we obtain from the model is bolometric and we have applied our analytic bolometric LC model to bolometric LCs constructed from observations. Here we try to fit the $L = L_1 t^{\alpha}$ formula to optical and NIR LCs of SN 2005ip and SN 2006jd obtained by Stritzinger et al. 2012. We focus on the parameter α which is directly affected by the CSM density slope s for a given n.

Figure 3.9 and Table 3.3 show the results of the LC fits. As we can see, α obtained with different photometric bands have different values. This means that we need to construct bolometric LCs from observations to obtain accurate information. This can be clearly seen in Figure 7 of Stritzinger et al. 2012. The spectra evolve significantly with time and no single band can represent the entire evolution of the bolometric LC. We thus clearly need to construct a bolometric LC to apply our model to obtain CSM and SN properties of SNe IIn.

3.7 Summary

We have applied the analytic bolometric LC model for SNe powered by the interaction between SN ejecta and dense CSM developed in Section 2.3 to SN IIn bolometric LCs constructed from observations. By fitting the analytic model to the observed LC, the CSM and SN ejecta properties of SNe IIn are estimated.

To demonstrate the capability of the analytic model, we have applied our bolometric LC model to three well-observed SNe IIn, i.e., SN 2005ip, SN 2006jd, and SN 2010jl. The results show that their CSM density slopes are close to what is expected from the steady mass loss ($s = 2$ where $\rho_{\rm csm} \propto r^{-s}$) but slightly deviate from it ($s \simeq 2.3 - 2.4$ for SN 2005ip, $s \simeq 1.4 - 1.6$ for SN 2006jd, and $s \simeq 2.2$ for SN 2010jl). The derived mass-loss rates are consistent with LBVs (SN 2005ip: $\langle \dot{M} \rangle = 0.0012 - 0.0014\ M_{\odot}\ {\rm yr}^{-1}$, SN 2006jd: $\langle \dot{M} \rangle = 0.0013 - 0.0017\ M_{\odot}\ {\rm yr}^{-1}$ and SN 2010jl: $\langle \dot{M} \rangle = 0.039\ M_{\odot}\ {\rm yr}^{-1}$). We could not

Table 3.3: List of α from optical and NIR LCs

Band	α	
	SN 2005ip	SN 2006jd
bolometric	-0.536	-0.0708
u	-1.01	-0.300
B	-0.923	-0.374
g	-0.934	-0.387
V	-0.995	-0.451
r	-0.854	-0.557
i	-1.00	-0.592
Y	-0.706	-0.414
J	-0.630	-0.137
H	-0.171	0.0950

constrain SN ejecta properties strongly but $E_{\rm ej}$ of all three SNe likely exceeded 10^{52} erg if we assume that $M_{\rm ej} = 10\ M_{\odot}$ and that the conversion efficiency from kinetic energy to radiation is 10% ($\varepsilon_k = 0.1$).

We have also found that the energy inputs from the interaction and the radioactive decay of ^{56}Ni can be similar to each other up to about 100 days since the explosion. We need to have LCs at later phases to distinguish between the two luminosity sources from LCs alone.

Our bolometric LC model can only be applied for $s < 3$. For $s > 3$, we suggest that the shell-shocked diffusion model proposed by Smith & McCray 2007 (see also Section 4.3.4.5) may be applied for some cases. The new SN IIn sample from Taddia et al. 2013 includes SNe IIn with very fast decline and may be related to the $s > 3$ CSM.

In addition to the three SNe IIn we studied intensively, we analysed five additional SNe IIn recently reported by Taddia et al. 2013 in order to statistically discuss the CSM properties of SNe IIn. There is still not enough number of SNe IIn to have meaningful statistical arguments, we find that the CSM around SNe IIn are more or less consistent with what is expected from the steady mass loss but prefers a bit steeper density profile. This means that the mass-loss rates of SN IIn progenitors may typically increase as the progenitors get close to the time of the core collapse.

We have also compared our analytic LCs to synthetic ones calculated with a one-dimensional radiation hydrodynamics code `STELLA`. Our analytic LCs are well-reproduced by the numerical modeling.

We have applied our model to only six observed SNe IIn. We suggest to systematically study the SN ejecta and CSM properties of SNe IIn by applying our LC model to many other SNe IIn. Such a systematic study will lead to a comprehensive understanding of SNe IIn, i.e., their progenitors and the mass-loss mechanisms related to them.

This chapter is based on
T.J. Moriya, K. Maeda, F. Taddia, J. Sollerman, S.I. Blinnikov, E.I. Sorokina,
Monthly Notices of the Royal Astronomical Society, accepted (arXiv:1307.2644)

If you always put limit on everything you do, physical or anything else, it will spread into your work and into your life. There are no limits. There are only plateaus, and you must not stay there, you must go beyond them.

Bruce Lee (1940 - 1973)

4

Superluminous Supernovae

4.1 Overview

Superluminous supernovae (SLSNe) are a new class of SNe whose existence is recognized recently. Currently, SNe whose peak luminosities are brighter than $\simeq -21$ mag are observationally defined as SLSNe. As we introduced in Chapter 1, SLSNe show diversities and they are sub-divided into several types. In this chapter, we investigate the nature and origins of SLSNe and their diversities through the theoretical LC modeling of them.

First, in Section 4.2, we focus on the existence of two types in SLSN II. All of currently know SLSN II, except for SN 2008es, are classified as Type IIn. The only one exception, SN 2008es, was Type IIL without any signatures of narrow lines. We will show that the existence of the two types in SLSN II can be explained by the diversity in the density structures of the dense CSM. The shock breakout plays a key role here. Then, in Section 4.3, we study the LC of Type IIn SLSN 2006gy in detail based on the shock breakout model developed in Section 4.2.

SLSN R is SLSNe without any hydrogen features. Their LCs have a characteristic decline rate which is consistent with the decay timescale of ^{56}Co. Thus, their luminosities are presumed to be powered by the large amount of ^{56}Ni produced at the time of their explosions. However, the required ^{56}Ni to explain their luminosities are more than $\simeq 5\ M_{\odot}$. We discuss what kind of explosions can produce such amount of ^{56}Ni and possible progenitors of SLSN R in Section 4.4.

Finally, we discuss SLSN I in Section 4.5. SLSN I is the most puzzling kind of SLSNe. They do not show any hydrogen features nor LC declines which are consistent with the ^{56}Co decay. Currently, there seems no clue about their power sources from the observations of SLSN I. However, we argue that the 'dip' in the LC of SLSN I 2006oz between the precursor and the main LC can appear if there are dense CSM. Thus, we suggest that SLSN I is powered by the interaction between SN ejecta and dense C+O-rich CSM.

4.2 Type IIn and Type IIL SLSNe from Shock Breakout

As we introduced in Section 1.5, one SLSN II, SN 2008es, did not show the narrow lines which are expected to be observed if SLSN II is powered by the interaction between SN ejecta and dense CSM. Here, we show that even if a SLSN is powered by the interaction between SN ejecta and dense CSM, it may not show the narrow lines especially after the peak luminosity. This is a natural consequence of the shock breakout in dense CSM.

We discussed the shock breakout in dense CSM in Section 2.4.1. We found that, if the shock breakout occurs in the dense CSM, the ratio of the diffusion timescale t_d and the shock propagation timescale t_s after the shock breakout can vary depending on the CSM density slope s ($\rho_{\rm csm} \propto r^{-s}$). The diffusion timescale t_d corresponds to the rising time of the observed LC and the shock propagation timescale t_s corresponds to the period when we can observe the narrow spectral components which come form the unshocked CSM.

Let us first recall what happens if the ratio of the two timescales is different. If $t_d/t_s \simeq 1$, the shock wave reaches the surface of the dense CSM soon after the LC has reached the peak with the timescale t_d. Since the entire CSM is shocked just after the LC peak, no signature in spectra from the CSM is observable after the LC peak. On the other hand, if $t_d/t_s < 1$, the shock wave continues to propagate in the optically thin region of the CSM even after the LC peak. As there remain unshocked materials in the CSM even after the LC peak, we expect to see the spectral components from the unshocked CSM even after the LC peak.

In other words, Type IIL SLSNe can result from the dense CSM with $t_d/t_s \simeq 1$ while Type IIn SLSNe can result from the dense CSM with $t_d/t_s < 1$. The ratio of the two timescales is determined by the density slope s as we found in Section 2.4.1.

However, even if we do not observe the narrow components after the peak due to the density slope, the narrow Lorentzian line profiles which are suggested to be caused by the dense CSM (e.g., Chugai 2001, Dessart et al. 2009) can still appear before the LC peak depending on the optical depth of the CSM. If we apply the model of Chugai 2001, the ratio U of the unscattered Hα line flux to the total Hα line flux of the Lorentzian profile is

$$U \simeq \frac{1 - e^{-\tau_{\rm csm}}}{\tau_{\rm csm}}. \tag{4.1}$$

For the case of flat density slopes, $\tau_{\rm csm}$ remains too high until the forward shock reaches the surface (Figure 2.2) and U is expected to be very small for a long time before the LC peak. On the other hand, if the density decline is steep, the optical depth decreases gradually with time and the suitable optical depth for the appearance of Lorentzian profiles would be realized for a long while. Therefore, Lorentzian lines are expected to be observed well before the LC peak for Type IIn SLSNe.

The LC evolution of SLSN II is also consistent with our models. In our models for both Type IIn and Type IIL SLSNe, the forward shock stays in the dense CSM until the LC peak. As the CSM with $\tau_{\rm csm} > 1$ is shocked with the timescale of t_d, the dense CSM adiabatically cools down after the LC peak. Thus, the LCs of SLSN II are supposed to follow the shell-shocked diffusion model presented by Smith & McCray 2007 after the peak. The shell-shocked diffusion model is based on the adiabatic cooling of the shocked dense CSM, which is basically the same as the LC model suggested for SNe II by Arnett 1980. The model had been already shown to be consistent with the declining phase of the LC of

SN 2006gy (Smith & McCray 2007). It should be noted, however, that the model is too simplified and many effects which cannot be treated by the formulation of Arnett 1980 are ignored in Smith & McCray 2007 (see Section 4.3.4.5). For example, the model assumes a constant opacity and it ignores the presence of a recombination wave which is supposed to be created in the diffusing shocked shell. Thus, we cannot confirm that our model is consistent with the LCs of SLSN II just by the comparison with the shell-shocked diffusion model and numerical LC modeling is required to see if our models are consistent with SLSN II LCs. We show the results of numerical LC modeling in Section 4.3.

4.2.1 Comparison with Observations

So far, we have shown that, if the shock breakout occurs inside a dense CSM ($x < 1$), the ratio of the timescale of the photon diffusion to that of the shock propagation in the CSM depends on the CSM density slope and thus the different density slope can result in two kinds of SLSN II, i.e., Type IIn and Type IIL. As an example, we apply our model to two SLSNe: Type IIn SLSN 2006gy and Type IIL SLSN 2008es. If we look into Type IIn SLSN 2006gy and Type IIL SLSN 2008es, one important difference is the existence of narrow P-Cygni profiles in the spectra of SN 2006gy after the LC peak. Based on the observational feature, we can guess that Type IIL SLSN 2008es came from the dense CSM with $t_d/t_s \simeq 1$ while Type IIn SLSN 2006gy resulted from the dense CSM with $t_d/t_s < 1$. We apply those models to the two SLSNe. $\kappa_{\rm csm}$ is set to 0.34 cm^2 g^{-1} in this section.

4.2.1.1 Type IIn SLSNe (SN 2006gy)

The observations of SN 2006gy are briefly summarized in Section 4.3.1. It is classified as SNe IIn and the luminosity reached $\simeq -22$ mag in the R band. The detailed spectral evolution is summarized in Smith et al. 2010a. The narrow P-Cygni Hα lines with the absorption minimum of $\simeq$ 100 km s^{-1} are considered to come from the CSM. As SN 2006gy shows narrow P-Cygni profiles after the maximum luminosity, an unshocked CSM is supposed to remain after the maximum. Thus, models with $t_d/t_s < 1$ and $y_1 < 1$ are preferred. Based on the observations of Smith et al. 2010a, we adopt the following parameters in this section:

$$v_s \simeq 5,200 \text{ km s}^{-1}, \tag{4.2}$$

$$t_d \simeq 70 \text{ days}. \tag{4.3}$$

v_s is constrained by the evolution of the blackbody radius and t_d is obtained from the rising time of the LC. As the narrow Hα P-Cygni profile is detected at 179 days[1] and disappears at 209 days (Smith et al. 2010a), we presume that the forward shock has gone through the entire CSM between 179 days and 209 days. We simply take the central date (194 days) as the time when the forward shock has gone through the entire CSM, i.e., $t_s \simeq 194$ days. With t_d, t_s, and v_s, we can estimate x and R_o for a given s from Equations 2.62 and 2.63.

If we adopt the model with $s = 2$, for example, x and R_o are estimated to be 0.0095 and 8.8×10^{15} cm, respectively. In this case, the shock breakout occurs at $xR_o \simeq 3.2 \times 10^{14}$ cm and the last scattering surface is $y_1 R_o \simeq 3.2 \times 10^{15}$ cm. The total CSM mass is $M_{\rm CSM} \simeq 0.81\ M_\odot$

[1] Days since the explosion. The explosion date is set to be the same as in Smith et al. 2010a.

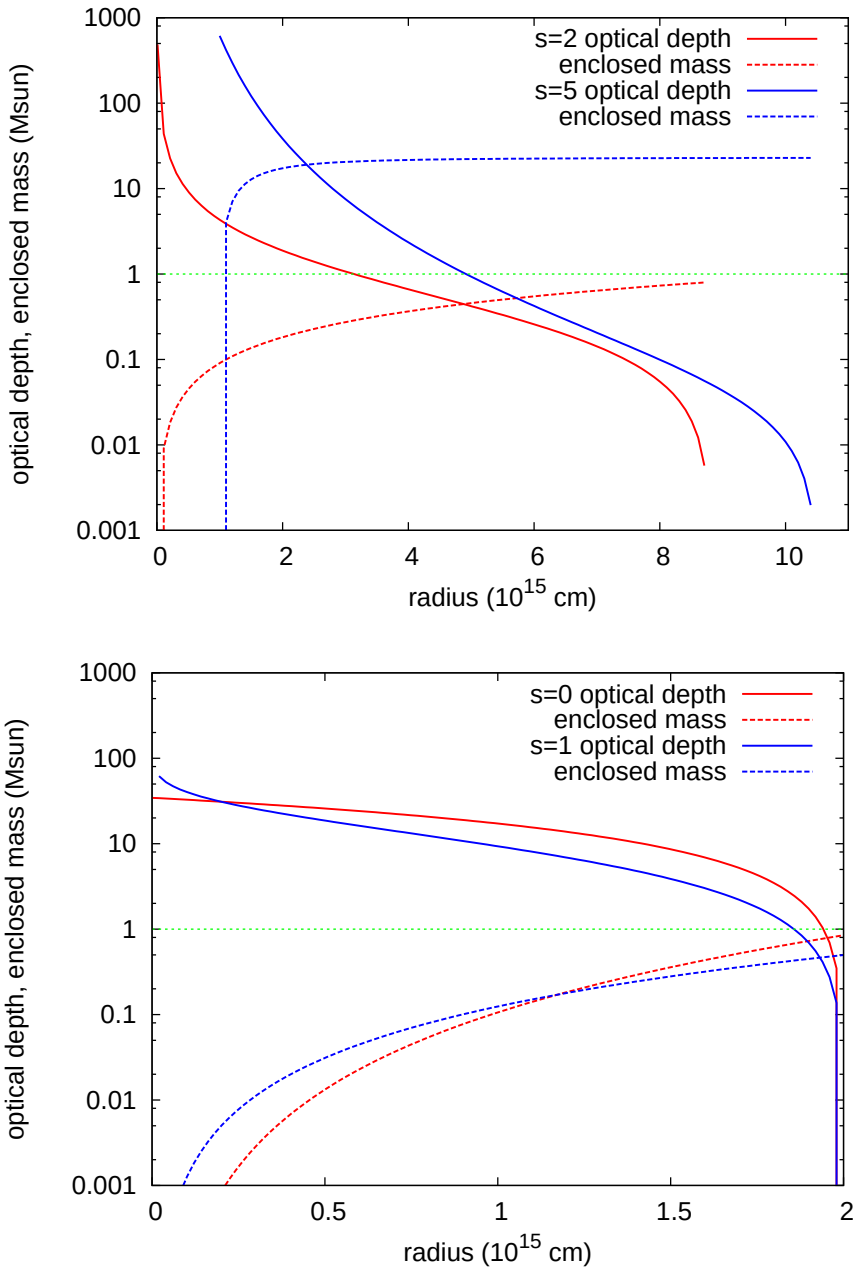

Figure 4.1: *Top:* Optical depth and enclosed mass distribution of the models $s = 2$ and $s = 5$ applied for Type IIn SLSN 2006gy. *Bottom:* Same as the top panel but for the models of Type IIL SLSN 2008es ($s = 0, 1$).

($R_i \ll R_o$) and is much smaller than the value estimated from the shell-shocked diffusion LC model ($\sim 10\ M_\odot$; Smith & McCray 2007). The shell-shocked diffusion model is a too simplified model and we cannot exclude this model just because of the inconsistency with it, as is noted in the previous section. However, we will find in the next section that the numerical modeling of the $s = 2$ model cannot reproduce the observational properties of SN 2006gy. Alternatively, if we adopt a steeper density gradient $s = 5$, x and R_o are estimated to be 0.17 and 1.05×10^{16} cm, respectively, and thus $xR_o \simeq 1.8 \times 10^{15}$ cm and $y_1 R_o \simeq 4.9 \times 10^{15}$ cm. $y_1 R_o$ is consistent with the blackbody radius at the LC peak estimated from the observations (6×10^{15} cm). If we assume that $R_i \simeq 10^{15}$ cm, the mass contained in the optically thick region ($R_i < r < y_1 R_o$) is 22 $M_\odot$ in our $s = 5$ model. The mass of the entire CSM becomes $M_{\rm CSM} \simeq 23\ M_\odot$. The top panel of Figure 4.1 is the optical depth and the enclosed mass distributions.

The spectral evolution of SN 2006gy is also consistent with our model. For example, for the case $s = 5$, $\tau_{\rm csm}$ become $\simeq 10$ at around 3×10^{15} cm (Figure 4.1). This is consistent with $\tau_{\rm csm} \simeq 15$ at 36 days which is estimated from the observed ratio U derived from Hα (Smith et al. 2010a). In our model, the Lorentzian line profiles are expected to be observed before the forward shock wave goes through the optically thick region of the CSM, i.e., before t_d, and thus, the Lorentzian spectra should disappear after the LC peak. This is also consistent with the spectra of SN 2006gy (Smith et al. 2010a).

Narrow Hα P-Cygni profiles can be created at the optically thin CSM above the last scattering surface of the continuum photons ($y_1 R_o < r < R_o$) because of the larger line opacities. Whether the narrow Hα P-Cygni profiles can be formed or not depends also on the ionization level of the CSM and thus the spectral modeling must be performed to see whether the narrow Hα profiles are actually synthesized in the unshocked CSM in our model.

We adopted $v_s \simeq 5,200$ km s^{-1} based on the observed photospheric radius evolution. However, we will find through the numerical LC modeling that the model obtained by assuming $v_s \simeq 5,200$ km s^{-1} is inconsistent with the huge luminosity of SN 2006gy in Section 4.3. We will show that the model with $v_s \simeq 10,000$ km s^{-1} becomes consistent with both the LC and the photospheric LC evolution in Section 4.3.

4.2.1.2 Type IIL SLSNe (SN 2008es)

Now, we apply our model to Type IIL SLSN 2008es (Miller et al. 2009, Gezari et al. 2009). In our model, the lack of the CSM features after the LC peak can be explained by the small difference in t_d and t_s because the entire dense CSM is shocked by the forward shock just after the LC peak. In other words, y_1 should be close to 1. This can be achieved by the CSM slope with $s \lesssim 1$ for the case of $x < 1$ (Figure 2.3).

The following parameters are estimated from the observations of SN 2008es:

$$v_s \simeq 10,000 \text{ km s}^{-1}, \tag{4.4}$$

$$t_d \simeq t_s \simeq 23 \text{ days}. \tag{4.5}$$

If we adopt the model of $s = 0$, y_1 is close to 1 and $R_o \simeq v_s t_s \simeq y_1 R_o \simeq 2 \times 10^{15}$ cm. $y_1 R_o$ is consistent with the blackbody radius at the LC peak estimated from the observations (3×10^{15} cm). Assuming $x = 0.1$ and $R_i \ll R_o$, the CSM mass is $M_{\rm CSM} \simeq 0.85\ M_\odot$. $M_{\rm CSM}$

does not vary so much on x unless it is close to 1. The model with $s = 1$ also gives $y_1 \simeq 1$ with $M_{\rm CSM} \simeq 0.50\ M_\odot$. The bottom panel of Figure 4.1 shows the optical depth and mass distributions. Miller et al. 2009 estimated $M_{\rm CSM} \simeq 5\ M_\odot$ based on the shell-shocked diffusion LC model. Gezari et al. 2009 obtained $M_{\rm CSM} \simeq 0.2\ M_\odot$ based on the peak luminosity. $M_{\rm CSM}$ of both $s = 0$ and $s = 1$ models are almost consistent with those estimates.

Lack of the Lorentzian H Balmer lines before the LC peak is another important difference between Type IIL SLSN 2008es and Type IIn SLSN 2006gy. For the case of the flat density slope, the CSM optical depth remains to be very large until the forward shock reaches the CSM surface (Figure 4.1). Hence, narrow H lines, even if they are emitted from the dense region of the CSM, are scattered by the dense CSM with a large optical depth for a long while. Then, U (Equation 4.1) will be very small until the forward shock reaches the CSM surface and the Lorentzian H lines will be very weak. Thus, it is likely that the Lorentzian H lines are missed. Detailed spectral modeling is required to see the actual spectral evolution expected from the density profile of our model.

4.2.2 Discussion

We have shown that the difference in the density slopes of the dense CSM can make a variety of SLSN II after the shock breakout in the dense CSM. Flat density slopes result in Type IIL SLSNe and steep density slopes result in Type IIn SLSNe. A model with the shock breakout in the dense CSM is first applied to SLSNe by Chevalier & Irwin 2011. Their idea for SN 2006gy is basically the same as our suggestion for Type IIn SLSNe: the shock breakout inside the dense CSM ($x < 1$). However, as they only consider the case $s = 2$, non-Type IIn SLSNe are related to the shock breakout at the surface ($x \simeq 1$) of the dense CSM. Here, we show that the shock breakout does not necessarily occur at the surface to explain non-Type IIn SLSNe, especially Type IIL SLSNe, if the progenitor stars experience non-steady mass loss. Currently, both models can explain Type IIL SLSNe. For the case of the shock breakout inside the dense CSM ($x < 1$), the Lorentzian spectral lines might be able to be observed just before the LC peak when a suitable optical depth is realized. The detailed spectral observations near the LC peak can distinguish the two scenarios. Note that we do not exclude the possibility that steep density slopes can become Type IIL SLSNe. If the density is high enough up to the surface, the steep dense CSM can end up with Type IIL SLSNe, i.e., y_1 becomes close to 1 at $x = 1$ no matter what the density decline is. This configuration corresponds to the shock breakout at the surface and exactly the same as what is suggested by Chevalier & Irwin 2011.

An important difference between our treatment of the shock breakout in a dense CSM from those of the previous works is that we adopt Equation 2.57 for the shock breakout condition instead of Equation 2.56. If we use Equation 2.56, the differences caused by the different density slopes are missed. For example, with Equation 2.56, we do not expect to see narrow spectral lines from the dense CSM after the LC peak of all SLSNe with the shock breakout in the dense CSM and they are all expected to be observed as Type IIL SLSNe. This is because the forward shock is regarded to go through the entire CSM at the LC peak in Equation 2.56.

The different density slope in the dense CSM is naturally expected to be caused by

the non-steady mass loss of the progenitor just before the explosion[2]. If Type IIL SLSNe are actually caused by the shock breakout in the CSM with $t_d/t_s \simeq 1$, it indicates that non-steady mass loss producing the flat dense CSM ($s \lesssim 1$) may take place just before the explosions of some massive stars. In addition, our model for Type IIn SLSN 2006gy prefers $s \neq 2$ because $M_{\rm CSM}$ of the $s = 2$ model may be too small to account for the LC of SN 2006gy after the peak. This will be confirmed in Section 4.3 by numerical modeling. This also supports the existence of the non-steady mass loss at the pre-SN stage of the massive stars (see also Chapter 3). Although the CSM densities of SNe treated in Chapter 3 are not high enough to be SLSNe, it is highly possible that the dense CSM from higher mass-loss rates also result in flat or steep density slopes. The presence of the two kinds of slopes can end up with two different kinds of SLSN II.

So far, we just consider a single slope in the dense CSM. The essential difference between Type IIn and Type IIL SLSNe is the existence of the spatially-large optically-thin region in the CSM of Type IIn SLSNe which can make narrow P-Cygni profiles. Although we show that large s can make such spatially-large optically-thin region with the optically thick region inside, the similar condition can also be achieved by assuming the two components in the CSM, i.e., optically thick (inside) and thin (outside) regions with any density slopes. The two-component CSM configuration is suggested for, e.g., SN IIn 1998S (Chugai 2001). Both models can explain Type IIn SLSNe. In either case, the P-Cygni profiles can be observed not only after but also before the LC peak. Currently, there are no spectral observations of Type IIn SLSNe before the LC peak with resolutions sufficient to resolve the narrow P-Cygni profile and the high resolution spectroscopic observations before the LC peak are important to reveal the CSM around SLSN II.

While we focus on the origin of Type IIL SLSNe in this section, the understanding of other SNe IIL, i.e., less-luminous SNe IIL, is also lacking. Currently, there are many models for SNe IIn but only a few models exist for SNe IIL (e.g., Blinnikov & Bartunov 1993, Swartz et al. 1991). Although the diversity in the CSM condition may be related to other SNe IIL, there can be other important, but currently ignored, ingredients for the full understanding of SNe IIL.

4.2.3 Summary

We have investigated the effect of the non-steady mass loss on the shock breakout in the dense CSM in this section. The non-steady mass loss varies the density slope of the CSM ($\rho_{\rm csm} \propto r^{-s}$) and the density slope alters the ratio of the diffusion timescale in the optically thick CSM (t_d) and the shock propagation timescale of the entire CSM (t_s) after the shock breakout in the CSM. Both timescales are comparable ($t_d/t_s \simeq 1$) for $s \lesssim 1$ and t_d/t_s becomes smaller as s gets larger (Section 2.4.1.2). The difference can only be obtained by the careful treatment of the shock breakout condition in the dense CSM (Section 2.4.1.1, Equation 2.57).

If the two timescales are comparable ($t_d/t_s \simeq 1$), the forward shock goes through the entire CSM just after the LC reaches the peak with the timescale t_d. In this case, no signature on

[2] Note that the flat density distribution of the CSM can also be caused by the steady mass loss of two different evolutionary stages (e.g., Dwarkadas 2011). Although the model shown in Dwarkadas 2011 is not dense enough to result in SLSNe, the flat density slope might result in Type IIL SLSNe if sufficiently high density is achieved.

the spectra from the CSM is expected to be observed especially after the LC peak because the entire CSM is already shocked after the LC peak. On the other hand, if the two timescales are different ($t_d/t_s < 1$), the shock continues to propagate in the CSM after the LC peak and the unshocked CSM remains after the LC peak. Thus, narrow P-Cygni profiles from the CSM are expected to be observed even after the LC peak. The former case corresponds to Type IIL SLSNe and the latter to Type IIn SLSNe. The difference in the density slope can also account for the lack of the Lorentzian emission profiles in Type IIL SLSNe.

Our results imply that the luminosity of Type IIL SLSNe can be explained in the context of the interaction between SN ejecta and the dense CSM even if they do not show the signature of the CSM in their spectra. We propose that the difference between Type IIn and Type IIL SLSNe can stem from the density slope of the dense CSM which results from the non-steady mass loss of their progenitors.

4.3 Type IIn SLSN 2006gy

SN 2006gy is the best observed SLSN ever. It is SLSN II and had very narrow H lines (Type IIn). Here in this section, we model SN 2006gy in detail to know the nature and the progenitor of SN 2006gy. Through this modeling, we aim at having a better understanding of SLSN II. As we will see, we constrain the initial conditions by using the analytical timescale estimates of the previous sections and show numerically that the simple analytic estimates can constrain the CSM properties of SLSN II well.

4.3.1 Brief Summary of Observations

We briefly summarize the observational properties of SN 2006gy. SN 2006gy was discovered by Texas Supernova Search on September 18, 2006 (UT) near the nucleus of an early-type galaxy NGC 1260 (Quimby 2006). There are several suggested values for the extinction by the host galaxy (Ofek et al. 2007, Smith et al. 2007, Agnoletto et al. 2009). We adopt $E(B-V)_{\rm host} = 0.40$ mag following Agnoletto et al. 2009 with the Milky Way extinction $E(B-V)_{\rm MW} = 0.16$ mag (Schlegel et al. 1998). Thus, the total extinction is $E(B-V) = 0.56$ mag or $A_R = 1.3$ mag with $R_V = 3.1$ (Cardelli et al. 1989). The distance modulus μ of the host galaxy is also taken from Agnoletto et al. 2009 ($\mu = 34.53$ mag).

Follow-up spectral observations classified SN 2006gy as Type IIn because of the narrow H emission lines presented in the spectra. The luminosity of SN 2006gy kept rising until October 25, 2006 (UT) and the peak R band luminosity got close to $\simeq -22$ mag. The rising time is estimated as about 70 days (hereafter, days are in the rest frame). After reaching the peak luminosity, the LC declined slowly ($\simeq 0.02$ mag day^{-1}) for $\simeq 120$ days and then the LC stayed almost constant for $\simeq 20$ days until SN 2006gy hid behind the Sun. NIR LCs in these early epochs are consistent with the blackbody temperature obtained from the optical spectra and no significant excess was detected (Miller et al. 2010). No X-ray was detected when the LC was rising (Ofek et al. 2007) but weak X-rays may have been detected during the declining phase (Smith et al. 2007). No radio emission is detected at any observed epochs (Ofek et al. 2007, Chandra et al. 2007, Argo et al. 2007, Bietenholz & Bartel 2007, Bietenholz & Bartel 2008a, Bietenholz & Bartel 2008b).

Optical spectra of the early epochs are also taken intensively (e.g., Smith et al. 2010a, Agnoletto et al. 2009). Spectra taken before the LC peak are characterized by Lorentzian Hα emission lines (Smith et al. 2010a). The origin of the Lorentzian profile is related to the existence of optically thick CSM (e.g., Chugai 2001, Dessart et al. 2009). Except for the narrow H emission lines, the spectra are featureless and characterized by blackbody with depletion in blue (Smith et al. 2010a, Agnoletto et al. 2009). The reason for the lack of features may be partly because the spectra before the LC peak were taken only with low resolutions. After the LC peak, overall Hα line profiles can be fitted by two Gaussian components with full widths at half-maximum of 1,800 km s^{-1} and 5,200 km s^{-1} and they are presumed to come from the interacting region between the ejecta and dense CSM (e.g., Smith et al. 2010a). There also exists a broad absorption in the blue part of the Hα profile which is suggested to originate from the ejecta inside. In addition, the spectra of SN 2006gy show narrow P-Cygni profiles from several elements (e.g., H, Fe) with the outflowing velocity $\simeq$ 100 km s^{-1}. As the velocity is too slow to attribute it to the ejecta inside, those narrow lines are presumed to originate from the unshocked CSM. The strengths of these narrow lines decline with time and they are barely seen in the spectrum taken at $\simeq$ 140 days since the LC peak (Smith et al. 2010a).

About 100 days later, SN 2006gy came out of the Sun and was observed again (Agnoletto et al. 2009, Kawabata et al. 2009, Miller et al. 2010). The optical luminosity of SN 2006gy declined dramatically (about 2 mag in the R band) which was almost constant for $\simeq$ 20 days before the SN went behind the Sun. The luminosity declined very slowly ($\simeq$ 0.002 mag day^{-1}) since it appeared from the Sun for more than 400 days until the last reported observation on November 22, 2008 (UT) (Kawabata et al. 2009, Miller et al. 2010). The decline rate is much slower than that of ^{56}Co decay (0.01 mag day^{-1}) and the main source of the luminosity cannot be the ^{56}Co decay. Because of the high NIR luminosities, Smith et al. 2008, Miller et al. 2010 suggest that the late time luminosity is due to light echoes. The optical spectra of those epochs are dominated by intermediate width emission lines ($\simeq 2,000$ km s^{-1}, Kawabata et al. 2009). H emission lines were weaker than those observed in the previous epochs and suggest that the interaction is weaker in those epochs and it is no longer a main source of the radiation (Agnoletto et al. 2009, Kawabata et al. 2009). Weakness of Fe lines in those epochs seems inconsistent with the large ^{56}Ni production (Kawabata et al. 2009).

4.3.2 Initial Conditions

In this section, we show how the initial conditions of our LC calculations are constructed. Two components exist in the initial conditions: SN ejecta inside and a dense CSM outside. We assume that there is a gap between the progenitor and the dense CSM. Then, it takes some time for the SN ejecta to reach the dense CSM and start to collide. We assume that the SN ejecta freely expands in the gap before the collision. We numerically follow the LCs after the collision. The initial conditions of the two components, SN ejecta and a dense CSM, are constructed based on the two timescales which are analytically estimated in Section 2.4.1 and observationally constrained in Section 4.2.1.1, i.e., the diffusion timescale t_d and the shock propagation timescale t_s in dense CSM. The validity of these initial conditions will

be confirmed by our numerical LC calculations as we show in the later sections. The initial density structures of two representative models are shown in Figure 4.2 as examples. Both SN ejecta and CSM are assumed to have solar metallicity and no ^{56}Ni is included in our calculations unless it is otherwise mentioned. The summary of the models is given in Table 4.1.

4.3.2.1 Supernova Ejecta

SN ejecta structures are constructed by using the same assumption made in the previous chapters. We briefly summarize them here. SN ejecta before the collision is assumed to be freely expanding with a homologous velocity profile. The analytic approximation for the density structure of SN ejecta provided by, e.g., Chevalier & Soker 1989 is adopted:

$$\rho_{\rm ej}\left(v_{\rm ej},t\right)=\begin{cases}\frac{1}{4\pi(n-\delta)}\frac{[2(5-\delta)(n-5)E_{\rm ej}]^{(n-3)/2}}{[(3-\delta)(n-3)M_{\rm ej}]^{(n-5)/2}}t^{-3}v_{\rm ej}^{-n} & (v_{\rm ej}>v_t),\\ \frac{1}{4\pi(n-\delta)}\frac{[2(5-\delta)(n-5)E_{\rm ej}]^{(\delta-3)/2}}{[(3-\delta)(n-3)M_{\rm ej}]^{(\delta-5)/2}}t^{-3}v_{\rm ej}^{-\delta} & (v_{\rm ej}<v_t),\end{cases} \tag{4.6}$$

where v_t is defined in Section 2.3. In this section, we adopt $\delta=1$ and $n=7$, which is assumed by Chevalier & Irwin 2011. The maximum velocity of the SN ejecta before the interaction is chosen to be high enough, so that most of the assumed $E_{\rm ej}$ is contained in the SN ejecta. It is around $20,000-50,000$ km s^{-1}.

$M_{\rm ej}$ is difficult to be constrained only by the observations of the LC of SN 2006gy because the LC is mainly affected by CSM as is shown in the following sections. In most of the models, we adopt $M_{\rm ej}=20\ M_\odot$ because the progenitors of SNe IIn are presumed to be originated from relatively massive stars. Effect of $M_{\rm ej}$ on LCs is discussed in Sections 4.3.3.2 and 4.3.4.1.

4.3.2.2 Circumstellar Media

Dense CSM in the calculations is assumed to exist from R_i to R_o from the center and have a density structure $\rho_{\rm csm}\propto r^{-s}$. The outflowing velocity of the CSM is 100 km s^{-1}. It is estimated from the narrow P-Cygni profile of Hα appeared in the spectra of SN 2006gy (e.g., Smith et al. 2010a). The CSM is assumed to be optically thick enough to cause the shock breakout within it. We estimate the physical conditions of the CSM from the observations by using the shock breakout condition described in Sections 2.4.1. One main purpose of this section is to see how well the properties of the dense CSM predicted by this simple shock breakout model in the CSM can explain the overall LC features of SN 2006gy. We use following three values which can be estimated from the observations to derive the CSM properties: the photon diffusion time t_d in the CSM, the propagation time t_s of the forward shock through the CSM, and the forward shock velocity v_s. As discussed in Section 2.4, t_d corresponds to the rising time of the LC and t_s corresponds to the time when the narrow P-Cygni Hα profiles from the CSM disappears. We adopt $t_d=70$ days and $t_s=194$ days (Section 4.2.1). v_s can be estimated from the spectral evolution.

With t_d, t_s, and v_s, we can estimate the outer radius R_o of the CSM and the radius xR_o where the shock breakout occurs ($R_i/R_o<x<1$) for a given s based on the shock breakout model. The shock breakout condition predicts the following relations for the three values

Table 4.1: List of LC models

Name	v_s	$M_{\rm ej}$	$E_{\rm ej}$	s	R_o	$y_1 R_o$	$x R_o$	R_i	$M_{\rm CSM}$	$\left\langle \dot{M} \right\rangle^a$	B_q
	km s^{-1}	$M_\odot$	10^{51} erg		10^{15} cm	10^{15} cm	10^{15} cm	10^{15} cm	$M_\odot$	$M_\odot$ yr^{-1}	
A1	5,200	20	50	5	11	4.9	1.8	1.0	22	0.70	1
A2	5,200	20	50	5	11	4.9	1.8	1.5	10	0.33	1
B1	5,200	20	10	2	8.8	3.3	0.090	0.090	0.83	0.030	1
B2	5,200	20	30	2	8.8	8.3	2.0	0.090	27	0.98	1
C1	5,200	20	50	0	4.9	4.8	1.8	1.0	14	1.1	1
D1	10,000	20	10	5	21	11	4.6	4.5	22	0.42	1
D2	10,000	20	10	5	21	11	4.6	5.0	18	0.36	1
E1	10,000	20	30	2	17	6.3	0.32	0.10	3.2	0.060	1
E2	10,000	2	10	2	17	6.3	0.32	0.10	3.2	0.060	1
F1	10,000	20	10	0	11	11	4.6	5.0	15	0.45	1
D3	10,000	10	10	5	21	11	4.6	5.0	18	0.36	1
D4	10,000	30	10	5	21	11	4.6	5.0	18	0.36	1
D5	10,000	10	5	5	21	11	4.6	5.0	18	0.36	1
D6	10,000	20	10	5	21	11	4.6	5.0	18	0.36	0.33
D7	10,000	20	10	5	21	11	4.6	5.0	18	0.36	3

[a] Average mass-loss rate. $\left\langle \dot{M} \right\rangle = v_{\rm w} M_{\rm CSM}/(R_o - R_i)$ where $v_{\rm w} = 100$ km s^{-1} is the assumed CSM velocity.

(Section 2.4):

$$t_d \simeq \begin{cases} \frac{R_o}{v_s}\left[\left(\frac{c/v_s+x^{1-s}}{c/v_s+1}\right)^{\frac{1}{1-s}}-x\right] & (s\neq 1), \\ \frac{R_o}{v_s}\left(x^{\frac{1}{1+c/v_s}}-x\right) & (s=1), \end{cases} \tag{4.7}$$

$$t_s \simeq \frac{R_o - xR_o}{v_s}. \tag{4.8}$$

We try $s = 0, 2, 5$. The models with $s = 2$ corresponds to the case of the steady mass loss and they are naturally expected structures for CSM. A steep CSM density gradient with $s = 5$ is suggested for SN 2006gy in Section 4.2.1. We also show $s = 0$ models which are difficult to be excluded only by the LC modeling.

It turns out in the later sections that it is difficult to estimate v_s from observational values self-consistently. This is partly because v_s is not an independent parameter and, in principle, can be derived for a given CSM structure if we specify $E_{\rm ej}$ and $M_{\rm ej}$. However, v_s is also strongly affected by the conversion efficiency from the kinetic energy to radiation through the interaction and it is unknown at first. Thus, it is difficult to estimate v_s from the first principles. Hence, we set v_s as a free parameter in this section. At first, we try to estimate it from the observations. As the blackbody radius of SN 2006gy expands linearly with the velocity $5,200$ km s^{-1}, one may estimate that $v_s = 5,200$ km s^{-1}. However, the required $E_{\rm ej}$ for the $v_s = 5,200$ km s^{-1} models to explain the peak luminosity of SN 2006gy is found to be very high and it becomes inconsistent with the relatively low v_s. In other words, the SLSN models obtained by setting $v_s = 5,200$ km s^{-1} are not self-consistent. Thus, we also try models with higher v_s, namely, $v_s = 10,000$ km s^{-1}. The $v_s = 10,000$ km s^{-1} models are found to work well self-consistently as is shown in the following sections. In addition, the linear evolution of the blackbody radius with $5,200$ km s^{-1} is found to be able to be explained by the $v_s = 10,000$ km s^{-1} models. With $t_d = 70$ days, $t_s = 194$ days, and the given v_s, we can derive R_o and xR_o from Equations 4.7 and 4.8 for a specified s. In the rest of this section, we show the details of the two v_s models.

$v_s = 5,200$ km s^{-1} Model

This model corresponds to the SN 2006gy model we adopted in Section 4.2.1. The shock velocity $v_s = 5,200$ km s^{-1} is estimated from the observed evolution of the blackbody radius of SN 2006gy (Smith et al. 2010a). For $s = 5$, we get $R_o = 1.1\times10^{16}$ cm and $xR_o = 1.8\times10^{15}$ cm from Equations 4.7 and 4.8. The inner radius R_i of the CSM cannot be constrained by the above observables and it is a free parameter. Two R_i are tried: 10^{15} cm (A1) and 1.5×10^{15} cm (A2). With $s = 2$ (steady mass loss), we get $R_o = 8.8\times10^{15}$ cm and $xR_o = 9.0\times10^{13}$ cm (B1). We set $R_i = xR_o$ in the $s = 2$ models. The results do not depend so much on R_i in this case because most of the mass in the $s = 2$ CSM is distributed in the outer part of the CSM. We also calculate LCs from the model (B2) in which the CSM mass is artificially increased 30 times of the model B1.

In the $s = 0$ models, t_s becomes similar to t_d ($t_s \simeq t_d$) (Section 2.4). Thus, the entire CSM is shocked with t_d and no unshocked CSM remains after the LC peak. This is against

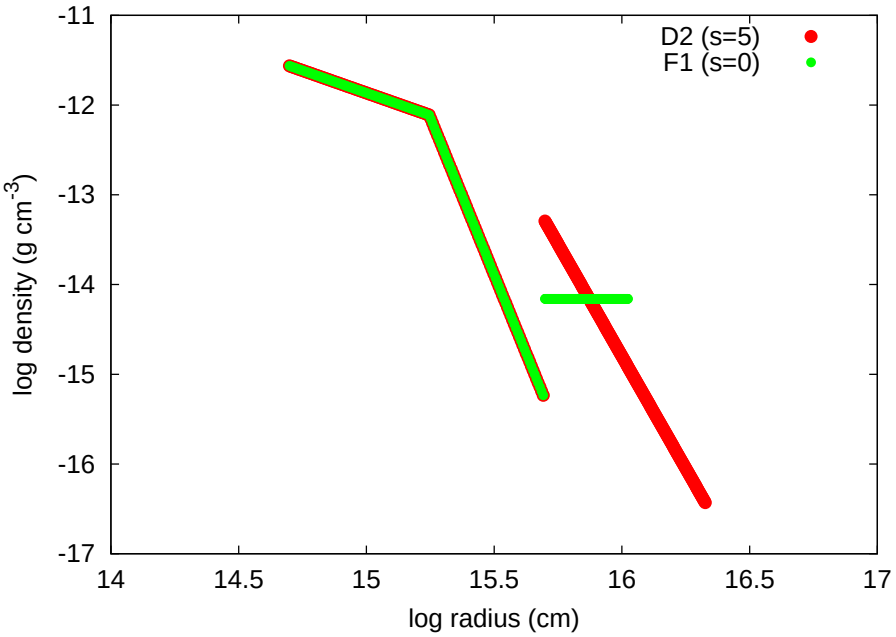

Figure 4.2: The density structures of the models D2 ($s = 5$) and F1 ($s = 0$) before the collision. These density structures are set as the initial conditions of the numerical LC calculations. The structure inside the density jump corresponds to the SN ejecta which is assumed to be freely expanding before the collision. The dense CSM exists above the density jump. The initial condition of the dense CSM is obtained based on the shock breakout model within the CSM.

the observations of SN 2006gy because narrow P-Cygni profiles are observed after the LC peak. However, this is only true when we only think a single $s = 0$ CSM component. If there is another CSM component outside the main CSM which is not dense enough to affect the LC but the spectra, SN 2006gy-like SNe can appear. Thus, the $s = 0$ models are difficult to be excluded only by the LC. From the rising time of the LC, we can presume $y_1 R_o - xR_o \simeq R_o - xR_o \simeq v_s t_d = 3.1 \times 10^{15}$ cm. $y_1 R_o$ is the radius where the optical depth from the surface of the CSM becomes 1 and $y_1 R_o \simeq R_o$ when $s = 0$ (see Section 2.4 for the details). We set the last scattering surface of the $s = 5$ model ($y_1 R_o = 4.9 \times 10^{15}$ cm) as R_o so that we can compare the results with those of the $s = 5$ models. Thus, $xR_o = 1.8 \times 10^{15}$ cm is also the same as the $s = 5$ model and we adopt $R_i = 10^{15}$ cm (C1).

$v_s = 10,000$ km s^{-1} Model

$v_s = 10,000$ km s^{-1} models are constructed by following the same way as the $v_s = 5,200$ km s^{-1} models. With $t_d = 70$ days, $t_s = 194$ days, and $v_s = 10,000$ km s^{-1}, $R_o = 2.1 \times 10^{16}$ cm and $xR_o = 4.6 \times 10^{15}$ cm are obtained for $s = 5$. We try two R_i: 4.5×10^{15} cm (D1) and 5×10^{15} cm (D2 - D7). Although $R_i = 5 \times 10^{15}$ cm is slightly larger than the shock breakout radius $xR_o = 4.6 \times 10^{15}$ cm, it turns out that the model gets

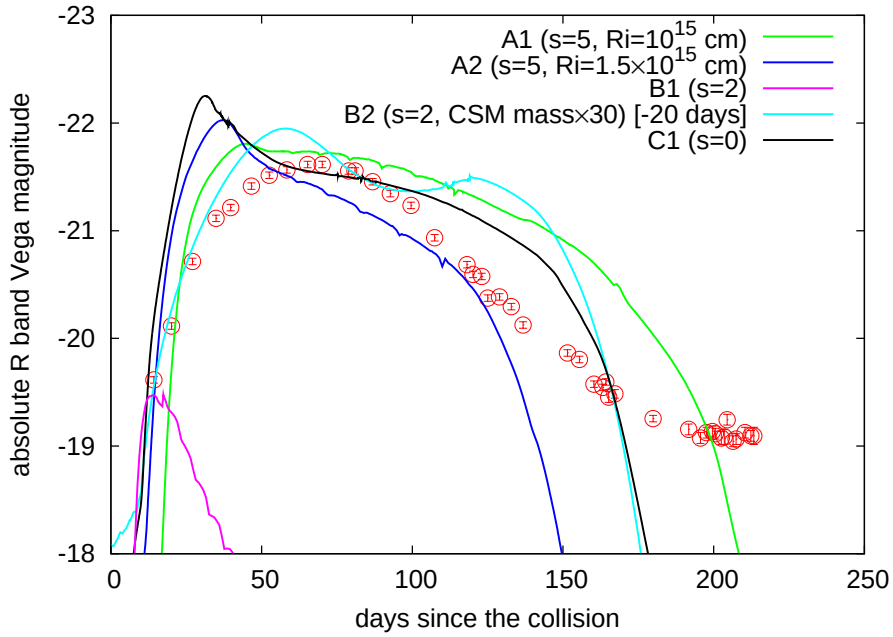

Figure 4.3: Absolute R band LCs of the $v_s = 5,200$ km s^{-1} models. These models are not self-consistent. The origin of time axis is set to when our numerical calculations start, i.e., when the SN ejecta and CSM start to collide, except for B2. The time of the model B2 is shifted -20 days.

closer to the SN 2006gy LC. Given the approximated way of our estimations, the difference is within an acceptable range. The steady mass-loss models ($s = 2$) gives $R_o = 1.7 \times 10^{16}$ cm and $xR_o = 3.2 \times 10^{14}$ cm (E1, E2). For $s = 0$, $R_o - xR_o \simeq v_s t_d = 6 \times 10^{15}$ cm ($y_1 R_o \simeq R_o$). As $y_1 R_o = 1.1 \times 10^{16}$ cm in $s = 5$ model, we adopted $R_o = 1.1 \times 10^{16}$ cm and $xR_o = R_i = 5 \times 10^{15}$ cm (F1).

4.3.3 Light Curve Models

Starting from the initial conditions obtained in Section 4.3.2, we perform the numerical LC calculations with `STELLA`. We show that the $v_s = 5,200$ km s^{-1} models cannot explain the huge luminosity of SN 2006gy self-consistently. LCs obtained from $v_s = 10,000$ km s^{-1} models are broadly consistent with the observational properties of SN 2006gy.

4.3.3.1 $v_s = 5,200$ km s^{-1} Model

Figure 4.3 shows the LCs from the $v_s = 5,200$ km s^{-1} models with the observed R band LC. $E_{\rm ej}$ is chosen so that the peak luminosities of the model LCs can be as luminous as that of SN 2006gy. However, $E_{\rm ej}$ should be very high ($\simeq 5 \times 10^{52}$ erg) for the $v_s = 5,200$ km s^{-1} models to be as luminous as SN 2006gy and assuming the relatively low $v_s = 5,200$ km s^{-1} is not consistent with the high kinetic energy. This inconsistency can also be seen from the rising times of the models. Although the models are constructed so that the rising times of

the LCs become $t_d = 70$ days, the rising times of the numerical results are much shorter than 70 days. If we set smaller $E_{\rm ej}$, the rising times can be the same as that of SN 2006gy but then the luminosities become much smaller than that of SN 2006gy. Shortly, the models derived by assuming $v_s = 5,200$ km s^{-1} are not compatible with the large luminosity of SN 2006gy. Given these results, we adopt models with a higher v_s, $v_s = 10,000$ km s^{-1}, and they are found to be able to explain the LC of SN 2006gy self-consistently (Section 4.3.3.2).

One important question of the interaction model is whether the CSM from the steady mass loss ($s = 2$) can explain the properties of SLSNe and we look into the $s = 2$ models more carefully. If it can, a mechanism to achieve such huge steady mass loss may exist. If not, it is indicated that explosive non-steady mass loss takes place in their progenitors and there should exist some mechanisms to cause such mass loss shortly before their explosions.

The $s = 2$ model B1 reaches only $\simeq -19.5$ mag in the R band at the LC peak. This is because $M_{\rm CSM} = 0.83\ M_\odot$ in the B1 model is much smaller than $M_{\rm CSM}$ of the models with the other s. The fraction of the kinetic energy converted to radiation in the model B1 is much smaller than those in the models A1, A2, and C1, as the amount of energy converted from kinetic energy to radiation strongly depends on the relative mass of CSM and SN ejecta (see Section 4.3.4.1). Thus, more kinetic energy is required for the B1 model to be as luminous as SN 2006gy. However, the rising time of the B1 model is already much less than that of SN 2006gy and it becomes shorter if we increase kinetic energy. Thus, the $v_s = 5,200$ km s^{-1} model with the steady mass loss ($s = 2$, B1) is hard to be compatible with SN 2006gy. For demonstration, we also calculated a model (B2) in which $M_{\rm CSM}$ is increased 30 times more than that of the model B1. Then, the amount of energy converted increases because of the high efficiency for the energy conversion. In addition, the photospheric radius is increased due to the increased density. As a result, the luminosity of the model becomes as large as that of SN 2006gy.

4.3.3.2 $v_s = 10,000$ km s^{-1} Model

As $v_s = 5,200$ km s^{-1} models are not able to explain SN 2006gy self-consistently, we investigate models with higher v_s, $v_s = 10,000$ km s^{-1}. $v_s = 5,200$ km s^{-1} is estimated from the evolution of the blackbody radius but it is shown that the evolution of the blackbody radius in the $v_s = 10,000$ km s^{-1} models is consistent with that of SN 2006gy.

Light Curve

The R band LCs from the $v_s = 10,000$ km s^{-1} models are shown in Figure 4.4. Multicolor LCs of the models D2 ($s = 5$) and F1 ($s = 0$) are shown in Figure 4.5 and the bolometric LCs of the two models are shown in Figure 4.6. The color and spectral evolution of the models D2 and F1 are shown in Figures 4.7 and 4.8, respectively.

The rising parts and the peak luminosities of the LCs of the $s = 0, 5$ models are consistent with SN 2006gy. Thus, the $v_s = 10,000$ km s^{-1} models are self-consistent with the assumed $E_{\rm ej}$ and $M_{\rm ej}$. The $v_s = 10,000$ km s^{-1} models only require $E_{\rm ej} = 10^{52}$ erg to achieve the peak luminosity of SN 2006gy, instead of $E_{\rm ej} \simeq 5 \times 10^{52}$ erg required for the $v_s = 5,200$ km s^{-1} models. This is because the blackbody radius in the CSM can be larger in the

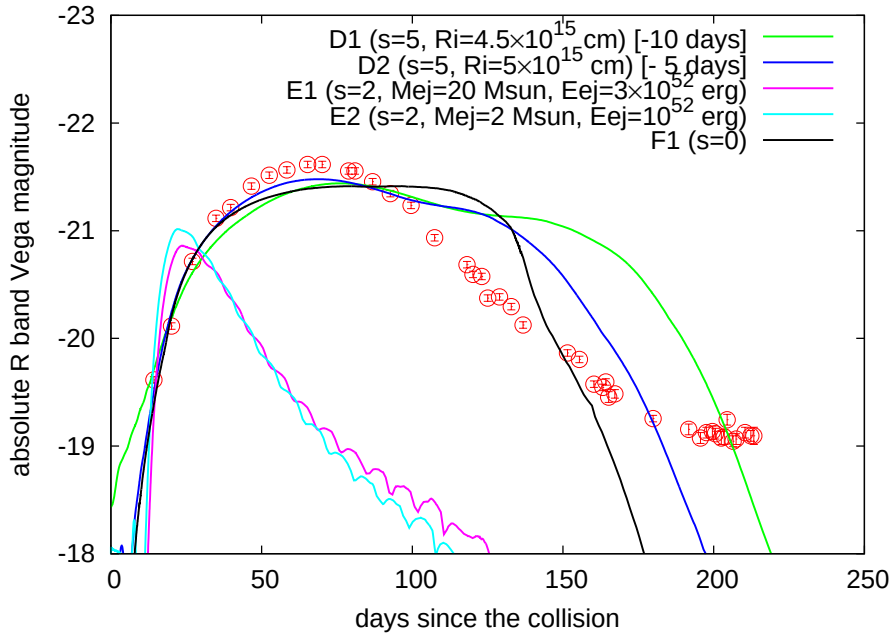

Figure 4.4: Absolute R band LCs of the $v_s = 10,000$ km s^{-1} models. These models can self-consistently explain the rising time and the peak luminosity of SN 2006gy. The origin of the time axis is +10 days (D1), +5 days (D2), 0 days (E1, E2, and F1) since the collision.

$v_s = 10,000$ km s^{-1} models and less energy is required to achieve the same luminosity. The steady mass-loss models ($s = 2$) are, however, still not consistent with SN 2006gy.

The model LCs with $s = 0, 5$ after the peak start to deviate from the observed LCs, but the deviations stay less than one magnitude before the plateau in the observed LC at around 200 days. Our model R band LCs take some time after the LCs have reached the peak until the LCs start to decline, contrary to the observed R band LC of SN 2006gy. This is because there remains unshocked optically thick CSM even after the LC peak in our numerical models and the photosphere remains there for a while. The analytic model in Section 2.4 which we use to estimate the initial conditions assumes a constant v_s. However, v_s actually reduces as the interaction goes on and the optically thick part of the CSM is not shocked away entirely at the time t_d when the optically thick CSM is assumed to be swept up by the forward shock in the model in Section 2.4. This effect is more significant in $s = 0$ models because $s = 0$ models suffer more from the deceleration than $s = 5$ models. A severe failure of our models is that all of them fail to reproduce the plateau in the LC of SN 2006gy at around 200 days. We discuss this separately in Section 4.3.4.2.

Looking at the multicolor LCs (Figure 4.5), the $s = 0$ model (F1) is closer to the observed LC, especially the B band LC of the rising epochs. This is presumed to be because the initial density jump between SN ejecta and CSM is smaller in the $s = 0$ model (Figure 4.2) and the temperature becomes lower in the $s = 0$ model. However, the LCs in the B bands can be affected by many weak absorption lines of Fe group elements which are not taken into account in our opacity. Those weak absorptions may reduce the luminosity of the B band

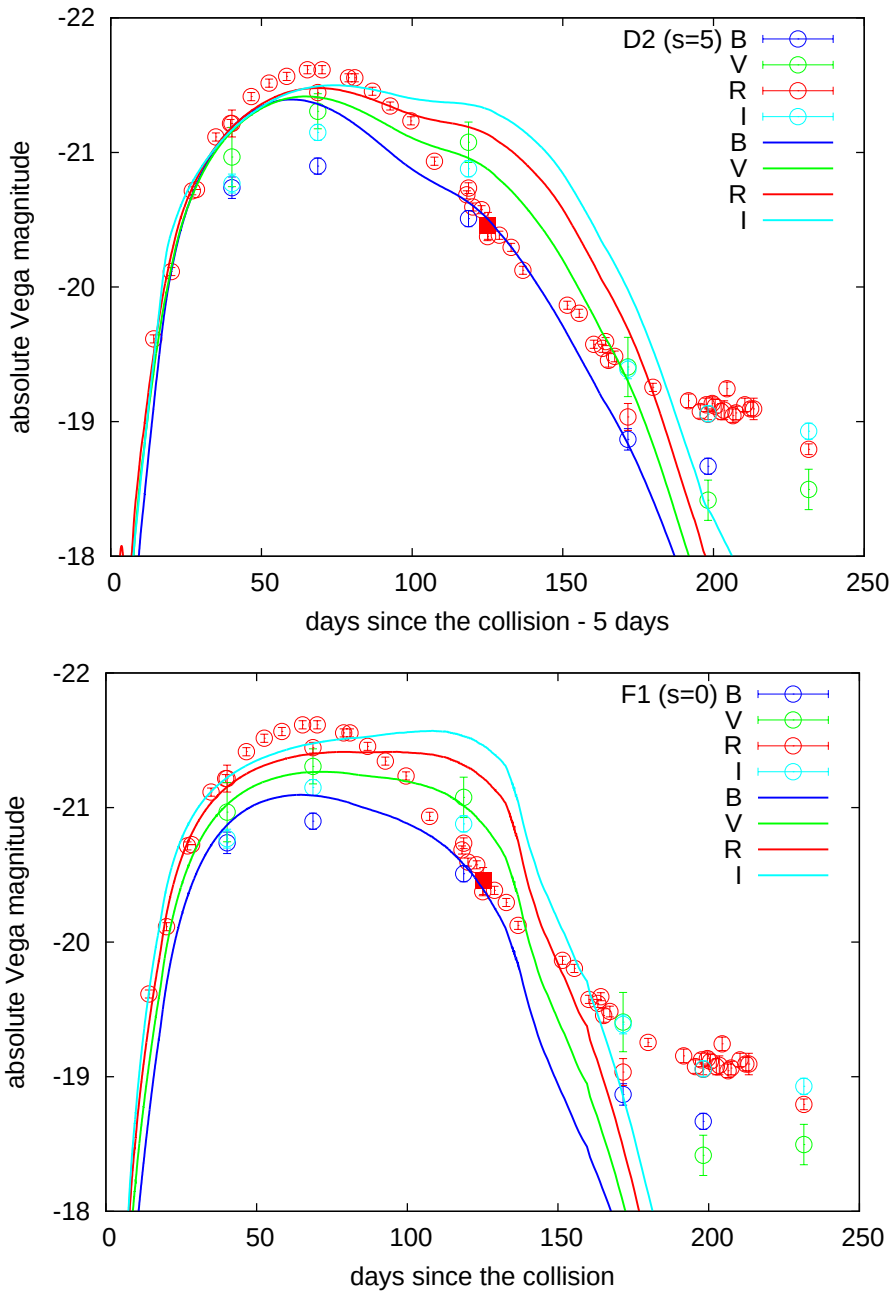

Figure 4.5: Multicolor LCs of the models D2 ($s = 5$, top) and F1 ($s = 0$, bottom). The observational data are from Smith et al. 2007, Agnoletto et al. 2009, Kawabata et al. 2009. The origin of the time axis in the top (bottom) panel is 5 (0) days since the collision.

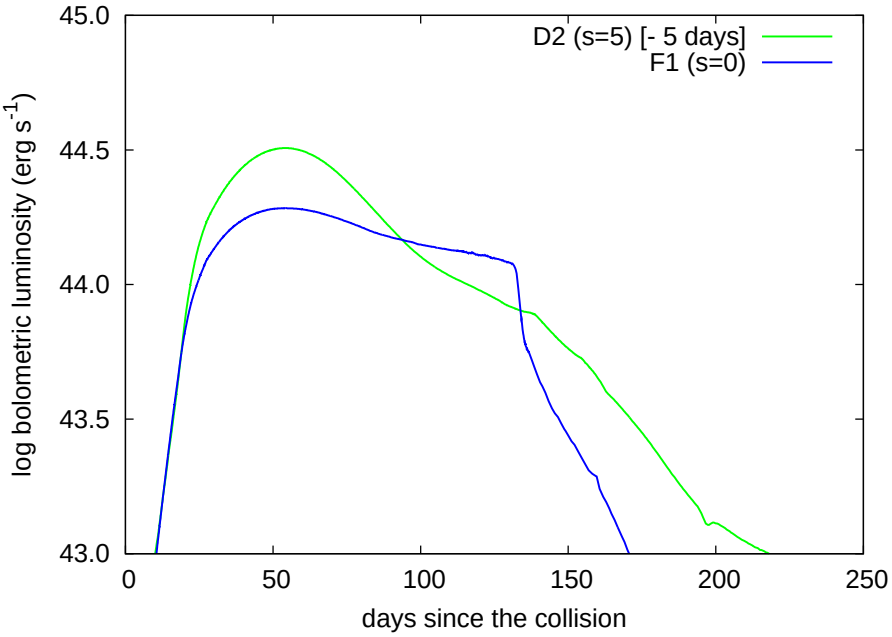

Figure 4.6: Bolometric LCs of the models D2 ($s = 5$) and F1 ($s = 0$). The origin of the time axis in the D2 (F1) model is 5 (0) days since the collision.

LCs and we cannot judge which model is better based just on the blue part of the LCs. In addition, the difference is $\simeq 0.5$ mag and they are not significant. The color evolution of the two models (Figure 4.7) roughly follows the observed evolution, although there exist some deviations especially in $R - I$ and $V - R$.

Although it is possible to continue LC modeling to get much better fits to the SN 2006gy LC, it does not necessarily lead us to the better understanding of the properties of the SN ejecta and the dense CSM involved in the progenitor system of SN 2006gy. This is mainly because of the simplified physics adopted in `STELLA`. Especially, `STELLA` is a one-dimensional code and multidimensional effects are approximately incorporated by adopting the smearing parameter. As the uncertainties involved in the parameter are large (see later discussion in this section), making a perfect fit to the observed LC does not necessarily provide us with the best parameters. In addition, the differences in the LCs in the declining phases are less than one magnitude (or a factor $\simeq 2$) and the differences in the rising phases are much less. Thus, the properties of the SN ejecta and the dense CSM in the D2 and F1 models are presumed not to be so different from the 'actual' values. Thus, we conclude that the CSM parameters predicted by the shock breakout model can explain the overall properties of SN 2006gy. We also note that a systematical study of the effect of the CSM properties on the LCs powered by the interaction between SN ejecta and dense CSM is summarized in Section 5.3. The durations of the LCs of the models D2 and F1 are a bit longer than that of SN 2006gy. To reduce the durations of the LCs by keeping the peak luminosities of them, we can, for example, change the radii of the CSM.

Finally, we look into the steady mass loss models to see whether they actually fail to

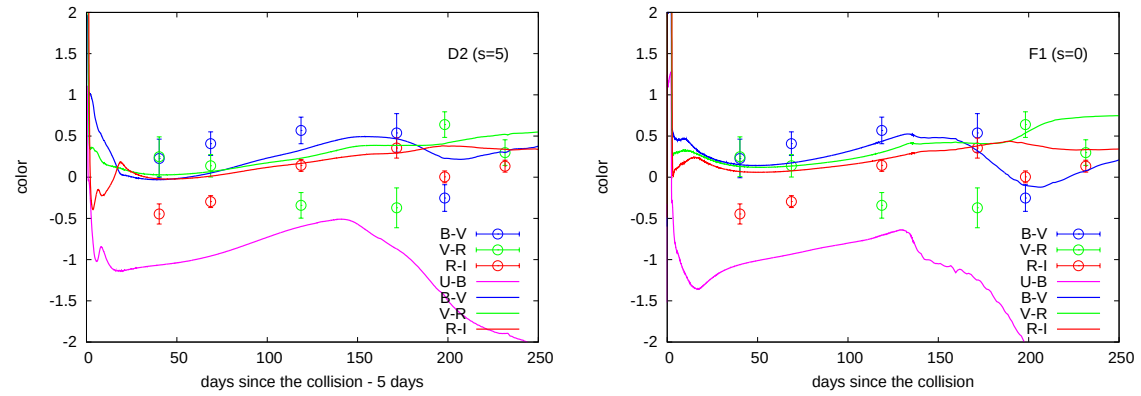

Figure 4.7: Color evolution of the models D2 ($s = 5$, left) and F1 ($s = 0$, right). Observational points are from Agnoletto et al. 2009.

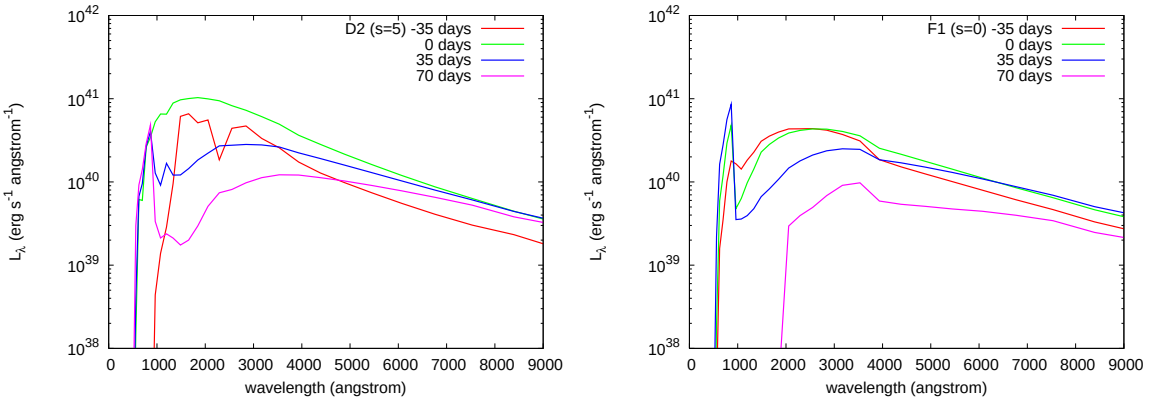

Figure 4.8: SEDs of the models D2 ($s = 5$, left) and F1 ($s = 0$, right). Days since the LC peak are shown in the figure.

reproduce the LC of SN 2006gy. The steady mass-loss model ($s = 2$, E1) is, again, too faint to explain SN 2006gy with $E_{\rm ej} = 3 \times 10^{52}$ erg. The rising time is already too short and reaching the peak luminosity of SN 2006gy by increasing $E_{\rm ej}$ does not work as is discussed in Section 4.3.3.1. This is because of the too small $M_{\rm CSM}$ and can be improved if $M_{\rm CSM}$ is increased (see the models B1 and B2). Another possible way to make $s = 2$ models work is to increase the conversion efficiency from $E_{\rm ej}$ to radiation energy so that $E_{\rm ej}$ can be reduced (see Section 4.3.4.1 for the discussion of the conversion efficiency). In the model E2, $M_{\rm ej}$ is set to be comparable to $M_{\rm CSM}$ so that the conversion efficiency becomes higher (Section 4.3.4.1). The similar peak luminosity to the model E1 is reached with less $E_{\rm ej}$ (10^{52} erg) in the model E2. However, as the diffusion time of the CSM is not affected so much by this, the LCs become similar to each other and increasing the efficiency does not revive the $s = 2$ models. To summarize, the dense CSM from the steady mass loss is still difficult to explain the LC of SN 2006gy with the shock breakout model.

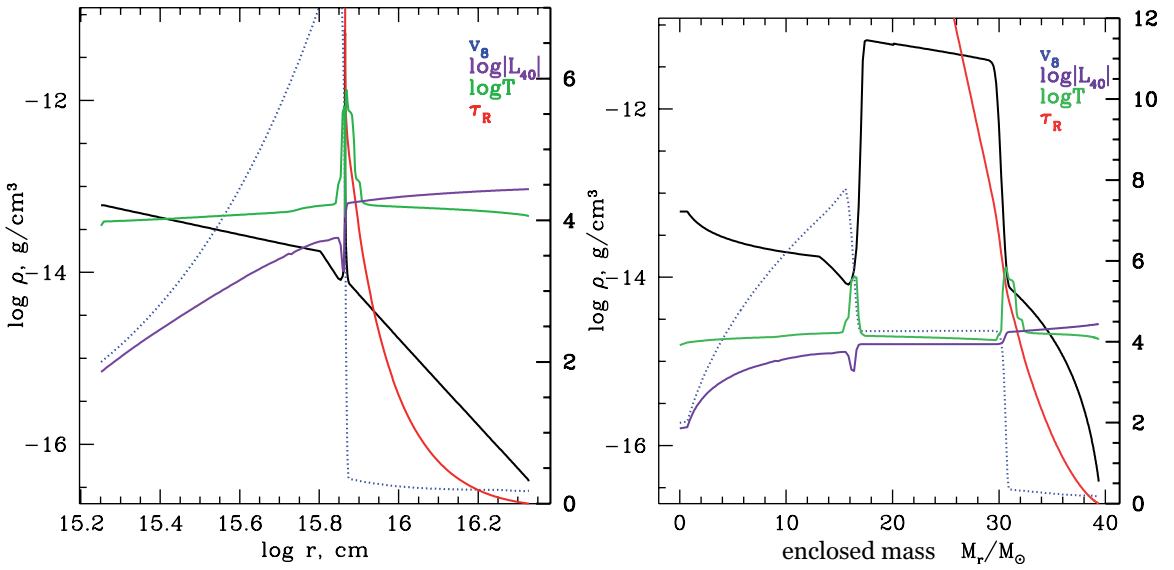

Figure 4.9: Physical structures of the model D2 in radius (left) and mass coordinate (right) at around the LC peak (74 days since the collision). Black lines show the density structure (left y-axis). Blue dotted lines are the velocity scaled by 10^8 cm s^{-1} (right y-axis), purple lines are the logarithm of the absolute value of luminosity scaled by 10^{40} erg s^{-1} (right y-axis), green lines are the logarithm of the temperature in Kelvin (right y-axis), and red lines are the Rosseland optical depth measured from the outside (right y-axis).

Dynamical Evolution

Figure 4.9 shows the dynamical structures of the model D2 ($s = 5$) at around the LC peak. The left panel shows the structure in the physical coordinate (radius) whereas the right panel shows the structure in the mass coordinate. The cool dense shell is created between SN ejecta and CSM in which about 10 $M_\odot$ of the shocked CSM and 3 $M_\odot$ of the shocked SN ejecta are contained.

Figure 4.10 shows the evolution of the color temperature ($T_{\rm col}$) and the effective temperature ($T_{\rm eff}$) of the model D2. The color temperature is derived by fitting the spectra obtained by the numerical calculations with the blackbody spectral distribution whereas the effective temperature is obtained by using the bolometric luminosity ($L_{\rm bol}$) and the radius ($R_{\tau_R=2/3}$) of the photosphere which is defined as the radius where the Rosseland mean optical depth τ_R from the surface becomes 2/3 in `STELLA` and is expressed as $T_{\rm eff} = \left(L_{\rm bol}/4\pi\sigma_{\rm SB}R^2_{\tau_{\rm R}=2/3}\right)^{1/4}$. Here, $\sigma_{\rm SB}$ is the Stephan-Boltzmann constant. As radiation mainly comes from the shell and the Thomson scattering is the dominant opacity source in the CSM above the shell, $T_{\rm col}$ roughly traces the temperature of the shell. The photosphere ($R_{\tau_R=2/3}$) is much above the shell and $T_{\rm eff}$ becomes very low because of the large $R_{\tau_R=2/3}$ (see also Figure 4.11). At the time when $T_{\rm col}$ starts to increase for the second time (from $\simeq$ 180 days), the photosphere is in the SN ejecta whose density structure and composition are expressed in the approximated way and the results around these epochs and later should not be taken seriously.

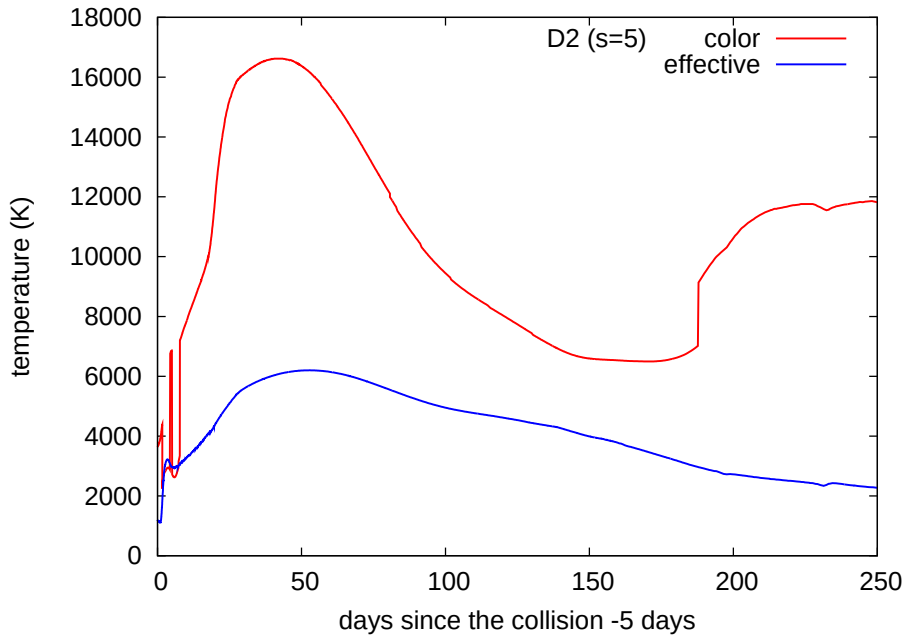

Figure 4.10: Evolution of the color temperature ($T_{\rm col}$) and the effective temperature ($T_{\rm eff}$) in the model D2. The origin of the time axis is 5 days since the collision.

Figure 4.11 shows the evolution of the blackbody radius $R_{\rm BB} = \sqrt{L_{\rm bol}/4\pi\sigma_{\rm SB}T_{\rm col}^4}$ and the photosphere $R_{\tau_R=2/3}$. The constant velocity line with $5,200$ km s^{-1} is the evolution of the blackbody radius obtained by Smith et al. 2010a along which $R_{\rm BB}$ follows until around 125 days. The evolution of $R_{\rm BB}$ in the models D2 and F1 is consistent with $5,200$ km s^{-1} although the radius is a bit smaller than the observed values. The bolometric correction of Smith et al. 2010a is based on $T_{\rm BB}$ and the correction may add extra luminosities because it ignores the effect of line depletion. Higher $L_{\rm bol}$ results in higher $R_{\rm BB}$ for a given $T_{\rm col}$ and this can be the reason why $R_{\rm BB}$ of Smith et al. 2010a is higher than ours.

$R_{\rm BB}$ obtained by our calculations tends to be smaller than the shell radius where the radiation is coming from. For example, $R_{\rm BB}$ of the model D2 shown in Figure 4.11 stays lower than the radius at which the interaction starts ($R_i = 5 \times 10^{15}$ cm). The reason is presumed to be similar to that of the discrepancy in $R_{\rm BB}$ obtained from observations and numerical calculations. $T_{\rm col}$ is obtained from the spectral fitting but actual spectra suffer from the line depletion especially in blue. Since $T_{\rm col}$ is reduced from the temperature at the photon production site, $L_{\rm bol}$ is the value affected by such depletion and is less than the value expected from the blackbody with $T_{\rm col}$. Thus, with the smaller $L_{\rm bol}$, $R_{\rm BB} = \sqrt{L_{\rm bol}/4\pi\sigma_{\rm SB}T_{\rm col}^4}$ becomes smaller than the actual emitting region.

As most of hydrogen in CSM remains to be ionized, $R_{\tau_R=2/3}$ continues to be at the radius where the Rosseland mean opacity from the surface of the CSM is 2/3 and remains to be constant until the shock wave comes close to the radius. Then, $R_{\tau_R=2/3}$ evolves roughly following the forward shock.

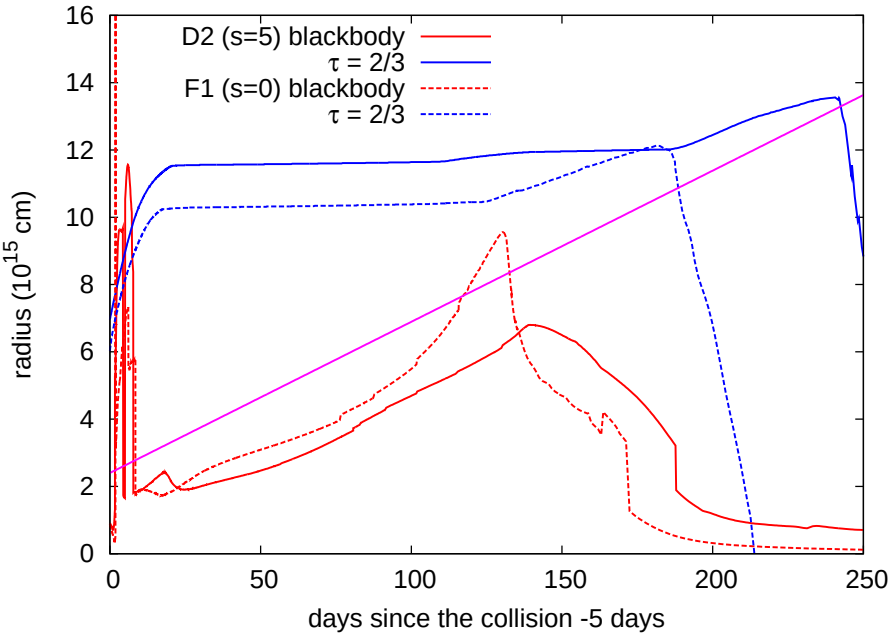

Figure 4.11: Evolution of the blackbody radius ($R_{\rm BB}$, solid line) and the photospheric radius ($R_{\tau=2/3}$, dashed line) of the models D2 ($s = 5$) and F1 ($s = 0$). The origin of the time axis is 5 days since the collision. The monotonically increasing linear line at the middle is the evolution of the blackbody radius obtained by Smith et al. 2010a, a constant velocity evolution with $5,200$ km s^{-1}. The observational blackbody radius follows the line until around 125 days and starts to decline (see Smith et al. 2010a for details).

$M_{\rm ej}$ and $E_{\rm ej}$

The properties of SN ejecta ($M_{\rm ej}$ and $E_{\rm ej}$) determine many aspects of SNe powered by the interaction (e.g., luminosities) because $E_{\rm ej}$ determines the available energy and $M_{\rm ej}$ affects the efficiency to convert the available kinetic energy to the radiation energy. We discuss the effect of $M_{\rm ej}$ and $E_{\rm ej}$ in Section 4.3.4.1 including the results of the $v_s = 5,200$ km s^{-1} models and here we just show the results of LC calculations with different $M_{\rm ej}$ and $E_{\rm ej}$ (Figure 4.12). LCs are similar to each others and we can see that it is difficult to constrain $M_{\rm ej}$ and $E_{\rm ej}$ only by the LC. This can also be seen by comparing the models E1 and E2 in Figure 4.4. The two models have different $M_{\rm ej}$ and $E_{\rm ej}$ with the same CSM but the resulting LCs are similar (see discussion in Section 4.3.4.1).

In the best LC model of the pulsational pair-instability model presented by Woosley et al. 2007, the ejecta with 5.1 $M_\odot$ and 2.9×10^{51} erg collides the CSM with 24.5 $M_\odot$. Our canonical models (D2 and F1) have much higher $E_{\rm ej}$ (10^{52} erg). One of the reasons is presumed to be the smaller photospheric radius ($y_1 R_o = 1.1 \times 10^{16}$ cm) in our models. The dense CSM in the pulsational pair-instability model extends to about 3×10^{16} cm and the photosphere can be larger than our models. This effect of the locations of the photosphere can also be seen in comparison to the $v_s = 5,200$ km s^{-1} models. The photospheric radii of

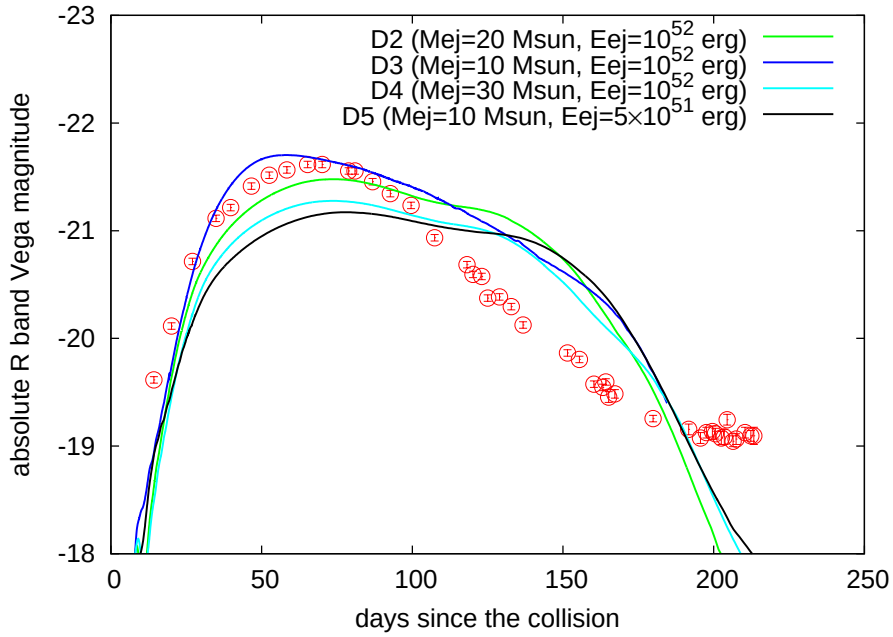

Figure 4.12: R band LCs from the same CSM but different $M_{\rm ej}$ and $E_{\rm ej}$. The models D2, D3, D4 have the same $E_{\rm ej}$ but different $M_{\rm ej}$, i.e., 10 $M_\odot$ (D3), 20 $M_\odot$ (D2), and 30 $M_\odot$ (D3). The model D5 has less $E_{\rm ej}$ (5×10^{51} erg) than other models (10^{52} erg) and $M_{\rm ej} = 10$ $M_\odot$. The calculation of the LC of the model D3 stopped at around 175 days since the collision and we show the LC until around 175 days.

them are only $y_1 R_o \simeq 5 \times 10^{15}$ cm at most and the required energy to achieve the maximum luminosity of SN 2006gy is 5×10^{52} erg which is even larger than 10^{52} erg required for the $v_s = 10,000$ km s^{-1} models ($y_1 R_o = 1.1 \times 10^{16}$ cm). This shows the difficulties to constrain $E_{\rm ej}$ only by the LC.

In addition, the efficiency to convert the kinetic energy to radiation is mainly determined by the relative mass of the ejecta and the collided CSM. It does not depend strongly on the ejecta mass if the CSM mass is much larger than the ejecta mass. To get high conversion efficiencies of the kinetic energy to the radiation energy, $M_{\rm ej}$ is better to be comparable or less than $M_{\rm CSM}$ and we can at least get some constraint on $M_{\rm ej}$ from the LC based on the view point of the conversion efficiency (Section 4.3.4.3).

Smearing

The dense shell which appears between SN ejecta and CSM is unstable in multidimension. As a result of the instabilities, less kinetic energy is expected to be converted to radiation because there would be the extra multidimensional motions caused by the instabilities. To take into account such multidimensional effects in one-dimensional code `STELLA`, we include a smearing term in the equation of motion (the parameter B_q, Section 2.5.2.3).

Figure 4.13 shows the LCs with different values of the smearing parameter B_q. With

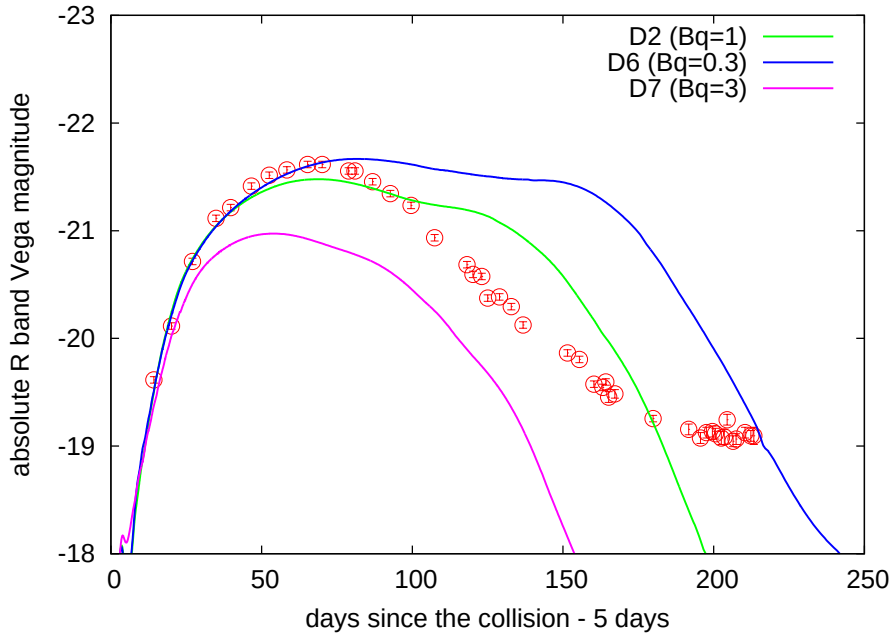

Figure 4.13: R band LCs with different B_q, i.e., D2 ($B_q = 1$), D6 ($B_q = 0.3$), and D7 ($B_q = 3$). The smearing parameter B_q changes the conversion efficiency from kinetic energy to radiation. With larger B_q, more kinetic energy remains and less radiation energy is emitted. The origin of the time axis is 5 days since the collision.

larger B_q, the effect of the smearing becomes larger and less kinetic energy is converted to radiation. In other words, radiative cooling becomes less efficient. The model D2 is calculated with our standard $B_q = 1$. The model D6 has $B_q = 0.33$ and the model D7 has $B_q = 3$. The shape of the LC is different even if we only change B_q with a factor 3. We discuss the efficiency in detail in Section 4.3.4.1.

The uncertainty in the smearing parameter adds one difficulty in our estimations of physical parameters of the progenitor system. This is one reason why we think that making the perfect fitting now does not lead us to the exact parameters of the progenitor system. The calibrations for the smearing parameter should be done at least. However, the rising time and the peak luminosity is not so sensitive to the smearing parameter and the parameters of SN ejecta and dense CSM we obtain with the current uncertainty are presumed to be close to the 'real' ones.

Effect of ^{56}Ni

We have also examined the effect of ^{56}Ni decay on the LCs. Figure 4.14 shows the results. We include ^{56}Ni at the center of the model D2. If we include ^{56}Ni, the length of the peak is extended due to the extra heat source. The significant effect can only be seen when we include $\sim 10\ M_\odot$ of ^{56}Ni. However, the amount of ^{56}Ni is observationally constrained to be less than $2.5\ M_\odot$ (Miller et al. 2010) and the effect of ^{56}Ni is negligible.

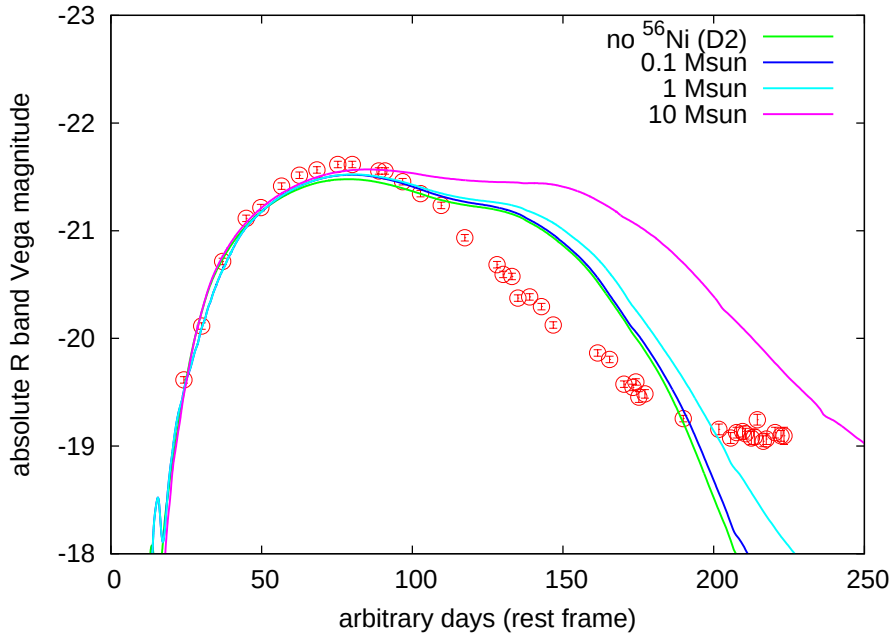

Figure 4.14: R band LCs with ^{56}Ni. 0.1 $M_{\odot}$, 1 $M_{\odot}$, and 10 $M_{\odot}$ of ^{56}Ni is included at the center of the model D2. Only 10 $M_{\odot}$ of ^{56}Ni makes significant effect on the LC.

4.3.4 Discussion

4.3.4.1 Conversion Efficiency

The source of radiation in our LC models is the kinetic energy of SN ejecta. The amount of energy converted from kinetic energy to radiation can be estimated by the conservation laws of energy and momentum. If we assume that the radiation pressure does not change the dynamics of the materials so much, the conservation of momentum requires

$$M_{\rm colej} v_{\rm colej} = (M_{\rm colej} + M_{\rm sCSM})\, v_{\rm sh}, \tag{4.9}$$

where $M_{\rm colej}$ is the mass of the collided SN ejecta, $v_{\rm colej}$ is the mean velocity of the collided SN ejecta, $M_{\rm sCSM}$ is the mass of the shocked CSM, and $v_{\rm sh}$ is the velocity of the dense shell between SN ejecta and CSM. Radiation energy $E_{\rm rad}$ emitted as a result of the interaction can be derived from the conservation of energy

$$E_{\rm rad} = \alpha \left[\frac{1}{2} M_{\rm colej} v_{\rm colej}^2 - \frac{1}{2} (M_{\rm colej} + M_{\rm sCSM})\, v_{\rm sh}^2 \right], \tag{4.10}$$

where α is the fraction of kinetic energy converted to radiation. From Equations 4.9 and 4.10,

$$\frac{E_{\rm rad}}{\frac{1}{2} M_{\rm colej} v_{\rm colej}^2} = \frac{\alpha M_{\rm sCSM}}{M_{\rm colej} + M_{\rm sCSM}}. \tag{4.11}$$

Table 4.2: Conversion efficiency from kinetic energy to radiation energy

Name	$E_{\rm rad}$ 10^{51} erg	$E_{\rm rad}/E_{\rm ej}$	$\frac{M_{\rm CSM}}{M_{\rm ej}+M_{\rm CSM}}$	α
A1	13	0.25	0.52	0.48
A2	12	0.24	0.33	0.72
B1	0.46	0.046	0.040	1.1
B2	8.7	0.29	0.57	0.50
C1	14	0.28	0.41	0.68
D1	2.7	0.27	0.52	0.51
D2	2.2	0.22	0.47	0.47
E1	2.6	0.086	0.14	0.63
E2	3.0	0.30	0.62	0.48
F1	2.9	0.29	0.64	0.46
D4	1.7	0.17	0.38	0.46
D5	1.6	0.32	0.64	0.50
D6	3.4	0.34	0.47	0.72
D7	0.89	0.089	0.47	0.19

If most of the SN ejecta and CSM are shocked, i.e., $M_{\rm colej} \simeq M_{\rm ej}$ and $M_{\rm sCSM} \simeq M_{\rm CSM}$, we get the rough estimate for the radiation energy emitted

$$E_{\rm rad} \simeq \frac{\alpha M_{\rm CSM}}{M_{\rm ej}+M_{\rm CSM}} E_{\rm ej}. \tag{4.12}$$

α is expected to be close to 1 without the smearing parameter B_q because most of thermal energy gained by the shock is eventually emitted as radiation. Since the parameter B_q adds additional acceleration to reduce the amount of energy converted to thermal energy, α is expected to become lower as B_q becomes larger. The rest of energy is mostly in the form of kinetic energy. We may also express the effect as the reduction of the radiative cooling efficiency because less radiation energy is emitted with the smearing term.

Table 4.2 is the list of radiation energy which is obtained by adding up the bolometric luminosity from the time of collision to around 300 days since the collision. The model D3 is excluded because we do not have the entire numerical LC. We also show the parameter α which is derived by using Equation 4.12. The efficiency $E_{\rm rad}/E_{\rm ej}$ to convert SN kinetic energy to radiation is plotted in Figure 4.15 as a function of $M_{\rm CSM}/\left(M_{\rm ej}+M_{\rm CSM}\right)$ with the results obtained by van Marle et al. 2010.

At the high $M_{\rm CSM}/\left(M_{\rm ej}+M_{\rm CSM}\right)$ region, our standard $B_q = 1$ results follow the line of $\alpha = 0.5$. This means that the efficiency to convert the kinetic energy to radiation is reduced by 50%. On the other hand, the results of van Marle et al. 2010 follow the $\alpha = 1$ line and the effect of multidimensional instabilities is not significant. Although van Marle et al. 2010 use a three-dimensional code and multidimensional instabilities are included in principle, their approximated way to treat the radiation and limited spatial resolution may have prevented multidimensional instabilities from growing.

As $M_{\rm CSM}/\left(M_{\rm ej}+M_{\rm CSM}\right)$ becomes lower, the results start to deviate from the constant α line. This is because $M_{\rm CSM}$ gets very small and most of the ejecta is not affected by the

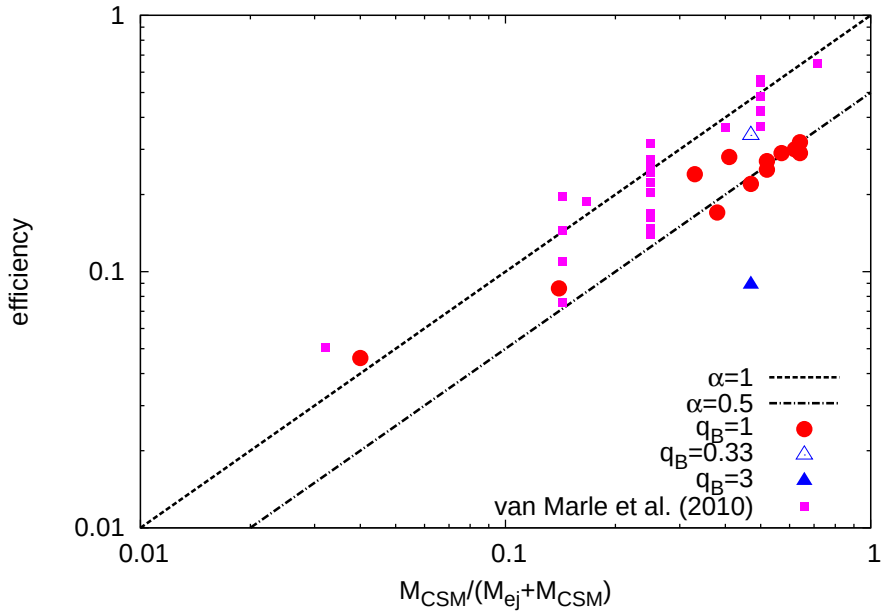

Figure 4.15: Efficiency of the conversion of kinetic energy to radiation. Most of the results from van Marle et al. 2010, including aspherical models, are also shown. α is a measure for the effect of the smearing parameter B_q. $\alpha = 1$ means no smearing effect and the smearing effect increases as α gets small.

interaction, i.e., the assumption $M_{\rm colej} = M_{\rm ej}$ is no longer valid and Equation 4.12 should not be used. We should use Equation 4.10 instead. As $M_{\rm colej} \ll M_{\rm ej}$ in this regime, the efficiencies tend to be higher than the values obtained from Equation 4.12.

The combinations of $E_{\rm ej}$ and $M_{\rm ej}$ which give a similar $[M_{\rm sCSM}/(M_{\rm colej} + M_{\rm sCSM})]\,\frac{1}{2}M_{\rm colej}v_{\rm ej}^2$ are expected to result in similar LCs and they are degenerated. Thus, it is difficult to constrain the exact value for $M_{\rm ej}$ and $E_{\rm ej}$ from LCs. This is clearly seen in the models E1 and E2 in Figure 4.4. Both the models have similar LCs. The CSM of the two models is exactly the same but $M_{\rm ej}$ and $E_{\rm ej}$ are different. Although $M_{\rm colej} < M_{\rm ej}$ in the model E1 and $M_{\rm colej} \simeq M_{\rm ej}$ in the model E2, $M_{\rm colej}$ and $\frac{1}{2}M_{\rm colej}v_{\rm ej}^2$ are happened to be similar in the two models with the similar $M_{\rm sCSM} \simeq M_{\rm CSM}$. Thus, the two models have similar $[M_{\rm sCSM}/(M_{\rm colej} + M_{\rm sCSM})]\,\frac{1}{2}M_{\rm colej}v_{\rm ej}^2$ and result in the similar LCs.

4.3.4.2 Origin of the Plateau Phase

There exists a plateau in the LC of SN 2006gy at around 200 days. None of our models are succeeded in producing the plateau. This is because the remaining CSM at these epochs is too thin to affect the LC. Note that the LC observations at later epochs reject the possibility to explain this plateau by ^{56}Ni heating (see also Section 4.3.3.2). There are several other possible ways to explain the plateau. One possibility is the recombination in the SN ejecta.

Because we use the simplified SN ejecta structures, our results of LC calculations after the photosphere gets inside of the SN ejecta are beyond the applicability of our simple models. Increasing the SN ejecta mass may also help because a plateau phase can be longer with larger hydrogen mass, although the conversion efficiency from kinetic energy to radiation is also affected at the same time (Section 4.3.4.1). By putting more realistic SN ejecta with realistic hydrogen-rich envelopes or more massive SN ejecta, the recombination wave may stay the envelope for a while and may end up with the plateau phase, as is the case in SNe IIP (see, e.g., Kasen & Woosley 2009). We note that the blackbody temperatures of these epochs are $\simeq 6,000$ K and they are consistent with this scenario. Recombination may also occur in the shocked CSM or the dense cool shell.

Light echoes from the remaining CSM may also play a role. The LC after this plateau phase remains almost constant for more than 200 days, although the luminosity is about 10 times smaller (Miller et al. 2010). Thus, it is possible that there existed another CSM component which caused the echoes at around 200 days and shocked away when SN 2006gy was behind the Sun.

4.3.4.3 Progenitor of SN 2006gy

It is difficult to get information on the progenitor from the LC of SN 2006gy, as the properties of the progenitor system which can be obtained from the LC modeling strongly depends on CSM. The CSM properties and the SN ejecta properties are degenerated. However, we can get some indications for it. As the origin of the luminosity is the kinetic energy of SN ejecta, the kinetic energy should be converted to radiation efficiently. If $M_{\rm CSM} \ll M_{\rm ej}$, the conversion efficiency $\alpha M_{\rm CSM}/\left(M_{\rm ej}+M_{\rm CSM}\right)$ is so small that the kinetic energy cannot be converted efficiently enough to explain the LC of SN 2006gy. Thus, the mass of the CSM should be close to or larger than $M_{\rm ej}$.

According to our modeling, $M_{\rm CSM}$ is required to be $\sim 10\ M_\odot$ and this means that $M_{\rm ej}$ is expected to be $\sim 10\ M_\odot$ or less. This indicates that the total mass of the system well exceeds $10\ M_\odot$ and the progenitor of SN 2006gy should be a very massive star. In addition, the progenitor should lose $M_{\rm CSM}$ within ~ 10 years before the explosion. Our models for SN 2006gy have $M_{\rm CSM} \simeq 18\ M_\odot$ and it may be difficult for RSGs to have such mass loss because of the following reason: To have CSM with $18\ M_\odot$, the ZAMS mass of RSGs should be very large but such massive stars suffer more from the radiation driven wind during their main-sequence phase because of their large luminosities. Thus, losing most of their mass only just before their explosions might be difficult. However, extensive mass loss of RSGs is suggested by many authors (e.g., Section 5.3, van Loon et al. 2005, Vanbeveren et al. 2007, Smith et al. 2009a, Boyer et al. 2010, Yoon & Cantiello 2010, Georgy 2012) and it is still possible that very massive RSGs lose $\sim 10\ M_\odot$ just before their explosions due to, e.g., pulsations (e.g., Yoon & Cantiello 2010, Heger et al. 1997, Li & Gong 1994), dust (e.g., van Loon et al. 2005), or g-mode oscillations (Quataert & Shiode 2012, see also Arnett & Meakin 2011).

The large CSM mass rather indicates that the progenitor of SN 2006gy is a very massive star. Among massive stars, LBVs are only known stars which can have some episodes with the huge mass-loss rates which are found to be required to explain SN 2006gy. Indeed, some of them, e.g., η Carinae, are known to have $\sim 10\ M_\odot$ CSM (e.g., Smith & Owocki 2006).

Their typical CSM velocities are also consistent with the CSM velocities estimated from the narrow P-Cygni Hα profiles in SN 2006gy (e.g., Smith et al. 2010a). However, as introduced in Chapter 1, LBVs are theoretically not thought to be a pre-SN stage. Recent stellar evolution theories are stating to show some possibilities for some LBVs to explode (e.g., Groh et al. 2013, Langer 2012) and this problem of LBV explosions is likely to be solved from the stellar evolution side and some important missing keys in the current stellar evolution theory can be revealed.

A shell created due to the interaction between the RSG wind and the WR wind is another possible way to have a massive CSM (e.g., Dwarkadas 2011). Alternatively, a shell created by pulsational instability can be followed up by the SN ejecta, instead of the ejecta of the next pulse as suggested by Woosley et al. 2007. Some binary interaction may cause extensive mass loss (e.g., Hachisu et al. 2008) but binary systems have not been considered deeply as a possible progenitor of SLSNe yet (see Chevalier 2012, Soker 2013). The collision of massive stars in a dense stellar cluster can make a massive star surrounded by a massive CSM and it may also result in SN 2006gy-like SLSNe (Portegies Zwart & van den Heuvel 2007, see also Pan et al. 2012b).

With the condition that $M_{\rm ej}$ is similar to or less than $M_{\rm CSM}$, the conversion efficiency of kinetic energy to radiation (Equation 4.11) is expected to be $\simeq$ 50 % at most (Section 4.3.4.1). As the radiation energy emitted by SN 2006gy exceeds 2×10^{51} erg, the SN ejecta should have more than $\simeq 4 \times 10^{51}$ erg. Thus, the SN explosion inside should be very energetic. As the energy of our models is comparable to those of energetic broad-line SNe Ic whose progenitors are suggested to be very massive (e.g., Nomoto et al. 2011), the estimated high energy may also indicate that the progenitor mass is rather close to those of LBVs. Note, however, that the host galaxy of SN 2006gy is not metal-poor (e.g., Ofek et al. 2007) while broad-line SNe Ic appear more preferentially in low metallicity environments (e.g., Arcavi et al. 2010, Modjaz et al. 2011, Sanders et al. 2012). In addition, the late time spectra of SN 2006gy are not similar to those of broad-line SNe Ic (Kawabata et al. 2009), although the late time spectra of SLSN I 2010gx show such features (Pastorello et al. 2010). The required high explosion energy can also be related to PISNe. PISNe with the explosion energy of 10^{52} erg which is required in our models to reproduce the SN 2006gy LC can be easily achieved by PISNe. PISNe are known to produce huge amount of ^{56}Ni but Heger & Woosley 2002 show that PISNe with the explosion energy of 10^{52} erg (He core of about 70 $M_{\odot}$) only produce about 0.01 $M_{\odot}$ of ^{56}Ni. Thus, combined with some instabilities which induce the extreme mass loss at the surface of PISN progenitors like that suggested by Woosley et al. 2007, PISNe can be SN 2006gy in spite of the small amount of ^{56}Ni observed. PISNe are suggested to be able to appear at relatively high metallicity environment due to the effects of, e.g., rotation (e.g., Langer & El Eid 1986, Langer et al. 2007, Langer 2012, Yoshida & Umeda 2011). However, the maximum metallicity for PISNe estimated by these works are still lower than the estimated metallicity of SN 2006gy environment.

4.3.4.4 Comparison with Semi-Analytic Model

Chatzopoulos et al. 2012 proposed a semi-analytic model of LCs powered by the interaction. The model involves several simplifications but the overall features predicted by the model

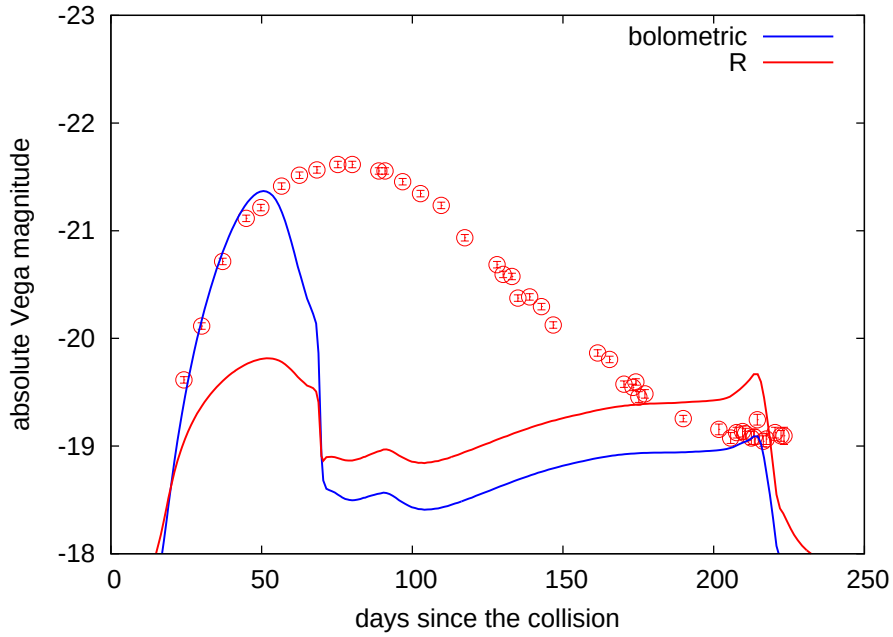

Figure 4.16: Observed R band LC and the bolometric and R band LCs calculated with the parameters suggested for SN 2006gy in Chatzopoulos et al. 2012. The observational points are shifted arbitrarily to match the numerical result in the figure.

are shown to match some numerical results. They show a LC model of SN 2006gy and we perform LC calculations with the same parameters which are obtained by them. The parameters are $\delta = 0$, $n = 12$, $s = 0$, $E_{\rm ej} = 4.4 \times 10^{51}$ erg, $M_{\rm ej} = 40\ M_\odot$, $R_i = 5 \times 10^{14}$ cm, and $R_o = 2.5 \times 10^{15}$ cm (corresponds to $M_{\rm CSM} = 5\ M_\odot$ with a constant CSM density 1.5×10^{-13} g cm^{-3}). Following the result of Chatzopoulos et al. 2012, we put 2 $M_\odot$ of ^{56}Ni at the center of the ejecta but the value is too small to affect the main part of the LC (Section 4.3.3.2). Except for the central region, the composition is set as the solar metallicity. We use our standard $B_q = 1$.

Figure 4.16 shows the result of the numerical calculation. Overall, the parameters suggested by Chatzopoulos et al. 2012 do not result in a similar LC to that of SN 2006gy. The peak luminosity of the bolometric LC is close to that of SN 2006gy but the duration is much shorter that that of SN 2006gy. In addition, the R band peak luminosity is much smaller than that of SN 2006gy because the photospheric temperature is much higher than that of SN 2006gy around the peak and the model has much bluer spectra. The duration can be longer if we use a smaller B_q but our results shown in Figure 4.13 imply that it is difficult to make the duration two times longer than the $B_q = 1$ LC to match the LC of SN 2006gy by just making the B_q small. What is more, changing B_q does not improve the color of the LC and the R band LC is expected to remain much fainter than the observed R band LC. The plateau phase after the drop in the LC is due to the recombination in 40 $M_\odot$ SN ejecta inside. The duration of the plateau phase should actually be much shorter than that in Figure 4.16, as the entire SN ejecta is composed of the solar metallicity in the model (except

for the central ^{56}Ni) and we use an approximate density structure for the SN ejecta.

There are several possible reasons for the discrepancy. The semi-analytic model assumes that the thermal energy gained by the forward shock is always released at the center of the CSM because the assumption is required to treat the transport equations analytically. However, this assumption keeps the diffusion time of the photons from the forward shock constant and the diffusion time is fixed with the initial value. In reality, the forward shock travels outward and the diffusion time decreases with time as the remaining unshocked CSM decreases. This effect leads to the overestimation of the duration of the LCs in the semi-analytic model. This is presumed to be the main reason why the duration of the LC obtained by the numerical calculation is much shorter than that obtained by the analytical model. This indicates that the semi-analytic model should not be applied to the system with the CSM of a large initial diffusion time in which the kinetic energy of shock waves is the main source of radiation.

Another possible reason is that the energy released by the reverse shock is overestimated in the semi-analytic model. In the semi-analytic model, the self-similar solution of Chevalier 1982a, Nadyozhin 1985 is used as the evolution of the hydrodynamical structure. However, in reality, the effect of cooling which is not taken into account in the adiabatic self-similar solution is so strong in the case of SLSNe powered by the shock interaction that a thin cool dense shell is created between the SN ejecta and the dense CSM. Thus, the reverse shock could not travel as fast as expected from the adiabatic self-similar solution and it rather stays close to the forward shock (see also Section 2.3).

In summary, many important effects which are essential in modeling the LC powered by the interaction between SN ejecta and a dense CSM with a large photon diffusion time lack in the semi-analytic model and it may not be appropriate to use it for the modeling of SLSNe powered by such a strong interaction.

4.3.4.5 Comparison with Shell-Shocked Diffusion Model

Smith & McCray 2007 (SM07 hereafter in this section) investigate a SLSN LC model resulting from a CSM through which a shock wave has gone through. They consider a dense CSM from which photons start to emit after the passage of a shock wave and they apply the LC model of adiabatically cooling SN ejecta formulated by Arnett 1980. By simply comparing the shape of the model LC to the R band LC of SN 2006gy, SM07 concluded that SN 2006gy can result from a shocked CSM.

However, there are many simplifications involved in the SM07 model which are not discussed so far. The existence of the recombination wave in shocked H-rich CSM is presumed to affect the LC as in the case of SNe IIP (e.g., Grassberg et al. 1971, Falk & Arnett 1977, Kasen & Woosley 2009, Bersten et al. 2011). In addition, SM07 compare a bolometric LC obtained from their model to the R band LC of SN 2006gy. As the shocked CSM should have temperature close to 10^4 K at the beginning to explain the observed SN 2006gy properties (Smith et al. 2010a), a large fraction of emitted photons is not in the R band and the bolometric correction should be considered.

To see the importance of these neglected effects in the SM07 analytic model, we numerically follow the system suggested to explain SN 2006gy in SM07 with `STELLA`. `STELLA` is a suitable code to see the effect of the bolometric correction and recombination which are not

Table 4.3: List of initial conditions

Name	v_o[a]	M_s[b]	R_o[c]	$T_{\rm ini}$[d]	composition
	km s^{-1}	$M_\odot$	10^{15} cm	10^4 K	
M01	4,000	10	2.4	1	solar
M02	4,000	10	2.4	4	solar
M03	4,000	20	7.2	1.7	solar
M04	2,000	20	7.2	1.7	solar
M05	8,000	20	7.2	1.7	solar
M06	4,000	20	0.72	13	solar

[a] velocity of the outermost layer of the shocked CSM
[b] mass of the shocked CSM
[c] radius of the shocked CSM
[d] initial temperature of the shocked CSM

taken into account in the SM07 analytic model. In this section, we apply the same distance to the host galaxy (73.1 Mpc) and extinctions (Galactic $A_R = 0.43$ mag + host $A_R = 1.25$ mag) as in SM07 to the observed LC of SN 2006gy. These values are slightly different from those adopted in the previous sections in this chapter.

Models

Initial conditions of the numerical calculations here are constructed based on SM07 at first. We do not follow shock propagation in the CSM to make the initial conditions the same as those of SM07. The initial conditions are supposed to result from the shock passage in the dense CSM. Since we do not treat the shock wave, the smearing term does not affect the results obtained here.

Table 4.3 is the list of our initial conditions. The initial radius of the SM07 model suggested for SN 2006gy is 2.4×10^{15} cm. The mass of the shocked CSM in the model is 10 $M_\odot$. We assume that the system is homologously expanding and the outermost layer velocity is $4,000$ km s^{-1}, as assumed in SM07. The initial temperature is set constant in the entire CSM. We try two temperatures for the SM07 system, namely, 10^4 K (Model 01 or M01) and 4×10^4 K (M02). The composition is solar in these models.

We also investigate several configurations other than those suggested in SM07. M03 has the same velocity but the initial radius is three times larger than that of the SM07 model. The temperature is set to 1.7×10^4 K to match the observed luminosity of SN 2006gy. The mass is increased to 20 $M_\odot$ in M03 to keep the shocked CSM optically thick. M04 and M05 have the same density structure as M03 but the velocity is 0.5 and 2 times of M03, respectively. We also show results of M06, which is more compact than the SM07 model. The composition is solar in M03-M06.

Synthetic Light Curves

Figure 4.17a shows the bolometric LCs of M01-M03. At first glance, we find that no LCs are consistent with that of SN 2006gy. Furthermore, the R band LCs shown in Figure

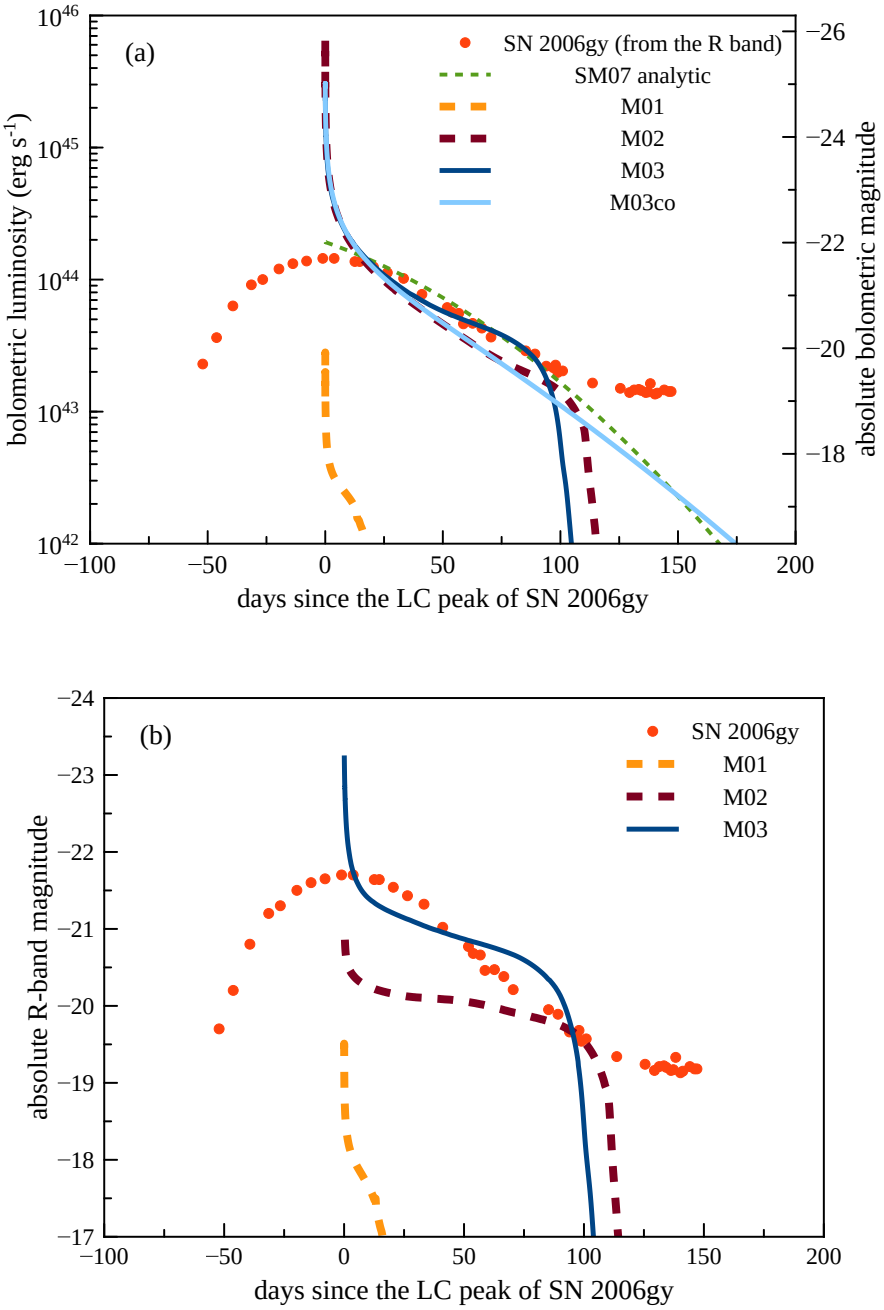

Figure 4.17: Bolometric (a) and R band (b) LCs of shocked CSM.

4.17b are found to be more different from the R band LC of SN 2006gy. This indicates the importance of the bolometric correction. We discuss the LC behaviors in this section but most of our discussion can be found in the previous studies, e.g., Grassberg et al. 1971, Falk & Arnett 1977.

The bolometric LCs start with the initial peak. The peak bolometric luminosity is $4\pi R_o^2 \sigma_{\rm SB} T_{\rm ini}^4$. At first, the bolometric luminosity decreases due to the adiabatic expansion of the shocked CSM. If we assume that the homologously-expanding shocked CSM is radiation-dominated at early phases, the bolometric luminosity should decrease following $\propto t^{-2}$. This rapid decrease in the bolometric luminosity appears in our numerical models.

SM07 suggest that the bolometric LC of the shocked CSM would rise following $\propto t^2$ at first because shocked materials expand homologously and the shocked CSM is just an expanding blackbody. However, if we take into account the decrease in the blackbody temperature of the shocked CSM due to the adiabatic expansion and the lack of any heat sources, the effect of the temperature decline on the bolometric luminosity ($\propto t^{-4}$ in radiation-dominated shocked CSM) is larger than the effect of the radius increase on the bolometric luminosity ($\propto t^2$). In fact, our synthetic LCs do not show the luminosity increase and the luminosity just declines.

After the initial rapid luminosity decline, bolometric LCs start to be affected by photons diffused in the shocked CSM and begin to follow the diffusion model of Arnett 1980. From this point, the SM07 analytic model starts to work. M01, whose initial temperature (10^4 K) is close to the blackbody temperature of SN 2006gy at the LC peak, is too faint at this epoch to explain SN 2006gy because of the initial rapid luminosity decline due to the adiabatic expansion. With the initial configuration suggested by SM07, the temperature should be around 4×10^4 K (M02) to explain the luminosity of SN 2006gy but it is inconsistent with the observed blackbody temperature (Figure 4.18). M03 has a larger radius than those of M01 and M02. Thus, the required temperature to get the same luminosity is small (1.7×10^4 K) and it is close to the observed values.

Although the bolometric LCs at these epochs seem to follow the observed bolometric LC, we should be careful because the bolometric LC of SN 2006gy is obtained by the R band LC without the bolometric correction. We need to compare LCs in the R band (Figure 4.17b). We find that the numerical R band LCs do not match the observed R band LC even in the models which give a good fit in Figure 4.17a. This is simply because of the high temperatures in the shocked CSM and most of the emitted photons are not in the R band. We note that the strong Hα line observed in SN 2006gy is in the R band and the direct comparison between our numerical R band LCs and the observed R band LC can be inappropriate. However, the Hα luminosities of SN 2006gy at the epochs we are interested in is just $\sim 10^{41}$ erg s^{-1} (Smith et al. 2010a) and the bolometric correction remains to be important.

Another unavoidable and important consequence of the SM07 model which is not discussed in SM07 is the existence of the recombination wave in the shocked CSM. In the SM07 model, there are no energy sources in the shocked CSM because the shock has already passed the CSM and the shocked CSM just cools down. At one epoch, the temperature should reach the recombination temperature as is the case for SNe IIP. This is not the case for the continuous ejecta-CSM interaction models because there remains an energy source (shock waves) which can keep the CSM ionized until the shock wave goes through the dense CSM.

The effect of the recombination can be seen by comparing M03 and M03co in Figure

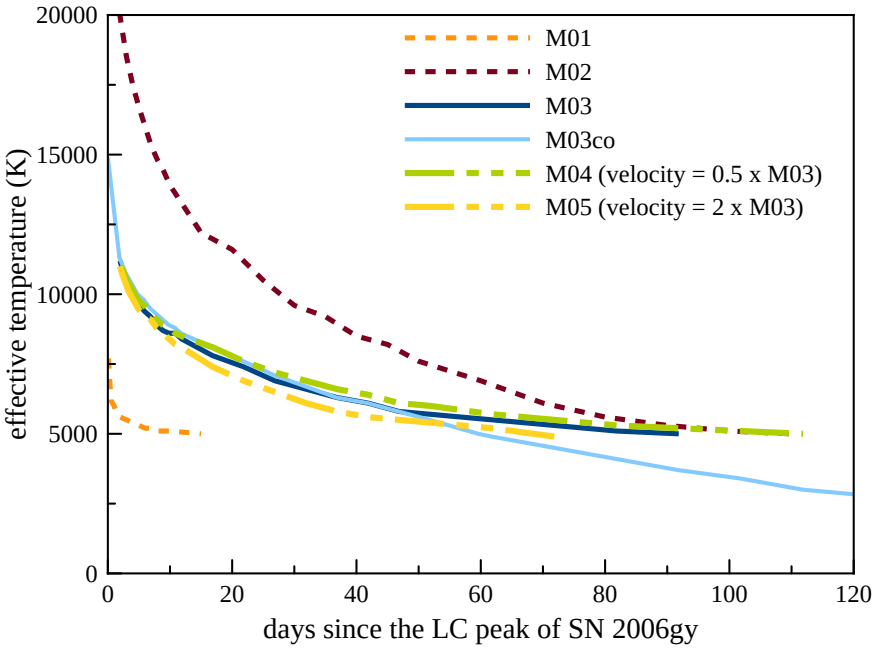

Figure 4.18: Evolution of the effective temperatures.

4.17a. M03 is calculated with our standard opacity table which takes recombination into account. M03co (M03 constant opacity) is calculated by forcing the scattering opacity of the system to be 0.34 cm^2 g^{-1}, which corresponds to the fully ionized solar composition materials. At first, when the CSM is above the recombination temperature, the two LCs follow almost the same track. Then, two LCs start to deviate when the outermost layer reaches the recombination temperature at around 40 days since the LC peak (Figure 4.18). The recombination wave, and thus the photosphere, moves inside (in Lagrangian sense) after this epoch. They eventually reach the bottom of the CSM and the LC suddenly drops. On the other hand, the LC with the constant opacity continues to decline monotonically, roughly following the SM07 analytic model. Figure 4.19 shows the photospheric radii of the models and the effect of the recombination is clear.

Another important consequence caused by the existence of the recombination is the strong dependency of LCs on the CSM velocity. The epoch when the outermost layers reach the recombination temperature and the recession velocity of the recombination wave in the CSM are affected by the CSM velocity. This is simply because adiabatic cooling becomes more efficient in faster shocked CSM. M04 and M05 have slower and faster shocked CSM, respectively, than M03 and their LCs are presented in Figure 4.20. At first, the LCs are expected to differ when the recombination start to play a role in the shocked CSM. However, the difference at this epoch is not significant according to our calculations. The time of the drop in the LCs clearly differs and the faster shocked CSM have earlier drops due to the faster recombination wave.

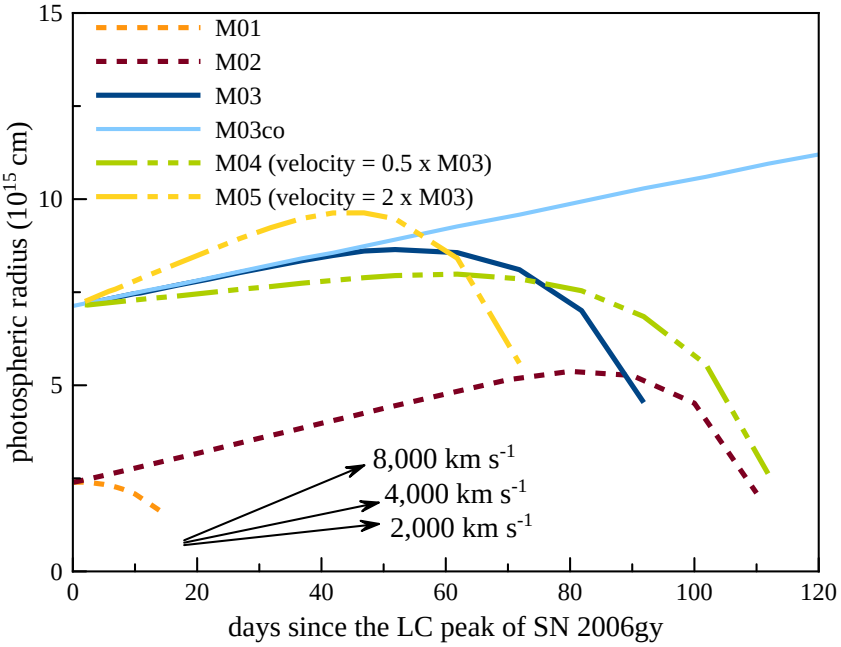

Figure 4.19: Evolution of the photospheric radii. The arrows in the figure shows the directions of the evolution of the radius with a given constant velocity.

Model with Initial R Band Luminosity Increase

All the models we have presented so far do not have a phase with luminosity increase and the luminosity just declines. However, it is possible to have a rising phase in optical LCs from a shocked CSM. Figure 4.21 shows one example of LC obtained from M06. The bolometric LC and optical LCs as well as the R band LC of SN 2006gy are shown in the same figure for the illustrative purpose. The evolution of the bolometric LC does not differ so much from the previous models but optical LCs of M06 have a rising phase. This is because of the initial small radius and high temperature. The optical luminosities are low at the beginning due to the initial high temperature. Then, as the adiabatic cooling is efficient due to the initial small CSM radius, the shocked CSM cools quickly and optical luminosities increase accordingly. Then, the R band LC can be similar to that of SN 2006gy, although the photospheric temperature is much higher in M06 and it is inconsistent with the SN 2006gy observations.

Possible Corresponding Supernovae

LCs of shocked CSM obtained by our numerical calculations have an initial rapid decline followed by a relatively long plateau. Although these features are not seen in SLSN 2006gy, SLSN 2003ma (SLSN II) qualitatively shows similar features (Rest et al. 2011, Figure 1.10). The LC of SN 2003ma is different from other known SLSNe. The LC of SN 2003ma has a quick rise and quick decline followed by a long plateau phase which lasts for about 100

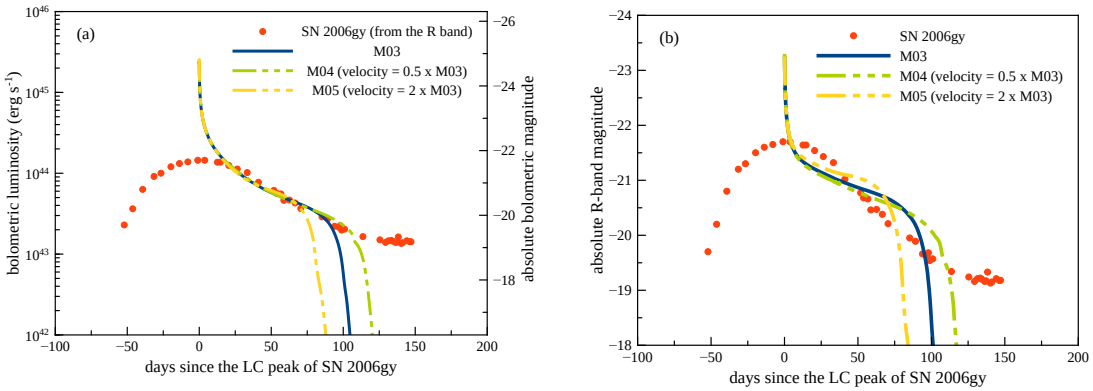

Figure 4.20: Bolometric (a) and R band (b) LCs of the models with different initial velocities.

days while other SLSNe evolves more slowly. Then the LC drops by about 1 mag in optical and the luminosity stays almost constant for about 1000 days after the drop. The initial rise and decline as well as the plateau phase which lasts for about 100 days can be seen in some synthetic optical LCs obtained in this study (e.g., Figure 4.17b), but the plateau phase after the drop which lasts for about 1000 days requires another emission mechanism like a continuous CSM interaction.

SN 1988Z has a similar feature to SN 2003ma, although the luminosity is about 3 magnitude smaller (e.g., Turatto et al. 1993, Aretxaga et al. 1999). Because of the LC similarity, SN 1988Z can also be related to shocked CSM (see also Chugai & Danziger 1994). Depending on, e.g., radii and temperatures of shocked CSM, their luminosities can vary. There can be many other similar SNe with variety of luminosities and plateau durations, depending on the CSM properties.

4.3.5 Summary

We have shown that the interaction between SN ejecta and dense CSM is a viable mechanism to power SLSNe such as SN 2006gy. The interaction in the dense CSM accounts for the huge luminosity and the long duration of the SN 2006gy LC. Shock breakout within the dense CSM is a key for the understanding of the interaction-powered SLSNe. Our canonical models have $M_{\rm ej} = 20\ M_\odot$, $E_{\rm ej} = 10^{52}$ erg, and $M_{\rm CSM} = 18\ M_\odot$ ($s = 5$) or $15\ M_\odot$ ($s = 0$) where the CSM is assumed to have a density profile of $\rho_{\rm csm} \propto r^{-s}$. The corresponding average mass-loss rate of the progenitor is about $0.4\ M_\odot\ {\rm yr}^{-1}$ if we assume that the dense CSM originates from a 100 km s^{-1} wind. Our steady mass-loss models ($s = 2$) fail to explain the SN 2006gy LC. No ^{56}Ni is required to explain the early LC of SN 2006gy.

It is difficult to break the degeneracy among $M_{\rm ej}$, $E_{\rm ej}$, and $M_{\rm CSM}$. One can obtain constraints on the progenitor of SN 2006gy based on the efficiency, as the conversion efficiency of the SN kinetic energy to radiation becomes high when $M_{\rm ej}$ is comparable to or less than $M_{\rm CSM}$. The progenitor of SN 2006gy should be a very massive star like LBVs or PISN progenitors because $M_{\rm CSM} = 18\ M_\odot$ or $15\ M_\odot$. As the conversion efficiency is $\simeq 50$ % at

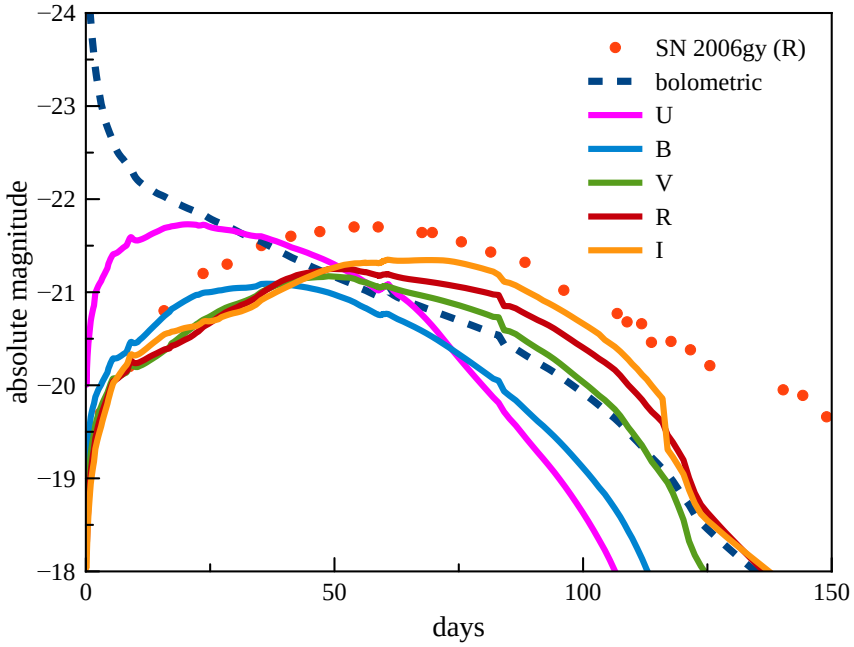

Figure 4.21: Bolometric and multicolor LCs from M06. The R band LC has a rising phase similar to that of SN 2006gy because of the initial high temperature 1.3×10^5 K. However, the high temperature is inconsistent with the SN 2006gy observations.

most and the radiation energy emitted by SN 2006gy is more than 2×10^{51} erg, $E_{\rm ej}$ should be larger than 4×10^{51} erg.

We have also examined the effect of multidimensional instabilities in the dense cool shell on the model LCs. Such instabilities are expected to reduce the amount of kinetic energy converted to radiation. Our LC modeling is based on a one-dimensional radiation hydrodynamics code in which the multidimensional instabilities are implemented only in an approximate way. We have thus explore the effect qualitatively. Further studies on the multidimensinal effects, perhaps using three-dimensional radiation hydrodynamics simulations, are needed for better understanding of SNe powered by the interaction.

4.4 SLSN R

We have discussed the origins of SLSN II so far. In this section, we discuss SLSN R which do not show H lines in their spectra but have the LC decline rates consistent with the ^{56}Co$\rightarrow$ ^{56}Fe decay time. The first reported SN of this kind in literature is SN 2007bi (Gal-Yam et al. 2009). Gal-Yam et al. 2009 compare the LC and spectra of SN 2007bi to some PISN models of Kasen et al. 2011 and conclude that SN 2007bi is a PISN. PISNe are known to produce huge amount of ^{56}Ni but Umeda & Nomoto 2008 show energetic core-collapse SNe can also produce the huge amount of ^{56}Ni required to explain the huge luminos-

ity of SN 2007bi. Here, in Section 4.4.1, we show that the LC of SN 2007bi can actually be explained by an energetic core-collapse explosion and SN 2007bi is not necessarily a PISN. However, this does not mean that SN 2007bi is not a PISN. We discuss the various possible origins for SLSN R (PISNe, energetic core-collapse SNe, and magnetars) and ways to distinguish the different possible origins.

4.4.1 Core-Collapse Supernova Model for SLSN-R 2007bi

4.4.1.1 Progenitor and Explosion Modeling

In this section, we assume that SN 2007bi is powered by the ^{56}Ni heating. The high peak luminosity and the long rise time of the LC of SN 2007bi (Gal-Yam et al. 2009, Young et al. 2010) require a large amount of ^{56}Ni ($> 3\ M_\odot$, Gal-Yam et al. 2009) and a large ejecta mass. These observations imply that the progenitor of SN 2007bi is massive. We apply a pre-SN model with $M_{\rm ZAMS} = 100\ M_\odot$ calculated by Umeda & Nomoto 2008 for our core-collapse SN model. Umeda & Nomoto 2008 assumed the metallicity of the progenitor models to be $Z = Z_\odot/200$, which is small enough to avoid a large amount of mass loss. Then the pre-SN model remains as massive as 83 $M_\odot$, whose C+O core is massive enough (43 $M_\odot$) to produce a large amount of ^{56}Ni.

However, the pre-SN model has a massive H-rich envelope, while SN 2007bi does not show the lines of either H or He. This is also true for PISN models (e.g., Heger & Woosley 2002, Umeda & Nomoto 2002). Therefore the progenitor must have lost its H-rich envelope (36 $M_\odot$) and He layer (4 $M_\odot$) during the pre-SN evolution, thus having only the bare C+O core at the explosion. We construct the pre-SN C+O star model of 43 $M_\odot$, by removing the H-rich envelope and He layer from the 83 $M_\odot$ star. Note that the metallicity of the host galaxy of SN 2007bi ($Z \simeq Z_\odot/3$, Young et al. 2010) is higher than that of our adopted progenitor ($Z = Z_\odot/200$). The mass loss is expected to work more efficiently and the ZAMS mass of the progenitor which has the C+O core mass of 43 $M_\odot$ might be more massive (c.f. Yoshida & Umeda 2011). The rotation of stars can also play a role in mass loss (e.g., Meynet & Maeder 2003, Hirschi et al. 2004, Meynet & Maeder 2005, Georgy et al. 2009, Ekström et al. 2012). Another possible cause of such envelope stripping is the formation of a common envelope during a close binary system, where the smaller mass companion star spirals into the envelope of the more massive star. The outcome depends on whether the energy available from the spiral-in exceeds the binding energy of the common envelope, thus being either a merging of the two stars or the formation of two compact stars, e.g., a C+O star and a He star (e.g., Nomoto et al. 1995).

The explosions of the SN progenitor are induced by a thermal bomb and followed by a one-dimensional Lagrangian code with the piecewise parabolic method (Colella & Woodward 1984). Note that the explosion energy is a free parameter in core-collapse SN explosion models while it is not in PISN explosion models. Explosive nucleosynthesis is calculated as post-processing for the thermodynamical history obtained by the hydrodynamical calculations. The resultant abundance distribution is basically very similar to those calculated by Umeda & Nomoto 2008 (see Figures 5 and 6 in Umeda & Nomoto 2008).

The dynamics of the ejecta is followed until 1 day after the explosion, when the expansion already becomes homologous. For simplicity, the bolometric LCs are calculated

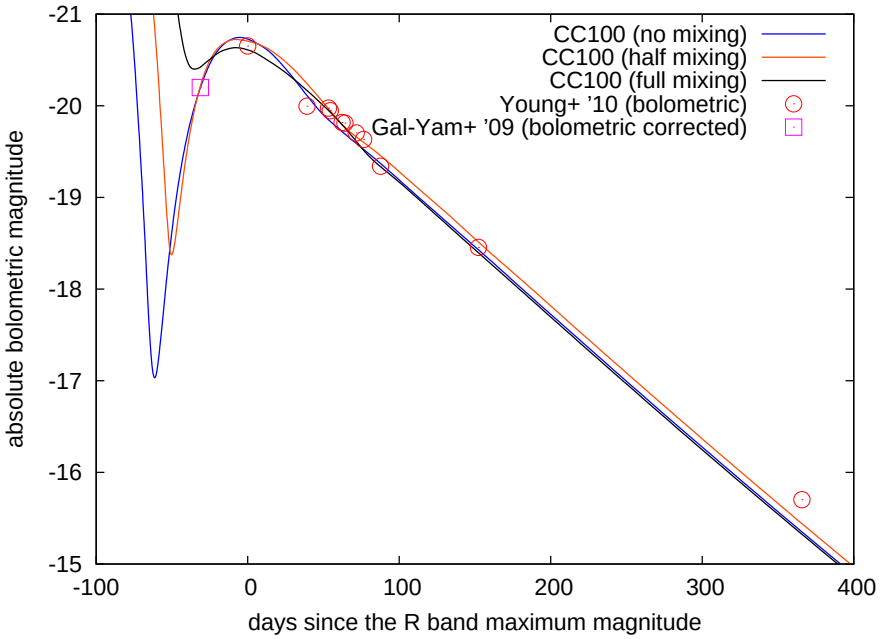

Figure 4.22: Bolometric LCs of the C+O star SN models CC100 ($M_{\rm ej} = 40\ M_\odot$, $E_{\rm ej} = 3.6 \times 10^{52}$ erg, and $M_{^{56}\rm Ni} = 6.1\ M_\odot$). The observed bolometric LC (open circles) is taken from Young et al. 2010. The bolometric magnitude of the rise part of SN 2007bi (open square) is estimated from the R band magnitude. All the calculated LC has the same physical structure but the degrees of mixing are different. The horizontal axis shows the days in the rest frame.

for the homologous ejecta by using a local thermodynamic equilibrium radiation transfer code (Iwamoto et al. 2000) that includes the radioactive decays of ^{56}Ni and ^{56}Co as energy sources. This code calculates the γ-ray transport for a constant γ-ray opacity (0.027 cm^2 g^{-1}, Axelrod 1980) and assumes all the emitted positrons are absorbed in situ[3]. For the general radiation transport, the Thomson scattering opacity is obtained by calculating the electron density from the Saha equation, and the Rosseland mean opacity is estimated from the empirical relation to the Thomson scattering opacity (Deng et al. 2005).

4.4.1.2 Results

We construct several core-collapse SN models and compare them with the observations of the bolometric LC and the line velocities of SN 2007bi shown in Young et al. 2010. Since the LC of Young et al. 2010 does not cover the rising part, we estimate the bolometric magnitude of the rising part from the R band observations (Gal-Yam et al. 2009) assuming the same bolometric correction (0.45 mag) as in the R band maximum. We also take into account mixing since it is possible that a jet emerges from the central remnant and causes the mixing of the ejecta (e.g., Maeda & Nomoto 2003, Tominaga 2009).

[3] This assumption of the positron absorption does not have much effect on the LCs we show in this section, because the contribution from the γ-rays are still dominant energy source of them.

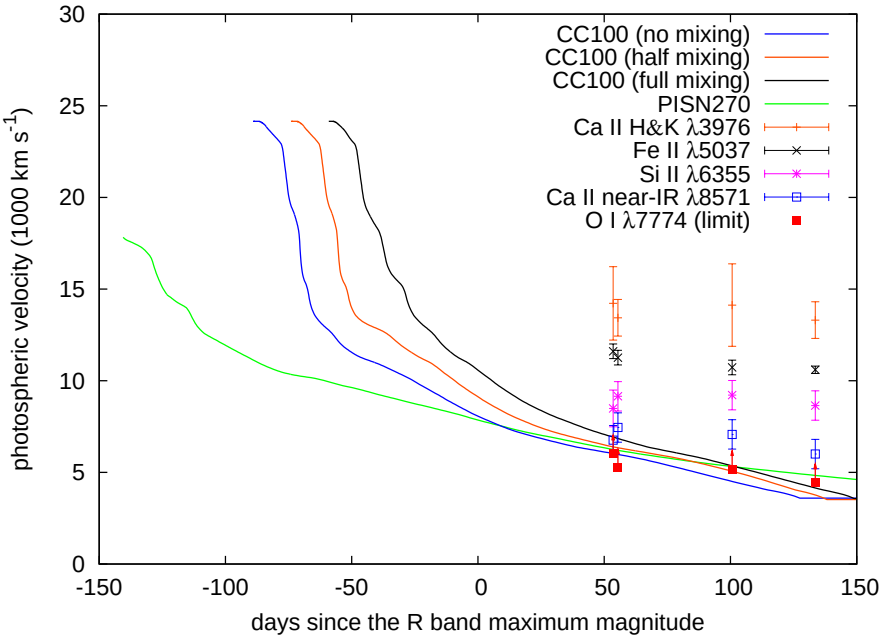

Figure 4.23: Photospheric velocities of the core-collapse SN and PISN models. The horizontal axis shows the days in the rest frame. The line velocities of SN 2007bi observed by Young et al. 2010 are also shown for comparison. The line velocities of OI λ7774 shows the lower limit. All the photospheric velocities are low enough to be consistent with the observed line velocities.

The LCs of the successful models (CC100) are shown in Figure 4.22. The kinetic energy ($E_{\rm ej}$), ejecta mass ($M_{\rm ej}$), and ^{56}Ni mass ($M_{^{56}\rm Ni}$) in the ejecta are $E_{\rm ej} = 3.6 \times 10^{52}$ erg, $M_{\rm ej} = 40\ M_\odot$, and $M_{^{56}\rm Ni} = 6.1\ M_\odot$, which are the same in all the models. The mass cut between the ejecta and the compact remnant is set at $M_r = 3\ M_\odot$, where M_r is the mass coordinate, so that the ejecta contains 6.1 $M_\odot$ of ^{56}Ni, which turns out to be consistent with the bolometric LC of SN 2007bi. The kinetic energy $E_{\rm ej}$ needs to be large to produce $M_{^{56}\rm Ni} = 6.1\ M_\odot$. The mass of some elements included in the ejecta are summarized in Table 4.4. The kinetic energy is as large as those of previously observed SNe which were associated with a gamma-ray burst (SNe 1998bw, 2003dh, 2003lw; e.g., Nomoto et al. 2006).

We adopt two different degrees of mixing to see its effects on the LC. The full-mixing model assumes that the whole ejecta are uniformly mixed. The half-mixing model assumes that the inner half of the ejecta (in the mass coordinate) is uniformly mixed. One of the effects of the mixing is seen in the rise time of the LC. With mixing, ^{56}Ni is distributed closer to the surface of the ejecta, so that the diffusion time is shorter and the rise time becomes shorter. The rise time of the model without mixing is 85 days while the rise times of the half-mixing model and the full-mixing model are 67 days and 52 days, respectively. As the rise time of SN 2007bi is not observationally well-determined, all the models are consistent with the bolometric LC of SN 2007bi. The initial decline part of the calculated LCs before maximum is formed by the shock heating of the envelope and its subsequent cooling due

Table 4.4: Amount of elements contained in the SN ejecta (in $M_\odot$)

^{12}C	^{16}O	^{20}Ne	^{24}Mg	^{28}Si	^{32}S	^{36}Ar	^{40}Ca	^{56}Ni
1.4	18.7	1.4	1.5	5.1	2.7	0.5	0.4	6.1

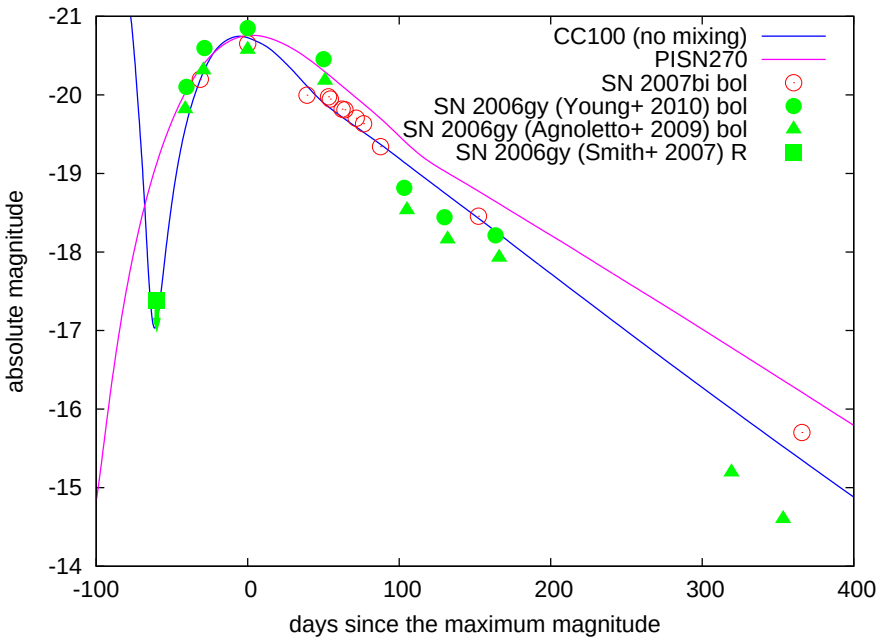

Figure 4.24: A PISN model for SN 2007bi (PISN270). The CC100 no-mixing model and observed bolometric LC of SN 2007bi in Figure 4.22 are also shown. The bolometric LC of SN 2006gy is taken from Young et al. 2010, Agnoletto et al. 2009 for comparison. The first point of SN 2006gy is the R band upper limit from Smith et al. 2007. The horizontal axis shows the days in the rest frame.

to the rapid expansion. Radiation hydrodynamical calculations are required to obtain the realistic LC at this epoch.

In Figure 4.23, we show the photospheric velocities obtained by the LC calculations. With the photospheric velocities, we also show the observed line velocities of SN 2007bi taken from Figure 17 of Young et al. 2010. The photospheric velocities of all the models are consistent with the observed lowest line velocities, which are thought to trace the photospheric velocity.

4.4.2 SLSN-R Models and their Characteristics

We show in the previous section that energetic core-collapse SN models can be consistent with SN 2007bi. Here, we discuss the characteristics of other suggested mechanisms and progenitors of SLSN R and possible ways to distinguish them observationally.

Let us first confirm that a PISN model can also be consistent with the bolometric LC of SN 2007bi by using the approximate PISN model PISN270 and discuss the differences between the two models. The PISN270 model is constructed by scaling the

physical structure of the homologously expanding model CC100 to the ejecta model with $M_{\rm ej} = 121\ M_\odot$ and $E_{\rm ej} = 7 \times 10^{52}$ erg. The ejecta mass $M_{\rm ej}$ is the same as the C+O core mass of the PISN model with $M_{\rm ZAMS} = 270\ M_\odot$(Umeda & Nomoto 2002), and $E_{\rm ej}$ is obtained from the nuclear energy released by explosive nuclear burning of the C+O core (Umeda & Nomoto 2002). Here the same amount of ^{56}Ni ($M_{^{56}\rm Ni} = 9.8\ M_\odot$) as in the 270 $M_\odot$ model (Umeda & Nomoto 2002) is assumed to be synthesized in the inner layers. Note that the 270 $M_\odot$ model of Umeda & Nomoto 2002 still has the H-rich and He envelopes at the time of explosion and, here, we assume that the envelopes were stripped off by some mechanism.

Figure 4.24 shows that the bolometric LC of PISN270 (the red line) is consistent with the bolometric LC of SN 2007bi (red open circles). The rise time to the LC peak for PISN270 is $\simeq 150$ days, being consistent with the PISN model in Gal-Yam et al. 2009. This rise time is longer than the core-collapse SN model CC100 (Figure 4.24), because the photon diffusion takes more time in more massive PISN270. Although $M_{^{56}\rm Ni}$ of PISN270 is $\simeq 1.6$ times larger than that of the core-collapse SN CC100 model, the longer rise time lowers the peak brightness powered by the radioactive decay. These two effects make the peak magnitude of PISN270 similar to CC100.

This difference in the rising time of the LC is important to distinguish between core-collapse SN and PISN models. For example, SN 2006gy was first suggested to be a PISN (e.g., Smith et al. 2007) but the fast rising time seen in Figure 4.24 as well as its spectral type (Type IIn) declined this possibility. Although SN 2007bi was not observed early enough, much earlier observations before the peak could constrain the progenitor from the LC.

Another difference in core-collapse SN models and PISN models is the abundance of the elements like Si and S. The abundance of our core-collapse SN model is consistent with the directly estimated abundances of Gal-Yam et al. 2009, i.e., C, O, Na, Mg, Ca, and ^{56}Ni. If SN 2007bi was a PISN, large amounts of Si and S should have been synthesized as shown by Gal-Yam et al. 2009 while core-collapse SN models predict much less amounts of Si and S. As Si and S have many emission lines in the infrared range, infrared spectra are also helpful to distinguish PISNe from core-collapse SNe. Note, however, that, although our core-collapse SN model is consistent with the estimated abundance of SN 2007bi by Gal-Yam et al. 2009, we still have not performed the numerical calculations of the nebular spectra based on our model. Elements whose abundances are not able to be estimated by the spectra could have played a role in line cooling processes and, to confirm that the abundance of the core-collapse SN model is consistent with the spectra, we have to perform the spectral synthesis calculations. We also point out that, if SN 2007bi is confirmed to be a PISN, we could expect that PISNe played a role in the chemical enrichment in the early Universe and there should be some old stars with chemical compositions expected from PISNe, although they are still not discovered (e.g., Cayrel et al. 2004).

We have shown that the LC and photospheric velocity of SN 2007bi are well-reproduced by the core-collapse SN model CC100. As some gamma-ray bursts are connected to such high energy SNe Ic, the extremely SLSNe like SN 2007bi could also be connected to gamma-ray bursts which result from very massive stars. If this is the case, extremely luminous SNe like SN 2007bi could be connected to gamma-ray bursts of much more massive star origin than known SNe associated with a gamma-ray burst. Even stars more massive than 300 $M_\odot$ could

be the origin of SLSNe (e.g., Ohkubo et al. 2006, Ohkubo et al. 2009).

We have been assuming that SLSN R is powered by the nuclear decay energy from ^{56}Ni to ^{56}Fe because of the timescale of the LC evolution. However, if a magnetar has a certain rotation period with an appropriate magnetic field, the LC decline can be similar to those of SLSN R (Kasen & Bildsten 2010). In addition, Dessart et al. 2012 argue that SLSN R has spectral temperatures which are higher than those expected from the ^{56}Ni heating. The progenitor mass of both PISN models and core-collapse SN models need to be large to produce the required large amount of ^{56}Ni ($\simeq 5\ M_{\odot}$). Dessart et al. 2012 show that the ^{56}Ni mass estimated from the LC is not enough to heat the huge ejecta mass as hot as is observed. For the case of the magnetar heating, the source of the energy is the rotational energy of the compact remnant and the ejecta mass does not need to be large and they can be easily heated up. However, the required magnetar spin period and magnetic field must be adjusted properly to mimic the ^{56}Ni-^{56}Co-^{56}Fe decay of SLSN R LCs. A natural explanation for having such magnetars seems to be required because a number of SLSN R are discovered so far and they always have the LC following the ^{56}Ni-^{56}Co-^{56}Fe decay.

4.5 SLSN I

SLSNe we have discussed so far have some hints for their power sources in their observations. SLSN II has narrow emission lines and SLSN R has LCs which are consistent with the ^{56}Co decay timescale. However, SLSN I does not have any clear signatures of their origin. There are several suggested mechanisms to power SLSN I. One possibility is the collision between SN ejecta and dense CSM with C and O (Blinnikov & Sorokina 2010). Others are some extra heating from inside C+O-rich SN ejecta. After the explosion of a WR star, magnetars inside (Kasen & Bildsten 2010, Woosley 2010, Maeda et al. 2007), fallback (Dexter & Kasen 2012), or the phase transition of the neutron star inside to a quark star (Ouyed et al. 2012, Kostka et al. 2012, Benvenuto & Lugones 1999) can heat the expanding C+O-rich SN ejecta from inside and make it very bright.

Here we focus on the interaction between SN ejecta and C+O-rich dense CSM and the observational signatures caused by the interaction. We show that this scenario predicts that the luminosity of SLSNe should decline for a while before the strong interaction that powers the huge luminosity begins. The 'dip' is an inevitable consequence of the shock breakout within the dense CSM (Section 2.4.1, Chevalier & Irwin 2011, Svirski et al. 2012, see also Ofek et al. 2010, Balberg & Loeb 2011). The possible dip observed in SLSN 2006oz (Leloudas et al. 2012) could be the first example of this and it indicates that the SN-CSM interaction is the power source of the SLSN I 2006oz.

4.5.1 Dense Circumstellar Medium around SN 2006oz

We explore a consequence of the SN-dense CSM interaction scenario to power the emission from SLSNe. Although our arguments apply to any SLSNe powered by interaction, we focus on SN 2006oz to provide our basic idea. This SLSN is the best example of SLSNe so far for which the early phase behavior was well observed. First, we estimate the physical properties of the dense CSM around the progenitor of SN 2006oz, under the assumption that the main

LC was powered by the interaction between SN ejecta and dense CSM. Then, with these constraints, we discuss what is expected to take place in the proposed system before the main LC.

Figure 4.25a presents the progenitor system required in the interaction scenario. A dense CSM shell exists between R_i and R_o. Once the SN ejecta reaches R_i, the interaction takes place until the ejecta reaches R_o, and this interaction powers the main LC. An early emission is created in the phase before the ejecta reaches to R_i. Our main arguments below do not depend on the nature of a power source for the early emission, and thus we proceed without specifying it (see Section 4.5.3 for possible origins for the early emission). The CSM should be dense enough to explain the peak luminosity of SN 2006oz by the interaction scenario, and the shock breakout is expected to take place within the CSM at the beginning of the interaction. The radius where the shock breakout occurs is expressed as xR_o ($R_i/R_o < x < 1$). As we focus on H-poor SLSNe, we assume that the CSM is mainly composed of C and O, and the progenitor star is a WR star. In the following, we assume that the dense CSM is uniformly distributed with a constant density. This is just for the sake of simplicity, and the main result is not sensitive to this assumption. Under these assumptions, we estimate the properties of the dense CSM by comparing the shock breakout prediction and the observed features of SN 2006oz.

The blackbody radius obtained from the spectrum near the main LC peak of SN 2006oz is about 2.5×10^{15} cm (Leloudas et al. 2012). Since the last scattering surface of the CSM at the main LC peak is expected to be at the outermost region of the dense CSM shell when the density is constant in the dense CSM (Section 2.4.1), we can estimate that $R_o \simeq 2.5 \times 10^{15}$ cm. On the other hand, the blackbody radius at the beginning of the main LC rising phase (i.e., at the beginning of the strong interaction just after the shock breakout within the CSM) is $\simeq 10^{15}$ cm (Leloudas et al. 2012). Thus, we can estimate that $xR_o \simeq 10^{15}$ cm.

By assuming that the rising time of the main LC of SN 2006oz ($\simeq 30$ days) corresponds to the diffusion time t_d of the dense CSM, the electron density n_e in the dense CSM can be estimated from the following equation:

$$t_d \simeq \frac{\tau_T (R_o - xR_o)}{c}, \tag{4.13}$$

where $\tau_T = \sigma_T n_e (R_o - xR_o)$ is the Thomson scattering optical depth within the dense CSM. From Equation 4.13,

$$n_e \simeq \frac{ct_d}{\sigma_T (R_o - xR_o)^2} \simeq 5 \times 10^{10}\ \mathrm{cm}^{-3}. \tag{4.14}$$

The last value of Equation 4.14 is estimated by adopting the parameters for SN 2006oz, i.e., $t_d = 30$ days, $xR_o = 10^{15}$ cm, and $R_o = 2.5 \times 10^{15}$ cm. $\tau_T = 52$ in this case and it is plausible that the shock breakout occurs in the CSM with a typical forward shock velocity $v_s \simeq 10,000$ km s^{-1} ($c/v_s \simeq 30$).

If the dense CSM is composed of 50 % C and 50 % O and both C and O are singly ionized in the entire CSM, the CSM density corresponding to $n_e \simeq 5 \times 10^{10}$ cm^{-3} is $\rho_{\rm csm} \simeq 10^{-12}$ g cm^{-3}. Then, the required CSM mass is $\simeq 35\ M_\odot$. If we further assume that the outflowing velocity of the dense CSM was 100 km s^{-1}, the 35 $M_\odot$ of C+O-rich materials must have been lost from the progenitor within 8 years before the explosion at a

Table 4.5: Model parameters of SN 2006oz

R_i	xR_o	R_o	n_e	CSM Density	CSM Mass
cm	cm	cm	cm^{-3}	$\mathrm{g\ cm}^{-3}$	$M_\odot$
10^{15}	10^{15}	2.5×10^{15}	5×10^{10}	10^{-12}	35

rate of $\simeq 7\ M_\odot\ \mathrm{yr}^{-1}$. Mechanisms by which WR stars experience such a huge mass loss just before the explosion have not yet been clarified, although there are some suggestions (e.g., Quataert & Shiode 2012). Alternatively, the dense CSM does not necessarily need to come from the huge mass ejection from the progenitor. Within a dense cluster, collisions of WR stars may leave dense C+O-rich envelopes that would persist until the time of the explosion. This is an alternative way to have a dense C+O-rich CSM around a SN (see also, e.g., Portegies Zwart & van den Heuvel 2007, Pan et al. 2012b, Chevalier 2012).

4.5.2 A Dip as a Signature of the SN-CSM Interaction

Based on the properties of the dense CSM required by the SN-CSM interaction scenario to power the main LC of SLSN 2006oz discussed above (Table 4.5), we now investigate a consequence of this scenario in the early phase before the main LC. We suggest that there must be a brief phase of the decreased luminosity lasting for a few days before the strong interaction energizes the main LC. This argument is independent of any assumptions regarding the nature of the early emission which will be discussed in Section 4.5.3. The only requirement is that there is a detectable, i.e., sufficiently luminous, early emission phase. The dip phase should then appear as the fading phase between the early emission and the main LC.

Figure 4.25 summarizes our model for the dip after the early emission. Before the explosion, most of C and O in the dense CSM is not ionized, and thus the CSM is transparent. This is because of the high CSM density which results in the high recombination rate ($\simeq 10^{-12}$ g cm^{-3} estimated for SN 2006oz). The emission rate of the ionizing photons from a typical WR star ($10^6 L_\odot$ and 10^5 K) is $\sim 10^{49}$ s^{-1}. With the recombination coefficient $\sim 10^{-13}$ cm^3 s^{-1}, the number of ionizing photons is too small to keep the dense CSM ionized.

Then, the central star explodes as a SN. Before the ejecta reaches R_i (Figure 4.25b), the SN ejecta expands within the rarefied region below R_i. We attribute the early emission in the LC to the light from the SN ejecta in this phase before the strong collision. The duration of the early emission in SN 2006oz before the main LC is about 10 days. Regardless of the nature of the early emission, the duration can be interpreted as the time required for the SN ejecta to reach the dense CSM (i.e., at R_i) in our scenario. With $v_s \simeq 10,000$ km s^{-1}, it reaches $\simeq 10^{15}$ cm in about 10 days and we can estimate that $R_i \simeq xR_o$. This is consistent with the estimated blackbody radius in this phase (Section 4.5.1).

Regardless of the mechanisms to power the early emission, if the majority of photons emitted from the SN ejecta is in the optical or near-UV, most of C and O in the dense CSM will still not be ionized during the early emission phase. For instance, the blackbody radius and temperature of SN 2006oz during the early emission phase are $\simeq 10^{15}$ cm and 15,000 K, respectively, and the emission rate of the ionizing photons ($\sim 10^{54}$ s^{-1}) is too small to

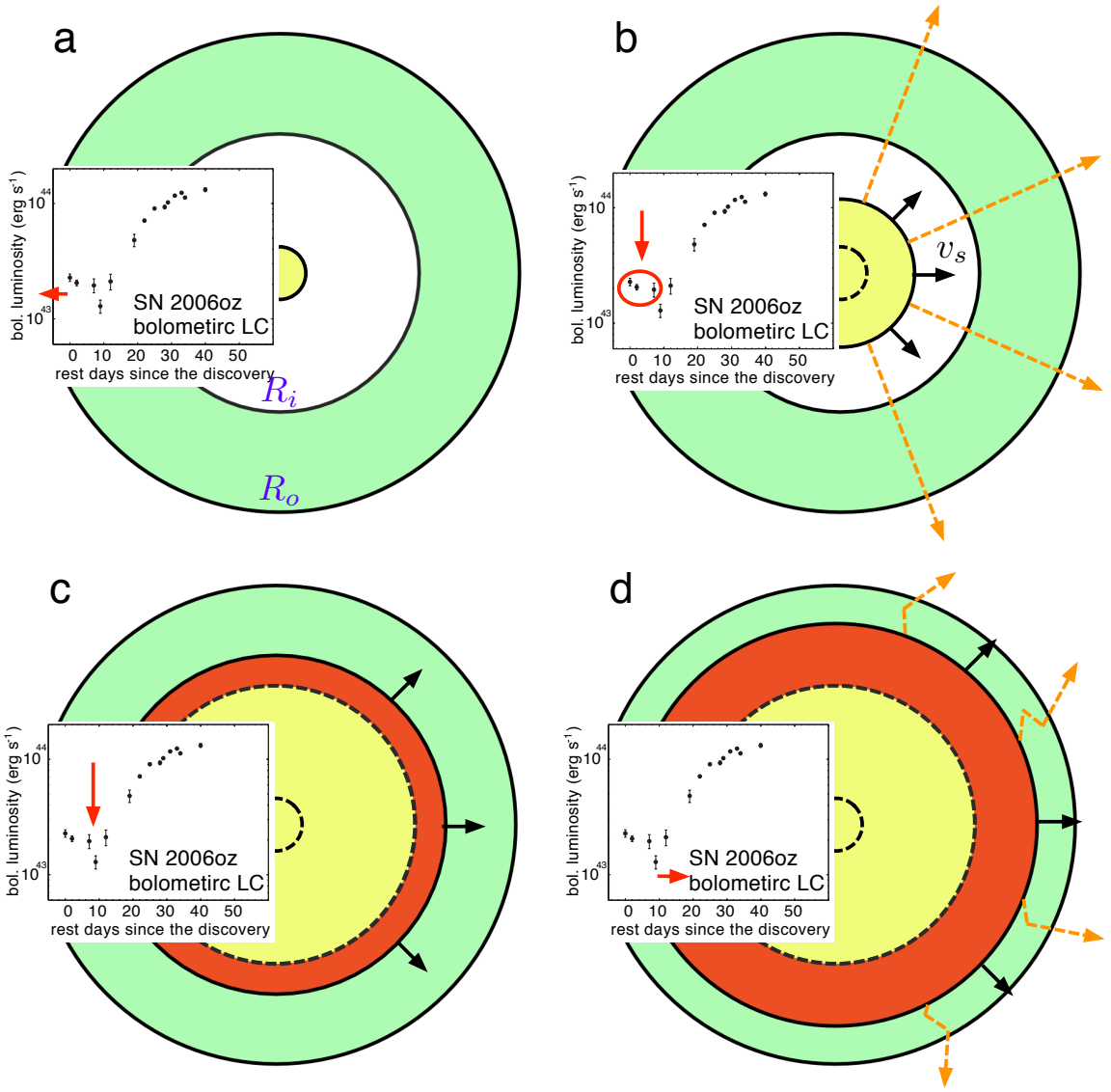

Figure 4.25: The proposed origin of the dip between the early emission and the main LC. The dense CSM, within which the shock breakout occurs, extends from R_i to R_o. A progenitor star explodes in this configuration (a). Before the forward shock reaches R_i (b), the dense CSM is transparent to optical photons from the SN ejecta and they can be observed as an early emission. When the forward shock reaches R_i (c), the opacity suddenly increases as ionization in the dense CSM is enhanced. Thus, even if the energy source of the early emission is still active, the dense CSM blocks the light, causing a dip in the LC. Then, after the shock breakout within the dense CSM (d), photons can escape from the shock again. The SN is now powered by the strong interaction reaching the large luminosity in the main peak. The LC shown in each inset is the bolometric LC of SN 2006oz obtained by Leloudas et al. 2012.

keep most of the dense CSM ionized. Only the innermost thin layer of the dense CSM (up to $\simeq 1.2 \times 10^{15}$ cm) can be ionized in this case. The optical depth to the Thomson scattering in this ionized region becomes $\simeq 7$. However, the ionizing region is confined in the thin layer, and the diffusion timescale within it is estimated to be less than a day. Thus, the photosphere can be located in this thin layer of ionized material, but the effect on the LC evolution is expected to be small. Some recombination lines may be found in spectra at this phase. Nonetheless, most of the dense CSM is still transparent to optical photons, and thus we can observe the early emission.

After about 10 days since the explosion, the SN ejecta starts to collide with the dense CSM. Because of the strong interaction, X-rays and UV photons are now efficiently produced at the forward shock, and the electron density in the dense CSM suddenly increases. The CSM gets ionized and the Thomson scattering makes the dense CSM opaque to any photons. Then, the diffusion velocity of photons can be less than the velocity of the shock wave, and photons cannot go out of the shock until the shock breakout takes place at xR_o (Figure 4.25c). During this optically thick phase before the shock breakout, the luminosity decreases. This sudden decline in the luminosity is a naturally-expected observable signature of the strong SN-CSM interaction scenario.

We suggest that the possible dip observed in SN 2006oz could be the first observed example of this signature. After this discovery, SNe IIn 2009ip (e.g., Prieto et al. 2013) and 2010mc (Ofek et al. 2013) was found to have similar dip in the precursor. As SNe 2009ip and 2010mc clearly have dense CSM because of its spectral type, our suggestion that the dip comes from dense CSM is strongly supported.

The duration of the dip in the LC of SN 2006oz was short. The luminosity at the single observed epoch after the early emission showed the decline, and the luminosity was back to the previous level by the next epoch (Leloudas et al. 2012, Figure 4.25). Therefore, the duration of the dip was at most 2 days. From this, we can place a constraint on the shock breakout: $xR_o - R_i$ should be less than 2×10^{14} cm, or xR_o should be less than 1.2×10^{15} cm, if $v_s = 10,000$ km s^{-1}. We note that the duration of the dip can be very short, and thus high cadence observations are important to capture this signature.

After the shock breakout at xR_o, photons are able to escape out of the interaction region. Then, the SN luminosity is powered by the SN-CSM interaction, and the SN becomes superluminous from the ongoing strong interaction (Figure 4.25d, Section 4.5.1).

4.5.3 Summary and Discussion

We have suggested a new way to distinguish proposed power sources of SLSNe in this section. Among scenarios proposed so far, the interaction scenario, which requires the existence of dense CSM, is distinguishable by the early phase LC before the rising part to the peak luminosity. The scenario predicts that a brief dip phase should appear before the main LC if there is an early emission which is bright enough to be observed, as was the case for the SLSN I 2006oz. SNe IIn 2009ip and 2010mc showed a similar dip in the LC and this fact supports our suggestion. This argument is irrespective of detailed nature and origin of the early emission itself. The existence of the dip reflects the change in the ionization condition in the dense CSM following the SN-CSM interaction which results in the shock breakout

within the CSM. The possible dip observed in SLSN I 2006oz indicates that the main power source of the huge luminosity for this SLSN is the strong interaction between the SN ejecta and the dense C+O-rich CSM whose mass is estimated as $\simeq 35\ M_{\odot}$. Other proposed power sources like magnetars may also happen to show a dip for a specific combination of model parameters and a dip may appear in some SLSNe but not in all SLSNe in these scenarios. On the other hand, a dip should always appear when the shock breakout occurs. Thus, more SLSN I samples in the early phase are required to see whether a dip is a common feature of SLSN I and it is actually due to the shock breakout.

The early emission of SN 2006oz itself is bright ($\sim 10^{43}$ erg s^{-1}), with the total radiation energy of $\sim 10^{49}$ erg within $\simeq 10$ days. There are a few possible mechanisms to power the early emission. ^{56}Ni produced in the SN inside is one possibility. The color of the early emission obtained by Leloudas et al. 2012 is similar to that of SNe Ia near the LC peak (e.g., Wang et al. 2009). The required ^{56}Ni mass to explain the early emission luminosity is $\sim 1\ M_{\odot}$. However, a difficulty in this model is that the rising time of the early emission is constrained to be 5 days at most (Leloudas et al. 2012), which is too short for the ^{56}Ni heating scenario. Another possibility is the interaction between the SN ejecta and CSM. It is possible that CSM which is less dense than the dense CSM above R_i exists below R_i. If there is additional CSM of $\sim 0.1\ M_{\odot}$ below R_i, this is enough to create the luminosity of $\sim 10^{43}$ erg s^{-1} through the SN-CSM interaction (Section 5.3). This small amount of CSM would not change the overall picture we suggest, since the total amount of the radiation energy emitted as the early emission ($\sim 10^{49}$ erg) is much smaller than the total available kinetic energy ($\sim 10^{51}$ erg or even more) by the SN explosion and the small amount of the CSM does not affect the dynamics of the shock wave so much.

The existence of $\sim 10\ M_{\odot}$ C+O-rich CSM around a WR star which is lost just before its explosion clearly challenges the current understanding of stellar mass loss and stellar evolution. This drastic mass loss could influence the final progenitor mass at the time of its explosion and its fate. For example, stars which are currently considered to end up with a black hole due to fallback may actually become a neutron star because of the extra mass loss which reduces the mass of the accreting envelope material at the time of the core collapse. We still do not have a large number of observations to confirm that a WR star can actually have such mass loss and the dip is a common feature of SLSN I. Future observations of SLSN I especially in the early phases are essential for understanding the origin of SLSN I and the final fates of WR stars.

4.6 Superluminous Supernovae as a Probe of the Early Universe

Thanks to their huge luminosities, SLSNe can be observed even if they appear at very high redshifts. The current most distant SN reported is a SLSN at $z = 3.9$ (Cooke et al. 2012). As SLSNe are likely from very massive stars as we have seen in this chapter, they can be a probe of the highest end of the initial mass function (IMF) at the early Universe.

The IMF of the local Universe observationally has been suggested to be uniform, regardless of the variety of the star forming environment (e.g., Kroupa 2002). The IMF of the local

Universe is empirically known to follow the Salpeter IMF[4] (Salpeter 1955). However, there exist several suggestions that the IMF is different from that of the local Universe at high redshifts. Especially, it is suggested that massive stars are preferably formed in the early Universe and the IMF is top-heavy at that time. For example, the Lyα emitters in the protocluster SSA22 at $z \sim 3$ are found to have the EWs of Lyα emission lines which can be explained by a top-heavy IMF (Morimoto 2008, see also Malhotra & Rhoads 2002).

The most strongly suggested possibility for a top-heavy IMF is the IMF of the first generation stars. The first stars are formed in clouds which are evolved from the primordial density fluctuations (e.g., Bromm 2013, Yoshida et al. 2008). The subsequent collapses of the clouds end up with the massive protostellar clouds of $\sim 10^4\ M_\odot$ which can be massive stars (e.g., Omukai 2001) and hence, result in a top-heavy IMF (see also Bromm et al. 1999, Abel et al. 2000, Nakamura & Umemura 2001). However, recent works suggest that the first stars may not be as massive as previously thought because of the radiative feedback (Hosokawa et al. 2011, McKee & Tan 2008, see also Susa 2013).

If the IMF of the early Universe is really top-heavy, we expect the significant increase of the SLSN rate at high redshifts (see Quimby et al. 2013b for the local rate). Tanaka et al. 2012 estimated the expected number of SLSN detection with the upcoming Subaru/Hyper Suprime-Cam (HSC) survey and an idealized NIR SN survey. As we can also see from Figure 4.26, which show the SN 2006gy model LC obtained in Section 4.3 at high redshifts observed by the Subaru/HSC i band, SLSNe can be detected up to about $z = 4-5$ by the HSC ultra-deep survey. If the Salpeter IMF is retained at the early Universe, the very low SLSN rate limits the expected highest redshift detection to $z \simeq 4$ in the ultra-deep survey and the deep survey can be more efficient to find high-redshift SLSNe because of the larger survey area (Tanaka et al. 2012, see also Lien & Fields 2009 for the case of *Large Synoptic Survey Telescope (LSST)*[5]). The spectral confirmations, however, are very difficult because of the faintness (see, e.g., Cooke 2008) and may require 30-m class telescope like *Thirty Meter Telescope (TMT)*[6] for the actual spectral confirmation of very high-redshift SLSNe discovered by Subaru/HSC. We can use the color information to select them before the age of *TMT*.

A promising alternative way to detect the explosions of the first stars at very high redshifts is going to NIR wavelength. Here, we show some NIR LCs of high-redshift SLSN LCs obtained based on the SN 2006gy model in Section 4.3 in Figures 4.27 and 4.28. We use the planned *James Webb Space Telescope (JWST)*[7]/NIRCam broad band filters which can be found at `http://www.stsci.edu/jwst/instruments/nircam/instrumentdesign/filters/index_html` for this purpose. Although SLSNe beyond $z = 10$ can be detected in principle with *JWST* (see also Scannapieco et al. 2005, Whalen et al. 2012), the estimated number of the detection is very small because of the small field of view of *JWST* (see also Hummel et al. 2012, Pan et al. 2012a). For the purpose of SLSNe detection at very high redshifts, it is better to use a wide-field NIR satellite like *Wide-field Imaging Surveyor for*

[4] Note that there are arguments that the Salpeter IMF is only valid for massive stars and low-mass stars do not follow the Salpeter IMF (e.g., Kroupa 2001).

[5] `http://www.lsst.org/`

[6] `http://www.tmt.org/`

[7] `http://www.jwst.nasa.gov/`

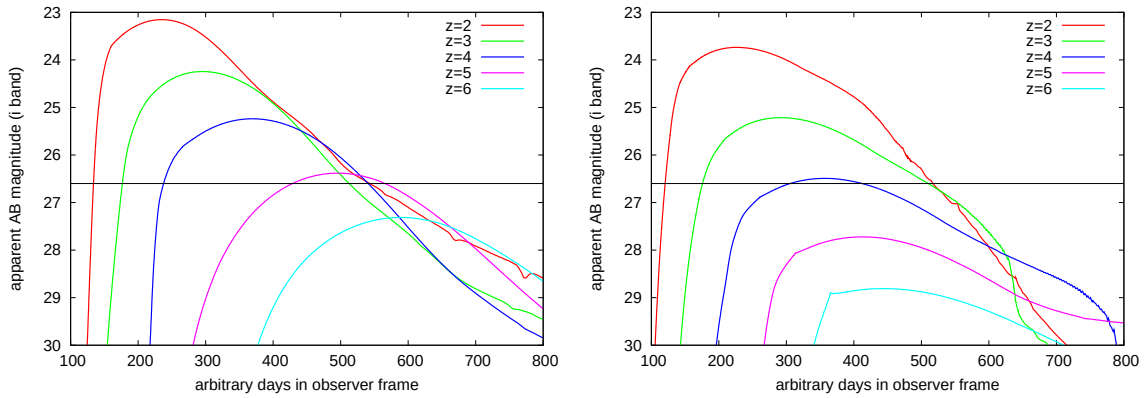

Figure 4.26: i band LCs of the models D2 ($s = 5$, left) and F1 ($s = 0$, right) at several redshifts. The horizontal line is the planed i band limiting magnitude of Subaru/HSC ultra-deep survey at one epoch (26.6 mag).

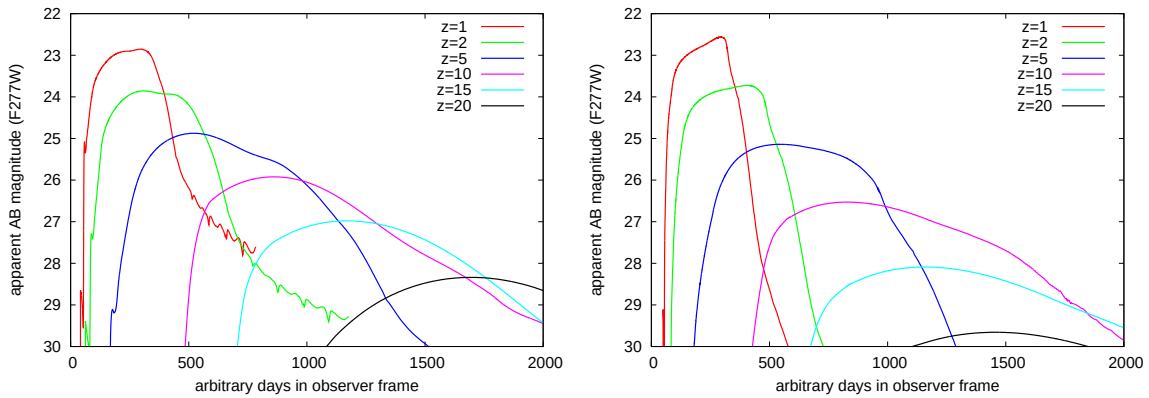

Figure 4.27: F277W band LCs of the models D2 ($s = 5$, left) and F1 ($s = 0$, right) at several redshifts.

High-redshift (WISH),[8] *Wide-Field Infrared Survey Telescope (WFIRST)*[9], or *Euclid*[10].

One last thing worth pointing out is that there is a growing evidence that the absolute peak luminosities of SLSN I do not have much diversities (Quimby et al. 2013b). If this is confirmed, SLSN I can be a new distance ladder which can reach redshifts much higher than those can be reached by SNe Ia and can be a new cosmological probe as well.

[8] http://www.wishmission.org/en/index.html
[9] http://wfirst.gsfc.nasa.gov
[10] http://sci.esa.int/euclid

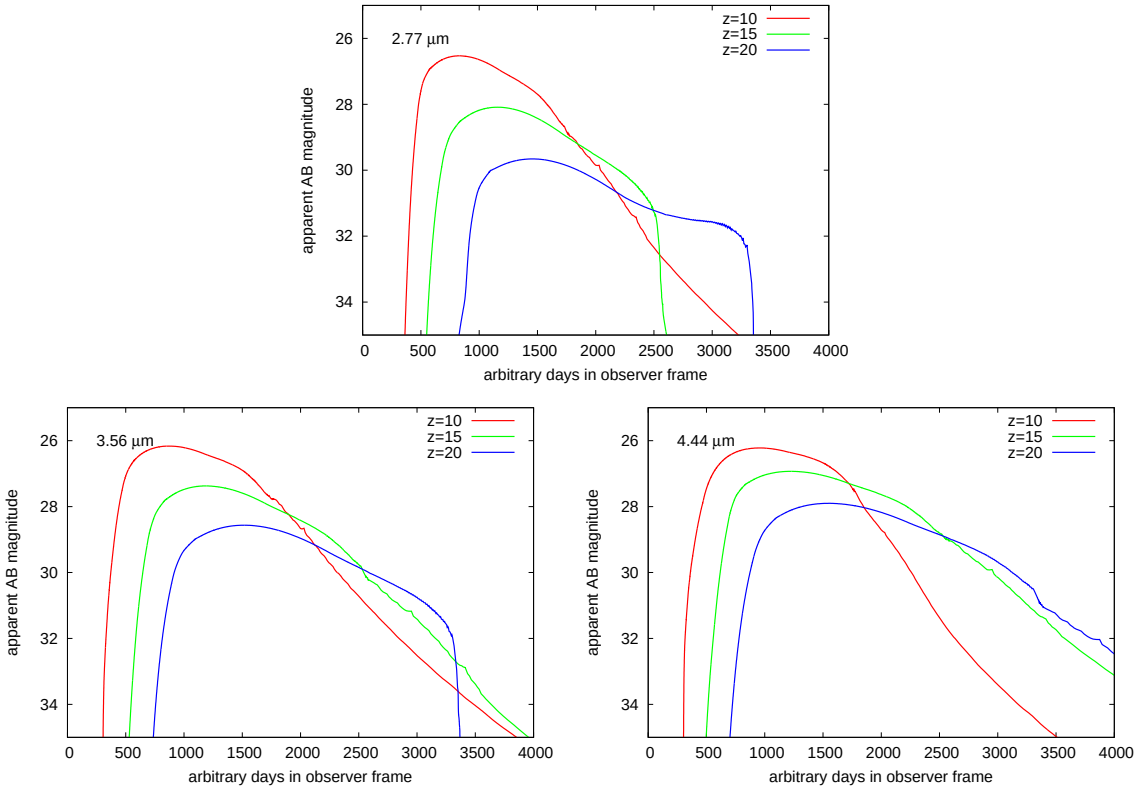

Figure 4.28: F277W, F356W, and F444W band LCs from the model F1 (s=0).

4.7 Summary

We have investigated the nature and origin of SLSNe in this chapter. We show that, except for SLSN R, the currently known observational diversities of SLSNe can be interpreted by the existence of the diversity in the dense CSM in the interaction between SN ejecta and dense CSM. Thus, the interaction between SN ejecta and dense CSM is likely to be a main reason for the huge luminosities of SLSNe.

We show that the shock breakout model naturally predicts that the diversity in SLSN II, i.e., the difference between Type IIn SLSNe and Type IIL SLSNe, is from the diversity in the density slope of the dense CSM (Section 4.2). We also show that the simple analytic shock breakout model can explain the LC properties of the best observed SLSN II 2006gy. Because of the existence of the dip in the precursor of SLSN I 2006oz, SLSN I is also likely to be related to the interaction between SN ejecta and dense C+O CSM.

The CSM mass required to explain the huge luminosities of SLSNe is extremely high and it is typically $\sim 10\ M_{\odot}$. This indicates that the progenitors of SLSNe are very massive stars. Moreover, they need to eject the dense CSM within several decades before their explosions with the mass-loss rates exceeding $0.1\ M_{\odot}\ \mathrm{yr}^{-1}$. No massive stars are known to experience such mass loss and SLSNe are clearly challenging our understanding of massive star evolution. Further SLSNe study will reveal what is lacking in the current understanding of the very

massive stellar evolution.

Finally, we show the expected LCs of SLSNe appeared at high redshifts and they can be observed with appropriate transient surveys. SLSNe are potential powerful tool to probe the IMF of the high-redshift Universe. In addition, SLSN I may turn out to be a distance ladder which can be used to probe the cosmology beyond the Universe that can be reached by SNe Ia.

This chapter is based on
T.J. Moriya, N. Tominaga,
The Astrophysical Journal, 747, 118, 2012
T.J. Moriya, S.I. Blinnikov, N. Tominaga, N. Yoshida, M. Tanaka, K. Maeda, K. Nomoto,
Monthly Notices of the Royal Astronomical Society, 428, 1020, 2013
T.J. Moriya, S.I. Blinnikov, P.V. Baklanov, E.I. Sorokina, A.D. Dolgov,
Monthly Notices of the Royal Astronomical Society, 430, 1402, 2013
T. Moriya, N. Tominaga, M. Tanaka, K. Maeda, K. Nomoto,
The Astrophysical Journal Letters, 717, L83, 2010
T.J. Moriya, K. Maeda,
The Astrophysical Journal Letters, 756, L22, 2012

We are all agreed that your theory is crazy. The question which divides us is whether it is crazy enough to have a chance of being correct. My own feeling is that it is not crazy enough.

Niels Bohr (1885 - 1962)

5

Proposed Supernova Progenitors with Dense Circumstellar Meida

5.1 Overview

We have mainly discussed SNe interacting with dense CSM from the observational point of view so far. We have developed their LC models and used them to interpret their LCs and obtain the CSM properties involved. We have shown that the estimated propterties are inconsistent with the current stellar evolution theory in many cases.

However, there do exsit some pre-SN models obtained by the stellar evolution theory which are suggested to explode within dense CSM. They can have extreme mass loss shortly before their explosions. Here, in this chapter, we look into these theoretical pre-SN models and show the observational properties expected from the pre-SN models. They may already be able to explain some SN properties within dense CSM. We calculate LCs within dense CSM expected from the stellar evolution model and compare the results to observations in this chapter.

We study three major pre-SN models which are suggested to have extensive mass loss shortly before their explosions, i.e., super-AGB stars (Section 5.2), massive RSGs (Section 5.3), and LBVs (Section 5.4).

5.2 Super-Asymptotic-Giant-Branch Stars

Core-collapse explosions of massive stars are not necessarily caused by the collapse of Fe cores. Massive stars with $M_{\rm ZAMS} \simeq 8 - 10\ M_\odot$ whose cores are not composed of Fe but O+Ne+Mg can cause electron capture reactions in their degenerated cores and the electron captures can induce the core collapse (e.g., Chapter 1, Miyaji et al. 1980, Nomoto 1984, Hillebrandt et al. 1984). The detailed numerical explosion modeling by Kitaura et al. 2006

shows that the core collapse of the O+Ne+Mg core can end up with a low-energy explosion of the star ($\simeq 10^{50}$ erg) by the neutrino explosion mechanism. Many theoretical works have been performed to investigate the evolution of stars which end up with the electron degenerate core potentially leading to ECSNe (e.g., Garcia-Berro & Iben 1994, Garcia-Berro et al. 1997, Siess 2007, Poelarends et al. 2008, Pumo et al. 2009, Takahashi et al. 2013). At the time of the electron capture, the star is believed to be at super-AGB stage. However, the evolution of super-AGB stars and thus the mass rage for ECSNe are strongly affected by the ways how the physical processes involved are numerically treated (e.g., mass loss, semi-convection, and convective overshooting) and they are not understood well. One remarkable feature of super-AGB stars is their high mass-loss rates (e.g., Poelarends et al. 2008). Thus, ECSNe, if they really exist, are quite likely to explode within dense CSM caused by the precedent super-AGB evolution.

Several observed SNe are also linked to ECSNe as we discussed in Chapter 1. Especially, SN 2008S is strongly linked to an ECSN because (1) SN 2008S was SN IIn and the absolute luminosity was very low indicating very low explosion energy (e.g., Thompson et al. 2009, Botticella et al. 2009) and (2) the progenitor observed in the pre-explosion image was $\simeq$ 10 $M_\odot$ (Prieto et al. 2008). There are other suggestive evidences of ECSNe exploding within dense CSM. Anderson et al. 2012 analysed the association between SN sites and Hα emitting regions in SN host galaxies. They found that the SN IIn sites are not strongly related to Hα emitting regions, which indicates that the majority of SNe IIn comes from low-mass progenitors like super-AGB stars. Wanajo et al. 2009 indicate that ECSNe can be a common SN from the nucleosynthesis perspective. Crab Nebula has been related to an ECSN and will be discussed in Section 6.3.2.

Although ECSNe have been suggested to explode within dense CSM, the effect of the dense CSM on their LCs has little been investigated. van Veelen 2010 did the first study of this kind and reported the modeling of the interaction between SN ejecta from ECSNe and dense CSM caused by super-AGB progenitors. van Veelen 2010 calculated the bolometric LCs of ECSNe within dense CSM with a simple treatment of the radiation energy loss as is used by van Marle et al. 2010. In this section, we investigate the interaction and its effect on the LCs in more detail with `STELLA`.

5.2.1 Dense CSM from Super-AGB Stars and Properties of ECSNe

We calculate the LCs of ECSNe within dense CSM following the same way as adopted by van Veelen 2010. Although there are many uncertainties in the super-AGB evolution caused by the ways to treat physical processes, the mass-loss rates of the super-AGB stars leading ECSNe are typically $\sim 10^{-4}$ $M_\odot$ yr^{-1}. The CSM velocity is set as 20 km s^{-1} following van Veelen 2010. This value is the 30% of the escape velocity (50 km s^{-1}) of the expected super-AGB stars with the luminosity $10^5 L_\odot$, the effective temperature 3,000 K, and 8 $M_\odot$ (see van Veelen 2010 for details).

As is assumed in the previous chapters, we assume that the SN ejecta has two density structure components and homologously expanding (see, e.g., Section 2.3). The explosion energy of the ECSN inside is set to 10^{50} erg based on the numerical explosion modeling (Kitaura et al. 2006). The SN ejecta mass depends strongly on the mass loss experienced

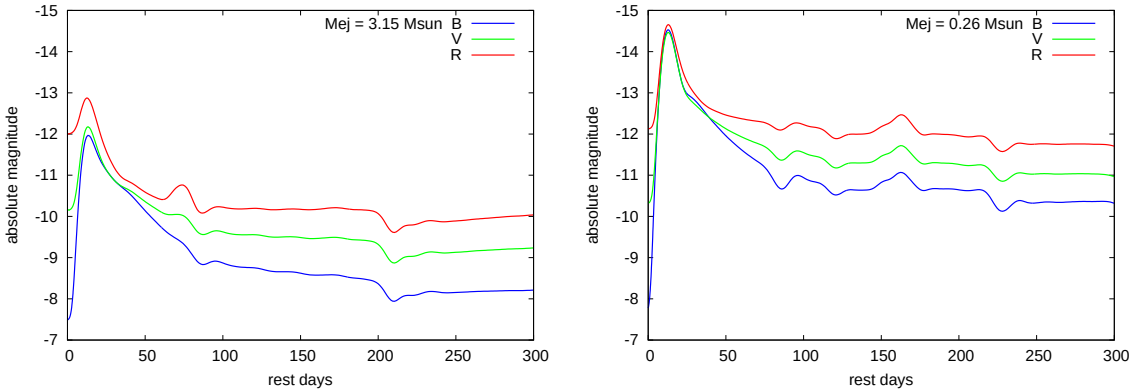

Figure 5.1: Optical LCs of ECSNe within dense CSM from super-AGB stars. The left panel shows the $M_{\rm ej} = 3.15\ M_\odot$ model and the right panel shows the $M_{\rm ej} = 0.26\ M_\odot$.

during the progenitor's super-AGB stage (see, e.g., Pumo et al. 2009). We adopt two SN ejecta mass which is used by van Veelen 2010 as well, i.e., 3.15 $M_\odot$ and 0.26 $M_\odot$. The actual progenitor mass at the time of the explosion is 1.4 $M_\odot$ larger, which is the mass of the compact remnant. The SN ejecta and the CSM is connected at 10^{14} cm and the CSM is extended to 10^{16} cm.

5.2.2 Synthetic Light Curves from ECSNe within Super-AGB CSM

The results of LC calculations are presented in Figure 5.1. Because of the low explosion energy, the luminosity does not become high. The model with the higher ejecta mass has lower luminosity because the specific kinetic energy is less in the model. The evolution of the LCs is qualitatively similar to those obtained by van Veelen 2010.

Figure 5.2 shows the comparison between our LCs and LCs of SNe suggested to be related to ECSNe, namely, SN 2008S (Botticella et al. 2009) and NGC 300-OT (Bond et al. 2009). Both SN 2008S and NGC 300-OT are SNe IIn and thus they were exploded within dense CSM. Two SNe have similar LC shapes and only the absolute luminosities are different. Comparing the model LCs and observed ECSN candidates, we find that they are different in many aspects. The model LCs show fast declines after the peak while the observed LCs decline slowly. After the initial LC declines, the model LCs stay rather constant. This is because of the continuous CSM interaction. The LCs from the interaction can stay constant for a long time if, for instance, the SN ejecta mass is much smaller than the CSM mass (see Section 2.3.2). The observed LCs, on the other hand, decline with the rate consistent with the ^{56}Co decay timescale after the initial decline (0.0098 mag day^{-1}).

5.2.3 Discussion and Summary

We have shown the numerical LCs of ECSNe exploded within dense CSM created by the super-AGB progenitors. We found that the observed LCs of low-luminosity SNe IIn which are suggested to be connected to ECSNe within dense CSM are not reproduced by the standard

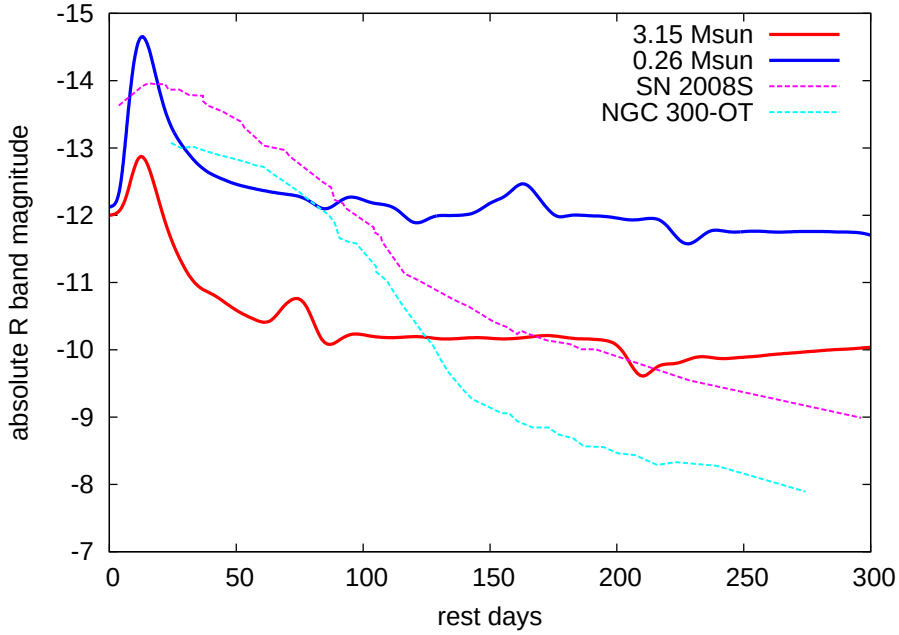

Figure 5.2: R band LCs of ECSNe within super-AGB CSM and the ECSN candidates SN 2008S (Botticella et al. 2009) and NGC 300-OT (Bond et al. 2009).

CSM which are expected from the super-AGB stars obtained by the current stellar evolution modeling.

Our results indicate that the observed SNe connected to ECSNe are actually from other progenitors or that there are missing pieces in the current super-AGB models. Especially, the mass loss of super-AGB stars are not known well and there may be additional mass-loss mechanisms like Ne flash which are not taken into account currently (see also Section 6.3.2). Here, we only investigated standard ECSNe and their dense CSM parameters. We need to investigate a wider parameter rage, especially of the dense CSM, to find out whether there are some combination of parameters which can explain the LCs of the ECSN candidates and see whether the required parameters are close to those expected from ECSNe from super-AGB stars or not.

5.3 Massive Red Supergiants

RSGs are progenitors of SNe IIP. RSGs, especially massive ones, are theoretically suggested to have some mechanisms to enhance mass-loss rates. Especially, the enhancement of the mass-loss rates by the pulsations of RSGs is likely to occur shortly before their explosions (Yoon & Cantiello 2010, Heger et al. 1997, Paxton et al. 2013, Li & Gong 1994). Yoon & Cantiello 2010 show that this mechanism can potentially make the mass-loss rates of RSGs as high as $\sim 10^{-2}\ M_\odot\ \mathrm{yr}^{-1}$. What is more, for RSGs with the ZAMS masses around $\simeq 17\ M_\odot$, the pulsations get unstable just before their explosions and the CSM can remain dense until the time of their explosions. Coincidentally, the minimum ZAMS mass to

Table 5.1: List of LC models without CSM

Name	Progenitor	Explosion Energy 10^{51} erg	Radiation Energy[a] 10^{49} erg
s13e3	s13	3	3.0
s15e1	s15	1	1.3
s15e3	s15	3	3.2
s15e5	s15	5	4.9
s18e3	s18	3	3.7
s20e3	s20	3	4.2

[a] Radiation energy emitted in 50 days since the explosion.

cause the pulsations obtained by Yoon & Cantiello 2010 is roughly the same as the maximum ZAMS mass of SN IIP progenitors indicated by observations (17 $M_{\odot}$, Smartt et al. 2009). Such extensive mass loss in massive SN IIP progenitors may suppress the upper limit on the ZAMS mass of SN IIP progenitors because such mass loss can take the whole hydrogen layer out of the progenitors. Mass loss due to nuclear flash may also be a driving force of the extensive mass loss (Weaver & Woosley 1979, Dessart et al. 2010b).

There are also observed potential SN IIP progenitors (RSGs) which are losing their mass with very high mass-loss rates. For example, a RSG VY Canis Majoris is estimated to be losing its mass with the rate $1 - 2 \times 10^{-3}$ $M_{\odot}$ yr^{-1} from the direct observations of CSM around it (Smith et al. 2009a). Observations of dusts around another RSG IRAS05280-6910 also indicate the extensive mass loss ($\sim 10^{-3}$ $M_{\odot}$ yr^{-1}) of the RSG (Boyer et al. 2010). Some IIP SNe are reported to show the possible effect of dense CSM in their LCs and spectra. A representative example of this kind is UV-bright SN IIP 2009kf (Botticella et al. 2010). SN 2009kf was bright in UV for ~ 10 days during its early epochs as well as in optical. Later, the LC transformed to that of a SN IIP and the spectra taken at later epochs are classified as Type IIP. The fact that SN 2009kf was bright in UV and optical at the same time makes it difficult to explain SN 2009kf without the CSM interaction. This is because usual SNe IIP cool adiabatically in their early epochs and they become optically bright after UV brightness gets weaker. Utrobin et al. 2010 show a LC model of SN 2009kf without CSM interaction but the required explosion energy is found to be very high (2.2×10^{52} erg). Another SN IIP 2007od (Andrews et al. 2010) had late phase spectra similar to those of SN IIn 1998S, which are considered to result from CSM interaction (Pozzo et al. 2004). Also, SN 2007od showed the possibility of the existence of light echos in its LC and it may indicate the existence of CSM around the progenitor (Andrews et al. 2010).

Here, given the possibilities that RSGs can have enhanced mass-loss rates and that dense CSM can exist around RSGs at the time of the explosions, we investigate the effect of dense CSM on LCs from SNe of RSGs with dense CSM. Some works (e.g., Falk & Arnett 1973, Falk & Arnett 1977) have already done with the similar conditions but, in this section, we model them more systematically and with better treatments of physics using `STELLA`.

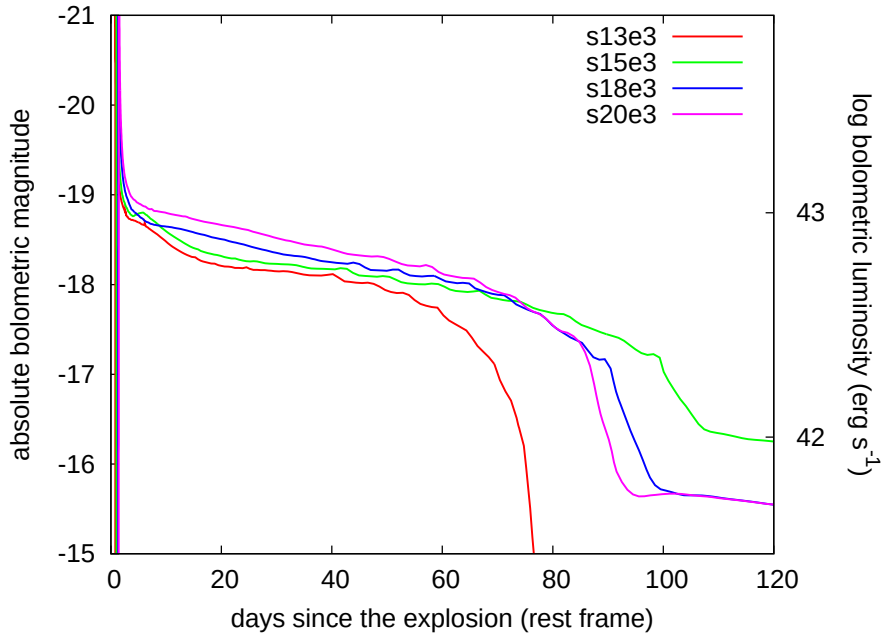

Figure 5.3: Bolometric LCs of the SNe from the progenitors without CSM.

5.3.1 Pre-Supernova Models

We construct pre-SN models by attaching CSM to the RSG progenitor models calculated by Woosley et al. 2002. As the progenitor models of Woosley et al. 2002 do not take into account of the extensive mass loss we are interested in, we artificially attach the CSM to the outer most layer of the progenitor models. The composition of the CSM is solar metallicity and is the same as the surface of the RSG models which we adopt. Compared to the effect of the CSM parameters, the LCs are less affected by the RSG models adopted inside (Section 5.3.2.2). This justifies our simple way to construct the pre-SN models. Among the pre-SN models shown in Woosley et al. 2002, we use the solar-metallicity single star models of RSGs: s13, s15, s18, and s20. The ZAMS masses of the models s13, s15, s18, and s20 are 13 $M_{\odot}$, 15 $M_{\odot}$, 18 $M_{\odot}$, and 20 $M_{\odot}$, respectively. If they are exploded without CSM, their LCs show a long plateau phase and thus they are SN IIP progenitors (Section 5.3.2.1). Although we do not follow explosive nucleosynthesis, ^{56}Ni exists in the core of the pre-SN models because of the nuclear statistical equilibrium established in the core. However, at the early epochs we are interested in (first $\simeq$ 50 days since the explosions), the photons originated from ^{56}Ni decay do not leak from the ejecta so much and contribute little to LCs. According to Figure 2 of Kasen & Woosley 2009, the effect of ^{56}Ni on SN IIP LCs appear after $\simeq$ 50 days since the explosions and thus our LC models are not applicable from around that epoch. The density structures of the pre-SN models are shown accordingly in the following sections.

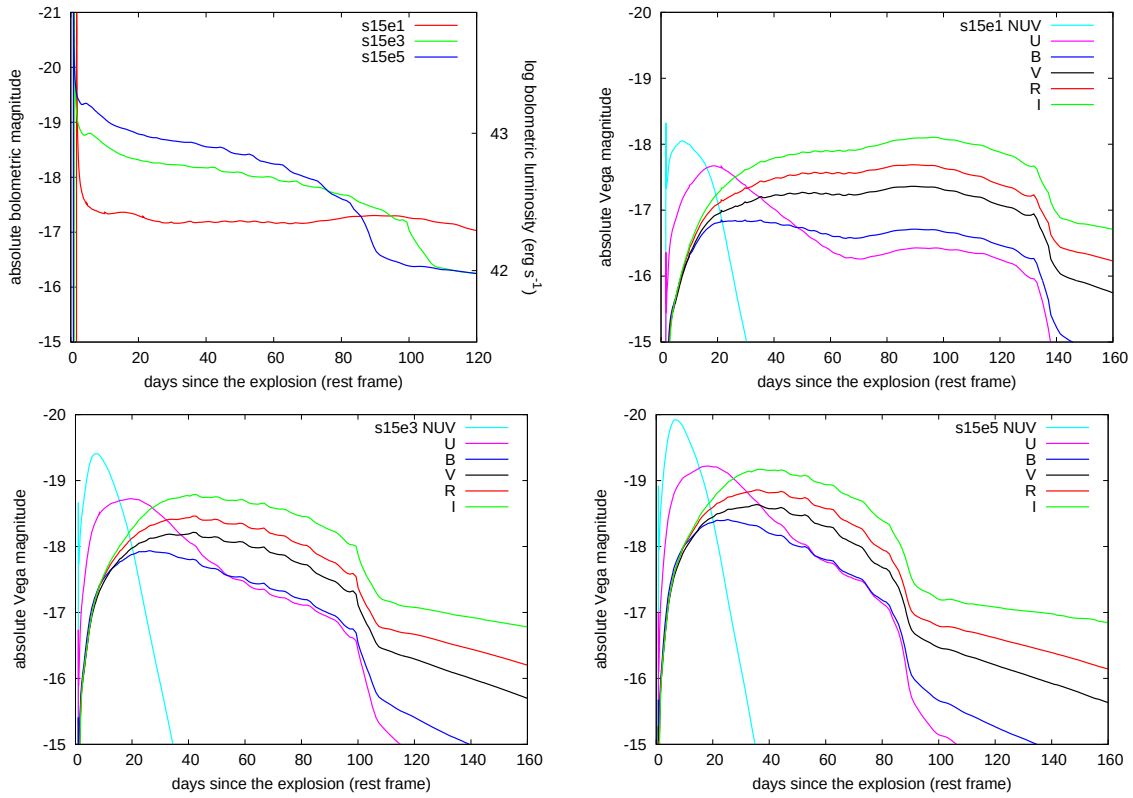

Figure 5.4: Bolometric (top left) and multicolor (the others) LCs of the SNe from the progenitor s15 without CSM. Models with several explosion energies are shown.

5.3.2 Light Curves

In this section, we present LCs calculated by `STELLA`. First, we show LCs of the explosions of the RSG progenitors without CSM for references (Section 5.3.2.1) and then LCs of the explosions with CSM (Section 5.3.2.2).

5.3.2.1 Explosions without CSM

In this section, we present the LCs for the RSG progenitors without CSM. The aim of these calculations is to provide references to be compared with LCs with CSM. Note that, as mentioned in Section 5.3.1, the LCs shown here are not applicable after $\simeq$ 50 days since the explosions because we do not follow explosive nucleosynthesis. Table 5.1 is the list of the LCs shown in this section. Previous studies also calculated the multicolor LCs of SNe IIP from the same progenitor models with different numerical codes (Kasen & Woosley 2009, Dessart et al. 2010a, Dessart & Hillier 2010) and from different progenitor models with the same numerical code (Baklanov et al. 2005, Tominaga et al. 2009, Tominaga et al. 2011).

In Figure 5.3, the bolometric LCs with the same explosion energy (3×10^{51} erg) are presented. When a shock emerges from a stellar surface, a bolometric LC is suddenly brightened due to the shock breakout. Then, the ejecta cools adiabatically. When the outer layer of the

ejecta reaches the recombination temperature of H, the LC becomes flat until the photosphere reaches the bottom of the H layer (plateau phase). After the plateau phase, the LC follows the decay line of ^{56}Co which existed as ^{56}Ni in the core of the pre-SN model even though we do not calculate the explosive nucleosynthesis (Section 5.3.1). Note that our LC models are not applicable after the late epochs of the plateau phase.

The bolometric LCs with the same progenitor (s15) but different explosion energies are shown in the top left panel of Figure 5.4. In the other panel of Figure 5.4, we also show the multicolor LCs of each model. Optical LCs are obtained by applying the Bessell *UBVRI* filters (Bessell 1990) and UV LCs are derived by using the near-UV (NUV) imaging filter of the *Galaxy Evolution Explorer* (*GALEX*) satellite whose central wavelength is around 2,300 Å (Morrissey et al. 2005). After the first brightening due to shock breakout, NUV first become bright because of the adiabatic cooling of the ejecta. Then, LCs become bright in optical as NUV become fainter. This is an important feature of usual SNe IIP. They are not bright in UV and optical at the same time. The behavior of the multicolor LCs of the other progenitors is qualitatively the same as the multicolor LCs shown in Figure 5.4.

5.3.2.2 Explosions with CSM

In this section, we investigate the effect of CSM around RSGs on SN LCs. After the core collapse of a progenitor, a shock wave propagates inside the progenitor. At these epochs, CSM is not ionized and optically thin. Then, after the shock wave has gone through the surface of the progenitor, a precursor wave appears in the CSM and CSM is ionized. The precursor wave propagates very fast and soon reaches to the surface of CSM. The optical depth ($\tau_{\rm csm}$) of CSM after the shock wave reached the surface of the progenitor is expressed as

$$\tau_{\rm csm} = \int_{R_i}^{R_o} \kappa_{\rm csm}(r)\rho_{\rm csm}(r)dr \simeq \int_{R_i}^{R_{\rm ion}} \kappa_{\rm csm}(r)\rho_{\rm csm}(R_i)\left(\frac{r}{R_o}\right)^{-s} dr, \tag{5.1}$$

where $\kappa_{\rm csm}$ is the CSM opacity, $\rho_{\rm csm}$ is the CSM density, R_o is the CSM radius, R_i is the radius of the inner edge of CSM where CSM is connected to the progenitor inside, i.e., the radius of the progenitor inside, and $R_{\rm ion}$ is the ionization front in CSM. $\tau_{\rm csm}$ depends on the thickness of the ionized layer because $\kappa_{\rm csm}$ above the ionization front is very low ($\kappa_{\rm csm} \sim 10^{-4}$ cm^2 g^{-1}). In order to estimate a condition in which CSM can affect the radiation from inside, we assume that CSM below $R_{\rm ion}$ is fully ionized and the Thomson scattering is the predominant source of opacity ($\kappa_{\rm csm}(r) = 0.34$ cm^2 g^{-1} with solar metallicity). With $R_i \simeq 5 \times 10^{13}$ cm (Figure 5.5; Section 5.3.2.2), $R_i \ll R_{\rm ion}$, and $s \gtrsim 1$, the condition to be $\tau_{\rm csm} > 1$ is

$$\rho(R_i) \gtrsim 6 \times 10^{-14}\,(s-1)\ \ {\rm g\ cm^{-3}}. \tag{5.2}$$

Thus, when the density of CSM at the radius where CSM is connected to the progenitor model inside is more than $\sim 10^{-13}$ g cm^{-3}, CSM becomes optically thick and photons from inside are expected to be affected by the CSM. CSM with mass-loss rates higher than $\sim 10^{-4}\ M_\odot$ yr^{-1} satisfy this condition, assuming that the CSM velocity is 10 km s^{-1} (Figure 5.5).

In the following sections, we also investigate the dependence of LCs on several physical parameters of CSM and progenitors. The parameters of CSM adopted are mass-loss rates

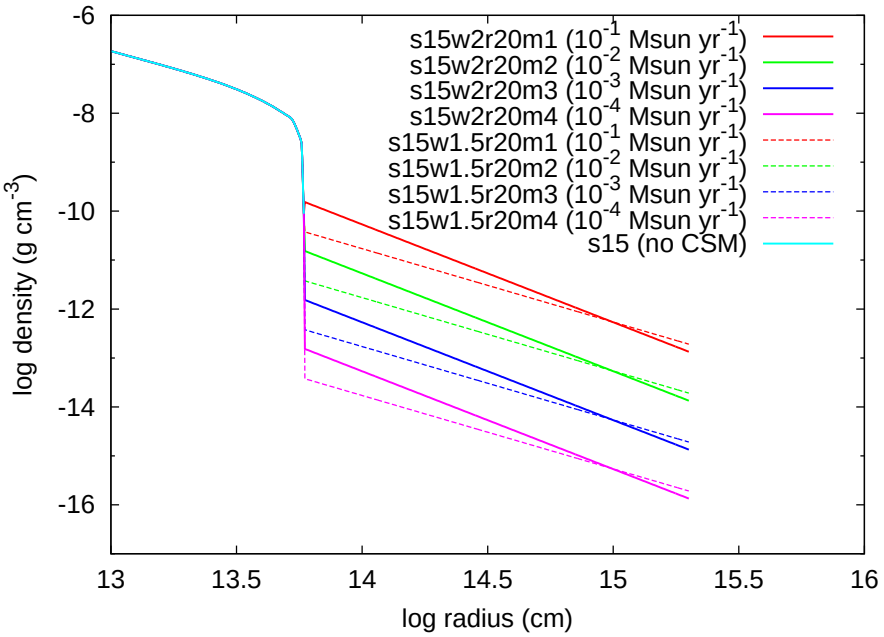

Figure 5.5: Density structures of the pre-SN models with different mass-loss rates and density slopes. The density structures shown with solid lines have CSM density slope of $\rho_{\rm csm} \propto r^{-2}$ and those shown with dashed lines have CSM density slope of $\rho_{\rm csm} \propto r^{-1.5}$. The pre-SN models are constructed by attaching CSM to the progenitor model s15.

$[10^{-1} - 10^{-4} M_\odot$ yr$^{-1}]$, radii of the outer edge of CSM (CSM radii) $[5\times10^{14} - 3\times10^{15}cm]$, and density slopes ($\rho_{\rm csm} \propto r^{-s}$) $[s = 2, 1.5]$. Several progenitor models inside are also adopted [s13, s15, s18, s20]. The density structures of the pre-SN models with CSM are shown accordingly in the following sections. The model parameters and results are summarized in Tables 5.2 and 5.3.

Effect of CSM

Typical bolometric LCs which are affected by the CSM are shown in Figure 5.6 with the bolometric LC from the model without CSM (s15e3). We focus on the model s15w2r20m3e3 to describe the effect of the CSM in this section. The CSM mainly affects the LCs at the early epochs, roughly until the sudden drop in the LCs which can be seen at around 25 days in the model s15w2r20m3e3 (10^{-3} $M_\odot$ yr^{-1}). At first, LCs have round shapes (until $\simeq$ 15 days in s15w2r20m3e3). The round phase is followed by a flat LC which lasts until the sudden drop ($\simeq 15 - 25$ days in s15w2r20m3e3). LCs are mainly powered by the interaction of SN ejecta and CSM at these epochs. We call these epochs as an interaction-powered phase (IPP) in this section.

The IPP appears in the LCs of the SNe with the dense CSM. When the temperature and the CSM density are high enough, the CSM become optically thick and the photosphere locates in the CSM. The photosphere during the IPP is in the CSM. This can clearly seen

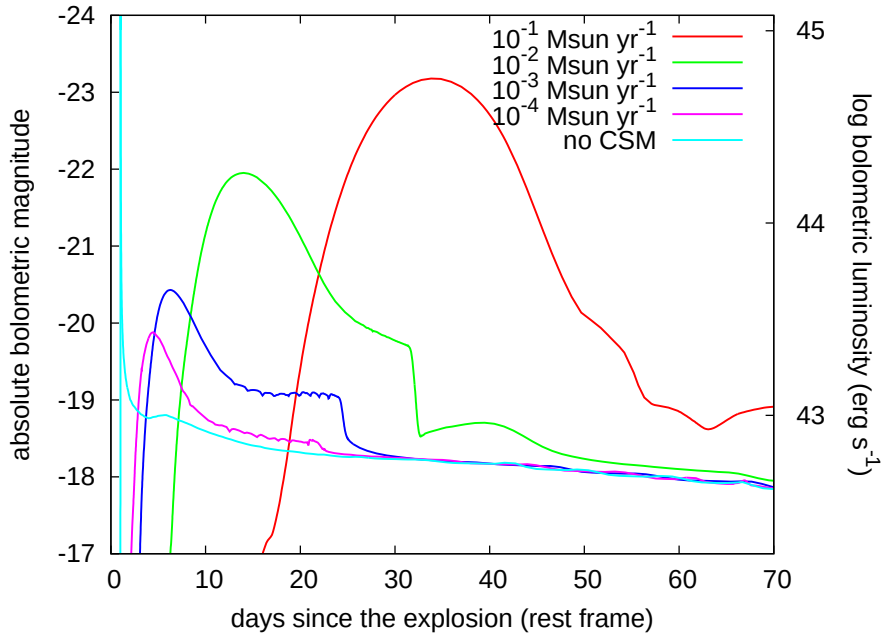

Figure 5.6: Bolometric LCs of the models with different mass-loss rates. The models shown are s15w2r20m1e3 (10^{-1} $M_\odot$ yr^{-1}), s15w2r20m2e3 (10^{-2} $M_\odot$ yr^{-1}), s15w2r20m3e3 (10^{-3} $M_\odot$ yr^{-1}), and s15w2r20m4e3 (10^{-4} $M_\odot$ yr^{-1}). The bolometric LC of the model s15e3 (no CSM) is also shown for comparison.

in Figure 5.7. Looking into the model s15w2r20m3e3, the photospheric velocity is at first 10 km s^{-1}, which is the initial CSM velocity. This is a characteristic feature of the explosions within the dense CSM. Then, the photospheric velocity increases due to the acceleration of the CSM by the precursor wave. At around $\simeq 15$ days in s15w2r20m3e3, the photosphere reaches the dense shell between the SN ejecta and the CSM (Figure 5.8). Then, the photosphere goes into the SN ejecta at $\simeq 25$ days.

All the LCs affected by CSM have round shapes at first (Figure 5.6). We briefly discuss why the round phase appears. As our models have $\tau_{\rm csm} > 1$, photons cannot escape freely from the CSM. In addition, our models satisfy the following condition at some moment when the shock wave is propagating in the CSM:

$$\tau_{\rm sh} \equiv \int_{R_{\rm sh}}^{R_o} \kappa_{\rm csm}(r)\rho_{\rm csm}(r)dr < \frac{c}{v_s}, \tag{5.3}$$

where $R_{\rm sh}$ is the radius of the shock wave and v_s is the shock velocity. Therefore, photons can diffuse out from the shock wave and a precursor wave propagates ahead of the shock wave (see the left panels of Figure 5.8). As the shock velocity is typically $\sim 10,000$ km s^{-1} when the shock wave reach R_i, c/v_s is typically ~ 10 at that time. Thus, photons in the models with

$$\rho_{\rm csm}(R_i) \lesssim 6 \times 10^{-13}\ {\rm g\ cm^{-3}} \tag{5.4}$$

Table 5.2: List of LC models with CSM

Name	Progenitor	Explosion Energy 10^{51} erg	Mass-Loss Rate[a] $M_\odot$ yr^{-1}	Radius 10^{15} cm	Density Slope s ($\rho_{\rm csm} \propto r^{-s}$)	CSM Mass $M_\odot$	Radiation Energy[b] 10^{49} erg
s13w2r20m2e3	s13	3	10^{-2}	2	2	0.65	20
s15w2r05m2e3	s15	3	10^{-2}	0.5	2	0.15	9.8
s15w2r05m3e3	s15	3	10^{-3}	0.5	2	0.015	3.8
s15w2r10m2e3	s15	3	10^{-2}	1	2	0.31	13
s15w2r10m3e3	s15	3	10^{-3}	1	2	0.031	4.2
s15w2r20m2e1	s15	1	10^{-2}	2	2	0.65	5.6
s15w2r20m1e3	s15	3	10^{-1}	2	2	6.5	75
s15w1.5r20m1e3	s15	3	–	2	1.5	6.5	80
s15w2r20m2e3	s15	3	10^{-2}	2	2	0.65	19
s15w1.5r20m2e3	s15	3	–	2	1.5	0.65	15
s15w2r20m2e5	s15	5	10^{-2}	2	2	0.65	32
s15w2r20m2e7	s15	7	10^{-2}	2	2	0.65	45
s15w2r20m3e3	s15	3	10^{-3}	2	2	0.065	5.0
s15w1.5r20m3e3	s15	3	–	2	1.5	0.065	4.8
s15w2r20m4e3	s15	3	10^{-4}	2	2	0.0065	3.4
s15w1.5r20m4e3	s15	3	–	2	1.5	0.0065	3.4
s15w2r30m2e3	s15	3	10^{-2}	3	2	0.98	23
s15w2r30m3e3	s15	3	10^{-3}	3	2	0.098	5.6
s18w2r20m2e3	s18	3	10^{-2}	2	2	0.65	17
s20w2r20m2e3	s20	3	10^{-2}	2	2	0.65	17

[a] Derived by assuming a constant CSM velocity 10 km s^{-1}.
[b] Radiation energy emitted in 50 days since the explosion.

Table 5.3: Properties of SNe from s15 at some selected epochs

	$L_{\rm bol}$[a] (10^{43} erg s^{-1})				$v_{\rm ph}$[b] (km s^{-1})				$T_{\rm BB}$[c] (10^3 K)			
Epoch[d] (days)	10	20	30	40	10	20	30	40	10	20	30	40
s15e1	0.27	0.26	0.23	0.23	6900	6500	5900	5000	15	9.8	7.9	7.0
s15e3	0.84	0.65	0.60	0.57	12000	11000	9500	7800	16	9.8	8.0	7.1
s15e5	1.3	1.0	0.90	0.81	15000	13000	12000	9200	15	9.9	8.0	7.1
s15e7	1.7	1.4	1.2	1.0	17000	16000	13000	10000	16	9.9	8.1	7.1
s15w2r05m2e3	1.1	0.63	0.73	0.57	8100	8300	8300	7800	15	9.0	7.7	7.2
s15w2r05m3e3	0.82	0.69	0.61	0.56	10000	10000	9400	7800	13	9.6	8.0	7.2
s15w2r10m2e3	22	0.78	0.73	0.64	950	7800	7500	7600	42	9.1	7.9	7.2
s15w2r10m3e3	1.5	0.72	0.61	0.56	9800	9800	9400	7800	14	9.1	8.0	7.2
s15w2r20m2e1	0.81	3.2	1.2	0.67	14	86	130	150	15	21	14	10
s15w2r20m1e3	0.049	1.9	47	36	10	15	410	1200	6.0	13	37	32
s15w1.5r20m1e3	0.064	1.5	45	46	10	12	400	1400	6.0	12	36	34
s15w2r20m2e3	9.1	8.4	2.5	0.92	65	500	7200	6800	29	23	11	7.2
s15w1.5r20m2e3	5.0	7.9	3.0	0.64	43	290	6300	5600	23	25	16	7.5
s15w2r20m2e5	29	7.6	1.2	1.1	670	1000	8900	9000	39	20	7.9	7.3
s15w2r20m2e7	58	8.1	1.7	1.3	570	11000	11000	10000	42	16	8.2	7.4
s15w2r20m3e3	2.1	1.3	0.62	0.57	420	9400	9200	7800	18	9.5	8.0	7.2
s15w1.5r20m3e3	2.1	1.5	0.62	0.36	270	9200	9200	7800	18	9.8	8.1	7.2
s15w2r20m4e3	0.96	0.74	0.61	0.57	11000	10000	9400	7800	16	10	8.1	7.1
s15w1.5r20m4e3	0.90	0.77	0.61	0.56	11000	10000	9500	7800	17	11	8.1	7.2
s15w2r30m2e3	2.8	15	4.4	2.5	21	210	300	330	20	26	16	10
s15w2r30m3e3	3.5	1.3	1.1	0.61	30	9400	9100	8000	21	9.8	8.7	7.3

[a]Bolometric luminosity.
[b]Photospheric velocity. Photosphere is where the Rosseland optical depth is 2/3.
[c]Color temperature at photosphere. Photosphere is where the Rosseland optical depth is 2/3.
[d]Epoch since the explosion.

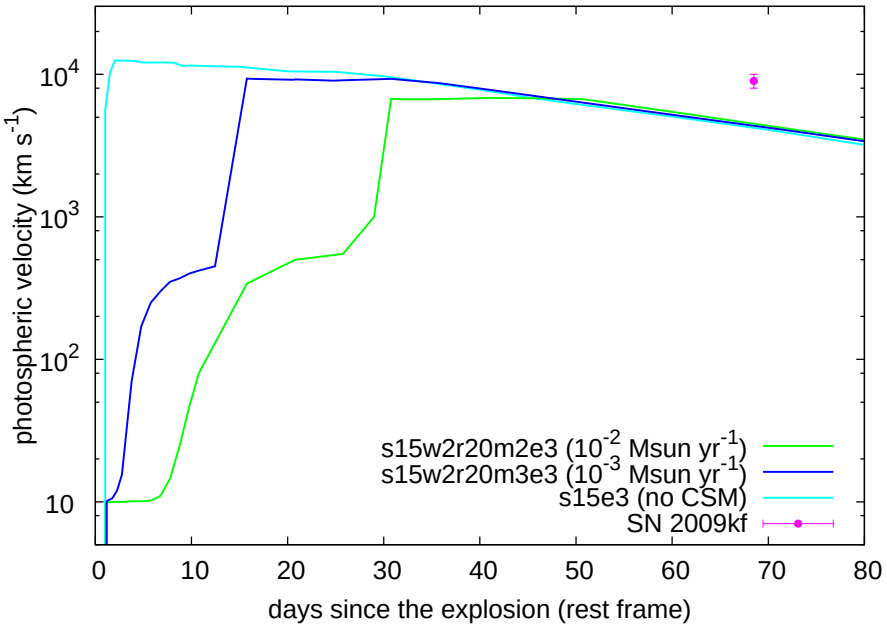

Figure 5.7: Evolutions of photospheric velocity of the models s15w2r20m2e3, s15w2r20m3e3, and s15e3. The photosphere is defined as the location where the Rosseland optical depth becomes 2/3. Observed Hα line velocity of SN 2009kf is also plotted in the figure. The explosion date of SN 2009kf is set as the same as in Figure 5.18.

start to leak photons from the shock wave just after the shock wave reach R_i. The other models satisfy Equation 5.3 when the shock wave propagates in the CSM because the deceleration of the shock wave makes c/v_s higher and the propagation of the shock wave reduces $\tau_{\rm sh}$. Once Equation 5.3 is satisfied, photons start to leak out from the shock wave and this phenomenon is usually observed as the shock breakout. However, since there is the remaining dense CSM above at the time of the shock breakout, photons diffuse out in the CSM and the shock breakout signal become longer compared with the explosions without the CSM (see also Falk & Arnett 1973, Falk & Arnett 1977).

In addition, SN ejecta is decelerated by the dense CSM. The dense CSM is massive and it has the density structure $\rho_{\rm csm} \propto r^{-2}$ if it is from steady mass loss. Thus, the shock wave between the SN ejecta and the CSM is decelerated and the kinetic energy of the SN ejecta is converted to thermal energy which is released as radiation energy. As a result, SNe with the dense CSM emit more photons and become brighter than those without the dense CSM. For further discussion, see, e.g., Chapter 4. Comparing radiation energy emitted during early epochs (Tables 5.1 and 5.2), it is clear that the effect of the SN ejecta deceleration is dominant radiation source during the IPP. In other words, the round phase is not just due to the elongation of the shock breakout signal seen in the models without the CSM.

The differences in the rising times and the durations of the round LCs during the IPP come from the difference in the diffusion timescales of the CSM (Figure 5.6). The models with the higher mass-loss rates have the denser CSM and thus the longer diffusion timescales.

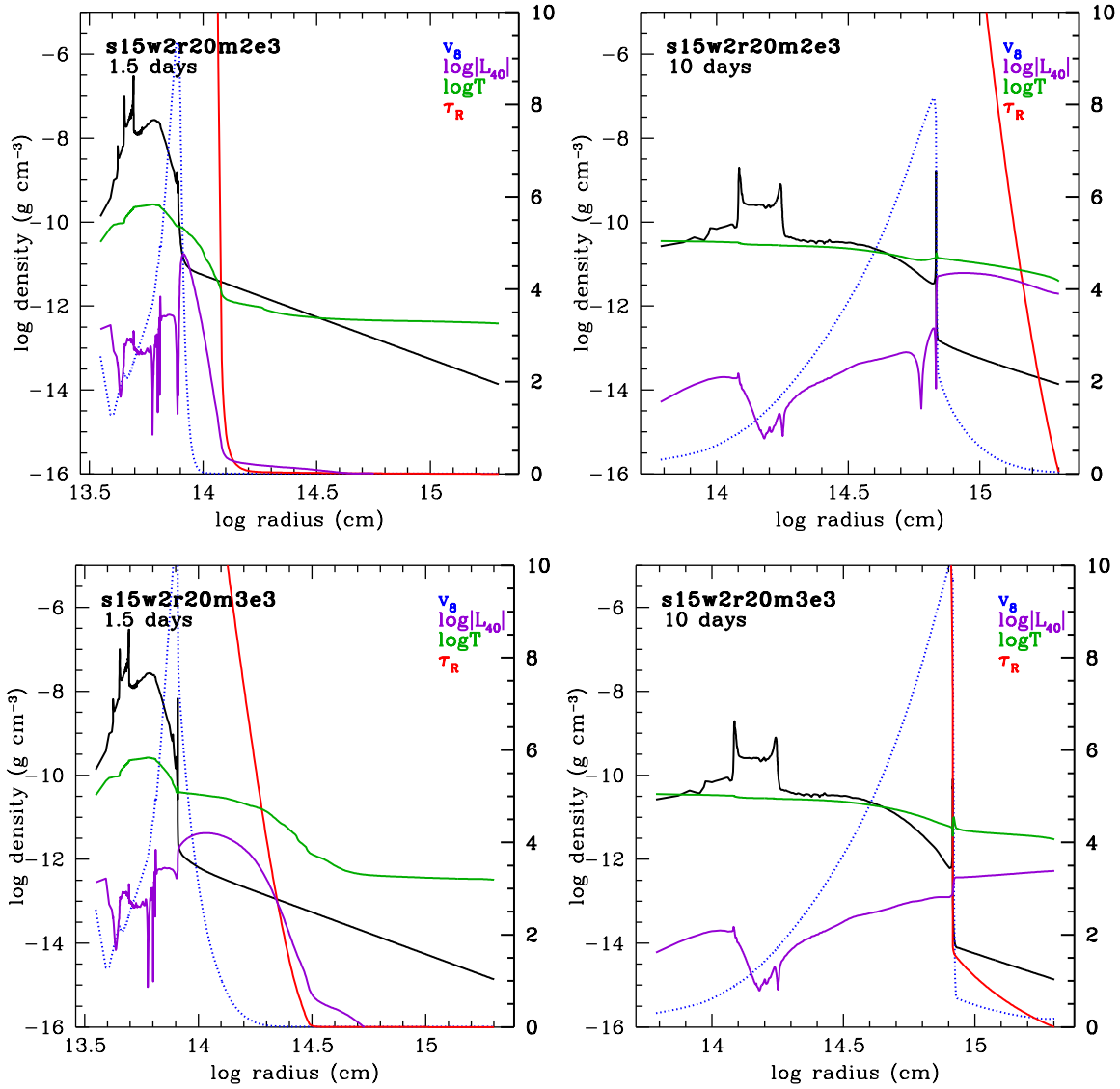

Figure 5.8: Physical structures of the models s15w2r20m2e3 and s15w2r20m3e3 at two epochs. The epochs are the days since the explosion. Black lines show the density structure (left y-axis). Blue lines are the velocity scaled by 10^8 cm s^{-1} (right y-axis), purple lines are the logarithm of the absolute value of luminosity scaled by 10^{40} erg s^{-1} (right y-axis), green lines are the logarithm of the temperature in Kelvin (right y-axis), and red lines are Rosseland optical depth measured from the outside (right y-axis).

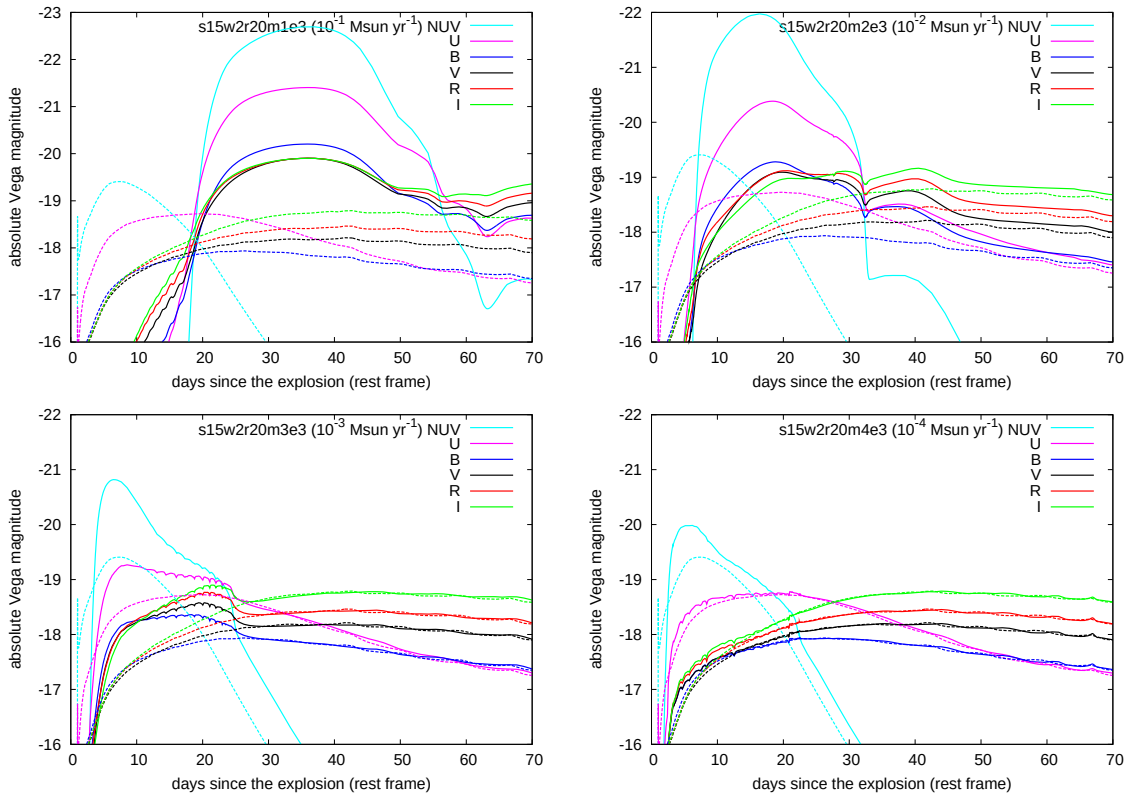

Figure 5.9: Multicolor LCs of the models with different mass-loss rates (solid lines). The dashed lines are the multicolor LCs of the model s15e3 for comparison. LCs of the same color are from the same filter. Note that top left panel has different y-axis range from the other panels.

This difference due to the diffusion timescales can be clearly seen in Figure 5.8. The upper panels and the lower panels represent the same epoch of the explosion with the different CSM densities, i.e., the different CSM diffusion timescales. As is indicated by the temperature waves in the CSM which are pushed by the photon diffusion, photons in the CSM with the shorter diffusion timescales diffuse out more quickly into the CSM. Therefore, the rising times and the durations of the round phase in the IPP are shorter for the models with the smaller CSM diffusion timescales. Those differences are also discussed in Falk & Arnett 1973, Falk & Arnett 1977.

The round LC in the IPP is followed by the flat LC which lasts until the sudden drop in the LC (between around 15 days and 25 days in s15w2r20m3e3). During this flat phase, the photosphere locates at the dense shell between the SN ejecta and the CSM. The photospheric velocity does not change so much during the flat phase (Figure 5.7). After the CSM above the dense shell has become optically thin, the photosphere remains at the dense shell until the temperature and the density of the shell become low enough to be optically thin.

One of the clear characteristics of the LCs with CSM is the sudden drop in the LCs. The time of this sudden drop corresponds to the time when the dense shell becomes optically

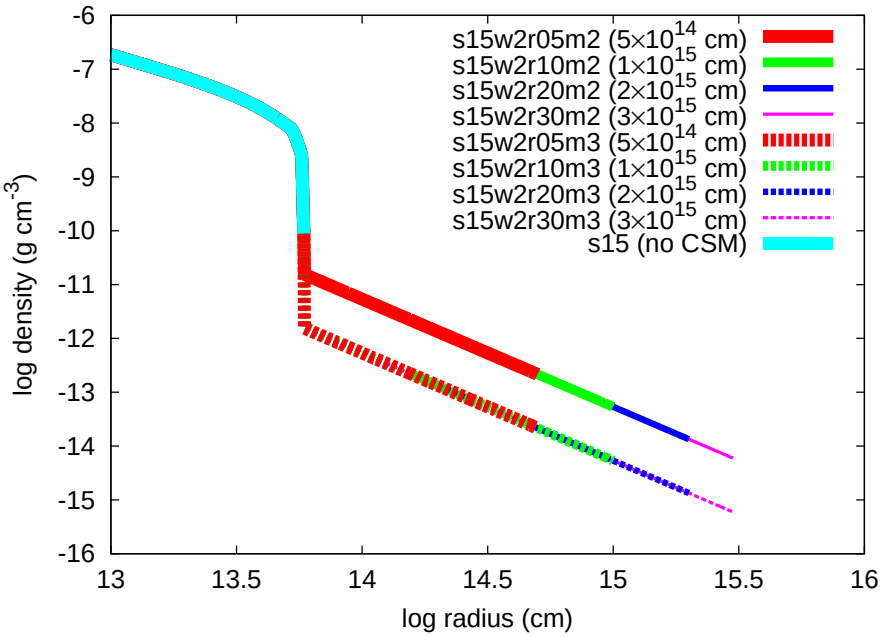

Figure 5.10: Density structures of the pre-SN models with the different radii. Models with the solid lines have the mass-loss rate 10^{-2} $M_{\odot}$ yr^{-1} and those with the dashed lines have 10^{-3} $M_{\odot}$ yr^{-1}. The pre-SN models are constructed by attaching the CSM to the progenitor model s15.

thin and the photosphere proceeds inward to the SN ejecta. This can also be seen in the photospheric velocity evolution (Figure 5.7). The brightness can drop as low as the LC without CSM because now the photons are emitted from the SN ejecta and the physical conditions are the same as those of SNe without dense CSM. However, the brightness is still slightly more luminous than the LC without CSM for several days after the sudden drop. This could be because of the extra-heating due to shock and/or the deceleration of SN ejecta by CSM which makes the adiabatic cooling of the SN ejecta less efficient.

There are many differences between our models (RSG + CSM) and RSGs with extended envelopes. First of all, it is difficult to have RSGs extended to $\sim 10^{15}$ cm (e.g., Woosley et al. 2002). What is more, the density and the temperature in RSGs are much higher in RSG envelopes than in the CSM. This does not allow the shock wave in RSGs to satisfy Equation 5.3 until the shock wave reaches the surface of RSGs. In other words, the shock wave does not break out until it reaches near the surface. On the contrary, in our models, Equation 5.3 is satisfied inside the CSM and the precursor wave propagates ahead of the shock wave. In addition, the kinetic energy of the SN ejecta efficiently converted to radiation energy because of the deceleration of the SN ejecta by the dense CSM. This precursor wave due to the shock breakout in the CSM and an additional heating source causes the IPP phase.

Dependence on Mass-Loss Rate

In this section, we show the effect of mass-loss rates on LCs. We adopt the mass-loss rates of 10^{-1}, 10^{-2}, 10^{-3}, and 10^{-4} $M_\odot$ yr^{-1} (the corresponding model names are s15w2r20m1, s15w2r20m2, s15w2r20m3, and s15w2r20m4, respectively). For the case of 10^{-1} $M_\odot$ yr^{-1}, CSM mass is 6.5 $M_\odot$ and the sum of the mass of the RSG inside and the CSM exceeds the ZAMS mass of the progenitor. This is unrealistic but we show the results just to see the effect of CSM. Every CSM in the models is optically thick (Equation 5.2, Figure 5.5). These mass-loss rates are derived by assuming that the CSM velocity is 10 km s^{-1}. However, the escape velocity of the surface of s15 is 76 km s^{-1}. This means that the CSM velocity can be higher than 10 km s^{-1} at least at the late stages of the evolution of the progenitors and thus the actual mass-loss rate for a given CSM density could be higher than the values we show. The flow from the progenitor may not be even steady. However, we assume that the CSM result from the steady flow from the progenitors with the velocity 10 km s^{-1} for simplicity because the CSM velocity has little effect on the LCs. To see the effect of the mass-loss rates on the LCs, we fix the radius of the CSM to 2×10^{15} cm and the density slope to $\rho_{\rm csm} \propto r^{-2}$ in this section. Also, the explosion energy and the progenitor of the SNe are fixed to 3×10^{51} erg and s15. The density structures of the progenitors with the CSM are shown in Figure 5.5.

Figure 5.6 shows the bolometric LCs of the SNe with the different mass-loss rates. Since the diffusion timescale of the CSM becomes larger for the denser CSM, the rising times and the durations of the round phases in the LCs are longer for the models with the higher mass-loss rates. The maximum luminosity of the LCs becomes larger as the CSM becomes denser. This is because the shock wave is more decelerated by the CSM due to the more massive CSM, i.e., more kinetic energy is converted to thermal energy and thus radiation energy. The radiation energies of the models are summarized in Table 5.2.

The multicolor LCs of the models in this section are shown in Figure 5.9. Each LC is plotted with the multicolor LCs of no CSM model s15e3. It is clear that the LCs during the IPP become bright especially in the short wavelengths because of the high temperatures at the photosphere.

Dependence on Radius

In this section, the effect of the CSM radius on LCs is investigated. To see the effect of the CSM radius, we fix the following parameters: the explosion energy (3×10^{51} erg), the density slope ($s = 2$), and the progenitor inside (s15). We try two mass-loss rates, 10^{-2} $M_\odot$ yr^{-1} and 10^{-3} $M_\odot$ yr^{-1}. We adopt four CSM radii to see the effect, i.e., 5×10^{14} cm (s15w2r05m2 and s15w2r05m3), 1×10^{15} cm (s15w2r10m2 and s15w2r10m3), 2×10^{15} cm (s15w2r20m2 and s15w2r20m3), and 3×10^{15} cm (s15w2r30m2 and s15w2r30m3). With the constant CSM velocity 10 km s^{-1}, the mass loss in the models lasts 16 years, 32 years, 64 years, and 96 years, respectively. The density structures of the pre-SN models are shown in Figure 5.10.

Figure 5.11 shows the bolometric LCs of the models with the different CSM radii. The durations of the round phases in the IPP are longer for the models with the larger CSM radius. This is because the diffusion times of the LCs are longer for the models with the larger CSM radius. On the other hand, the maximum luminosities of the round phases

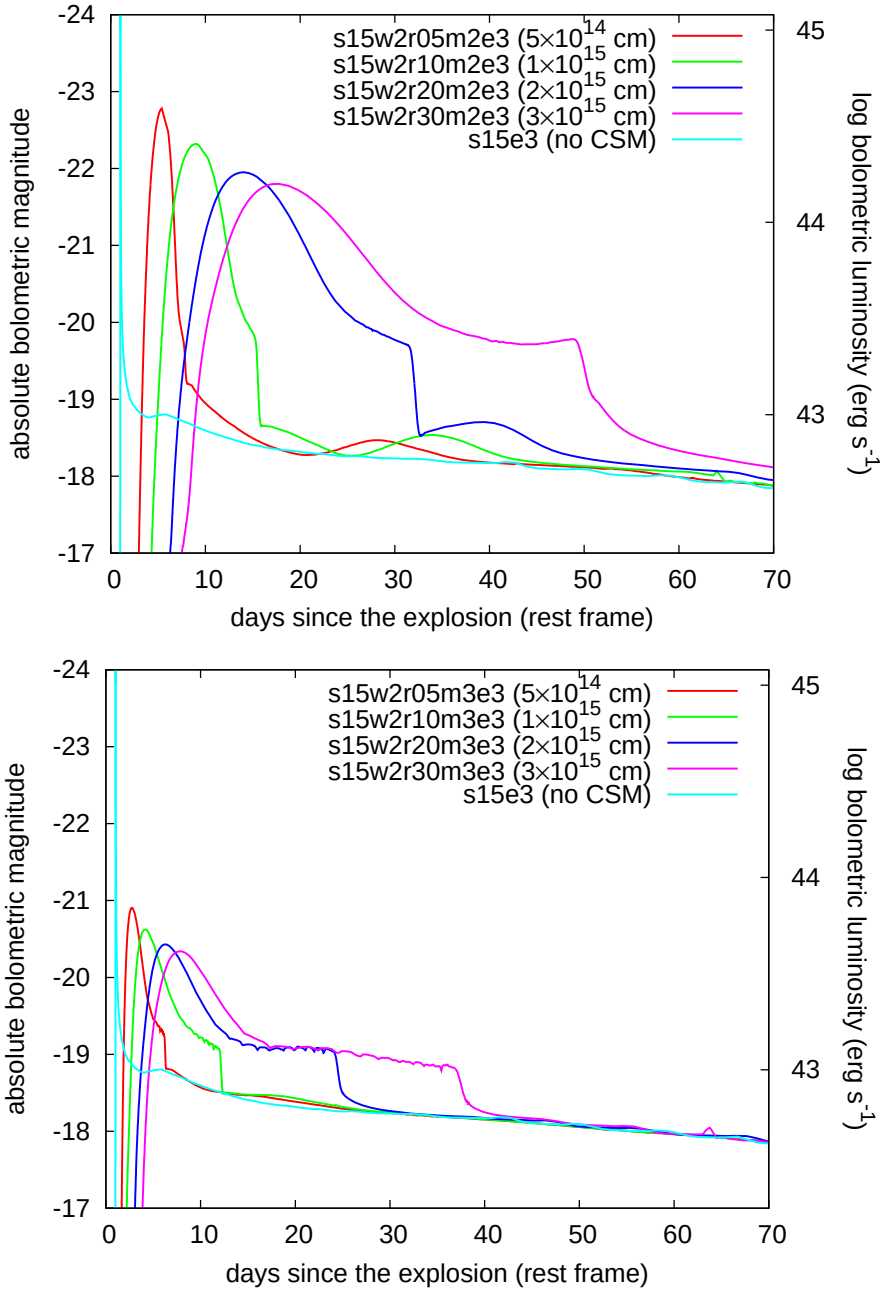

Figure 5.11: Bolometric LCs of the models with the different CSM radii. The top panel shows the LCs from the models with the mass-loss rate 10^{-2} $M_{\odot}$ yr^{-1} and the bottom panel shows those with 10^{-3} $M_{\odot}$ yr^{-1}. The bolometric LC of the model s15e3 is also shown for comparison.

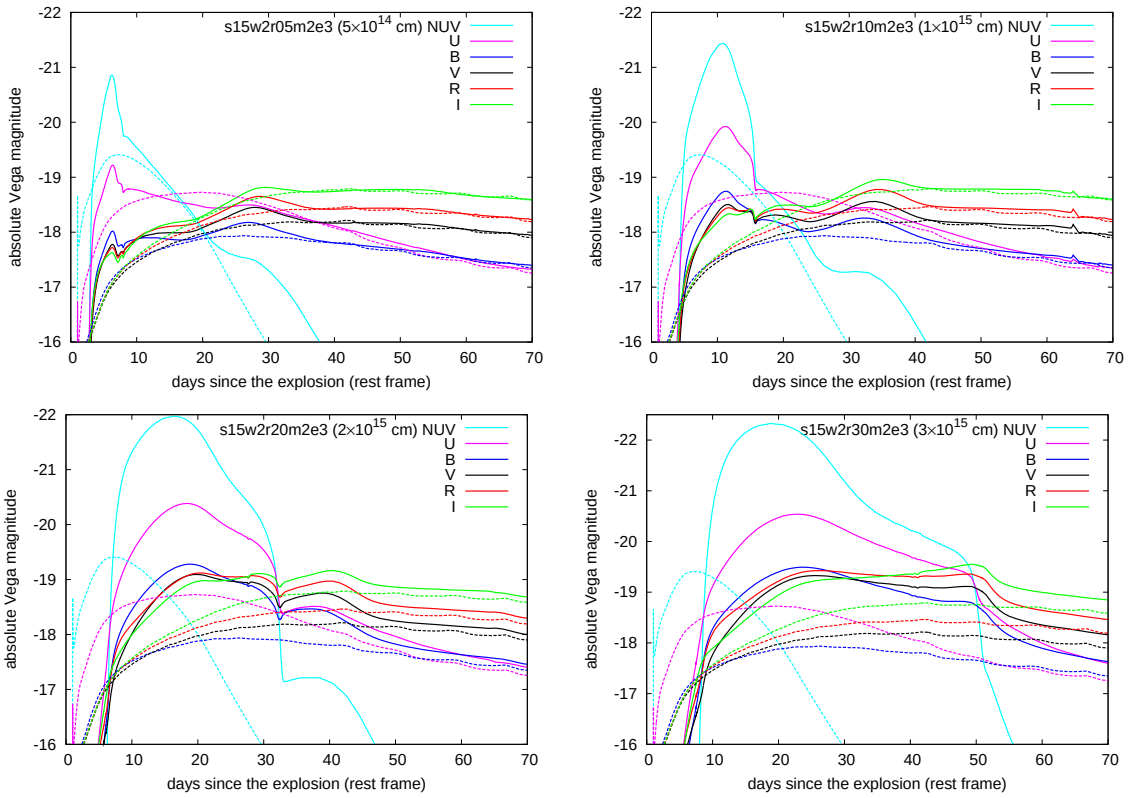

Figure 5.12: Multicolor LCs of the models with different radii (solid lines). The dashed lines are the multicolor LCs of the model s15e3 for comparison. LCs of the same color are from the same filter. Note that the scale of y-axis in the right bottom panel (s15w2r30m2e3) is different from those in the other panels.

decrease as the CSM radius increases. As the explosion energy and the density structure are similar in each model, the radiation energy released by the shock interaction is also close to each other (see Table 5.2 for the radiation energy emitted in each model). Therefore, the difference in the maximum luminosities is caused by the difference in the diffusion timescales. Even if the same energy is released in the same timescale, photons are more scattered and distribute more uniformly in the CSM for models with the longer diffusion timescales. Thus, the luminosity, i.e., radiation energy released from the CSM surface in a unit time, becomes lower for the models with the larger CSM radii. The flat phase of the IPP is also longer for the models with the larger radius.

The multicolor LCs of the models with 10^{-2} $M_\odot$ yr^{-1} are shown in Figure 5.12. Although s15w2r05m2e3 has the brightest peak bolometric luminosity among the models, the NUV and $UBVRI$ band LCs of the model are the faintest. This is because the more compact CSM is, the hotter CSM becomes. The photosphere of the model s15w2r05m2e3 is too hot during the IPP to emit the radiation in the NUV and $UBVRI$ bands. The SEDs of the models at the bolometric peak are shown in Figure 5.13.

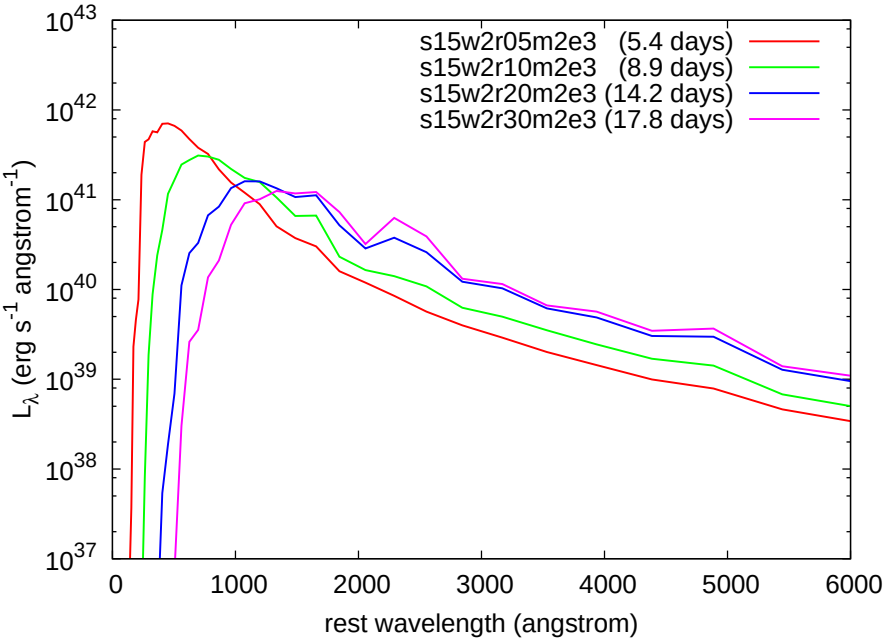

Figure 5.13: SEDs of the models with the different radii at the epoch of the maximum bolometric luminosity. The mass-loss rate of the models is 10^{-2} $M_\odot$ yr^{-1}.

Dependence on Density Slope

The CSM density slope of $\rho_{\rm csm} \propto r^{-2}$ results from the steady flow from the central progenitor. However, if mass loss is not steady, the density slope does not necessarily have the density structure $\rho_{\rm csm} \propto r^{-2}$ and can be shallower ($s < 2$) or steeper ($s > 2$) (c.f. Chapter 3). We calculate the LCs with the slope $s = 1.5$ as an example. As we are fixing the CSM velocity, the mass-loss rates should change with time to have the density slope $s = 1.5$. The CSM radius (2×10^{15} cm), the explosion energy (3×10^{51} erg), and the progenitor inside (s15) are fixed in this section. To see the effect of density slopes, we calculate the models with the same CSM masses as the models with the density slope $s = 2$, i.e., 6.5 $M_\odot$ (s15w1.5r20m1), 0.65 $M_\odot$ (s15w1.5r20m2), 0.065 $M_\odot$ (s15w1.5r20m3), 0.0065 $M_\odot$ (s15w1.5r20m4). The density structures of the pre-SN models are shown in Figure 5.5.

Figure 5.14 shows the bolometric LCs. The dependence on the CSM mass in the case $s = 1.5$ is similar to that of the case $s = 2$. Looking into the bolometric LCs with the same CSM mass, the LCs with $s = 1.5$ are fainter until around the bolometric peak and then become brighter. This is because in the case of $s = 1.5$, the CSM is denser outside and thinner inside compared to the case of $s = 2$ (Figure 5.5). Since the kinetic energy is more efficiently converted to the radiation energy with the denser CSM, the LCs from shallower CSM become brighter at later epochs. Although the luminosity of LCs is affected by density slopes, the durations of the round phase and the epochs of the sudden drop in the cases of $s = 1.5$ are similar to the cases of $s = 2$ and are not strongly affected by the density slopes.

The multicolor LCs are similar to those shown in Figure 5.9. The NUV absolute Vega mag-

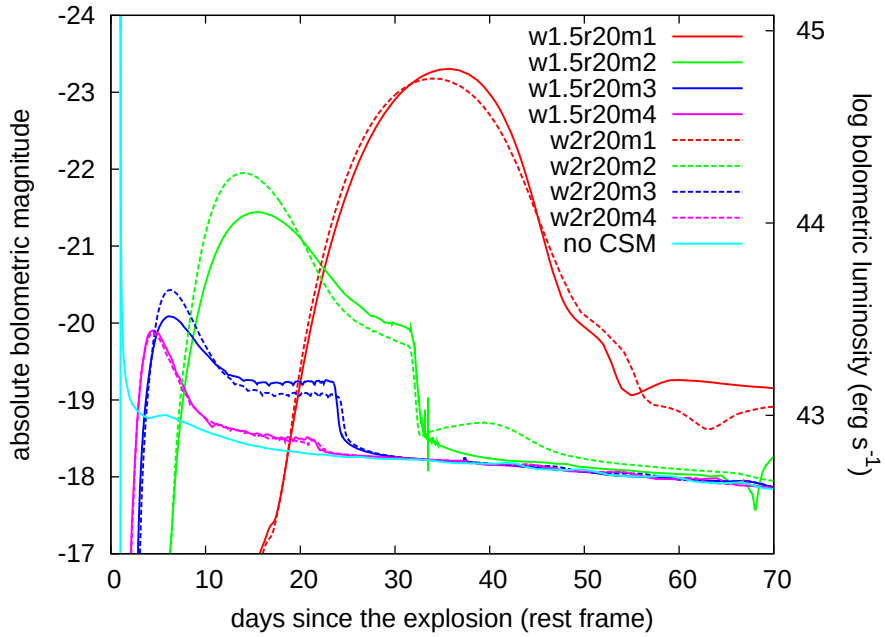

Figure 5.14: Bolometric LCs of the models with the different CSM density slopes and the mass-loss rates. The bolometric LCs shown with the solid lines have the CSM density slope of $\rho_{\rm csm} \propto r^{-1.5}$ and those shown with the dashed lines have the CSM density slope of $\rho_{\rm csm} \propto r^{-2}$. 's15' in the model names are omitted in the figure. The bolometric LC of the model s15e3 (no CSM) is also shown for comparison.

nitudes become as bright as -22.8 mag, -21.7 mag, -20.7 mag, and -20.0 mag for the models s15w1.5r20m1e3, s15w1.5r20m2e3, s15w1.5r20m3e3, and s15w1.5r20m4e3, respectively.

Dependence on Explosion Energy

In this section, we look into the effect of the explosion energy on the LCs. As the higher explosion energy leads to the higher kinetic energy of the SN ejecta, the luminosities of the LCs during the IPP are expected to be higher with the higher explosion energies. The fixed parameters in this section are the mass-loss rate (10^{-2} $M_\odot$ yr^{-1}), the CSM radius (2×10^{15} cm), the density slope ($s = 2$), and the progenitor (s15). The explosion energies we adopt are 1×10^{51} erg (s15w2r20m2e1), 3×10^{51} erg (s15w2r20m2e3), 5×10^{51} erg (s15w2r20m2e5), and 7×10^{51} erg (s15w2r20m2e7). The density structures of the models in this section are the same as that of the model s15w2r20m2 (Figure 5.5).

Figure 5.15 is the bolometric LCs of the explosions with the different explosion energies. As expected, the LCs become brighter with the higher explosion energies. Since the shock propagates faster in a higher energy model, the model has a shorter rising time and a shorter duration. However, the LCs are less sensitive to explosion energies than mass-loss rates and radii. This is because the CSM parameters have the direct effect on the diffusion timescales, while the explosion energy determines the strength of the shock wave where photons are

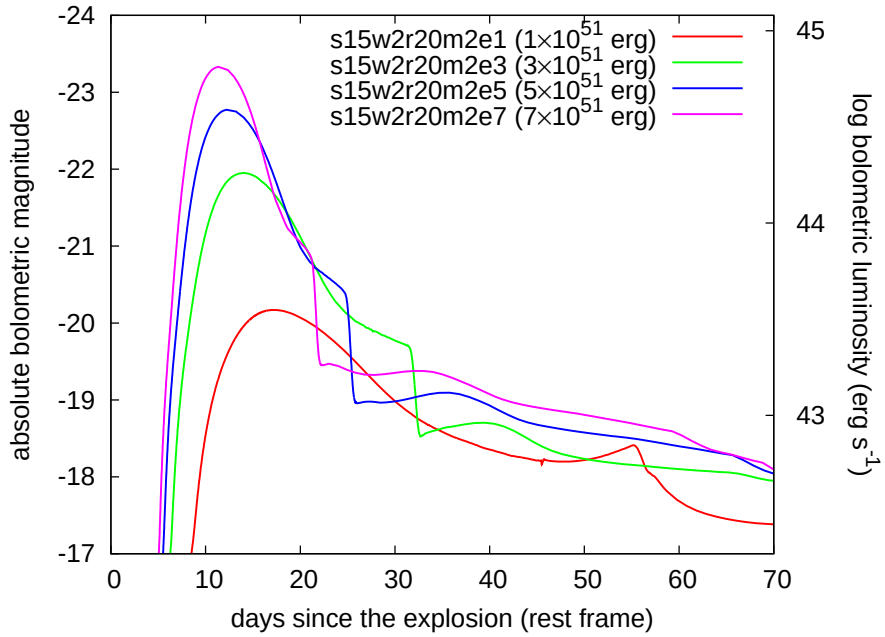

Figure 5.15: Bolometric LCs from the model s15w2r20m2 with the different explosion energies.

emitted.

The multicolor LCs of all the models shown in this section are similar to those of the model s15w2r20m2e3 in Figure 5.9 with the different rising times, durations, and brightness. The rising times and the durations are the same as those of the corresponding bolometric LCs and the NUV absolute Vega magnitudes become as bright as -21.0 mag, -22.4 mag, and -22.8 mag for the models s15w2r20m2e1, s15w2r20m2e5, and s15w2r20m2e7, respectively.

Dependence on Progenitor

In the previous sections, the progenitor model inside the CSM is fixed to s15. As the LCs during the IPP are powered by the interaction of SN ejecta and CSM, the effect on the LCs due to the difference in the progenitors (RSGs) inside is expected to be small. To confirm this, we calculate the LCs of the models which have different progenitors but the same CSM parameters. The CSM parameters fixed are the mass-loss rate (10^{-2} $M_\odot$ yr^{-1}), the CSM radius (2×10^{15} cm), and the density slope ($s = 2$). The explosion energy is also fixed to 3×10^{51} erg. We use SN IIP progenitors s13 (s13w2r20m2), s15 (s15w2r20m2), s18 (s18w2r20m2), and s20 (s20w2r20m2) to see the effect. Figure 5.16 shows the density structures of the models. We note that the CSM density structures of the models are slightly different from each other because the radius where the CSM is connected to the central progenitor is different depending on the pre-SN models.

Figure 5.17 shows the LCs with the different progenitors. Roughly speaking, the LCs are similar to each other because all the progenitors are RSGs and the properties of the

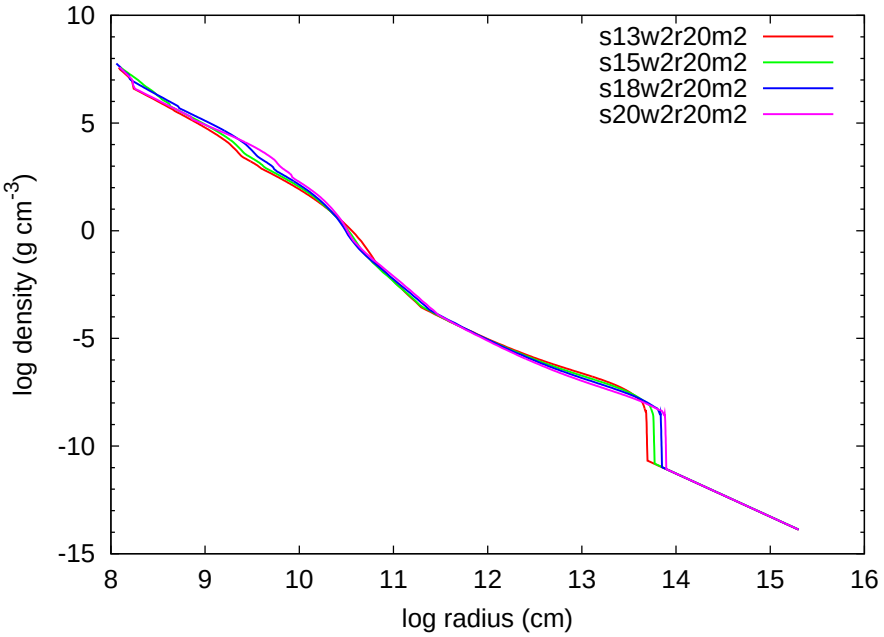

Figure 5.16: Density structures of the pre-SN models with the different progenitor models inside.

progenitors, like radii or density structures, are not dramatically different from each other. There are slight differences in the maximum luminosities and the epochs of the sudden drop in the LCs due to the slight difference in those properties of the progenitors.

The multicolor LCs are also similar to those of the model s15w2r20m2e3 (Figure 5.9). The NUV absolute Vega magnitudes become as bright as -22.0 mag, -21.8 mag, and -21.9 mag for the models s13w2r20m2e3, s18w2r20m2e3, and s20w2r20m2e3, respectively.

5.3.3 Discussion

In this section, we compare our LCs obtained in the previous section to that of UV-bright SN IIP 2009kf whose LC is suggested to be affected by dense CSM (Botticella et al. 2010). We show that the LC of SN 2009kf is actually reproduced by the LC models with dense CSM and we get constraints on the state of the CSM around the progenitor of SN 2009kf at the pre-SN stage.

5.3.3.1 Observations of SN 2009kf and Light Curve Modeling

SN 2009kf was discovered by Pan-STARRS 1 survey and observed by *GALEX* using the NUV filter (Botticella et al. 2010). The observations of SN 2009kf by *GALEX* revealed its distinguishing features: SN 2009kf was continued to be bright in NUV for more than 10 days and it was also bright in the optical bands during the same period. This feature is difficult to be explained by SN IIP models without the dense CSM. This is because, after the shock breakout, the UV LCs of SNe IIP without the dense CSM decline rapidly due to

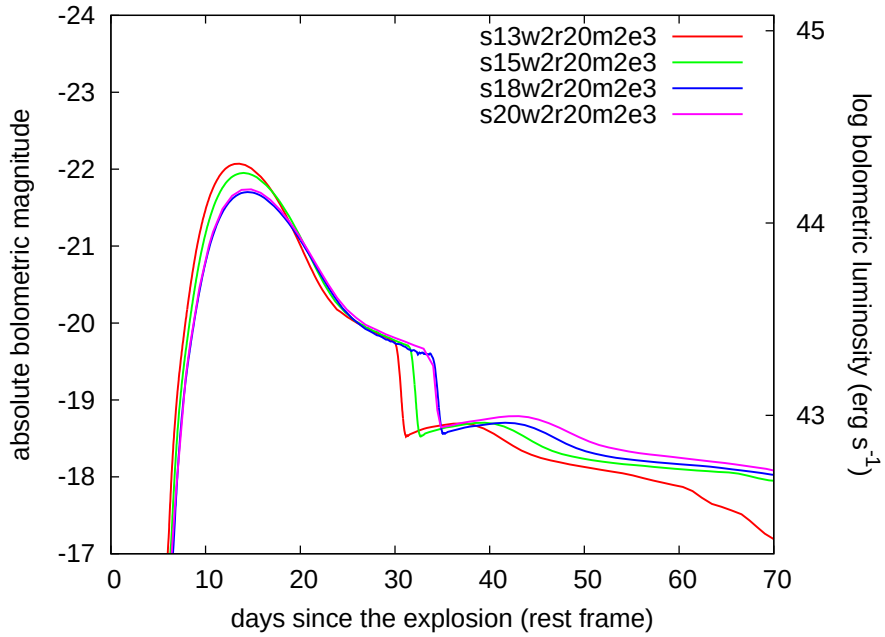

Figure 5.17: Bolometric LCs of the models with different progenitors inside.

the adiabatic cooling of the ejecta and the absorptions by iron group elements. Therefore, the optical brightness of SNe IIP without the dense CSM increases as the ejecta cools down with the decreasing UV brightness (Figure 5.4). Utrobin et al. 2010 try to model the LC of SN 2009kf without dense CSM and they find that large explosion energy (2×10^{52} erg) is required to obtain the LC of SN 2009kf.

One big uncertainty is in the extinction of SN 2009kf. Although the galactic extinction is negligible ($E(B-V) = 0.009$ mag; Schlegel et al. 1998), the host extinction is estimated as $E(B-V) = 0.32 \pm 0.5$ mag (Botticella et al. 2010). The large uncertainty in the host extinction makes it difficult to estimate its absolute NUV magnitudes. The redshift of the host galaxy is 0.182 ± 0.002 (Botticella et al. 2010).

In Figure 5.18, we show a comparison of the model s15w2r20m2e3 with the LCs of SN 2009kf. The SED derived at each time step in `STELLA` is reddened with the host extinction assuming the extinction law of Cardelli et al. 1989 and then shifted to the redshift 0.182 by using the standard ΛCDM cosmology with $H_0 = 70$ km s^{-1} Mpc^{-1}, $\Omega_{\rm M} = 0.3$, and $\Omega_\Lambda = 0.7$. The host extinction we apply here is $E(B-V) = 0.22$ mag. The top panel of Figure 5.18 shows the LCs in the first 60 days since the explosion in the observer frame. The solid lines are the model LCs and the points are the observations by Botticella et al. 2010. The epochs of observations are shifted arbitrarily. There is little contribution of ^{56}Ni produced by explosive nucleosynthesis on LCs at these epochs. The model LCs are in good agreement with the observations. Especially, the characteristic observational feature that the NUV LC and the optical LCs are bright at the same epochs is well-reproduced, as well as the NUV brightness. In the bottom panel of Figure 5.18, the LCs at the later epochs are also shown. Since the explosive nucleosynthesis (amount of ^{56}Ni produced), the progenitor model

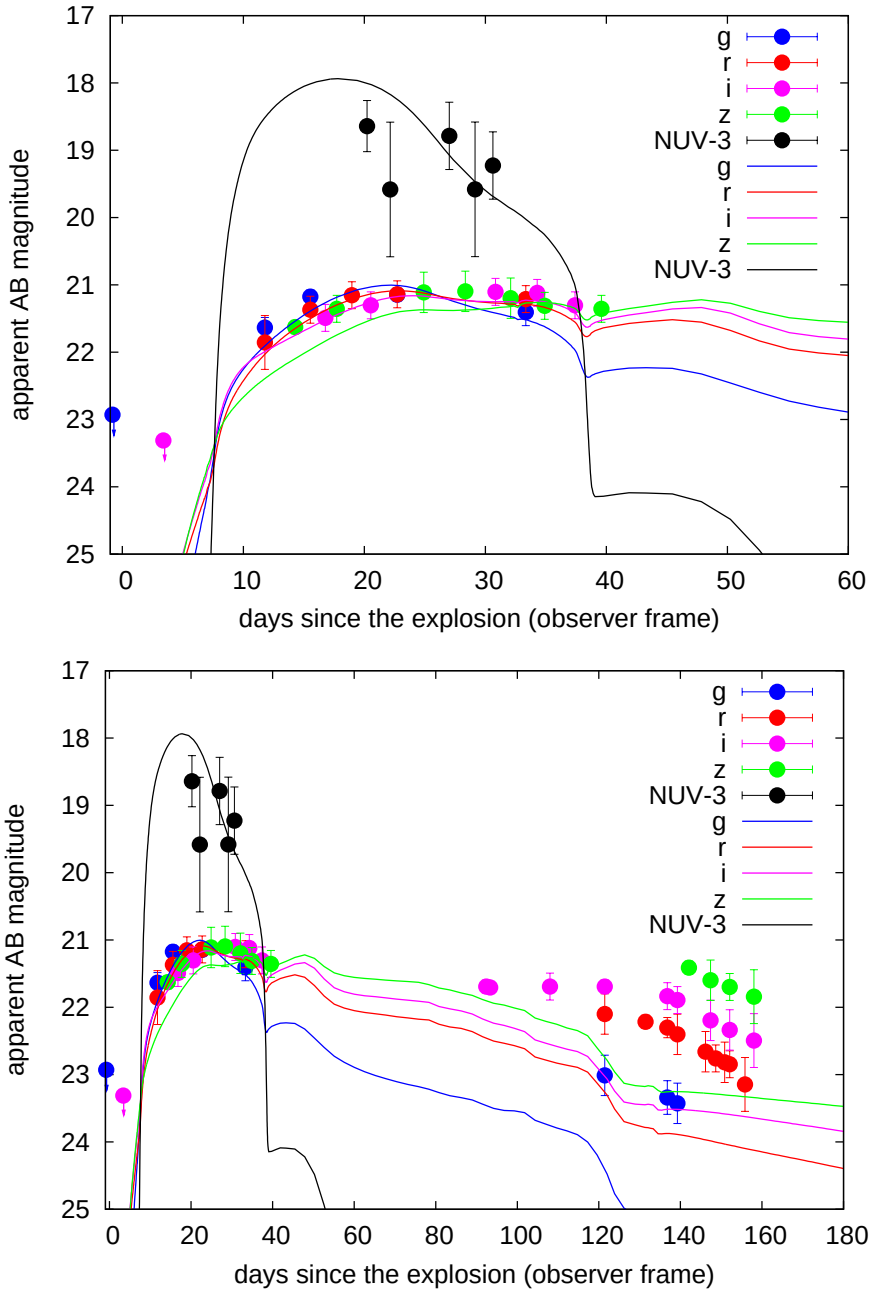

Figure 5.18: Comparison of the model LCs from s15w2r20m2e3 with the observed LCs of SN 2009kf. Each point is the observed LCs and the solid lines are the model LCs shifted to the observer frame. The epochs of the observation points are shifted arbitrarily. The model LCs are obtained by reddening the SEDs obtained by the numerical calculations with the host extinction of $E(B-V) = 0.22$ mag and then adopting the redshift 0.182. Magnitudes of NUV are shifted by 3 magnitudes in this figure.

inside (mass of hydrogen layer), and the degree of mixing of ^{56}Ni in H-rich layer mainly affect the LCs at the epochs after the IPP (e.g., Kasen & Woosley 2009, Dessart et al. 2010a, Dessart & Hillier 2010, Bersten et al. 2011), modeling this part of the LCs is out of our scope. Especially, if we include such effect, the photosphere is expected to be located outer than our model and the photospheric velocity becomes faster. The model shown in Figure 5.18 has the explosion energy of 3×10^{51} erg and the evolution of the photospheric velocity is shown in Figure 5.7 with the observed Hα line velocity. Although our model LCs have slower photospheric velocity, it is expected to increase as is mentioned above. Large amount of ^{56}Ni production is expected from the long plateau phase after the IPP. In addition, the observational facts that the bolometric luminosity at the plateau phase is very high and the Hα line velocities of SN 2009kf are very large also indicate large explosion energy of SN 2009kf. Note that the LCs during the IPP are not sensitive to the central progenitor model (Section 5.3.2.2) and the progenitor models other than s15 can also work.

5.3.3.2 CSM around the Progenitor of SN 2009kf

Given that the only observational data we are able to compare with our model LCs are those during the IPP and that the difference in the progenitors inside (RSGs) does not have much effect on LCs during the IPP (Section 5.3.2.2; Figure 5.17), it is difficult to constrain the ZAMS mass of the progenitor of SN 2009kf. However, as we show in Section 5.3.2.2, the LCs of the IPP is strongly affected by the CSM parameters and we can get constraints on them. In this section, we try to make constraints on the CSM around the progenitor of SN 2009kf at the pre-SN stage.

First, as discussed in Section 5.3.2.2, the mass-loss rate of the progenitor should be larger than $\sim 10^{-4}\ M_\odot\ \mathrm{yr}^{-1}$ to see the effect of the CSM on LCs. The duration of the UV-bright phase of SN 2009kf indicates that the CSM radius is larger than $\sim 1 \times 10^{15}$ cm (Section 5.3.2.2; Figure 5.11). Although a model with low explosion energy and a small CSM radius can result in LCs with a duration similar to that of SN 2009kf, the high bolometric luminosity and the large line velocities of SN 2009kf are difficult to be reproduced by such low-energy explosion.

The absolute NUV magnitude of the UV-bright phase is required to make further constraints on CSM. However, due to the uncertainty in the host extinction, it is difficult to get the absolute NUV magnitude of SN 2009kf. Therefore, what we can confidently conclude is that SN 2009kf has a LC naturally explained by the CSM interaction (long-lasting UV brightness during the period when it is also bright in optical) and the mass-loss rate of its progenitor should be higher than $10^{-4}\ M_\odot\ \mathrm{yr}^{-1}$ just before or at the time of the explosion to see such effect on the LCs, assuming that the CSM velocity is 10 km s^{-1}. The CSM radius which is larger than $\sim 1 \times 10^{15}$ cm is inferred from the duration and brightness of the NUV LC. If the host extinction is assumed to be $E(B-V) = 0.22$ mag, the multicolor LC model of the IPP shown in Figure 5.18, which has the CSM with the mass-loss rate $10^{-2}\ M_\odot\ \mathrm{yr}^{-1}$ and the radius 2×10^{15} cm, is consistent with the UV-bright phase of SN 2009kf. We note that the density slope of the CSM does not have much effect on the duration of the IPP as shown in Section 5.3.2.2 and we cannot constrain the density slope well with our model.

5.3.3.3 Progenitor of SN 2009kf and Its Extensive Mass Loss

The high bolometric luminosity at the plateau phase and very high line velocities of SN 2009kf imply that SN 2009kf had a high explosion energy. In addition, the long plateau phase indicates that the amount of ^{56}Ni produced by the explosive nucleosynthesis is large. Since SNe IIP from higher ZAMS mass progenitors tend to be more energetic and produce more ^{56}Ni (e.g., Hamuy 2003, Utrobin & Chugai 2009), the progenitor of SN 2009kf is indicated to be one of the most massive RSGs and may come from the high mass end of RSGs. Therefore, it is indicated that the most massive RSGs can have a very high mass-loss rate and that such extensive mass loss can occur just before the explosions of the massive RSGs.

Not only LCs but also spectra can be affected by the existence of dense CSM. During the IPP phase of SNe from RSGs with dense CSM, the photosphere is located in CSM and very narrow P-Cygni profiles, which are similar to those of SNe IIn, are expected to be observed (Figure 5.7). Then, after the IPP, their spectra shift to those of SNe IIP. In other words, SN 2009kf-like SNe can be a hybrid type of Type IIn and Type IIP (Figure 5.19). If extensive mass loss of massive RSGs happens just before their explosions, CSM mass and/or radius can be so small that the interaction of dense CSM and SN ejecta ends in early epochs. Then, the corresponding SN may be observed as a hybrid of Type IIn and Type IIP and SN 2009kf might be classified as Type IIn if early spectra were taken. If there is large and/or massive enough CSM or a shell exists that is created long before the explosion due to extensive mass loss, the SNe may be purely Type IIn and may not show the feature of SNe IIP (Figure 5.19). Our prediction that the early spectra of SN 2009kf-like SNe have narrow lines is what clearly differs from theoretical models suggested by Utrobin et al. 2010.

While no spectra of SN 2009kf were taken during the IPP, SN 1987C are suggested to have shown such transition of the spectra from a Type IIn-like blue spectrum with narrow hydrogen emission lines to Type IIP spectra (Schlegel & Kirshner 1998). The Type IIn-like spectrum of SN 1987C is taken at 52 days since its discovery when SN 1987C could have been approaching to the end of the IPP. At 79 days after the discovery, the spectrum showed the P-Cygni profile of hydrogen lines and the line velocity of Hα was high ($6,800$ km s^{-1}). Although SN 1987C was not observed by UV, this transition of the spectra could indicate that SN 1987C may be another sample of an explosion of a RSG within a dense CSM. The high Hα line velocities indicates that the progenitor of SN 1987C was a massive RSG. Another luminous SN II 2007pk, whose LC evolution is likely in between those of SNe IIP and SNe IIL, is suggested to have the early spectral transition from Type IIn to Type II (Inserra et al. 2012). Such early observations of SN spectra are important to find other candidate SNe which are the hybrid of Type IIn and Type IIP.

Rareness of UV-bright SNe IIP similar to SN 2009kf can be interpreted as a relatively small ZAMS mass range of this event. For example, no SNe IIP observed with *Swift* satellite show the long term UV-brightening which is expected by the CSM interaction (Brown et al. 2009). The rareness of UV-bright SNe IIP also supports that they may come from the high mass end of SN IIP progenitors (Figure 5.19). Note, however, that the rareness can also be interpreted in different ways. For example, it is possible that RSGs generally have extensive mass loss (due to, e.g., nuclear flashes) but it usually occurs long before their explosions and the mass range of the progenitors which experience extensive mass loss just before the explosions is small. Future early spectral and UV observations of SNe IIP are required to get more samples

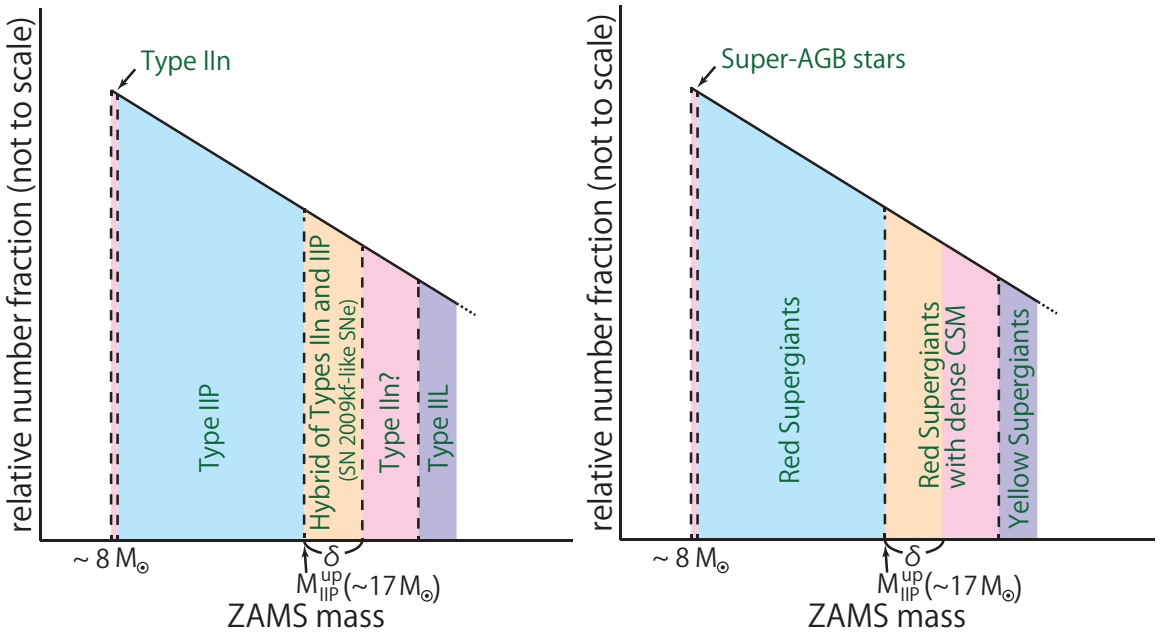

Figure 5.19: *Left:* Possible relation between ZAMS mass and SN types. We set the maximum ZAMS mass of SNe IIP as $M_{\rm IIP}^{\rm up}$, which is observationally suggested to be $\simeq 17\ M_\odot$ (Smartt et al. 2009). Dense CSM may be left at the time of SN explosions at a ZAMS mass range above $M_{\rm IIP}^{\rm up}$. If there is enough CSM, the SNe can be Type IIn. On the other hand, there can be a small ZAMS mass range from $M_{\rm IIP}^{\rm up}$ to $M_{\rm IIP}^{\rm up} + \delta$ (with small δ), in which there is not enough CSM for the SN to continue to be Type IIn and the SN can be a hybrid of Type IIP and Type IIn. SN 2009kf, SN 1987C, and SN 2007pk are possible candidates for such a hybrid SN. The number fraction of SNe (y-axis) is determined by an initial mass function. *Right:* The same as left but plotted with progenitor stars. The explosions of RSGs without dense CSM are expected from $\simeq 8\ M_\odot$ to $M_{\rm IIP}^{\rm up}$. RSGs explode within dense CSM above $M_{\rm IIP}^{\rm up}$. A yellow supergiant is observationally found to be the progenitor of SN IIL 2009kr. The ZAMS mass of the yellow supergiant is estimated as $\simeq 18 - 24\ M_\odot$ (Elias-Rosa et al. 2010) and $15^{+5}_{-4}\ M_\odot$ (Fraser et al. 2010), which is consistent with our picture.

of SN 2009kf-like SNe so that we can make constraint on the mass range of SN 2009kf-like SNe and on the driving force of such extensive mass loss. Observations of nebular phase spectra are also important for determining the ZAMS mass of such SNe (e.g., Dessart et al. 2010a).

5.3.4 Summary

We show that the existence of dense CSM around massive RSGs theoretically suggested affects LCs from the explosions of massive RSGs. This is because (1) the shock breakout signals are elongated by the CSM and (2) SN ejecta is decelerated by the CSM. In particular, because of the deceleration, kinetic energy of SN ejecta is converted to thermal energy which is emitted as radiation and SNe can be brighter than usual. The LC becomes bright in UV as well as in optical. In addition, the photospheric velocity of early epochs is very low because the photosphere is located in the CSM at early epochs. The most influential parameters of the CSM are mass-loss rates and radii. The mass-loss rate should be higher than $\sim 10^{-4}\ M_{\odot}\ \mathrm{yr}^{-1}$ to show the effect of the CSM. The higher mass-loss rates and/or the larger radii lead to the longer diffusion timescales of the CSM and thus, the longer durations and rising times of the LCs powered by the interaction. Density slopes and explosion energies also slightly change the LCs. The difference in SN IIP progenitor (RSG) models inside the CSM are not so sensitive to the LCs. (Section 5.3.2)

The LCs of SN IIP 2009kf, which were bright in UV as well as in optical in early phases (Botticella et al. 2010), can be explained by the pre-SN models with dense CSM. The mass-loss rate of the progenitor of SN 2009kf should be higher than $10^{-4}\ M_{\odot}\ \mathrm{yr}^{-1}$. The CSM radius is expected to be larger than $\sim 1 \times 10^{15}$ cm. The explosion energy of SN 2009kf is likely to be very high because of its high bolometric luminosity at the plateau phase and its high line velocities. The long duration of the plateau phase of SN 2009kf implies that the large amount of ^{56}Ni is produced by the explosion.

The high explosion energy and the large amount of ^{56}Ni produced indicate that the progenitor of SN 2009kf is a massive RSG. Our results show that massive RSGs are likely to experience extensive mass loss exceeding $10^{-4}\ M_{\odot}\ \mathrm{yr}^{-1}$ just before their explosions. The explosions of such massive RSGs with extensive mass loss will be SN 2009kf-like SNe. Their spectra show the transition from Type IIn-like spectra to Type IIP spectra which is likely observed in SN 1987C (Schlegel & Kirshner 1998) and SN 2007pk (Inserra et al. 2012). The existence of such SNe indicates that there is actually some mechanism to enhance mass loss of massive RSGs, like pulsations discussed by Yoon & Cantiello 2010 or nuclear flashes suggested by Weaver & Woosley 1979. Such a mechanism may reduce the maximum ZAMS mass of SN IIP progenitors predicted by the single star evolution modeling ($\simeq 25 M_{\odot}$; e.g., Heger et al. 2003) as low as the observationally implicated value ($\simeq 17 M_{\odot}$; e.g., Smartt et al. 2009) (Figure 5.19).

Future early spectral and UV observations of SNe will find other SNe similar to SN 2009kf and provide LCs with long time coverage and spectra at the IPP. Large samples and detailed observations of SN 2009kf-like SNe can reveal the mass-loss mechanism of RSGs as well as the nature of SN 2009kf-like SNe.

5.4 Luminous Blue Variables

As is introduced in Chapter 1, LBVs have not been considered to be SN progenitors. Recently, however, Groh et al. 2013 show that the spectra of the rotating 20 $M_{\odot}$ and 25 $M_{\odot}$ pre-SN model obtained by Ekström et al. 2012 become similar to those of LBVs and these relatively low-mass stars may be at an LBV stage at the time of the core collapse. This is the first theoretical LBV SN progenitors reported.

The possibility of LBV explosions is first suggested by Kotak & Vink 2006 by interpreting SN radio LCs, not from SN IIn observations. Radio emission from SNe is caused by the interaction between SN ejecta and the progenitor's CSM (see Section 2.2.1) and the mass-loss history of the SN progenitor is imprinted in SN radio LCs (e.g., Weiler et al. 2002, Chevalier et al. 2006, Chevalier & Fransson 2006). Radio emission from some SNe is known to have episodic luminosity enhancements. They are clearly observed in, e.g., SN IIb 2011ei (Milisavljevic et al. 2013), SN IIb 2008ax (Roming et al. 2009), SN IIb 2003bg (Soderberg et al. 2006), SN IIb 2001ig (Ryder et al. 2004), SN Ic 1998bw (Kulkarni et al. 1998), and SN IIL 1979C (Weiler et al. 1992). Kotak & Vink 2006 suggested that the timescales of the episodic radio modulations are consistent with S Doradus-type mass loss which LBVs experience and these SNe can be related to LBVs.

In this section, we investigate the CSM properties of the LBV SN progenitors reported by Groh et al. 2013 and the effect of the CSM to observational properties of SNe. Unfortunately, we find that the mass-loss rates of the LBV SN progenitors are too low to be SNe IIn. However, we show that the LBV SN progenitor from the rotating 20 $M_{\odot}$ star which is suggested to be SN IIb by Groh et al. 2013 actually experiences the episodic mass loss shortly before the core collapse and the model can naturally explain the episodic radio LC modulations. This result supports the idea that a fraction of LBVs can be the end stage of massive stars.

5.4.1 LBV SN Progenitor Models and their CSM

The rotating 20 $M_{\odot}$ and 25 $M_{\odot}$ LBV progenitors are computed by Ekström et al. 2012. The models are computed with the solar metallicity ($Z = 0.014$, Asplund et al. 2009). We first shortly summarize the stellar evolution modeling of Ekström et al. 2012. The initial rotational velocities of the models are 274 km s^{-1} and 295 km s^{-1}, respectively (both are 40% of the critical rotational velocity). The rotational velocities change with time and the average rotational velocities are 217 km s^{-1} (20 $M_{\odot}$) and 209 km s^{-1} (25 $M_{\odot}$). The radiative mass-loss rate is mainly adopted from Vink et al. 2001. The mass-loss rate of the parameter range in which Vink et al. 2001 does not cover is adopted from de Jager et al. 1988. A correction for the mass-loss rates due to the rotation are applied according to Maeder & Meynet 2000a but the correction does not have much effect on the two models we consider here. When the outermost layers of the stellar envelope exceed the Eddington luminosity in the RSG phase, the mass-loss rates are increased by a factor of 3 and the mass loss enhancement in RSGs shown by van Loon et al. 2005 is effectively taken into account in this way.

The rotating 20 $M_{\odot}$ and 25 $M_{\odot}$ models end their lives at the blue side of the HR diagram (Figure 5.20a). Groh et al. 2013 show that their spectra look like those of quiescent LBVs. An interesting feature we can find from Figure 5.20a is that the effective temperature of the 20 $M_{\odot}$ model at the end stage of the evolution is around 20,000 K. At around 20,000 K, the

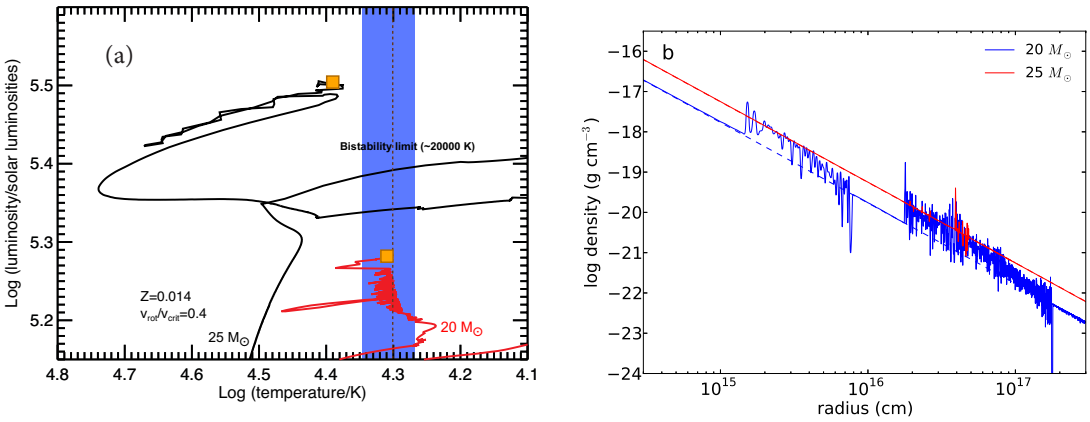

Figure 5.20: Evolutions of the LBV SN progenitors on the HR diagram (a) and CSM density structures obtained from them (solid lines in b). The CSM densities with dashed lines are the CSM without the mass loss variations and used to obtain the reference LCs.

ionization level of Fe is known to change dramatically and small changes in the effective temperature cause a huge variation in the mass-loss rate (Lamers et al. 1995, Vink et al. 1999). This phenomenon is know as the bistability jump and its relation to LBVs is proposed by Vink & de Koter 2002, Smith et al. 2004. The mass-loss rate of the 20 $M_\odot$ model rapidly changes from 1.2×10^{-5} $M_\odot$ yr^{-1} (hot side) to 1.5×10^{-4} $M_\odot$ yr^{-1} (cool side) many times shortly before the core collapse due to the bistability. On the other hand, the effective temperature of the 25 $M_\odot$ model is not close to 20,000 K at the end stage of the evolution and the mass-loss rate does not change rapidly.

To construct the CSM density structure from the mass-loss rates and the CSM velocities obtained by the stellar evolution model, we perform one-dimensional spherically-symmetric numerical hydrodynamics calculations with `ZEUS-MP2` version 2.1.2 (Hayes et al. 2006). The CSM structure of the region between 1.5×10^{13} cm and 3×10^{17} cm is followed by setting the inner boundary condition at 1.5×10^{13} cm based on the mass-loss rates and CSM velocities.

The CSM density structures obtained are shown in Figure 5.20b. In the 20 $M_\odot$ model, there exist two extended high-density regions. The two regions correspond to the two enhanced mass-loss periods (around 175-20 years and 10-1 years before the explosion) when the surface of the star is at the bistability. The small-scale density variations are due to the rapid variations in the mass-loss rate. On the contrary, the 25 $M_\odot$ model does not have significant enhancement in the mass-loss rate shortly before the core collapse and it does not have any extended high-density regions in CSM near the progenitor.

The mass-loss rates of the two LBV progenitors shortly before the core collapse are below 10^{-4} $M_\odot$ yr^{-1} on average and it is below the mass-loss rates required to explain SN IIn observations (Chapter 3). Thus, these LBV progenitors are not progenitors of SNe IIn. However, we show in the following that the 20 $M_\odot$ model shows an interesting radio LC feature which is observed in SNe IIb, IIL, and Ic.

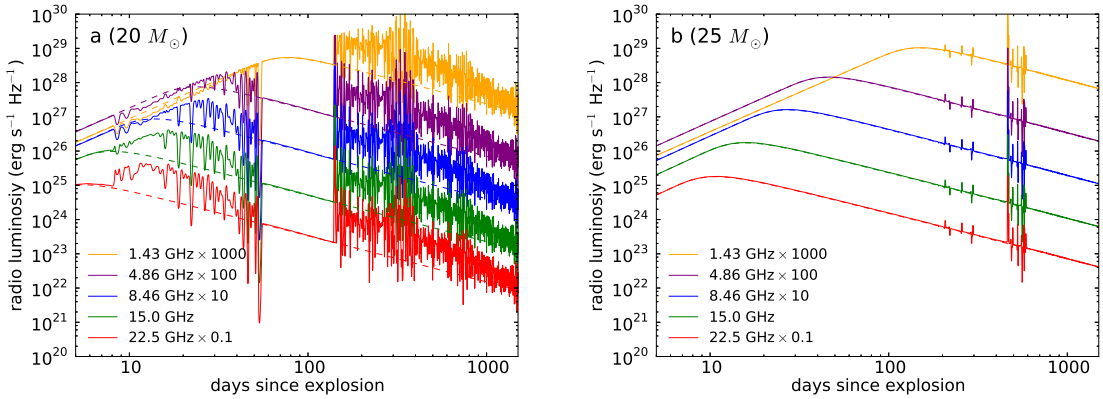

Figure 5.21: Synthesized radio LCs (solid lines) of (a) 20 $M_\odot$ model and (b) 25 $M_\odot$ model. The reference LCs from the models without the CSM density jumps are also shown (dashed lines, see Figure 5.20).

5.4.2 SN Radio Light Curves from the LBV SN Progenitors

We synthesize radio LCs following the formalism in Section 2.2.1. The radio emission is from synchrotron at the forward shock. As the CSM density is not high, we ignore the effect of the free-free absorption and take account of the SSA as absorption process. We adopt the standard parameters $\varepsilon_B = 0.1$, $\varepsilon_e = 0.1$, $p = 3$, and $\gamma_{\rm min} \sim 1$ used in SN radio studies (e.g., Chevalier et al. 2006, Chevalier & Fransson 2006, but see also Maeda 2012, Maeda 2013). The dynamical evolution ($r_{\rm sh}$ and $v_{\rm sh}$) is derived by the self-similar solution of Chevalier 1982a which is essentially the same as what we derived in Section 2.3. The SN ejecta with the kinetic energy $E_{\rm ej}$ and the mass $M_{\rm ej}$ is assumed to have the density structure with the two power-law components ($\rho_{\rm ej} \propto r^{-n}$ outside and $\rho_{\rm ej} \propto r^{-\delta}$ inside). We adopt $n = 10.2$ and $\delta = 1.1$ which approximate the numerical explosion of SN IIb/Ib/Ic progenitors (Matzner & McKee 1999). For simplicity, we ignore the effect of the density jump in the CSM on $r_{\rm sh}$ and $v_{\rm sh}$ as is also assumed in Soderberg et al. 2006. The mass-loss rate and the CSM velocity used to obtain $r_{\rm sh}$ and $v_{\rm sh}$ are 1.2×10^{-5} $M_\odot$ yr^{-1} and 270 km s^{-1} (20 $M_\odot$ model) and 4.6×10^{-5} $M_\odot$ yr^{-1} and 330 km s^{-1} (25 $M_\odot$ model) (see Groh et al. 2013). We assume $E_{\rm ej} = 10^{51}$ erg. We constrain $M_{\rm ej}$ by subtracting the remnant mass 1.4 $M_\odot$ from the progenitor mass obtained by Ekström et al. 2012 and $M_{\rm ej} = 5.7$ $M_\odot$ (20 $M_\odot$ model) and $M_{\rm ej} = 8.2$ $M_\odot$ (25 $M_\odot$ model).

SN radio LCs obtained from the LBV SN progenitors are presented in Figure 5.21. The radio LCs from the 20 $M_\odot$ model show two episodic modulations. They result from the two density jumps caused by the mass-loss enhancements shortly before the core collapse. The forward shock reaches the first jump in the density at around 8 days since the explosion. At this time, the effect of the SSA is still dominant at 1.43 GHz, 4.86 GHz, and 8.46 GHz and the radio luminosities at these frequencies decrease due to the density enhancement. As time passes, the SSA gets less effective and the radio luminosities start to be enhanced after the LC peak in the reference LC without the density jump. At the time when the forward shock reaches the second density jump, the SSA is negligible in all the frequencies shown in Figure 5.21 and the radio luminosities are enhanced about ~ 4 times on average in all the bands.

The radio LCs also have very short variations which are caused by the small-scale density variations seen in Figure 5.20b. However, these short time variations should be smoothed by the light-traveling-time effect which is not taken into account in our LC modeling.

On the contrary, the 25 $M_{\odot}$ model does not show episodic LC modulations as its surface temperature deviates from the bistability temperature and there is no episodic mass-loss increase shortly before the explosion (Figure 5.20).

We also find that the 20 $M_{\odot}$ model can explain the observational radio LCs of SNe IIb 2001ig and 2003bg by just slightly changing the parameters. In Figure 5.22, we compare our modified radio LCs from the 20 $M_{\odot}$ model to those of SNe IIb 2001ig (Ryder et al. 2004) and 2003bg (Soderberg et al. 2006). The absolute radio luminosities of SNe 2001ig and 2003bg are higher than those of the 20 $M_{\odot}$ model presented above. Hence, we need to increase the kinetic energy of SN ejecta and the CSM density to increase the luminosities (see Section 2.2.1). We change ε_e and ε_B to 0.2 and 0.08, respectively, to account for the time of the radio LC peaks in both cases. The model for SN 2001ig have $E_{\rm ej} = 4 \times 10^{51}$ erg and the CSM density is increased three times. The synthesized LC luminosity matches the observed LC luminosity within a factor of a few. The episodic radio LC jump observed at around 130 days matches to the epoch when the model LCs show the second modulation. The observed radio luminosities increase about a factor 4 and this also matches the radio luminosity increase in our model.

To have close match to the SN 2003bg radio LCs, we increased the SN ejecta energy to $E_{\rm ej} = 5 \times 10^{51}$ erg and the CSM density is increased by eight times. However, the model radio luminosity is still 20% of the observed luminosity. The spectra of SN 2003by are reported to have very broad component and the SN energy can be larger (Hamuy et al. 2009). However, the time of the bump become much earlier with the increased energy and we find that the location of the radio bump is difficult to be explained by the larger kinetic energy with the current CSM profile. The time of the bump is mostly determined by when the mass-loss variation occurs in the progenitor and it depends on the progenitor model. The 20 $M_{\odot}$ model just happens not to have the mass loss enhancement at the correct time to explain the SN 2003bg. Thus, we conclude that the basic features of SN 2003bg are consistent with the LBV progenitor model.

5.4.3 Summary

We have shown that the LBV SN progenitor from the rotating 20 $M_{\odot}$model obtained by Ekström et al. 2012 can explain episodic radio LC modulations observed in some SNe. The connection between the radio modulations and LBVs is suggested by Kotak & Vink 2006 and we show that the relatively low mass LBV SN progenitor actually show them. Unfortunately, the LBV progenitor does not become a SN IIn and SN IIn progenitors must be investigated. However, our result that the radio modulation can be actually explained by the LBV SN progenitors suggest that LBVs may rather be a common SN progenitor.

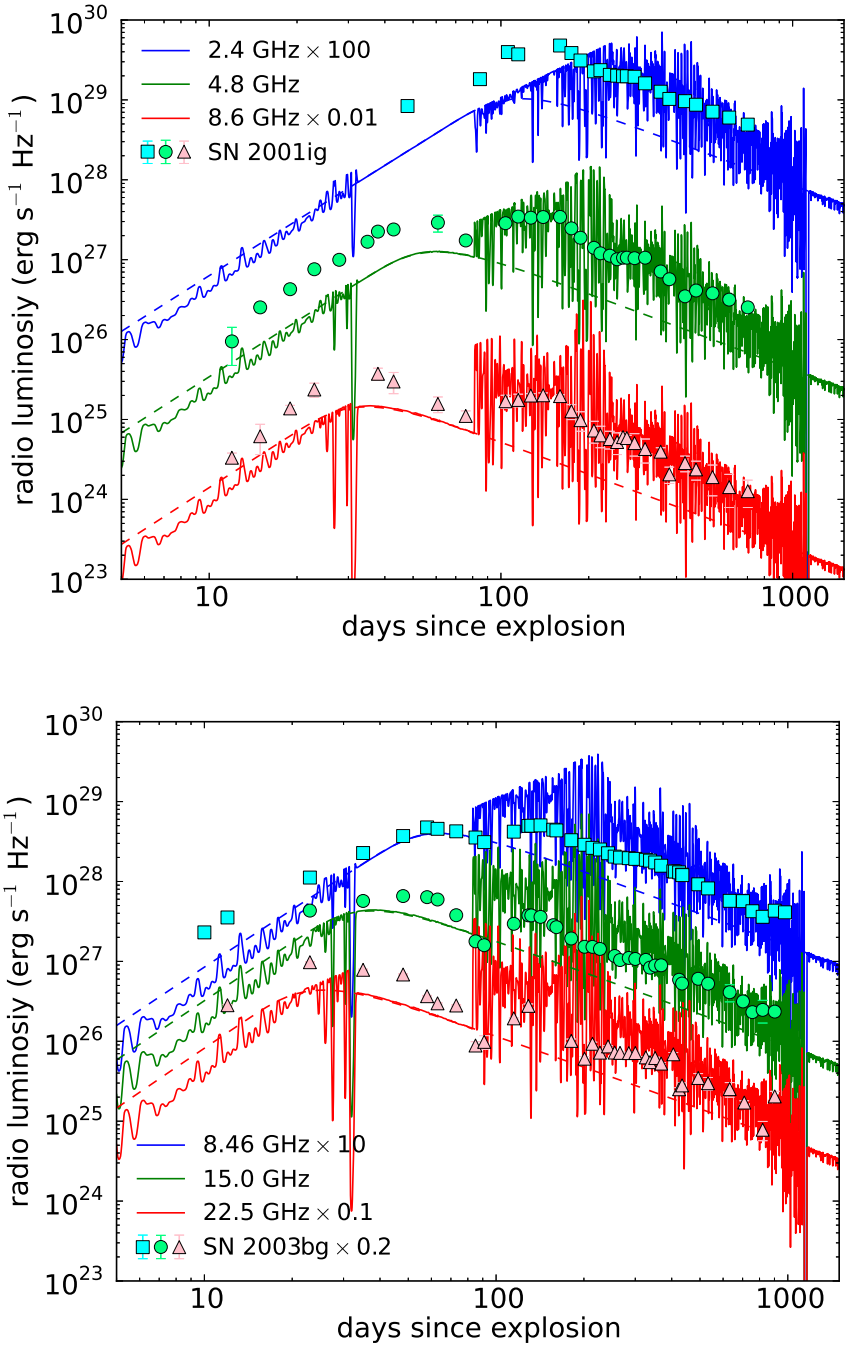

Figure 5.22: Comparisons between the model radio LCs from the 20 $M_{\odot}$ model and the observed radio LCs of SNe IIb 2001ig (Ryder et al. 2004) and 2003bg (Soderberg et al. 2006). The frequencies of the observed radio LCs are 2.4 GHz (square), 4.8 GHz (circle), and 8.6 GHz (triangle) in the top panel. The LCs of 2.4 GHz and 8.6 GHz are shifted 100 and 0.01 times, respectively, for the illustrative purpose. In the bottom panel, the frequencies of the observed radio LCs are 8.46 GHz (square), 15.0 GHz (circle), and 22.5 GHz (triangle). The LCs of 8.46 GHz and 22.5 GHz are shifted 10 and 0.1 times, respectively. The radio LCs of SN 2003bg are shifted 0.2 times additionally to match the synthesized LCs.

5.5 Summary

We have investigated properties of SNe whose progenitors are theoretically suggested to explode within dense CSM. We have considered three kinds of the progenitors, namely, super-AGB stars (Section 5.2), massive RSGs (Section 5.3), and LBVs (Section 5.4). We found that these suggested SN progenitors can explain some properties of peculiar SNe which are not SNe IIn, none of them will be SNe IIn. We conclude that there are still no SN IIn progenitor expected from the theoretical stellar evolution modeling and there are missing important keys in it. The missing keys are presumed to be related to mass loss of massive stars which are a critical ingredient in the stellar evolution modeling and SN IIn studies will provide us with important hints to reveal them.

This chapter is based on
T. Moriya, N. Tominaga, S.I. Blinnikov, P.V. Baklanov, E.I. Sorokina,
Monthly Notices of the Royal Astronomical Society, 415, 199, 2011
T.J. Moriya, J.H. Groh, G. Meynet,
Astronomy & Astrophysics Letters, accepted (arXiv:1306.0605)

The future is something which everyone reaches at the rate of 60 minutes an hour, whatever he does, whoever he is.

Clive Staples Lewis (1898 - 1963)

6

Remnants of Supernovae Interacting with Dense Circumstellar Media

6.1 Overview

We have looked into the effect of the dense CSM at the early stages of the SN evolution. SNe will eventually evolve to SNRs. What kind of SNRs is expected from SNe interacting with dense CSM? In this chapter, we show that recombining SNRs are likely to be an answer. In Section 6.2, we introduce recombining SNRs and discuss the progenitors from which they can emerge. We also discuss other SNRs which are suggested to be exploded within the dense CSM in Section 6.3.

6.2 Recombining Supernova Remnants

Recombining SNRs are SNRs in which the ionization temperature is higher than the electron temperature. The existence of recombining SNRs are recently confirmed by the X-ray observations by the *Suzaku* satellite (Yamaguchi et al. 2009, Yamaguchi et al. 2012, Ozawa et al. 2009, Ohnishi et al. 2011, Sawada & Koyama 2012). The forward shock wave emerged at the time of a SN explosion propagates in the interstellar medium (ISM). As the typical density of the ISM is very small ($n_e \sim 1$ cm^{-3} or less where n_e is the electron number density), the timescale to reach collisional ionization equilibrium (CIE) in the shocked ISM is typically $\sim 10^4$ years or longer (e.g., Masai 1984). Electrons heated by the Coulomb interaction with ions in the shocked ISM collisionally excite ions and SNRs reach CIE with this timescale. Thus, young SNRs before CIE are supposed to be ionizing SNRs in which the electron temperature is higher than the ionization temperature and evolve to SNRs in CIE. Most of SNRs are known to be in either the ionizing stage or CIE (e.g., Kawasaki et al. 2005). In this simple picture, SNRs cannot be recombining SNRs and the confirmation of the re-

combining SNRs challenges the current understanding of the evolution of SNRs.

There are several suggested mechanisms to make recombining plasma in SNRs (see, e.g., Yamaguchi et al. 2012 and the references therein). The existence of dense CSM is one possible way to explain the recombining SNRs (e.g., Itoh & Masai 1989, Shimizu et al. 2012, Zhou et al. 2011). If a dense CSM is around a SN, CIE can be achieved in much shorter timescale [$\sim 10^4/(n_e/1\ \mathrm{cm}^{-3})$ years]. When the shock wave reaches the outer edge of the dense CSM, the shocked CSM suddenly expands adiabatically and the electron temperature suddenly becomes low and the plasma starts to recombine.

Although the existence of the dense CSM at the time of the SN explosion has been suggested as a possible mechanism to realize recombining SNRs, we still do not have a clear picture about possible SN progenitors that can have a CSM which is dense enough to make recombining SNRs. In this section, we look into the properties of the CSM around several SN progenitors at the time of SN explosions and investigate the progenitors which can evolve to recombining SNRs. We focus on massive star progenitors because two recombining SNRs, IC 443 and W49B, are clearly associated with massive star forming regions (e.g., Yamaguchi et al. 2012) but we also investigate possible channels for white dwarfs to be recombining SNRs.

6.2.1 Possible Progenitors of Recombining SNRs

6.2.1.1 Red Supergiants & Wolf-Rayet Stars

RSGs and WR stars explode inside the CSM created by the preceding stellar evolution. If we assume that the CSM is from steady mass loss with the velocity v_w and the mass-loss rate $\dot{M}$, the CSM density ρ_csm becomes

$$\rho_\mathrm{csm} = \frac{\dot{M}}{4\pi r^2 v_\mathrm{w}}. \tag{6.1}$$

If the star inside the CSM explodes, a forward shock propagates in the CSM. Assuming that the adiabatic index of the system is 3/5, the density ρ_scsm of the shocked CSM just behind the forward shock becomes $\rho_\mathrm{scsm} = 4\rho_\mathrm{csm}$. As the forward shock propagates in the CSM, it is decelerated, especially if the CSM is dense. However, the mass of the CSM swept up by the forward shock is still small compared to the progenitor mass in the early epochs we are interested in and we assume that it is freely expanding with the velocity v_s for simplicity. Note that the deceleration makes the time of the interaction between the shock wave and the CSM longer and CIE can be achieved easier with the deceleration. The typical v_s of standard SN explosions is $v_s \sim 10{,}000$ km s^{-1} (e.g., Suzuki & Nomoto 1995, Fransson et al. 1996, Dwarkadas 2005, Dwarkadas 2007). The location of the forward shock at the time t after the explosion is $r = v_s t$ and ρ_scsm can be expressed as

$$\rho_\mathrm{scsm} = \frac{\dot{M}}{\pi v_s^2 t^2 v_\mathrm{w}}. \tag{6.2}$$

Although Equation 6.2 is the evolution of the density just behind the shock, the remaining entire shocked CSM has similar densities when the shock is traveling in the density structure close to $\rho_\mathrm{csm} \propto r^{-2}$ (see, e.g., Chevalier 1982a, Suzuki & Nomoto 1995, Fransson et al. 1996,

Dwarkadas 2005, Dwarkadas 2007) and we assume that $\rho_{\rm scsm}$ is a typical value in the shocked CSM. The actual densities in the shocked CSM are slightly higher than $\rho_{\rm scsm}$.

Since the CSM properties of RSGs and WR stars differ, we consider two cases separately.

Red Supergiants

The typical mass-loss rate and wind velocity of RSGs are $\sim 10^{-5}\ M_\odot\ {\rm yr}^{-1}$ and $\sim 10\ {\rm km\ s}^{-1}$, respectively (e.g., Mauron & Josselin 2011) and they are consistent with those estimated from the observations of SN explosions from RSGs (SNe IIP, e.g., Chevalier et al. 2006). If we assume that the RSG wind has the solar metallicity and H and He in the wind are fully ionized when the forward shock passes, $\rho_{\rm scsm} = 2.0 \times 10^{-24} n_{es}$ where n_{es} is the electron number density in the shocked CSM. From Equation 6.2, the time evolution of n_{es} is

$$n_{es} t^2 = 10^{20} \dot{M}_{-5} v_{s,9}^{-2} v_{\rm w,6}^{-1}\ {\rm cm}^{-3}\ {\rm sec}^2, \tag{6.3}$$

where $\dot{M}_{-5}$ is $\dot{M}$ scaled by $10^{-5}\ M_\odot\ {\rm yr}^{-1}$, $v_{s,9}$ is v_s scaled by $10,000\ {\rm km\ s}^{-1}$, and $v_{\rm w,6}$ is $v_{\rm w}$ scaled by $10\ {\rm km\ s}^{-1}$.

Electrons and ions in plasma can reach CIE with the timescale of

$$n_{es} t \sim 10^{12}\ {\rm cm}^{-3}\ {\rm sec}, \tag{6.4}$$

(e.g., Masai 1984, Smith & Hughes 2010). Note that only ions are presumed to be heated by the forward shock and electrons are heated up by the subsequent Coulomb interaction between ions and electrons. The timescale of the electron heating is (e.g., Masai 1994)

$$n_{es} t = 3 \times 10^{14} v_{s,9}^3 \left(\frac{\mu}{0.5}\right)^{1.5} \left(\frac{\ln \Lambda}{30}\right)^{-1}\ {\rm cm}^{-3}\ {\rm sec}, \tag{6.5}$$

where μ is the mean molecular weight and $\ln \Lambda$ is the Coulomb logarithm. Although the timescale of temperature equilibrium is a few orders of magnitudes longer than that of CIE, the electron temperature can reach about 10 % of the ion temperature ($\sim 10^9$ K) in the CIE timescale (Masai 1994) and becomes high enough to explain the ionization temperature of recombining SNRs. Recombining plasma in SNRs can appear if electrons cool down after CIE is achieved (e.g., Itoh & Masai 1989).

Figure 6.1 shows the comparison of the evolution of the typical density in the shocked CSM (Equation 6.3) and the CIE timescale (Equation 6.4). CIE can be achieved at early epochs of SNRs from RSGs with the typical mass-loss rate if we take account of the existence of the CSM. This is contrary to the general belief that it takes much time to be CIE because SNRs evolve in ISM. Note that v_s in the early time is presumed to be higher than the value assumed in Figure 6.1 (e.g., Dwarkadas 2005) and this effect can make the evolution of the electron number density faster. In addition, the mass of the recombining plasma estimated from Figure 6.1 in the case of the standard mass loss is $\simeq 3 \times 10^{-2}\ M_\odot$ and rather small. Massive RSGs, yellow supergiants, or RSGs in binary systems can have higher mass-loss rates than less massive RSGs especially just before their explosions (see, e.g., Section 5.3, Georgy 2012 and the references therein) and they are more likely to become recombining SNRs among RSGs.

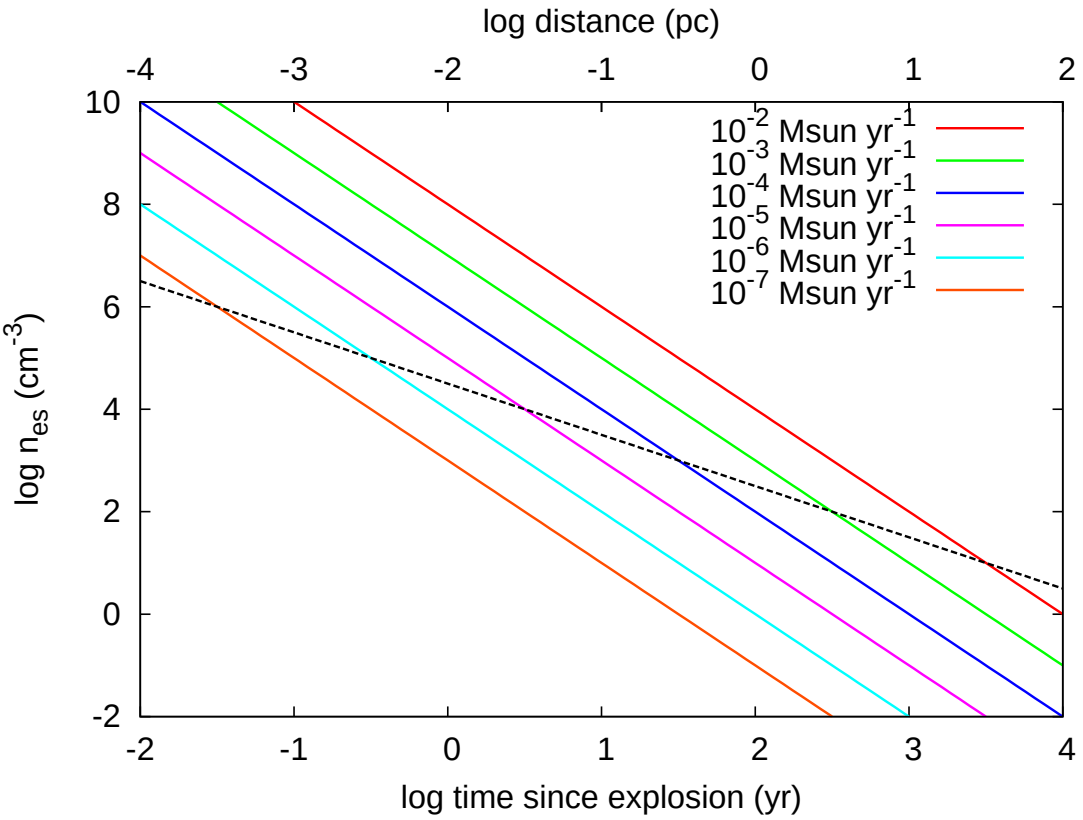

Figure 6.1: Evolution of the electron number density in the shocked CSM from RSG winds. $v_s = 10{,}000$ km s^{-1} and $v_{\rm w} = 10$ km s^{-1} is fixed and lines with several mass-loss rates are shown. The distance in the horizontal axis is the distance which can be reached by the forward shock with $v_s = 10{,}000$ km s^{-1} in the corresponding time. If we assume that the progenitor is in the RSG stage for 10^5 years before the explosion, the CSM can reach 1 pc with $v_{\rm w} = 10$ km s^{-1}. The dashed line follows $n_{es}t = 10^{12}$ cm^{-3} sec and corresponds to the minimum density required to reach CIE at the time. Shocked CSM above this line is presumed to be at CIE.

The early X-ray observations of SN IIb 1993J whose progenitor is an RSG in a binary system (e.g., Maund et al. 2004) revealed the existence of the CIE plasma at a few days since the explosion (e.g., Uno et al. 2002) and the progenitor's mass-loss rate is suggested to be $\simeq 5 \times 10^{-5}\ M_\odot\ \mathrm{yr}^{-1}$ (e.g., Suzuki & Nomoto 1995, Fransson et al. 1996). This is consistent with our estimate and explosions of RSGs can establish CIE in the early epochs and evolve to recombining SNRs.

Wolf-Rayet Stars

The typical mass-loss rate and CSM velocity of WR stars are $\sim 10^{-5}\ M_\odot\ \mathrm{yr}^{-1}$ and $\sim 1,000\ \mathrm{km\ s}^{-1}$, respectively (e.g., Crowther 2007). If we assume that the wind from WR stars is composed of 50 % of C and 50 % of O and they are fully ionized when the CSM is shocked, $\rho_{\mathrm{scsm}} = 3.3 \times 10^{-24} n_{es}$. With these values, the following equation is obtained from Equation 6.2:

$$n_{es} t^2 = 6 \times 10^{17} \dot{M}_{-5} v_{s,9}^{-2} v_{\mathrm{w},8}^{-1}\ \mathrm{cm}^{-3}\ \mathrm{sec}^2, \tag{6.6}$$

where $v_{\mathrm{w},8}$ is v_{w} scaled by $1,000\ \mathrm{km\ s}^{-1}$.

The evolution of n_{es} is compared to the CIE timescale $n_{es}t \sim 10^{12}\ \mathrm{cm}^{-3}$ sec in Figure 6.2. With the canonical mass-loss rate $10^{-5}\ M_\odot\ \mathrm{yr}^{-1}$, the evolution of the shocked CSM can be comparable to the CIE timescale just after the explosion. However, v_s is presumed to be larger than $v_s = 10,000\ \mathrm{km\ s}^{-1}$ in the early epochs and the evolution of n_{es} can be faster, as noted in the previous section. Contrary to the case of RSGs, CIE can be only established at the very early epochs with the optimistic v_s and it is likely that CIE is not achieved at early phases of the typical explosions of WR stars with the canonical mass-loss history. This is because the typical CSM velocity is about 100 times larger than the typical RSG CSM velocity and the CSM is less dense. Although recent radio observations of explosions of WR stars (SNe Ibc) are revealing the existence of WR stars with high mass-loss rates ($\sim 10^{-4}\ M_\odot\ \mathrm{yr}^{-1}$, e.g., Wellons et al. 2012), the amount of recombining plasma is very small ($\sim 10^{-4}\ M_\odot$, Figure 6.2) even if such a high mass-loss rate is maintained for the entire WR phase. Thus, WR stars may be difficult to have dense CSM which is massive enough to make them recombining SNRs. Since some elements can reach the CIE in smaller timescales than $n_{es}t \sim 10^{12}\ \mathrm{cm}^{-3}$ sec at the typical temperature in the shocked CSM (Smith & Hughes 2010), at least some elements may reach CIE. In addition, it is also known that some WR stars experience explosive mass loss just before their explosions which can eject massive CSM, as is indicated by the progenitor of SN Ib 2006jc (e.g., Pastorello et al. 2007). Explosions of this kind of WR stars can also result in recombining SNRs but they are also expected to be rare.

6.2.1.2 Type IIn Supernova Progenitors

As have been discussed in this dissertation, the progenitors of SNe IIn are not known well. In this section, for simplicity, we assume that SNe IIn have a dense CSM with $\tau_T = \sigma_T \overline{n}_{\mathrm{ecsm}} \Delta R \sim 1$, where σ_T is the Thomson cross section, $\overline{n}_{\mathrm{ecsm}}$ is the mean CSM electron number density, and ΔR is the CSM length. We use the mean density $\overline{n}_{\mathrm{ecsm}}$ because the mass loss of SN IIn progenitors just before their explosions can be non-steady (Chapters 3 and 4). The shock wave with the velocity v_s can propagate through the CSM with $t_s = \Delta R / v_s$. As CSM or ISM with much lower density exists outside the dense CSM and

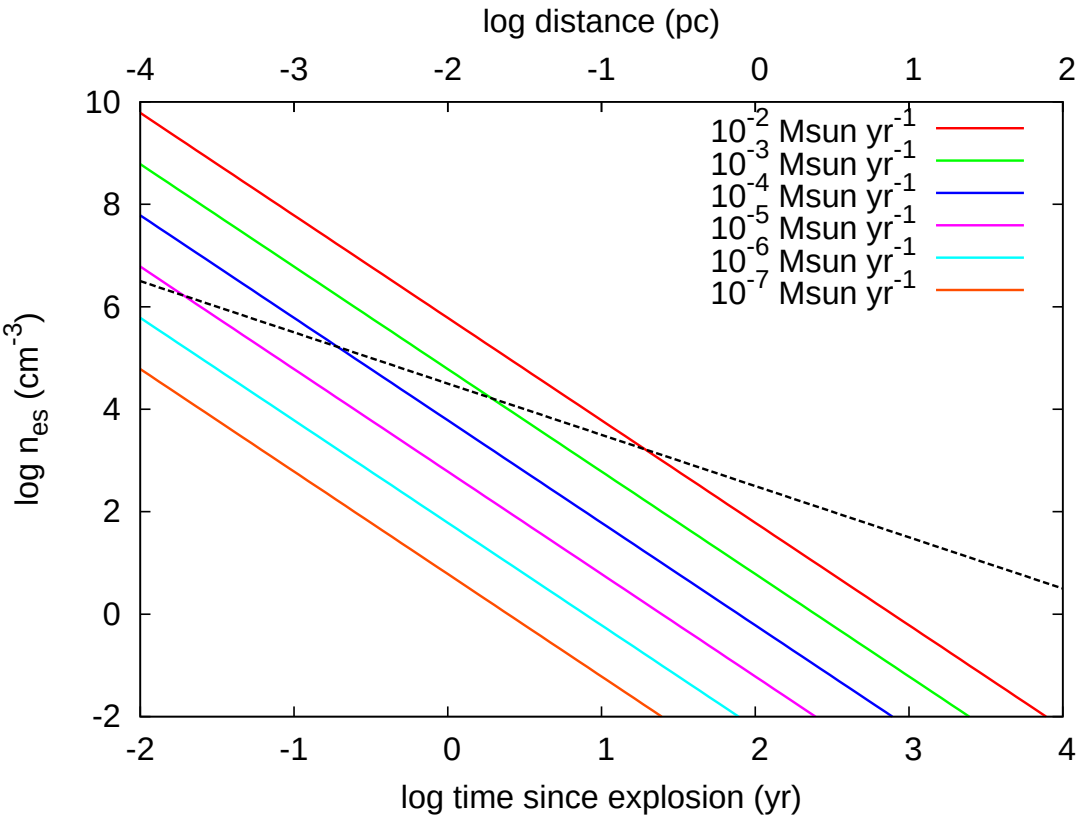

Figure 6.2: Evolution of the electron number density in the shocked CSM from WR star winds. $v_s = 10,000$ km s^{-1} and $v_{\rm w} = 1,000$ km s^{-1} is fixed and lines with several mass-loss rates are shown. The distance in the horizontal axis is the distance which can be reached by the forward shock with $v_s = 10,000$ km s^{-1} in the corresponding time. If we assume that the progenitor is in the WR stage for 10^5 years before the explosion, the CSM can reach 100 pc with $v_{\rm w} = 1,000$ km s^{-1}. The dashed line follows $n_{es}t = 10^{12}$ cm^{-3} sec and corresponds to the minimum density required to reach CIE at the time. Shocked CSM above this line is presumed to be at CIE.

the shocked CSM is rarefied after the shock wave goes out of the dense CSM, recombining plasma can be easily synthesized once the CIE is achieved in the shocked CSM. Assuming $\overline{n}_{\rm es} = 4\overline{n}_{\rm ecsm}$ and the solar metallicity, the typical timescale before the rarefaction is

$$\overline{n}_{\rm es} t_s \sim 6 \times 10^{15} v_{s,9}^{-1} \ {\rm cm}^{-3} \ {\rm sec}. \tag{6.7}$$

This is much larger than the timescale required to achieve the CIE, $n_e t \sim 10^{12}$ cm^{-3} sec. In reality, v_s can be smaller than 10,000 km s^{-1} because of the deceleration by the dense CSM but this makes t_s longer. One caveat is that we use a constant mean electron density $\overline{n}_{\rm ecsm}$ to estimate the density evolution. If the density declines very steeply, this assumption can be very crude and SNe IIn from very steep CSM may not end up with recombining SNRs. Nonetheless, as explosions of RSGs (SNe II) occurs much more frequently than SNe IIn (e.g., Li et al. 2011b), the major progenitors of recombining SNRs are likely to be RSGs.

6.2.1.3 White Dwarfs

Although most of the recombining SNRs currently discovered are likely to originate from core-collapse SNe (e.g., Yamaguchi et al. 2012), SNe Ia can also evolve to recombining SNRs although it is expected to be quite rare. SNe Ia are explosions of white dwarfs. As discussed in Chapter 1, there are two major suggested paths for white dwarfs to explode: single degenerate (SD) channel (e.g., Nomoto 1982) and double degenerate (DD) channel (e.g., Iben & Tutukov 1984). In the SD scenario, a white dwarf is in a binary system with a main-sequence star and the mass of the companion accretes to the white dwarf. The white dwarf explodes when its mass gets close to the Chandrasekhar mass limit. On the other hand, the DD scenario suggests that SNe Ia are caused by the merger of two white dwarfs in a binary system. The main channel of SNe Ia is still unknown (see Chapter 1 for details).

In the SD scenario, the exploding white dwarf is surrounded by the accreting materials with a typical rate of $\sim 10^{-7}$ $M_\odot$ yr^{-1} (Nomoto 1982) but the rate is presumed to be too small to make the recombining SNR. Mass loss from the companion star can also make CSM around the progenitor but the companion is likely to be a less evolved red giant with too small mass-loss rates to establish CIE ($\sim 10^{-7}$ $M_\odot$ yr^{-1} or less, e.g., Hachisu et al. 1999). However, there are rare ways to make the mass-loss rate of the system high during the binary evolution (Hachisu et al. 2008) and some SNe Ia are actually suggested to be a hybrid of Type Ia and Type IIn, i.e., SNe Ia exploded in a CSM as dense as those discussed in Section 6.2.1.2 (Silverman et al. 2013). Thus, it is possible that a SN Ia from the SD scenario evolve to a recombining SNR but the number is expected to be very small.

In the DD scenario, we do not expect the CSM from the progenitor system because two binary stars are white dwarfs. However, stripped materials at the time of the merger are suggested to remain when the merged white dwarf explodes (Fryer et al. 2010). These materials are quite dense ($n_{\rm ecsm} > 10^{18}$ cm^{-3} within $r = R_\odot$, see Figure 5 of Fryer et al. 2010) and SNe Ia exploded in such environment can reach CIE and may end up with recombining SNRs. However, such a dense envelope is not obtained in a similar DD simulation of Pakmor et al. 2012. The fact that we do not see recombining SNRs of SNe Ia may already suggest that the model obtained by Fryer et al. 2010 is not the major path to be a SN Ia. Because of the uncertainty in the theoretical prediction of SNe Ia from the DD scenario, we

still cannot exclude the possibility that SNe Ia from the DD scenario can be recombining SNRs.

To sum up, although all the recombining SNRs currently discovered are likely from core-collapse SNe, SNe Ia from both the SD and DD channels have possibility to become recombining SNRs. When the detailed theoretical predictions are fixed, like the existence of the dense envelope in the DD channel, recombining SNRs may be able to be a probe to indicate the progenitor system of SNe Ia.

6.3 Other Possible Remnants from SNe Interacting with Dense CSM

6.3.1 [Fe II]-Bright SNRs

Fe^+ is easily ionized at the post shock region of SNRs and SNRs are a strong [Fe II] emitter (see, e.g., Koo 2013 for a short recent review). There are two kinds of [Fe II]-bright SNRs. One is middle-aged SNRs and the other is young SNRs. The former SNRs become [Fe II]-bright because of the interaction between the SN ejecta and ISM or interstellar clouds. The latter SNRs are supposed to get [Fe II]-bright earlier than the former SNRs because of the existence of the dense CSM around the SN. Indeed, some of recombining SNRs we discussed in the previous section are also known to be [Fe II]-bright SNRs (e.g., W49B).

6.3.2 Crab Nebula (SN 1054)

Crab Nebula (M1) is related to the 'guest star' of the year 1054 which is recorded in the ancient Chinese documents (see Stephenson & Green 2002 for a summary of the records) in 1920s (Lundmark 1921, Hubble 1928). As Crab Nebula has a compact remnant at its center, SN 1054 is known to be a core-collapse SN. Especially, SN 1054 is related to an ECSN because of the relatively low estimated ejecta mass and explosion energy (e.g., Hester 2008, Sollerman et al. 2000, Davidson et al. 1982, Nomoto et al. 1982). Smith 2013, Collins et al. 1999 estimated the LC of SN 1054 based on the ancient Chinese record. The estimated LC is found to be much brighter than the LCs expected from ECSNe (e.g., Kitaura et al. 2006). In addition, the region which is bright and we observe today is too small to be from an explosion in 1054 and it is suggested that the observed region just corresponds to the region inside the contact discontinuity (Chevalier 1977). Smith 2013 suggests that these two puzzles can be solved if Crab Nebula is a remnant of SN interacting with dense CSM. If the dense CSM surrounds the SN ejecta from an ECSN, its luminosity can be higher. Also, the location of the forward shock can be similar to that of the contact discontinuity because of the radiative cooling caused by the CSM interaction. Indeed, the estimated LC is shown to be similar to some SNe IIn which indicate the existence of the CSM interaction (Smith 2013).

However, as shown in Section 5.2 (Figure 5.1), even if we consider the mass-loss rate of the model super-AGB stars which end up with ECSNe, the model LC peak luminosity is far beyond the expected LC peak luminosity of SN 1054 ($\simeq -18$ mag). This means that the mass-loss rate of super-AGB star which is higher than those of other SN progenitors is

not enough to explain the luminosity of SN 1054. If SN 1054 is actually an ECSN, this may indicate that super-AGB stars which end up with ECSNe have some episodes with unexpected high mass-loss rates due to, e.g., Ne flash of the degenerated core (Smith 2013, Arnett 1974, Hillebrandt 1982, Weaver & Woosley 1979).

6.4 Summary

We have investigated possible SNRs resulting from SNe interacting with dense CSM. We have focused on recombining SNRs and discussed possible progenitors of them. If a CSM which is dense enough to establish CIE in the early epochs of the SNR evolution exists around a progenitor, the plasma in the shocked CSM can be overionized and the SNR can become a recombining SNR. RSGs, especially massive ones as discussed in Section 5.3, and SN IIn progenitors can have the CSM which is dense enough to establish CIE at the early stage of their explosions and can evolve to recombining SNRs. As explosions of RSGs (SNe II) occurs much more frequently than SNe IIn, the major progenitors of recombining SNRs are likely to be RSGs.

WR stars and white dwarfs are difficult to make recombining SNRs with their standard mass-loss histories but they are suggested to have mechanisms to enhance their mass-loss rates and they can be recombining SNRs if such mechanisms enhance their mass-loss rates. However, these mechanisms are presumed to work on a small fraction of these stars and such progenitors are expected to be a minor way to have recombining SNRs.

There are other SNRs which may be related to SNe interacting with dense CSM. One is [Fe II]-bright young SNRs. SN ejecta need to collide to CSM or ISM to excite [Fe II] and high [Fe II] brightness in young SNRs are likely due to the existence of dense CSM. Crab Nebula is recently suggested to have had been affected by the dense CSM and may indicate some super-AGB stars experience extensive mass loss shortly before they explode as ECSNe.

This chapter is based on
T.J. Moriya,
The Astrophysical Journal Letters, 750, L13, 2012

No one but a theorist believes his theory; everyone puts faith in a laboratory result but the experimenter himself.

Albert Einstein (1879 - 1955)

7 Conclusion

7.1 Summary

We have studied SNe interacting with CSM from both SN observational and stellar evolution theoretical points of view. We mainly focused on SNe whose major luminosity source is kinetic energy of SN ejecta. If CSM are dense enough, SN ejecta is decelerated by the CSM and its kinetic energy is efficiently converted to radiation energy. Hence, SNe can be powered by dense CSM surrounding them. The dense CSM are created by their progenitors' mass loss immediately prior to their explosions. By studying these SNe, mass loss of massive exploding stars shortly before their explosions has been revealed.

We started our study from the observational point of view. We developed an analytic bolometric LC model whose power source is kinetic energy of SN ejecta. This model can be applied to SNe whose major power source is the kinetic energy but their dense CSM are optically thin. We applied our bolometric LC model to observed bolometric LCs of SNe IIn which clearly show the signatures of the dense CSM in their spectra. We found that the mass-loss rates of SNe IIn we modeled exceed $10^{-3}\ M_{\odot}\ \mathrm{yr}^{-1}$, which is far beyond the mass-loss rates which can be achieved by the standard line-driven mass-loss mechanism and there should be other mechanisms to enhance the mass-loss rates of SN IIn progenitors shortly before their explosions. We also found that mass loss of SN IIn progenitors shortly before their explosions is generally non-steady. Surprisingly, their mass-loss rates generally seem to increase as the progenitors get closer to the time of their explosions. Thus, the mass-loss mechanisms related to SN IIn progenitors may somehow be related to the evolution toward their core collapse. However, it is still possible that a mass-loss mechanism whose mass-loss rates increase with time happens to be activated in some SN progenitors shortly before their explosions. The number of SNe IIn which we can model and get information of their CSM is still limited and we need to have more observational samples to know the mass-loss mechanisms involved better.

We also investigated the observational properties of SLSNe in the context of the interaction between SN ejecta and dense CSM. Most of SLSNe are SNe IIn and have signatures of dense CSM in their spectra. Thus, SLSNe are presumed to be very bright because of the existence of very dense CSM which decelerate SN ejecta very efficiently. Indeed, the CSM should be optically thick to explain the huge luminosities of SLSNe by the interaction and the analytic bolometric LC model we developed cannot be used to model SLSN LCs. In addition, the dense CSM are suggested to be optically thick enough to cause the shock breakout within them. We have shown that the ratio of the diffusion timescale and the shock propagation timescale of a dense CSM in which the shock breakout occurs depends on the density slope of the dense CSM. This diversity of the ratio of the two timescales caused by the CSM density slope can explain the existence of the two kinds of SLSN II, namely, Type IIn and Type IIL. If the shock propagation timescale is much longer than the diffusion timescale, which is expected when the CSM density slope is very steep, there remains the unshocked CSM after the diffusion timescale and the corresponding SLSNe can be observed as SNe IIn. On the contrary, if the two timescales are comparable, which is expected when the CSM density slope is flat, the entire CSM is shocked with the diffusion timescale and the corresponding SLSNe can be observed as SNe IIL. Thus, the existence of the two spectral types in SLSN II also indicates that various non-steady mass loss occurs shortly before the explosions of some massive stars.

Based on the shock breakout model we developed to interpret the observed properties of SLSNe, we estimated the dense CSM properties of SLSN 2006gy (Type IIn). To confirm that the estimated CSM properties can actually explain the observed properties of SN 2006gy, we performed numerical modeling of the LCs powered by the interaction with a numerical one-dimensional multigroup radiation hydrodynamics code `STELLA`. We found that the CSM properties estimated by the shock breakout model can reproduce the observed LC of SN 2006gy. Through the numerical modeling, we found that CSM from the steady mass loss are difficult to explain SN 2006gy and the mass loss of the progenitor shortly before the explosion should be non-steady. In addition, the mass-loss rate is estimated to exceed 0.1 $M_\odot$ yr^{-1}. The only known stars which can experience mass loss with such huge mass-loss rates are LBVs. However, LBVs are not considered to be SN progenitors and the progenitor of SN 2006gy remains to be a mystery. Moreover, the estimated SN ejecta kinetic energy is 10^{52} erg and is much higher than the normal SN ejecta kinetic energy ($\simeq 10^{51}$ erg).

The power sources and progenitors of SLSNe without any features of H in their spectra were also discussed. SLSN R has LCs whose decline rates are consistent with the ^{56}Co decay timescale and they are presumed to be powered by large amount of ^{56}Ni produced at their explosions. However, the required amount of ^{56}Ni to explain the huge luminosities is more than 5 $M_\odot$ and this amount of ^{56}Ni is difficult to be produced by normal SNe. Thus, it has been suggested that PISNe are progenitors of SLSN R but we showed that an energetic core-collapse SN of a massive star can also make the required amount of ^{56}Ni and SLSN R does not necessarily come from PISNe. SLSN I has not shown any features of its luminosity source in their observations but we find that the short-time luminosity decline observed between the precursor and the main LC of SLSN I 2006oz strongly indicates the existence of the dense CSM. Hence, we suggest that SLSN I is also powered by the interaction between SN ejecta and dense C+O CSM. However, the required mass-loss rate exceeds 0.1 $M_\odot$ yr^{-1} again and

no WR stars are known to have such mass loss either observationally nor theoretically.

So far, we have interpreted the observations of SNe interacting with CSM and estimated the CSM properties and mass loss of their progenitors. We have found that the estimated mass-loss properties are difficult to be explained by the current stellar evolutionary model. However, there do exist theoretical SN progenitor models which are suggested to have high mass-loss rates shortly before their explosions. Starting from the stellar evolutionary point of view, we investigated the expected observational properties of such SNe theoretically suggested to explode within dense CSM. We explored three kinds of such SN progenitor models, namely, super-AGB stars, massive RSGs, and LBVs.

ECSNe are suggested to explode within super-AGB winds but the theoretical modeling of super-AGB stars is challenging and there are few established models of ECSN progenitors followed with the super-AGB evolution. We used canonical mass-loss properties of super-AGB stars and obtained LCs assuming that an ECSN explode in the CSM. We found that there are no observed SNe which have similar LCs to those we obtained and our LCs are different from the SNe whose progenitors are suggested to be super-AGB stars (e.g., SN 2008S and NGC 300-OT).

Massive RSGs have several suggested mechanisms to enhance their mass-loss rates. If the suggested mass-loss enhancement occurs shortly before their explosions, massive RSGs are expected to explode within dense CSM. We numerically modeled LCs of SNe from RSGs exploded within dense CSM. We found that the UV luminosity of the corresponding SNe can be high at the same time when the optical luminosity is high in the early epochs before their plateau phase while usual SNe from RSGs become bright in optical after the UV luminosity declines. This property is observed in SN 2009kf and we suggested that SN 2009kf is from a massive RSG which experienced the mass-loss enhancement shortly before its explosion. We also predicted that the SNe of this kind will show the spectral transition from Type IIn to Type IIP, which may have been already observed in SN 1987C and SN 2007pk.

LBVs have not been considered to be SN progenitors but recent stellar evolution modeling starts to find possible SN progenitors with LBV spectra. We constructed the CSM of recently reported LBV SN progenitors. Although we found that the mass-loss rates of the LBV progenitors recently reported are not high enough to be SNe IIn, one of them experiences short-term mass-loss rate variations shortly before its explosion because of the bistability. We found that they can explain the episodic SN radio LC modulations observed in some SNe IIb. As SNe from the LBV progenitors recently reported are likely to be SNe IIb because of their surface composition, these newly found LBV SN progenitors were found to provide a theoretical explanation for the mysterious episodic radio LC modulations.

Finally, we discussed the possible remnants of SNe exploded within dense CSM. Recombining SNRs have been suggested to come from SNe exploded within dense CSM. We studied what kind of SN progenitors can have CSM which are dense enough to be recombining SNRs. We found that massive RSGs and SN IIn progenitors are the major progenitors of recombining SNRs.

7.2 Concluding Remarks

A decade ago, when the number of SN progenitors observed in their pre-explosion images was still small, the theoretical understanding of the stellar evolution was considered to be well-established. However, the emerging observed SN progenitors are challenging to it. Many discrepancies found in the observed and predicted SN progenitors seem to come from our lack of understanding in the mass loss of massive stars. Here in this dissertation, we have investigated the properties of the extreme mass loss which occurs within decades to centuries before their explosions. This kind of mass loss is not taken into account in the standard stellar evolution theory but the existence of it is now clear and it is playing an important role in determining the fates of some massive stars.

We started to catch some properties of such mass loss in this dissertation from SN studies but there are still many unsolved problems which must be studied. One of them is the effect of multidimensionality. We assumed the spherical symmetry of CSM and SNe in modeling LCs in this dissertation. However, just by looking the pictures of η Carinae, which is suggested to be a possible SN IIn progenitor, the existence of the multidimensionality in CSM is clear. In addition, SNe exploding inside can also have multidimensional structures. We need to study how the multidimensional effect changes the LC and mass-loss properties we obtained assuming the spherical symmetry. For this purpose, the development of a numerical multidimensional radiation hydrodynamics code is required. The formation processes of the complicated spectra from the interaction are also still not understood and studied well. We need to develop a theoretical framework to interpret the spectral properties of SNe interacting with CSM.

Of course, to fully understand the extreme mass loss occurring shortly before explosions of massive stars, we need to find out what is missing in the current stellar evolution theory. Especially, the mechanisms of the mass loss of this kind are mystery. The required mass-loss rates to explain the observed properties of SNe interacting with CSM are beyond the rates which can be achieved by the current standard mass-loss mechanisms. What is more puzzling in this kind of mass loss is that it seems to be linked to the time of the explosions of massive stars. Whether some kind of mass loss occurs shortly before the explosions accidentally or there exist some mass-loss mechanisms which are activated when massive stars evolve toward their deaths is unclear. One important missing key in the current stellar evolution theory may also exist in a lack of the multidimensional effects in it. The current stellar evolution theory treat multidimensional effects approximately in one-dimensional stellar evolution codes. However, many important multidimensional effects like rotations or chaotic multidimensional motions caused by multidimensional instabilities are killed in such treatments. Multidimensional motions occurring at the center of the stars shortly before their explosions may be linked to the extreme mass loss we found. As was found in the modeling of core-collapse SN explosions, the multidimensional effects are very likely to turn out to be an essential ingredient.

We have considered the mass loss in the context of the single stellar evolution so far. However, the binary evolution can also be an important missing key in the mass-loss enhancement. The major fraction of massive stars is known to be in a binary system. A massive star known to have had the extreme mass loss, η Carinae, is known to be in a binary system. Although

the mass loss enhancement due to the binary evolution does not necessarily occur shortly before the explosion of a star, it may accidentally happen shortly before the explosion in some cases.

Understanding the evolution and fates of stars is one of the most fundamental goals in astronomy. Especially, understanding those of massive stars which are eventually expected to explode is essential in understanding the evolution of the Universe as a whole. Explosions of stars provide large amount of energy and elements based on which the Universe is enriched. In addition, thanks to the huge luminosities of SNe, we can observe them even if they appear at very high redshifts and SNe can be probes of many properties of the early Universe. To use them as probes, understanding SNe themselves is a must. As we have seen in this dissertation, understanding the mass loss occurring exactly prior to the explosions of the massive stars is inevitable in understanding the evolution and fates of them and we need further efforts to unveil it.

Bibliography

[Abel et al. 2000] T. Abel, G. L. Bryan and M. L. Norman. *The Formation and Fragmentation of Primordial Molecular Clouds.* The Astrophysical Journal, vol. 540, page 39, September 2000.

[Agnoletto et al. 2009] I. Agnoletto, S. Benetti, E. Cappellaro, L. Zampieri, M. Turatto, P. Mazzali, A. Pastorello, M. Della Valle, F. Bufano, A. Harutyunyan, H. Navasardyan, N. Elias-Rosa, S. Taubenberger, S. Spiro and S. Valenti. *SN 2006gy: Was it Really Extraordinary?* The Astrophysical Journal, vol. 691, page 1348, February 2009.

[Akiyama et al. 2003] S. Akiyama, J. C. Wheeler, D. L. Meier and I. Lichtenstadt. *The Magnetorotational Instability in Core-Collapse Supernova Explosions.* The Astrophysical Journal, vol. 584, page 954, February 2003.

[Anderson et al. 2012] J. P. Anderson, S. M. Habergham, P. A. James and M. Hamuy. *Progenitor mass constraints for core-collapse supernovae from correlations with host galaxy star formation.* Monthly Notices of the Royal Astronomical Society, vol. 424, page 1372, August 2012.

[Andrews et al. 2010] J. E. Andrews, J. S. Gallagher, G. C. Clayton, B. E. K. Sugerman, J. P. Chatelain, J. Clem, D. L. Welch, M. J. Barlow, B. Ercolano, J. Fabbri, R. Wesson and M. Meixner. *SN 2007od: A Type IIP Supernova with Circumstellar Interaction.* The Astrophysical Journal, vol. 715, page 541, May 2010.

[Andrews et al. 2011] J. E. Andrews, G. C. Clayton, R. Wesson, B. E. K. Sugerman, M. J. Barlow, J. Clem, B. Ercolano, J. Fabbri, J. S. Gallagher, A. Landolt, M. Meixner, M. Otsuka, D. Riebel and D. L. Welch. *Evidence for Pre-existing Dust in the Bright Type IIn SN 2010jl.* The Astronomical Journal, vol. 142, page 45, August 2011.

[Arcavi et al. 2010] I. Arcavi, A. Gal-Yam, M. M. Kasliwal, R. M. Quimby, E. O. Ofek, S. R. Kulkarni, P. E. Nugent, S. B. Cenko, J. S. Bloom, M. Sullivan, D. A. Howell, D. Poznanski, A. V. Filippenko, N. Law, I. Hook, J. Jönsson, S. Blake, J. Cooke, R. Dekany, G. Rahmer, D. Hale, R. Smith, J. Zolkower, V. Velur, R. Walters, J. Henning, K. Bui, D. McKenna and J. Jacobsen. *Core-collapse Supernovae from the Palomar Transient Factory: Indications for a Different Population in Dwarf Galaxies.* The Astrophysical Journal, vol. 721, page 777, September 2010.

[Aretxaga et al. 1999] I. Aretxaga, S. Benetti, R. J. Terlevich, A. C. Fabian, E. Cappellaro, M. Turatto and M. della Valle. *SN 1988Z: spectro-photometric catalogue and energy*

estimates. Monthly Notices of the Royal Astronomical Society, vol. 309, page 343, October 1999.

[Argo et al. 2007] M. K. Argo, R. J. Beswick, T. W. B. Muxlow and A. Pedlar. *Radio observations of SN 2006gy with MERLIN.* The Astronomer's Telegram, vol. 1084, page 1, May 2007.

[Arnett & Meakin 2011] W. D. Arnett and C. Meakin. *Turbulent Cells in Stars: Fluctuations in Kinetic Energy and Luminosity.* The Astrophysical Journal, vol. 741, page 33, November 2011.

[Arnett 1974] W. D. Arnett. *Advanced evolution of massive stars. V - Neon burning.* The Astrophysical Journal, vol. 193, page 169, October 1974.

[Arnett 1980] W. D. Arnett. *Analytic solutions for light curves of supernovae of Type II.* The Astrophysical Journal, vol. 237, page 541, April 1980.

[Arnett 1982] W. D. Arnett. *Type I supernovae. I - Analytic solutions for the early part of the light curve.* The Astrophysical Journal, vol. 253, page 785, February 1982.

[Asplund et al. 2009] M. Asplund, N. Grevesse, A. J. Sauval and P. Scott. *The Chemical Composition of the Sun.* Annual Review of Astronomy and Astrophysics, vol. 47, page 481, September 2009.

[Axelrod 1980] T. S. Axelrod. *Late time optical spectra from the Ni-56 model for Type 1 supernovae.* PhD thesis, California Univ., Santa Cruz., July 1980.

[Baade & Zwicky 1934] W. Baade and F. Zwicky. *On Super-novae.* Proceedings of the National Academy of Science, vol. 20, page 254, May 1934.

[Baklanov et al. 2005] P. V. Baklanov, S. I. Blinnikov and N. N. Pavlyuk. *Parameters of the classical type-IIP supernova SN 1999em.* Astronomy Letters, vol. 31, page 429, July 2005.

[Balberg & Loeb 2011] S. Balberg and A. Loeb. *Supernova shock breakout through a wind.* Monthly Notices of the Royal Astronomical Society, vol. 414, page 1715, June 2011.

[Barbon et al. 1999] R. Barbon, V. Buondí, E. Cappellaro and M. Turatto. *The Asiago Supernova Catalogue - 10 years after.* Astronomy & Astrophysics Supplement Series, vol. 139, page 531, November 1999.

[Barkat et al. 1967] Z. Barkat, G. Rakavy and N. Sack. *Dynamics of Supernova Explosion Resulting from Pair Formation.* Physical Review Letters, vol. 18, page 379, March 1967.

[Basko 1985] M. M. Basko. *Metallic equation of state in the mean ion approximation.* High Temperature, vol. 23, page 388, November 1985.

[Benvenuto & Lugones 1999] O. G. Benvenuto and G. Lugones. *The phase transition from nuclear matter to quark matter during proto-neutron star evolution.* Monthly Notices of the Royal Astronomical Society, vol. 304, page L25, April 1999.

[Benvenuto et al. 2013] O. G. Benvenuto, M. C. Bersten and K. Nomoto. *A Binary Progenitor for the Type IIb Supernova 2011dh in M51.* The Astrophysical Journal, vol. 762, page 74, January 2013.

[Berger et al. 2012] E. Berger, R. Chornock, R. Lunnan, R. Foley, I. Czekala, A. Rest, C. Leibler, A. M. Soderberg, K. Roth, G. Narayan, M. E. Huber, D. Milisavljevic, N. E. Sanders, M. Drout, R. Margutti, R. P. Kirshner, G. H. Marion, P. J. Challis, A. G. Riess, S. J. Smartt, W. S. Burgett, K. W. Hodapp, J. N. Heasley, N. Kaiser, R.-P. Kudritzki, E. A. Magnier, M. McCrum, P. A. Price, K. Smith, J. L. Tonry and R. J. Wainscoat. *Ultraluminous Supernovae as a New Probe of the Interstellar Medium in Distant Galaxies.* The Astrophysical Journal Letters, vol. 755, page L29, August 2012.

[Bersten et al. 2011] M. C. Bersten, O. Benvenuto and M. Hamuy. *Hydrodynamical Models of Type II Plateau Supernovae.* The Astrophysical Journal, vol. 729, page 61, March 2011.

[Bessell 1990] M. S. Bessell. *UBVRI passbands.* Publications of the Astronomical Society of the Pacific, vol. 102, page 1181, October 1990.

[Bietenholz & Bartel 2007] M. Bietenholz and N. Bartel. *Radio non-detection of SN 2006gy with the VLA at 8.4 and 43 GHz.* The Astronomer's Telegram, vol. 1254, page 1, November 2007.

[Bietenholz & Bartel 2008a] M. Bietenholz and N. Bartel. *Continued Radio Non-Detection of SN 2006gy with the VLA at 8.4 and 43 GHz.* The Astronomer's Telegram, vol. 1525, page 1, May 2008.

[Bietenholz & Bartel 2008b] M. Bietenholz and N. Bartel. *Continued Radio Non-Detection of SN 2006gy with the VLA at 8.4 and 43 GHz.* The Astronomer's Telegram, vol. 1657, page 1, August 2008.

[Bisnovatyi-Kogan et al. 1976] G. S. Bisnovatyi-Kogan, I. P. Popov and A. A. Samokhin. *The magnetohydrodynamic rotational model of supernova explosion.* Astrophysics and Space Science, vol. 41, page 287, June 1976.

[Björnsson & Fransson 2004] C.-I. Björnsson and C. Fransson. *The X-Ray and Radio Emission from SN 2002ap: The Importance of Compton Scattering.* The Astrophysical Journal, vol. 605, page 823, April 2004.

[Blinnikov & Bartunov 1993] S. I. Blinnikov and O. S. Bartunov. *Non-Equilibrium Radiative Transfer in Supernova Theory - Models of Linear Type-II Supernovae.* Astronomy & Astrophysics, vol. 273, page 106, June 1993.

[Blinnikov & Sorokina 2010] S. I. Blinnikov and E. I. Sorokina. *Supernova Explosions inside Carbon-Oxygen Circumstellar Shells.* ArXiv e-prints, September 2010.

[Blinnikov & Tolstov 2011] S. I. Blinnikov and A. G. Tolstov. *Multigroup radiative transfer in supernova shock breakout models.* Astronomy Letters, vol. 37, page 194, March 2011.

[Blinnikov et al. 1998] S. I. Blinnikov, R. Eastman, O. S. Bartunov, V. A. Popolitov and S. E. Woosley. *A Comparative Modeling of Supernova 1993J.* The Astrophysical Journal, vol. 496, page 454, March 1998.

[Blinnikov et al. 2000] S. Blinnikov, P. Lundqvist, O. Bartunov, K. Nomoto and K. Iwamoto. *Radiation Hydrodynamics of SN 1987A. I. Global Analysis of the Light Curve for the First 4 Months.* The Astrophysical Journal, vol. 532, page 1132, April 2000.

[Blinnikov et al. 2006] S. I. Blinnikov, F. K. Röpke, E. I. Sorokina, M. Gieseler, M. Reinecke, C. Travaglio, W. Hillebrandt and M. Stritzinger. *Theoretical light curves for deflagration models of type Ia supernova.* Astronomy & Astrophysics, vol. 453, page 229, July 2006.

[Blinnikov et al. 2012] S. Blinnikov, M. Potashov, P. Baklanov and A. Dolgov. *Direct determination of the hubble parameter using type IIn supernovae.* Soviet Journal of Experimental and Theoretical Physics Letters, vol. 96, page 153, October 2012.

[Blondin et al. 2003] J. M. Blondin, A. Mezzacappa and C. DeMarino. *Stability of Standing Accretion Shocks, with an Eye toward Core-Collapse Supernovae.* The Astrophysical Journal, vol. 584, page 971, February 2003.

[Bond et al. 2009] H. E. Bond, L. R. Bedin, A. Z. Bonanos, R. M. Humphreys, L. A. G. B. Monard, J. L. Prieto and F. M. Walter. *The 2008 Luminous Optical Transient in the Nearby Galaxy NGC 300.* The Astrophysical Journal Letters, vol. 695, page L154, April 2009.

[Botticella et al. 2009] M. T. Botticella, A. Pastorello, S. J. Smartt, W. P. S. Meikle, S. Benetti, R. Kotak, E. Cappellaro, R. M. Crockett, S. Mattila, M. Sereno, F. Patat, D. Tsvetkov, J. T. van Loon, D. Abraham, I. Agnoletto, R. Arbour, C. Benn, G. di Rico, N. Elias-Rosa, D. L. Gorshanov, A. Harutyunyan, D. Hunter, V. Lorenzi, F. P. Keenan, K. Maguire, J. Mendez, M. Mobberley, H. Navasardyan, C. Ries, V. Stanishev, S. Taubenberger, C. Trundle, M. Turatto and I. M. Volkov. *SN 2008S: an electron-capture SN from a super-AGB progenitor?* Monthly Notices of the Royal Astronomical Society, vol. 398, page 1041, September 2009.

[Botticella et al. 2010] M. T. Botticella, C. Trundle, A. Pastorello, S. Rodney, A. Rest, S. Gezari, S. J. Smartt, G. Narayan, M. E. Huber, J. L. Tonry, D. Young, K. Smith, F. Bresolin, S. Valenti, R. Kotak, S. Mattila, E. Kankare, W. M. Wood-Vasey, A. Riess, J. D. Neill, K. Forster, D. C. Martin, C. W. Stubbs, W. S. Burgett, K. C. Chambers, T. Dombeck, H. Flewelling, T. Grav, J. N. Heasley, K. W. Hodapp, N. Kaiser, R. Kudritzki, G. Luppino, R. H. Lupton, E. A. Magnier, D. G. Monet, J. S.

Morgan, P. M. Onaka, P. A. Price, P. H. Rhoads, W. A. Siegmund, W. E. Sweeney, R. J. Wainscoat, C. Waters, M. F. Waterson and C. G. Wynn-Williams. *Supernova 2009kf: An Ultraviolet Bright Type IIP Supernova Discovered with Pan-STARRS 1 and GALEX.* The Astrophysical Journal Letters, vol. 717, page L52, July 2010.

[Boyer et al. 2010] M. L. Boyer, B. Sargent, J. T. van Loon, S. Srinivasan, G. C. Clayton, F. Kemper, L. J. Smith, M. Matsuura, P. M. Woods, M. Marengo, M. Meixner, C. Engelbracht, K. D. Gordon, S. Hony, R. Indebetouw, K. Misselt, K. Okumura, P. Panuzzo, D. Riebel, J. Roman-Duval, M. Sauvage and G. C. Sloan. *Cold dust in three massive evolved stars in the LMC.* Astronomy & Astrophysics, vol. 518, page L142, July 2010.

[Bromm et al. 1999] V. Bromm, P. S. Coppi and R. B. Larson. *Forming the First Stars in the Universe: The Fragmentation of Primordial Gas.* The Astrophysical Journal Letters, vol. 527, page L5, December 1999.

[Bromm 2013] V. Bromm. *Formation of the First Stars.* ArXiv e-prints, May 2013.

[Brown et al. 2009] P. J. Brown, S. T. Holland, S. Immler, P. Milne, P. W. A. Roming, N. Gehrels, J. Nousek, N. Panagia, M. Still and D. Vanden Berk. *Ultraviolet Light Curves of Supernovae with the Swift Ultraviolet/Optical Telescope.* The Astronomical Journal, vol. 137, page 4517, May 2009.

[Bruenn et al. 2013] S. W. Bruenn, A. Mezzacappa, W. R. Hix, E. J. Lentz, O. E. Bronson Messer, E. J. Lingerfelt, J. M. Blondin, E. Endeve, P. Marronetti and K. N. Yakunin. *Axisymmetric Ab Initio Core-collapse Supernova Simulations of 12-25 $M_{\odot}$ Stars.* The Astrophysical Journal Letters, vol. 767, page L6, April 2013.

[Buchler 1983] J. R. Buchler. *Radiation transfer in the fluid frame.* Journal of Quantitative Spectroscopy and Radiative Transfer, vol. 30, page 395, November 1983.

[Burrows et al. 2006] A. Burrows, E. Livne, L. Dessart, C. D. Ott and J. Murphy. *A New Mechanism for Core-Collapse Supernova Explosions.* The Astrophysical Journal, vol. 640, page 878, April 2006.

[Calzavara & Matzner 2004] A. J. Calzavara and C. D. Matzner. *Supernova properties from shock breakout X-rays.* Monthly Notices of the Royal Astronomical Society, vol. 351, page 694, June 2004.

[Cardelli et al. 1989] J. A. Cardelli, G. C. Clayton and J. S. Mathis. *The relationship between infrared, optical, and ultraviolet extinction.* The Astrophysical Journal, vol. 345, page 245, October 1989.

[Castor 1972] J. I. Castor. *Radiative Transfer in Spherically Symmetric Flows.* The Astrophysical Journal, vol. 178, page 779, December 1972.

[Castor 2004] J. I. Castor. Radiation Hydrodynamics. Cambridge University Press, 2004.

[Cayrel et al. 2004] R. Cayrel, E. Depagne, M. Spite, V. Hill, F. Spite, P. François, B. Plez, T. Beers, F. Primas, J. Andersen, B. Barbuy, P. Bonifacio, P. Molaro and B. Nordström. *First stars V - Abundance patterns from C to Zn and supernova yields in the early Galaxy.* Astronomy & Astrophysics, vol. 416, page 1117, March 2004.

[Chandra et al. 2007] P. Chandra, S. Chakraborti and A. Ray. *Radio non-detection of SN 2006gy with GMRT in the L-band.* The Astronomer's Telegram, vol. 1082, page 1, May 2007.

[Chandra et al. 2012a] P. Chandra, R. A. Chevalier, N. Chugai, C. Fransson, C. M. Irwin, A. M. Soderberg, S. Chakraborti and S. Immler. *Radio and X-Ray Observations of SN 2006jd: Another Strongly Interacting Type IIn Supernova.* The Astrophysical Journal, vol. 755, page 110, August 2012.

[Chandra et al. 2012b] P. Chandra, R. A. Chevalier, C. M. Irwin, N. Chugai, C. Fransson and A. M. Soderberg. *Strong Evolution of X-Ray Absorption in the Type IIn Supernova SN 2010jl.* The Astrophysical Journal Letters, vol. 750, page L2, May 2012.

[Chandrasekhar 1931] S. Chandrasekhar. *The Maximum Mass of Ideal White Dwarfs.* The Astrophysical Journal, vol. 74, page 81, July 1931.

[Chatzopoulos et al. 2012] E. Chatzopoulos, J. C. Wheeler and J. Vinko. *Generalized Semi-analytical Models of Supernova Light Curves.* The Astrophysical Journal, vol. 746, page 121, February 2012.

[Chen et al. 2013] T.-W. Chen, S. J. Smartt, F. Bresolin, A. Pastorello, R.-P. Kudritzki, R. Kotak, M. McCrum, M. Fraser and S. Valenti. *The Host Galaxy of the Super-luminous SN 2010gx and Limits on Explosive ^{56}Ni Production.* The Astrophysical Journal Letters, vol. 763, page L28, February 2013.

[Chevalier & Blondin 1995] R. Chevalier and J. M. Blondin. *Hydrodynamic instabilities in supernova remnants: Early radiative cooling.* The Astrophysical Journal, vol. 444, page 312, May 1995.

[Chevalier & Fransson 1994] R. A. Chevalier and C. Fransson. *Emission from circumstellar interaction in normal Type II supernovae.* The Astrophysical Journal, vol. 420, page 268, January 1994.

[Chevalier & Fransson 2003] R. A. Chevalier and C. Fransson. *Supernova Interaction with a Circumstellar Medium.* In K. Weiler, editeur, Supernovae and Gamma-Ray Bursters, volume 598 of *Lecture Notes in Physics, Berlin Springer Verlag*, page 171, 2003.

[Chevalier & Fransson 2006] R. A. Chevalier and C. Fransson. *Circumstellar Emission from Type Ib and Ic Supernovae.* The Astrophysical Journal, vol. 651, page 381, November 2006.

[Chevalier & Irwin 2011] R. A. Chevalier and C. M. Irwin. *Shock Breakout in Dense Mass Loss: Luminous Supernovae.* The Astrophysical Journal Letters, vol. 729, page L6, March 2011.

[Chevalier & Soker 1989] R. A. Chevalier and N. Soker. *Asymmetric envelope expansion of supernova 1987A.* The Astrophysical Journal, vol. 341, page 867, June 1989.

[Chevalier et al. 2006] R. A. Chevalier, C. Fransson and T. K. Nymark. *Radio and X-Ray Emission as Probes of Type IIP Supernovae and Red Supergiant Mass Loss.* The Astrophysical Journal, vol. 641, page 1029, April 2006.

[Chevalier 1977] R. A. Chevalier. *Was SN 1054 A Type II Supernova?* In D. N. Schramm, editeur, Supernovae, volume 66 of *Astrophysics and Space Science Library*, page 53, 1977.

[Chevalier 1982a] R. A. Chevalier. *Self-similar solutions for the interaction of stellar ejecta with an external medium.* The Astrophysical Journal, vol. 258, page 790, July 1982.

[Chevalier 1982b] R. A. Chevalier. *The radio and X-ray emission from type II supernovae.* The Astrophysical Journal, vol. 259, page 302, August 1982.

[Chevalier 1990] R. A. Chevalier. *Interaction of supernovae with circumstellar matter.* In A. G. Petschek, editeur, Supernovae, page 91, 1990.

[Chevalier 1998] R. A. Chevalier. *Synchrotron Self-Absorption in Radio Supernovae.* The Astrophysical Journal, vol. 499, page 810, May 1998.

[Chevalier 2012] R. A. Chevalier. *Common Envelope Evolution Leading to Supernovae with Dense Interaction.* The Astrophysical Journal Letters, vol. 752, page L2, June 2012.

[Chornock et al. 2013] R. Chornock, E. Berger, A. Rest, D. Milisavljevic, R. Lunnan, R. J. Foley, A. M. Soderberg, S. J. Smartt, A. J. Burgasser, P. Challis, L. Chomiuk, I. Czekala, M. Drout, W. Fong, M. E. Huber, R. P. Kirshner, C. Leibler, B. McLeod, G. H. Marion, G. Narayan, A. G. Riess, K. C. Roth, N. E. Sanders, D. Scolnic, K. Smith, C. W. Stubbs, J. L. Tonry, S. Valenti, W. S. Burgett, K. C. Chambers, K. W. Hodapp, N. Kaiser, R.-P. Kudritzki, E. A. Magnier and P. A. Price. *PS1-10afx at z = 1.388: Pan-STARRS1 Discovery of a New Type of Superluminous Supernova.* The Astrophysical Journal, vol. 767, page 162, April 2013.

[Chugai & Danziger 1994] N. N. Chugai and I. J. Danziger. *Supernova 1988Z - Low-Mass Ejecta Colliding with the Clumpy Wind.* Monthly Notices of the Royal Astronomical Society, vol. 268, page 173, May 1994.

[Chugai 2001] N. N. Chugai. *Broad emission lines from the opaque electron-scattering environment of SN 1998S.* Monthly Notices of the Royal Astronomical Society, vol. 326, page 1448, October 2001.

[Colella & Woodward 1984] P. Colella and P. R. Woodward. *The Piecewise Parabolic Method (PPM) for Gas-Dynamical Simulations.* Journal of Computational Physics, vol. 54, page 174, September 1984.

[Colgate & White 1966] S. A. Colgate and R. H. White. *The Hydrodynamic Behavior of Supernovae Explosions.* The Astrophysical Journal, vol. 143, page 626, March 1966.

[Colgate 1974] S. A. Colgate. *Early Gamma Rays from Supernovae.* The Astrophysical Journal, vol. 187, page 333, January 1974.

[Collins et al. 1999] G. W. Collins II, W. P. Claspy and J. C. Martin. *A Reinterpretation of Historical References to the Supernova of A.D. 1054.* Publications of the Astronomical Society of the Pacific, vol. 111, page 871, July 1999.

[Cooke et al. 2009] J. Cooke, M. Sullivan, E. J. Barton, J. S. Bullock, R. G. Carlberg, A. Gal-Yam and E. Tollerud. *Type IIn supernovae at redshift z˜2 from archival data.* Nature, vol. 460, page 237, July 2009.

[Cooke et al. 2012] J. Cooke, M. Sullivan, A. Gal-Yam, E. J. Barton, R. G. Carlberg, E. V. Ryan-Weber, C. Horst, Y. Omori and C. G. Díaz. *Superluminous supernovae at redshifts of 2.05 and 3.90.* Nature, vol. 491, page 228, November 2012.

[Cooke 2008] J. Cooke. *Detecting $z > 2$ Type IIn Supernovae.* The Astrophysical Journal, vol. 677, page 137, April 2008.

[Crowther 2007] P. A. Crowther. *Physical Properties of Wolf-Rayet Stars.* Annual Review of Astronomy and Astrophysics, vol. 45, page 177, September 2007.

[Davidson & Humphreys 1997] K. Davidson and R. M. Humphreys. *Eta Carinae and Its Environment.* Annual Review of Astronomy and Astrophysics, vol. 35, page 1, 1997.

[Davidson & Humphreys 2012] K. Davidson and R. M. Humphreys, editeurs. Eta Carinae and the Supernova Impostors, volume 384 of *Astrophysics and Space Science Library*, 2012.

[Davidson et al. 1982] K. Davidson, T. R. Gull, S. P. Maran, T. P. Stecher, R. A. Fesen, R. A. Parise, C. A. Harvel, M. Kafatos and V. L. Trimble. *The ultraviolet spectrum of the Crab Nebula.* The Astrophysical Journal, vol. 253, page 696, February 1982.

[de Jager et al. 1988] C. de Jager, H. Nieuwenhuijzen and K. A. van der Hucht. *Mass loss rates in the Hertzsprung-Russell diagram.* Astronomy & Astrophysics Supplement Series, vol. 72, page 259, February 1988.

[Deng et al. 2005] J. Deng, N. Tominaga, P. A. Mazzali, K. Maeda and K. Nomoto. *On the Light Curve and Spectrum of SN 2003dh Separated from the Optical Afterglow of GRB 030329.* The Astrophysical Journal, vol. 624, page 898, May 2005.

[Dessart & Hillier 2010] L. Dessart and D. J. Hillier. *Non-LTE time-dependent spectroscopic modelling of Type II-plateau supernovae from the photospheric to the nebular phase: case study for 15 and 25 $M_{\odot}$ progenitor stars.* Monthly Notices of the Royal Astronomical Society, page 1716, November 2010.

[Dessart et al. 2009] L. Dessart, D. J. Hillier, S. Gezari, S. Basa and T. Matheson. *SN 1994W: an interacting supernova or two interacting shells?* Monthly Notices of the Royal Astronomical Society, vol. 394, page 21, March 2009.

[Dessart et al. 2010a] L. Dessart, E. Livne and R. Waldman. *Determining the main-sequence mass of Type II supernova progenitors.* Monthly Notices of the Royal Astronomical Society, vol. 408, page 827, October 2010.

[Dessart et al. 2010b] L. Dessart, E. Livne and R. Waldman. *Shock-heating of stellar envelopes: a possible common mechanism at the origin of explosions and eruptions in massive stars.* Monthly Notices of the Royal Astronomical Society, vol. 405, page 2113, July 2010.

[Dessart et al. 2012] L. Dessart, D. J. Hillier, R. Waldman, E. Livne and S. Blondin. *Superluminous supernovae: ^{56}Ni power versus magnetar radiation.* Monthly Notices of the Royal Astronomical Society, vol. 426, page L76, October 2012.

[Dessart et al. 2013] L. Dessart, R. Waldman, E. Livne, D. J. Hillier and S. Blondin. *Radiative properties of pair-instability supernova explosions.* Monthly Notices of the Royal Astronomical Society, vol. 428, page 3227, February 2013.

[Dexter & Kasen 2012] J. Dexter and D. Kasen. *Supernova Light Curves Powered by Fallback Accretion.* ArXiv e-prints, October 2012.

[Dilday et al. 2012] B. Dilday, D. A. Howell, S. B. Cenko, J. M. Silverman, P. E. Nugent, M. Sullivan, S. Ben-Ami, L. Bildsten, M. Bolte, M. Endl, A. V. Filippenko, O. Gnat, A. Horesh, E. Hsiao, M. M. Kasliwal, D. Kirkman, K. Maguire, G. W. Marcy, K. Moore, Y. Pan, J. T. Parrent, P. Podsiadlowski, R. M. Quimby, A. Sternberg, N. Suzuki, D. R. Tytler, D. Xu, J. S. Bloom, A. Gal-Yam, I. M. Hook, S. R. Kulkarni, N. M. Law, E. O. Ofek, D. Polishook and D. Poznanski. *PTF 11kx: A Type Ia Supernova with a Symbiotic Nova Progenitor.* Science, vol. 337, page 942, August 2012.

[Drake et al. 2011] A. J. Drake, S. G. Djorgovski, A. Mahabal, J. Anderson, R. Roy, V. Mohan, S. Ravindranath, D. Frail, S. Gezari, J. D. Neill, L. C. Ho, J. L. Prieto, D. Thompson, J. Thorstensen, M. Wagner, R. Kowalski, J. Chiang, J. E. Grove, F. K. Schinzel, D. L. Wood, L. Carrasco, E. Recillas, L. Kewley, K. N. Archana, A. Basu, Y. Wadadekar, B. Kumar, A. D. Myers, E. S. Phinney, R. Williams, M. J. Graham, M. Catelan, E. Beshore, S. Larson and E. Christensen. *The Discovery and Nature of the Optical Transient CSS100217:102913+404220.* The Astrophysical Journal, vol. 735, page 106, July 2011.

[Dwarkadas & Gruszko 2012] V. V. Dwarkadas and J. Gruszko. *What are published X-ray light curves telling us about young supernova expansion?* Monthly Notices of the Royal Astronomical Society, vol. 419, page 1515, January 2012.

[Dwarkadas 2005] V. V. Dwarkadas. *The Evolution of Supernovae in Circumstellar Wind-Blown Bubbles. I. Introduction and One-Dimensional Calculations.* The Astrophysical Journal, vol. 630, page 892, September 2005.

[Dwarkadas 2007] V. V. Dwarkadas. *The Evolution of Supernovae in Circumstellar Wind Bubbles. II. Case of a Wolf-Rayet Star.* The Astrophysical Journal, vol. 667, page 226, September 2007.

[Dwarkadas 2011] V. V. Dwarkadas. *On luminous blue variables as the progenitors of core-collapse supernovae, especially Type IIn supernovae.* Monthly Notices of the Royal Astronomical Society, vol. 412, page 1639, April 2011.

[Eastman & Pinto 1993] R. G. Eastman and P. A. Pinto. *Spectrum formation in supernovae - Numerical techniques.* The Astrophysical Journal, vol. 412, page 731, August 1993.

[Ekström et al. 2012] S. Ekström, C. Georgy, P. Eggenberger, G. Meynet, N. Mowlavi, A. Wyttenbach, A. Granada, T. Decressin, R. Hirschi, U. Frischknecht, C. Charbonnel and A. Maeder. *Grids of stellar models with rotation. I. Models from 0.8 to 120 $M_{\odot}$ at solar metallicity (Z = 0.014).* Astronomy & Astrophysics, vol. 537, page A146, January 2012.

[Eldridge & Tout 2004] J. J. Eldridge and C. A. Tout. *The progenitors of core-collapse supernovae.* Monthly Notices of the Royal Astronomical Society, vol. 353, page 87, September 2004.

[Elias-Rosa et al. 2010] N. Elias-Rosa, S. D. Van Dyk, W. Li, A. A. Miller, J. M. Silverman, M. Ganeshalingam, A. F. Boden, M. M. Kasliwal, J. Vinkó, J.-C. Cuillandre, A. V. Filippenko, T. N. Steele, J. S. Bloom, C. V. Griffith, I. K. W. Kleiser and R. J. Foley. *The Massive Progenitor of the Type II-linear Supernova 2009kr.* The Astrophysical Journal Letters, vol. 714, page L254, May 2010.

[Ensman & Burrows 1992] L. Ensman and A. Burrows. *Shock breakout in SN 1987A.* The Astrophysical Journal, vol. 393, page 742, July 1992.

[Falk & Arnett 1973] S. W. Falk and W. D. Arnett. *A Theoretical Model for Type II Supernovae.* The Astrophysical Journal Letters, vol. 180, page L65, March 1973.

[Falk & Arnett 1977] S. W. Falk and W. D. Arnett. *Radiation Dynamics, Envelope Ejection, and Supernova Light Curves.* The Astrophysical Journal Supplement Series, vol. 33, page 515, April 1977.

[Feautrier 1964] P. Feautrier. *Sur la resolution numerique de l'equation de transfert.* Comptes Rendus Academie des Sciences (serie non specifiee), vol. 258, page 3189, 1964.

[Filippenko 1997] A. V. Filippenko. *Optical Spectra of Supernovae.* Annual Review of Astronomy and Astrophysics, vol. 35, page 309, 1997.

[Fischer et al. 2010] T. Fischer, I. Sagert, G. Pagliara, M. Hempel, J. Schaffner-Bielich, T. Rauscher, F. -. Thielemann, R. Käppeli, G. Martínez-Pinedo and M. Liebendörfer. *The revival of an explosion mechanism of massive stars - the quark hadron phase transition during the early post bounce phase of core collapse supernovae.* ArXiv e-prints, November 2010.

[Foglizzo et al. 2012] T. Foglizzo, F. Masset, J. Guilet and G. Durand. *Shallow Water Analogue of the Standing Accretion Shock Instability: Experimental Demonstration and a Two-Dimensional Model.* Physical Review Letters, vol. 108, no. 5, page 051103, February 2012.

[Foley et al. 2007] R. J. Foley, N. Smith, M. Ganeshalingam, W. Li, R. Chornock and A. V. Filippenko. *SN 2006jc: A Wolf-Rayet Star Exploding in a Dense He-rich Circumstellar Medium.* The Astrophysical Journal Letters, vol. 657, page L105, March 2007.

[Foley et al. 2011] R. J. Foley, E. Berger, O. Fox, E. M. Levesque, P. J. Challis, I. I. Ivans, J. E. Rhoads and A. M. Soderberg. *The Diversity of Massive Star Outbursts. I. Observations of SN2009ip, UGC 2773 OT2009-1, and Their Progenitors.* The Astrophysical Journal, vol. 732, page 32, May 2011.

[Fox et al. 2009] O. Fox, M. F. Skrutskie, R. A. Chevalier, S. Kanneganti, C. Park, J. Wilson, M. Nelson, J. Amirhadji, D. Crump, A. Hoeft, S. Provence, B. Sargeant, J. Sop, M. Tea, S. Thomas and K. Woolard. *Near-Infrared Photometry of the Type IIn SN 2005ip: The Case for Dust Condensation.* The Astrophysical Journal, vol. 691, page 650, January 2009.

[Fox et al. 2010] O. D. Fox, R. A. Chevalier, E. Dwek, M. F. Skrutskie, B. E. K. Sugerman and J. M. Leisenring. *Disentangling the Origin and Heating Mechanism of Supernova Dust: Late-time Spitzer Spectroscopy of the Type IIn SN 2005ip.* The Astrophysical Journal, vol. 725, page 1768, December 2010.

[Fox et al. 2011] O. D. Fox, R. A. Chevalier, M. F. Skrutskie, A. M. Soderberg, A. V. Filippenko, M. Ganeshalingam, J. M. Silverman, N. Smith and T. N. Steele. *A Spitzer Survey for Dust in Type IIn Supernovae.* The Astrophysical Journal, vol. 741, page 7, November 2011.

[Fox et al. 2013] O. D. Fox, A. V. Filippenko, M. F. Skrutskie, J. M. Silverman, M. Ganeshalingam, S. B. Cenko and K. I. Clubb. *Late-Time Circumstellar Interaction in a Spitzer Selected Sample of Type IIn Supernovae.* ArXiv e-prints, March 2013.

[Fransson & Björnsson 1998] C. Fransson and C.-I. Björnsson. *Radio Emission and Particle Acceleration in SN 1993J.* The Astrophysical Journal, vol. 509, page 861, December 1998.

[Fransson et al. 1996] C. Fransson, P. Lundqvist and R. A. Chevalier. *Circumstellar Interaction in SN 1993J.* The Astrophysical Journal, vol. 461, page 993, April 1996.

[Fraser et al. 2010] M. Fraser, K. Takáts, A. Pastorello, S. J. Smartt, S. Mattila, M.-T. Botticella, S. Valenti, M. Ergon, J. Sollerman, I. Arcavi, S. Benetti, F. Bufano, R. M. Crockett, I. J. Danziger, A. Gal-Yam, J. R. Maund, S. Taubenberger and M. Turatto. *On the Progenitor and Early Evolution of the Type II Supernova 2009kr.* The Astrophysical Journal Letters, vol. 714, page L280, May 2010.

[Fraser et al. 2013] M. Fraser, C. Inserra, A. Jerkstrand, R. Kotak, G. Pignata, S. Benetti, M.-T. Botticella, F. Bufano, M. Childress, S. Mattila, A. Pastorello, S. J. Smartt, M. Turatto, F. Yuan, J. P. Anderson, D. D. R. Bayliss, F. E. Bauer, T.-W. Chen, F. Förster Burón, A. Gal-Yam, J. B. Haislip, C. Knapic, L. Le Guillou, S. Marchi, P. Mazzali, M. Molinaro, J. P. Moore, D. Reichart, R. Smareglia, K. W. Smith, A. Sternberg, M. Sullivan, K. Takáts, B. E. Tucker, S. Valenti, O. Yaron, D. R.

Young and G. Zhou. *SN 2009ip \'a la PESSTO: No evidence for core-collapse yet.* ArXiv e-prints, March 2013.

[Fryer et al. 2010] C. L. Fryer, A. J. Ruiter, K. Belczynski, P. J. Brown, F. Bufano, S. Diehl, C. J. Fontes, L. H. Frey, S. T. Holland, A. L. Hungerford, S. Immler, P. Mazzali, C. Meakin, P. A. Milne, C. Raskin and F. X. Timmes. *Spectra of Type Ia Supernovae from Double Degenerate Mergers.* The Astrophysical Journal, vol. 725, page 296, December 2010.

[Gal-Yam & Leonard 2009] A. Gal-Yam and D. C. Leonard. *A massive hypergiant star as the progenitor of the supernova SN 2005gl.* Nature, vol. 458, page 865, April 2009.

[Gal-Yam et al. 2007] A. Gal-Yam, D. C. Leonard, D. B. Fox, S. B. Cenko, A. M. Soderberg, D.-S. Moon, D. J. Sand, Caltech Core Collapse Program, W. Li, A. V. Filippenko, G. Aldering and Y. Copin. *On the Progenitor of SN 2005gl and the Nature of Type IIn Supernovae.* The Astrophysical Journal, vol. 656, page 372, February 2007.

[Gal-Yam et al. 2009] A. Gal-Yam, P. Mazzali, E. O. Ofek, P. E. Nugent, S. R. Kulkarni, M. M. Kasliwal, R. M. Quimby, A. V. Filippenko, S. B. Cenko, R. Chornock, R. Waldman, D. Kasen, M. Sullivan, E. C. Beshore, A. J. Drake, R. C. Thomas, J. S. Bloom, D. Poznanski, A. A. Miller, R. J. Foley, J. M. Silverman, I. Arcavi, R. S. Ellis and J. Deng. *Supernova 2007bi as a pair-instability explosion.* Nature, vol. 462, page 624, December 2009.

[Gal-Yam 2012] A. Gal-Yam. *Luminous Supernovae.* Science, vol. 337, page 927, August 2012.

[Garcia-Berro & Iben 1994] E. Garcia-Berro and I. Iben. *On the formation and evolution of super-asymptotic giant branch stars with cores processed by carbon burning. 1: SPICA to Antares.* The Astrophysical Journal, vol. 434, page 306, October 1994.

[Garcia-Berro et al. 1997] E. Garcia-Berro, C. Ritossa and I. Iben Jr. *On the Evolution of Stars That Form Electron-Degenerate Cores Processed by Carbon Burning. III. The Inward Propagation of a Carbon-burning Flame and Other Properties of a 9 $M_{\odot}$ Model Star.* The Astrophysical Journal, vol. 485, page 765, August 1997.

[Georgy et al. 2009] C. Georgy, G. Meynet, R. Walder, D. Folini and A. Maeder. *The different progenitors of type Ib, Ic SNe, and of GRB.* Astronomy & Astrophysics, vol. 502, page 611, August 2009.

[Georgy 2012] C. Georgy. *Yellow supergiants as supernova progenitors: an indication of strong mass loss for red supergiants?* Astronomy & Astrophysics, vol. 538, page L8, February 2012.

[Gezari et al. 2009] S. Gezari, J. P. Halpern, D. Grupe, F. Yuan, R. Quimby, T. McKay, D. Chamarro, M. D. Sisson, C. Akerlof, J. C. Wheeler, P. J. Brown, S. B. Cenko, A. Rau, J. O. Djordjevic and D. M. Terndrup. *Discovery of the Ultra-Bright Type II-L Supernova 2008es.* The Astrophysical Journal, vol. 690, page 1313, January 2009.

[Ginzburg & Balberg 2012] S. Ginzburg and S. Balberg. *Superluminous Light Curves from Supernovae Exploding in a Dense Wind.* The Astrophysical Journal, vol. 757, page 178, October 2012.

[Grassberg et al. 1971] E. K. Grassberg, V. S. Imshennik and D. K. Nadyozhin. *On the Theory of the Light Curves of Supernovate.* Astrophysics and Space Science, vol. 10, page 28, January 1971.

[Groh et al. 2013] J. H. Groh, G. Meynet and S. Ekström. *Massive star evolution: luminous blue variables as unexpected supernova progenitors.* Astronomy & Astrophysics, vol. 550, page L7, February 2013.

[Hachisu et al. 1999] I. Hachisu, M. Kato and K. Nomoto. *A Wide Symbiotic Channel to Type IA Supernovae.* The Astrophysical Journal, vol. 522, page 487, September 1999.

[Hachisu et al. 2008] I. Hachisu, M. Kato and K. Nomoto. *Young and Massive Binary Progenitors of Type Ia Supernovae and Their Circumstellar Matter.* The Astrophysical Journal, vol. 679, page 1390, June 2008.

[Hachisu et al. 2012] I. Hachisu, M. Kato and K. Nomoto. *Final Fates of Rotating White Dwarfs and Their Companions in the Single Degenerate Model of Type Ia Supernovae.* The Astrophysical Journal Letters, vol. 756, page L4, September 2012.

[Hamuy et al. 2001] M. Hamuy, P. A. Pinto, J. Maza, N. B. Suntzeff, M. M. Phillips, R. G. Eastman, R. C. Smith, C. J. Corbally, D. Burstein, Y. Li, V. Ivanov, A. Moro-Martin, L. G. Strolger, R. E. de Souza, S. dos Anjos, E. M. Green, T. E. Pickering, L. González, R. Antezana, M. Wischnjewsky, G. Galaz, M. Roth, S. E. Persson and R. A. Schommer. *The Distance to SN 1999em from the Expanding Photosphere Method.* The Astrophysical Journal, vol. 558, page 615, September 2001.

[Hamuy et al. 2003] M. Hamuy, M. M. Phillips, N. B. Suntzeff, J. Maza, L. E. González, M. Roth, K. Krisciunas, N. Morrell, E. M. Green, S. E. Persson and P. J. McCarthy. *An asymptotic-giant-branch star in the progenitor system of a type Ia supernova.* Nature, vol. 424, page 651, August 2003.

[Hamuy et al. 2009] M. Hamuy, J. Deng, P. A. Mazzali, N. I. Morrell, M. M. Phillips, M. Roth, S. Gonzalez, J. Thomas-Osip, W. Krzeminski, C. Contreras, J. Maza, L. González, L. Huerta, G. Folatelli, R. Chornock, A. V. Filippenko, S. E. Persson, W. L. Freedman, K. Koviak, N. B. Suntzeff and K. Krisciunas. *Supernova 2003bg: The First Type IIb Hypernova.* The Astrophysical Journal, vol. 703, page 1612, October 2009.

[Hamuy 2003] M. Hamuy. *Observed and Physical Properties of Core-Collapse Supernovae.* The Astrophysical Journal, vol. 582, page 905, January 2003.

[Hanke et al. 2013] F. Hanke, B. Mueller, A. Wongwathanarat, A. Marek and H.-T. Janka. *SASI Activity in Three-Dimensional Neutrino-Hydrodynamics Simulations of Supernova Cores.* ArXiv e-prints, March 2013.

[Hayes et al. 2006] J. C. Hayes, M. L. Norman, R. A. Fiedler, J. O. Bordner, P. S. Li, S. E. Clark, A. ud-Doula and M.-M. Mac Low. *Simulating Radiating and Magnetized Flows in Multiple Dimensions with ZEUS-MP.* The Astrophysical Journal Supplement Series, vol. 165, page 188, July 2006.

[Heger & Woosley 2002] A. Heger and S. E. Woosley. *The Nucleosynthetic Signature of Population III.* The Astrophysical Journal, vol. 567, page 532, March 2002.

[Heger et al. 1997] A. Heger, L. Jeannin, N. Langer and I. Baraffe. *Pulsations in red supergiants with high L/M ratio. Implications for the stellar and circumstellar structure of supernova progenitors.* Astronomy & Astrophysics, vol. 327, page 224, November 1997.

[Heger et al. 2003] A. Heger, C. L. Fryer, S. E. Woosley, N. Langer and D. H. Hartmann. *How Massive Single Stars End Their Life.* The Astrophysical Journal, vol. 591, page 288, July 2003.

[Herant et al. 1994] M. Herant, W. Benz, W. R. Hix, C. L. Fryer and S. A. Colgate. *Inside the supernova: A powerful convective engine.* The Astrophysical Journal, vol. 435, page 339, November 1994.

[Hester 2008] J. J. Hester. *The Crab Nebula: An Astrophysical Chimera.* Annual Review of Astronomy and Astrophysics, vol. 46, page 127, September 2008.

[Hillebrandt et al. 1984] W. Hillebrandt, K. Nomoto and R. G. Wolff. *Supernova explosions of massive stars - The mass range 8 to 10 solar masses.* Astronomy & Astrophysics, vol. 133, page 175, April 1984.

[Hillebrandt 1982] W. Hillebrandt. *An exploding 10 solar mass star - A model for the Crab supernova.* Astronomy & Astrophysics, vol. 110, page L3, June 1982.

[Hirata et al. 1987] K. Hirata, T. Kajita, M. Koshiba, M. Nakahata, Y. Oyama, N. Sato, A. Suzuki, M. Takita, Y. Totsuka, T. Kifune, T. Suda, K. Takahashi, T. Tanimori, K. Miyano, M. Yamada, E. W. Beier, L. R. Feldscher, S. B. Kim, A. K. Mann, F. M. Newcomer, R. Van, W. Zhang and B. G. Cortez. *Observation of a neutrino burst from the supernova SN1987A.* Physical Review Letters, vol. 58, page 1490, April 1987.

[Hirschi et al. 2004] R. Hirschi, G. Meynet and A. Maeder. *Stellar evolution with rotation. XII. Pre-supernova models.* Astronomy & Astrophysics, vol. 425, page 649, October 2004.

[Hosokawa et al. 2011] T. Hosokawa, K. Omukai, N. Yoshida and H. W. Yorke. *Protostellar Feedback Halts the Growth of the First Stars in the Universe.* Science, vol. 334, page 1250, December 2011.

[Hubble 1928] E. P. Hubble. *Novae or Temporary Stars.* Leaflet of the Astronomical Society of the Pacific, vol. 1, page 55, 1928.

[Hummel et al. 2012] J. A. Hummel, A. H. Pawlik, M. Milosavljević and V. Bromm. *The Source Density and Observability of Pair-instability Supernovae from the First Stars.* The Astrophysical Journal, vol. 755, page 72, August 2012.

[Humphreys & Davidson 1994] R. M. Humphreys and K. Davidson. *The luminous blue variables: Astrophysical geysers.* Publications of the Astronomical Society of the Pacific, vol. 106, page 1025, October 1994.

[Iben & Tutukov 1984] I. Iben Jr. and A. V. Tutukov. *Supernovae of type I as end products of the evolution of binaries with components of moderate initial mass (M not greater than about 9 solar masses).* The Astrophysical Journal Supplement Series, vol. 54, page 335, February 1984.

[Inserra et al. 2012] C. Inserra, A. Pastorello, M. Turatto, M. L. Pumo, S. Benetti, E. Cappellaro, M. T. Botticella, F. Bufano, N. Elias-Rosa, A. harutyunyan, S. Taubenberger, S. Valenti and L. Zampieri. *Luminous type II Supernovae.* ArXiv e-prints, October 2012.

[Inserra et al. 2013] C. Inserra, S. J. Smartt, A. Jerkstrand, S. Valenti, M. Fraser, D. Wright, K. Smith, T.-W. Chen, R. Kotak, A. Pastorello, M. Nicholl, F. Bresolin, R. P. Kudritzki, S. Benetti, M. T. Botticella, W. S. Burgett, K. C. Chambers, M. Ergon, H. Flewelling, J. P. U. Fynbo, S. Geier, K. W. Hodapp, D. A. Howell, M. Huber, N. Kaiser, G. Leloudas, L. Magill, E. A. Magnier, M. G. McCrumm, N. Metcalfe, P. A. Price, A. Rest, J. Sollerman, W. Sweeney, F. Taddia, S. Taubenberger, J. L. Tonry, R. J. Wainscoat, C. Waters and D. Young. *Super Luminous Ic Supernovae: catching a magnetar by the tail.* ArXiv e-prints, April 2013.

[Itoh & Masai 1989] H. Itoh and K. Masai. *The effect of a circumstellar medium on the X-ray emission of young remnants of Type II supernovae.* Monthly Notices of the Royal Astronomical Society, vol. 236, page 885, February 1989.

[Iwakami et al. 2008] W. Iwakami, K. Kotake, N. Ohnishi, S. Yamada and K. Sawada. *Three-Dimensional Simulations of Standing Accretion Shock Instability in Core-Collapse Supernovae.* The Astrophysical Journal, vol. 678, page 1207, May 2008.

[Iwamoto et al. 2000] K. Iwamoto, T. Nakamura, K. Nomoto, P. A. Mazzali, I. J. Danziger, P. Garnavich, R. Kirshner, S. Jha, D. Balam and J. Thorstensen. *The Peculiar Type IC Supernova 1997EF: Another Hypernova.* The Astrophysical Journal, vol. 534, page 660, May 2000.

[Janka et al. 2007] H.-T. Janka, K. Langanke, A. Marek, G. Martínez-Pinedo and B. Müller. *Theory of core-collapse supernovae.* Physics Reports, vol. 442, page 38, April 2007.

[Janka et al. 2012] H.-T. Janka, F. Hanke, L. Hüdepohl, A. Marek, B. Müller and M. Obergaulinger. *Core-collapse supernovae: Reflections and directions.* Progress of Theoretical and Experimental Physics, vol. 2012, no. 1, page 010000, December 2012.

[Jiang et al. 2013] Y.-F. Jiang, S. W. Davis and J. M. Stone. *Nonlinear Evolution of Rayleigh-Taylor Instability in a Radiation-supported Atmosphere.* The Astrophysical Journal, vol. 763, page 102, February 2013.

[Karp 1980] A. H. Karp. *A globally convergent method for computing the electron density of a partially ionized plasma.* Journal of Quantitative Spectroscopy and Radiative Transfer, vol. 23, page 285, March 1980.

[Kasen & Bildsten 2010] D. Kasen and L. Bildsten. *Supernova Light Curves Powered by Young Magnetars.* The Astrophysical Journal, vol. 717, page 245, July 2010.

[Kasen & Woosley 2009] D. Kasen and S. E. Woosley. *Type II Supernovae: Model Light Curves and Standard Candle Relationships.* The Astrophysical Journal, vol. 703, page 2205, October 2009.

[Kasen et al. 2011] D. Kasen, S. E. Woosley and A. Heger. *Pair Instability Supernovae: Light Curves, Spectra, and Shock Breakout.* The Astrophysical Journal, vol. 734, page 102, June 2011.

[Kasen 2010] D. Kasen. *Seeing the Collision of a Supernova with Its Companion Star.* The Astrophysical Journal, vol. 708, page 1025, January 2010.

[Katz et al. 2011] B. Katz, N. Sapir and E. Waxman. *X-rays, gamma-rays and neutrinos from collisoinless shocks in supernova wind breakouts.* ArXiv e-prints, June 2011.

[Kawabata et al. 2009] K. S. Kawabata, M. Tanaka, K. Maeda, T. Hattori, K. Nomoto, N. Tominaga and M. Yamanaka. *Extremely Luminous Supernova 2006gy at Late Phase: Detection of Optical Emission from Supernova.* The Astrophysical Journal, vol. 697, page 747, May 2009.

[Kawasaki et al. 2005] M. Kawasaki, M. Ozaki, F. Nagase, H. Inoue and R. Petre. *Ionization States and Plasma Structures of Mixed-Morphology Supernova Remnants Observed with ASCA.* The Astrophysical Journal, vol. 631, page 935, October 2005.

[Kepler et al. 2007] S. O. Kepler, S. J. Kleinman, A. Nitta, D. Koester, B. G. Castanheira, O. Giovannini, A. F. M. Costa and L. Althaus. *White dwarf mass distribution in the SDSS.* Monthly Notices of the Royal Astronomical Society, vol. 375, page 1315, March 2007.

[Kiewe et al. 2012] M. Kiewe, A. Gal-Yam, I. Arcavi, D. C. Leonard, J. Emilio Enriquez, S. B. Cenko, D. B. Fox, D.-S. Moon, D. J. Sand, A. M. Soderberg and T. CCCP. *Caltech Core-Collapse Project (CCCP) Observations of Type IIn Supernovae: Typical Properties and Implications for Their Progenitor Stars.* The Astrophysical Journal, vol. 744, page 10, January 2012.

[Kitaura et al. 2006] F. S. Kitaura, H.-T. Janka and W. Hillebrandt. *Explosions of O-Ne-Mg cores, the Crab supernova, and subluminous type II-P supernovae.* Astronomy & Astrophysics, vol. 450, page 345, April 2006.

[Klein & Chevalier 1978] R. I. Klein and R. A. Chevalier. *X-ray bursts from Type II supernovae.* The Astrophysical Journal Letters, vol. 223, page L109, August 1978.

[Knop et al. 1999] R. Knop, G. Aldering, S. Deustua, G. Goldhaber, M. Kim, P. Nugent, E. Helin, S. Pravdo, D. Rabinowitz and K. Lawrence. *Supernovae 1999as and 1999at in Anonymous Galaxies.* International Astronomical Union Circular, vol. 7128, page 1, March 1999.

[Koo 2013] B.-C. Koo. *Infrared [Fe II] and Dust Emissions from Supernova Remnants.* ArXiv e-prints, April 2013.

[Kostka et al. 2012] M. Kostka, N. Koning, R. Ouyed, D. Leahy and W. Steffen. *Quark Nova Signatures in Super-luminous Supernovae.* ArXiv e-prints, June 2012.

[Kotak & Vink 2006] R. Kotak and J. S. Vink. *Luminous blue variables as the progenitors of supernovae with quasi-periodic radio modulations.* Astronomy & Astrophysics, vol. 460, page L5, December 2006.

[Kotake et al. 2006] K. Kotake, K. Sato and K. Takahashi. *Explosion mechanism, neutrino burst and gravitational wave in core-collapse supernovae.* Reports on Progress in Physics, vol. 69, page 971, April 2006.

[Koyama 2010] Y. Koyama. *Galaxy Evolution in Growing Clusters.* PhD thesis, University of Tokyo, December 2010.

[Kromer et al. 2010] M. Kromer, S. A. Sim, M. Fink, F. K. Röpke, I. R. Seitenzahl and W. Hillebrandt. *Double-detonation Sub-Chandrasekhar Supernovae: Synthetic Observables for Minimum Helium Shell Mass Models.* The Astrophysical Journal, vol. 719, page 1067, August 2010.

[Kroupa 2001] P. Kroupa. *On the variation of the initial mass function.* Monthly Notices of the Royal Astronomical Society, vol. 322, page 231, April 2001.

[Kroupa 2002] P. Kroupa. *The Initial Mass Function of Stars: Evidence for Uniformity in Variable Systems.* Science, vol. 295, page 82, January 2002.

[Kulkarni et al. 1998] S. R. Kulkarni, D. A. Frail, M. H. Wieringa, R. D. Ekers, E. M. Sadler, R. M. Wark, J. L. Higdon, E. S. Phinney and J. S. Bloom. *Radio emission from the unusual supernova 1998bw and its association with the γ-ray burst of 25 April 1998.* Nature, vol. 395, page 663, October 1998.

[Kurucz 1991] R. L. Kurucz. *New Opacity Calculations.* In NATO ASIC Proc. 341: Stellar Atmospheres - Beyond Classical Models, page 441, 1991.

[Lamers et al. 1995] H. J. G. L. M. Lamers, T. P. Snow and D. M. Lindholm. *Terminal Velocities and the Bistability of Stellar Winds.* The Astrophysical Journal, vol. 455, page 269, December 1995.

[Langer & El Eid 1986] N. Langer and M. F. El Eid. *The evolution of very luminous stars. I - Presupernova evolution.* Astronomy & Astrophysics, vol. 167, page 265, October 1986.

[Langer et al. 2007] N. Langer, C. A. Norman, A. de Koter, J. S. Vink, M. Cantiello and S.-C. Yoon. *Pair creation supernovae at low and high redshift.* Astronomy & Astrophysics, vol. 475, page L19, November 2007.

[Langer 2012] N. Langer. *Presupernova Evolution of Massive Single and Binary Stars.* Annual Review of Astronomy and Astrophysics, vol. 50, page 107, September 2012.

[Leloudas et al. 2012] G. Leloudas, E. Chatzopoulos, B. Dilday, J. Gorosabel, J. Vinko, A. Gallazzi, J. C. Wheeler, B. Bassett, J. A. Fischer, J. A. Frieman, J. P. U. Fynbo, A. Goobar, M. Jelínek, D. Malesani, R. C. Nichol, J. Nordin, L. Östman, M. Sako, D. P. Schneider, M. Smith, J. Sollerman, M. D. Stritzinger, C. C. Thöne and A. de Ugarte Postigo. *SN 2006oz: rise of a super-luminous supernova observed by the SDSS-II SN Survey.* Astronomy & Astrophysics, vol. 541, page A129, May 2012.

[Levan et al. 2013] A. J. Levan, A. M. Read, B. D. Metzger, P. J. Wheatley and N. R. Tanvir. *Superluminous X-rays from a superluminous supernova.* ArXiv e-prints, April 2013.

[Li & Gong 1994] Y. Li and Z. G. Gong. *Red supergiant variables in the Large Magellanic Cloud: Their evolution and puslations.* Astronomy & Astrophysics, vol. 289, page 449, September 1994.

[Li et al. 2011a] W. Li, J. S. Bloom, P. Podsiadlowski, A. A. Miller, S. B. Cenko, S. W. Jha, M. Sullivan, D. A. Howell, P. E. Nugent, N. R. Butler, E. O. Ofek, M. M. Kasliwal, J. W. Richards, A. Stockton, H.-Y. Shih, L. Bildsten, M. M. Shara, J. Bibby, A. V. Filippenko, M. Ganeshalingam, J. M. Silverman, S. R. Kulkarni, N. M. Law, D. Poznanski, R. M. Quimby, C. McCully, B. Patel, K. Maguire and K. J. Shen. *Exclusion of a luminous red giant as a companion star to the progenitor of supernova SN 2011fe.* Nature, vol. 480, page 348, December 2011.

[Li et al. 2011b] W. Li, J. Leaman, R. Chornock, A. V. Filippenko, D. Poznanski, M. Ganeshalingam, X. Wang, M. Modjaz, S. Jha, R. J. Foley and N. Smith. *Nearby supernova rates from the Lick Observatory Supernova Search - II. The observed luminosity functions and fractions of supernovae in a complete sample.* Monthly Notices of the Royal Astronomical Society, vol. 412, page 1441, April 2011.

[Liebendörfer et al. 2005] M. Liebendörfer, M. Rampp, H.-T. Janka and A. Mezzacappa. *Supernova Simulations with Boltzmann Neutrino Transport: A Comparison of Methods.* The Astrophysical Journal, vol. 620, page 840, February 2005.

[Lien & Fields 2009] A. Lien and B. D. Fields. *Cosmic core-collapse supernovae from upcoming sky surveys.* Journal of Cosmology and Astroparticle Physics, vol. 1, page 47, January 2009.

[Lundmark 1921] K. Lundmark. *Suspected New Stars Recorded in Old Chronicles and Among Recent Meridian Observations.* Publications of the Astronomical Society of the Pacific, vol. 33, page 225, October 1921.

[Maeda & Nomoto 2003] K. Maeda and K. Nomoto. *Bipolar Supernova Explosions: Nucleosynthesis and Implications for Abundances in Extremely Metal-Poor Stars.* The Astrophysical Journal, vol. 598, page 1163, December 2003.

[Maeda et al. 2007] K. Maeda, M. Tanaka, K. Nomoto, N. Tominaga, K. Kawabata, P. A. Mazzali, H. Umeda, T. Suzuki and T. Hattori. *The Unique Type Ib Supernova 2005bf at Nebular Phases: A Possible Birth Event of a Strongly Magnetized Neutron Star.* The Astrophysical Journal, vol. 666, page 1069, September 2007.

[Maeda 2012] K. Maeda. *Injection and Acceleration of Electrons at a Strong Shock: Radio and X-Ray Study of Young Supernova 2011dh.* The Astrophysical Journal, vol. 758, page 81, October 2012.

[Maeda 2013] K. Maeda. *Young Supernovae as Experimental Sites for Studying the Electron Acceleration Mechanism.* The Astrophysical Journal Letters, vol. 762, page L24, January 2013.

[Maeder & Meynet 2000a] A. Maeder and G. Meynet. *Stellar evolution with rotation. VI. The Eddington and Omega-limits, the rotational mass loss for OB and LBV stars.* Astronomy & Astrophysics, vol. 361, page 159, September 2000.

[Maeder & Meynet 2000b] A. Maeder and G. Meynet. *The Evolution of Rotating Stars.* Annual Review of Astronomy and Astrophysics, vol. 38, page 143, 2000.

[Malhotra & Rhoads 2002] S. Malhotra and J. E. Rhoads. *Large Equivalent Width Lyα line Emission at z=4.5: Young Galaxies in a Young Universe?* The Astrophysical Journal Letters, vol. 565, page L71, February 2002.

[Masai 1984] K. Masai. *X-ray emission spectra from ionizing plasmas.* Astrophysics and Space Science, vol. 98, page 367, January 1984.

[Masai 1994] K. Masai. *Nonequilibria in thermal emission from supernova remnants.* The Astrophysical Journal, vol. 437, page 770, December 1994.

[Matzner & McKee 1999] C. D. Matzner and C. F. McKee. *The Expulsion of Stellar Envelopes in Core-Collapse Supernovae.* The Astrophysical Journal, vol. 510, page 379, January 1999.

[Mauerhan et al. 2013] J. C. Mauerhan, N. Smith, A. V. Filippenko, K. B. Blanchard, P. K. Blanchard, C. F. E. Casper, S. B. Cenko, K. I. Clubb, D. P. Cohen, K. L. Fuller, G. Z. Li and J. M. Silverman. *The unprecedented 2012 outburst of SN 2009ip: a luminous blue variable star becomes a true supernova.* Monthly Notices of the Royal Astronomical Society, vol. 430, page 1801, April 2013.

[Maund et al. 2004] J. R. Maund, S. J. Smartt, R. P. Kudritzki, P. Podsiadlowski and G. F. Gilmore. *The massive binary companion star to the progenitor of supernova 1993J.* Nature, vol. 427, page 129, January 2004.

[Mauron & Josselin 2011] N. Mauron and E. Josselin. *The mass-loss rates of red supergiants and the de Jager prescription.* Astronomy & Astrophysics, vol. 526, page A156, February 2011.

[McKee & Tan 2008] C. F. McKee and J. C. Tan. *The Formation of the First Stars. II. Radiative Feedback Processes and Implications for the Initial Mass Function.* The Astrophysical Journal, vol. 681, page 771, July 2008.

[Metzger 2010] B. D. Metzger. *Relic proto-stellar discs and the origin of luminous circumstellar interaction in core-collapse supernovae.* Monthly Notices of the Royal Astronomical Society, vol. 409, page 284, November 2010.

[Meynet & Maeder 2003] G. Meynet and A. Maeder. *Stellar evolution with rotation. X. Wolf-Rayet star populations at solar metallicity.* Astronomy & Astrophysics, vol. 404, page 975, June 2003.

[Meynet & Maeder 2005] G. Meynet and A. Maeder. *Stellar evolution with rotation. XI. Wolf-Rayet star populations at different metallicities.* Astronomy & Astrophysics, vol. 429, page 581, January 2005.

[Mihalas & Mihalas 1999] D. Mihalas and B. Mihalas. Foundations of Radiation Hydrodynamics. Dover, 1999.

[Mihalas 1978] D. Mihalas. Stellar Atmospheres. W.H. Freeman, 2nd edition, 1978.

[Milisavljevic et al. 2013] D. Milisavljevic, R. Margutti, A. M. Soderberg, G. Pignata, L. Chomiuk, R. A. Fesen, F. Bufano, N. E. Sanders, J. T. Parrent, S. Parker, P. Mazzali, E. Pian, T. Pickering, D. A. H. Buckley, S. M. Crawford, A. A. S. Gulbis, C. Hettlage, E. Hooper, K. H. Nordsieck, D. O'Donoghue, T.-O. Husser, S. Potter, A. Kniazev, P. Kotze, E. Romero-Colmenero, P. Vaisanen, M. Wolf, M. F. Bietenholz, N. Bartel, C. Fransson, E. S. Walker, A. Brunthaler, S. Chakraborti, E. M. Levesque, A. MacFadyen, C. Drescher, G. Bock, P. Marples, J. P. Anderson, S. Benetti, D. Reichart and K. Ivarsen. *Multi-wavelength Observations of Supernova 2011ei: Time-dependent Classification of Type IIb and Ib Supernovae and Implications for Their Progenitors.* The Astrophysical Journal, vol. 767, page 71, April 2013.

[Miller et al. 2009] A. A. Miller, R. Chornock, D. A. Perley, M. Ganeshalingam, W. Li, N. R. Butler, J. S. Bloom, N. Smith, M. Modjaz, D. Poznanski, A. V. Filippenko, C. V. Griffith, J. H. Shiode and J. M. Silverman. *The Exceptionally Luminous Type II-Linear Supernova 2008es.* The Astrophysical Journal, vol. 690, page 1303, January 2009.

[Miller et al. 2010] A. A. Miller, N. Smith, W. Li, J. S. Bloom, R. Chornock, A. V. Filippenko and J. X. Prochaska. *New Observations of the Very Luminous Supernova 2006gy: Evidence for Echoes.* The Astronomical Journal, vol. 139, page 2218, June 2010.

[Miyaji et al. 1980] S. Miyaji, K. Nomoto, K. Yokoi and D. Sugimoto. *Supernova Triggered by Electron Captures.* Publications of the Astronomical Society of Japan, vol. 32, page 303, 1980.

[Modjaz et al. 2011] M. Modjaz, L. Kewley, J. S. Bloom, A. V. Filippenko, D. Perley and J. M. Silverman. *Progenitor Diagnostics for Stripped Core-collapse Supernovae: Measured Metallicities at Explosion Sites.* The Astrophysical Journal Letters, vol. 731, page L4, April 2011.

[Morimoto 2008] N. Morimoto. *Kou Sekihou Hen'i Ni Okeru Henkou Tentai Tansaku* [in Japanese] (Searching for Transients at High Redshifts). Master's thesis, Tohoku University, 2008.

[Morrissey et al. 2005] P. Morrissey, D. Schiminovich, T. A. Barlow, D. C. Martin, B. Blakkolb, T. Conrow, B. Cooke, K. Erickson, J. Fanson, P. G. Friedman, R. Grange, P. N. Jelinsky, S.-C. Lee, D. Liu, A. Mazer, R. McLean, B. Milliard, D. Randall, W. Schmitigal, A. Sen, O. H. W. Siegmund, F. Surber, A. Vaughan, M. Viton, B. Y. Welsh, L. Bianchi, Y.-I. Byun, J. Donas, K. Forster, T. M. Heckman, Y.-W. Lee, B. F. Madore, R. F. Malina, S. G. Neff, R. M. Rich, T. Small, A. S. Szalay and T. K. Wyder. *The On-Orbit Performance of the Galaxy Evolution Explorer.* The Astrophysical Journal Letters, vol. 619, page L7, January 2005.

[Murase et al. 2011] K. Murase, T. A. Thompson, B. C. Lacki and J. F. Beacom. *New class of high-energy transients from crashes of supernova ejecta with massive circumstellar material shells.* Physical Review D, vol. 84, no. 4, page 043003, August 2011.

[Nadyozhin 1985] D. K. Nadyozhin. *On the initial phase of interaction between expanding stellar envelopes and surrounding medium.* Astrophysics and Space Science, vol. 112, page 225, May 1985.

[Nadyozhin 1994] D. K. Nadyozhin. *The properties of NI to CO to Fe decay.* The Astrophysical Journal Supplement Series, vol. 92, page 527, June 1994.

[Nakamura & Umemura 2001] F. Nakamura and M. Umemura. *On the Initial Mass Function of Population III Stars.* The Astrophysical Journal, vol. 548, page 19, February 2001.

[Nakano et al. 2006] S. Nakano, K. Itagaki, T. Puckett and R. Gorelli. *Possible Supernova in UGC 4904.* Central Bureau Electronic Telegrams, vol. 666, page 1, October 2006.

[Nakar & Sari 2010] E. Nakar and R. Sari. *Early Supernovae Light Curves Following the Shock Breakout.* The Astrophysical Journal, vol. 725, page 904, December 2010.

[Neill et al. 2011] J. D. Neill, M. Sullivan, A. Gal-Yam, R. Quimby, E. Ofek, T. K. Wyder, D. A. Howell, P. Nugent, M. Seibert, D. C. Martin, R. Overzier, T. A. Barlow, K. Foster, P. G. Friedman, P. Morrissey, S. G. Neff, D. Schiminovich, L. Bianchi, J. Donas, T. M. Heckman, Y.-W. Lee, B. F. Madore, B. Milliard, R. M. Rich and A. S. Szalay. *The Extreme Hosts of Extreme Supernovae.* The Astrophysical Journal, vol. 727, page 15, January 2011.

[Nomoto et al. 1982] K. Nomoto, D. Sugimoto, W. M. Sparks, R. A. Fesen, T. R. Gull and S. Miyaji. *The Crab Nebula's progenitor.* Nature, vol. 299, page 803, October 1982.

[Nomoto et al. 1984] K. Nomoto, F.-K. Thielemann and K. Yokoi. *Accreting white dwarf models of Type I supernovae. III - Carbon deflagration supernovae.* The Astrophysical Journal, vol. 286, page 644, November 1984.

[Nomoto et al. 1995] K. Nomoto, K. Iwamoto and T. Suzuki. *The evolution and explosion of massive binary stars and Type Ib-Ic-IIb-IIL supernovae.* Physics Reports, vol. 256, page 173, May 1995.

[Nomoto et al. 2006] K. Nomoto, N. Tominaga, M. Tanaka, K. Maeda, T. Suzuki, J. S. Deng and P. A. Mazzali. *Diversity of the supernova–gamma-ray burst connection.* Nuovo Cimento B Serie, vol. 121, page 1207, October 2006.

[Nomoto et al. 2011] K. Nomoto, K. Maeda, M. Tanaka and T. Suzuki. *Gamma-Ray Bursts and magnetar-forming Supernovae.* Astrophysics and Space Science, vol. 336, page 129, November 2011.

[Nomoto 1982] K. Nomoto. *Accreting white dwarf models for type I supernovae. I - Presupernova evolution and triggering mechanisms.* The Astrophysical Journal, vol. 253, page 798, February 1982.

[Nomoto 1984] K. Nomoto. *Evolution of 8-10 solar mass stars toward electron capture supernovae. I - Formation of electron-degenerate O + NE + MG cores.* The Astrophysical Journal, vol. 277, page 791, February 1984.

[Nordhaus et al. 2010] J. Nordhaus, A. Burrows, A. Almgren and J. Bell. *Dimension as a Key to the Neutrino Mechanism of Core-collapse Supernova Explosions.* The Astrophysical Journal, vol. 720, page 694, September 2010.

[Nugent et al. 2011] P. E. Nugent, M. Sullivan, S. B. Cenko, R. C. Thomas, D. Kasen, D. A. Howell, D. Bersier, J. S. Bloom, S. R. Kulkarni, M. T. Kandrashoff, A. V. Filippenko, J. M. Silverman, G. W. Marcy, A. W. Howard, H. T. Isaacson, K. Maguire, N. Suzuki, J. E. Tarlton, Y.-C. Pan, L. Bildsten, B. J. Fulton, J. T. Parrent, D. Sand, P. Podsiadlowski, F. B. Bianco, B. Dilday, M. L. Graham, J. Lyman, P. James, M. M. Kasliwal, N. M. Law, R. M. Quimby, I. M. Hook, E. S. Walker, P. Mazzali, E. Pian, E. O. Ofek, A. Gal-Yam and D. Poznanski. *Supernova SN 2011fe from an exploding carbon-oxygen white dwarf star.* Nature, vol. 480, page 344, December 2011.

[Nymark et al. 2006] T. K. Nymark, C. Fransson and C. Kozma. *X-ray emission from radiative shocks in type II supernovae.* Astronomy & Astrophysics, vol. 449, page 171, April 2006.

[Ofek et al. 2007] E. O. Ofek, P. B. Cameron, M. M. Kasliwal, A. Gal-Yam, A. Rau, S. R. Kulkarni, D. A. Frail, P. Chandra, S. B. Cenko, A. M. Soderberg and S. Immler. *SN 2006gy: An Extremely Luminous Supernova in the Galaxy NGC 1260.* The Astrophysical Journal Letters, vol. 659, page L13, April 2007.

[Ofek et al. 2010] E. O. Ofek, I. Rabinak, J. D. Neill, I. Arcavi, S. B. Cenko, E. Waxman, S. R. Kulkarni, A. Gal-Yam, P. E. Nugent, L. Bildsten, J. S. Bloom, A. V. Filippenko, K. Forster, D. A. Howell, J. Jacobsen, M. M. Kasliwal, N. Law, C. Martin, D. Poznanski, R. M. Quimby, K. J. Shen, M. Sullivan, R. Dekany, G. Rahmer, D. Hale, R. Smith, J. Zolkower, V. Velur, R. Walters, J. Henning, K. Bui and D. McKenna. *Supernova PTF 09UJ: A Possible Shock Breakout from a Dense Circumstellar Wind.* The Astrophysical Journal, vol. 724, page 1396, December 2010.

[Ofek et al. 2013] E. O. Ofek, M. Sullivan, S. B. Cenko, M. M. Kasliwal, A. Gal-Yam, S. R. Kulkarni, I. Arcavi, L. Bildsten, J. S. Bloom, A. Horesh, D. A. Howell, A. V. Filippenko, R. Laher, D. Murray, E. Nakar, P. E. Nugent, J. M. Silverman, N. J. Shaviv, J. Surace and O. Yaron. *An outburst from a massive star 40days before a supernova explosion.* Nature, vol. 494, page 65, February 2013.

[Ohkubo et al. 2006] T. Ohkubo, H. Umeda, K. Maeda, K. Nomoto, T. Suzuki, S. Tsuruta and M. J. Rees. *Core-Collapse Very Massive Stars: Evolution, Explosion, and Nucleosynthesis of Population III 500-1000 M_{solar} Stars.* The Astrophysical Journal, vol. 645, page 1352, July 2006.

[Ohkubo et al. 2009] T. Ohkubo, K. Nomoto, H. Umeda, N. Yoshida and S. Tsuruta. *Evolution of Very Massive Population III Stars with Mass Accretion from Pre-main Sequence to Collapse.* The Astrophysical Journal, vol. 706, page 1184, December 2009.

[Ohnishi et al. 2011] T. Ohnishi, K. Koyama, T. G. Tsuru, K. Masai, H. Yamaguchi and M. Ozawa. *X-Ray Spectrum of a Peculiar Supernova Remnant, G359.1-0.5.* Publications of the Astronomical Society of Japan, vol. 63, page 527, June 2011.

[Ohyama 1963] N. Ohyama. *On the Explosion of Type II Supernova.* Progress of Theoretical Physics, vol. 30, page 170, August 1963.

[Omukai 2001] K. Omukai. *Primordial Star Formation under Far-Ultraviolet Radiation.* The Astrophysical Journal, vol. 546, page 635, January 2001.

[Ostlie & Carroll 2006] D. A. Ostlie and B. W. Carroll. An Introduction to Modern Stellar Astrophysics. Benjamin Cummings, 2nd edition, 2006.

[Ouyed & Leahy 2012] R. Ouyed and D. Leahy. *The peculiar case of the "double-humped" super-luminous supernova SN2006oz.* ArXiv e-prints, February 2012.

[Ouyed et al. 2012] R. Ouyed, M. Kostka, N. Koning, D. A. Leahy and W. Steffen. *Quark nova imprint in the extreme supernova explosion SN 2006gy.* Monthly Notices of the Royal Astronomical Society, vol. 423, page 1652, June 2012.

[Ozawa et al. 2009] M. Ozawa, K. Koyama, H. Yamaguchi, K. Masai and T. Tamagawa. *Suzaku Discovery of the Strong Radiative Recombination Continuum of Iron from the Supernova Remnant W49B.* The Astrophysical Journal Letters, vol. 706, page L71, November 2009.

[Pakmor et al. 2012] R. Pakmor, M. Kromer, S. Taubenberger, S. A. Sim, F. K. Röpke and W. Hillebrandt. *Normal Type Ia Supernovae from Violent Mergers of White Dwarf Binaries.* The Astrophysical Journal Letters, vol. 747, page L10, March 2012.

[Pan et al. 2012a] T. Pan, D. Kasen and A. Loeb. *Pair-instability supernovae at the epoch of reionization.* Monthly Notices of the Royal Astronomical Society, vol. 422, page 2701, May 2012.

[Pan et al. 2012b] T. Pan, A. Loeb and D. Kasen. *Pair-instability supernovae via collision runaway in young dense star clusters.* Monthly Notices of the Royal Astronomical Society, vol. 423, page 2203, July 2012.

[Pan et al. 2013] T. Pan, D. J. Patnaude and A. Loeb. *Super-luminous X-ray Emission from the Interaction of Supernova Ejecta with Dense Circumstellar Shells.* ArXiv e-prints, March 2013.

[Pastorello et al. 2006] A. Pastorello, D. Sauer, S. Taubenberger, P. A. Mazzali, K. Nomoto, K. S. Kawabata, S. Benetti, N. Elias-Rosa, A. Harutyunyan, H. Navasardyan, L. Zampieri, T. Iijima, M. T. Botticella, G. di Rico, M. Del Principe, M. Dolci, S. Gagliardi, M. Ragni and G. Valentini. *SN 2005cs in M51 - I. The first month of evolution of a subluminous SN II plateau.* Monthly Notices of the Royal Astronomical Society, vol. 370, page 1752, August 2006.

[Pastorello et al. 2007] A. Pastorello, S. J. Smartt, S. Mattila, J. J. Eldridge, D. Young, K. Itagaki, H. Yamaoka, H. Navasardyan, S. Valenti, F. Patat, I. Agnoletto, T. Augusteijn, S. Benetti, E. Cappellaro, T. Boles, J.-M. Bonnet-Bidaud, M. T. Botticella, F. Bufano, C. Cao, J. Deng, M. Dennefeld, N. Elias-Rosa, A. Harutyunyan, F. P. Keenan, T. Iijima, V. Lorenzi, P. A. Mazzali, X. Meng, S. Nakano, T. B. Nielsen, J. V. Smoker, V. Stanishev, M. Turatto, D. Xu and L. Zampieri. *A giant outburst two years before the core-collapse of a massive star.* Nature, vol. 447, page 829, June 2007.

[Pastorello et al. 2010] A. Pastorello, S. J. Smartt, M. T. Botticella, K. Maguire, M. Fraser, K. Smith, R. Kotak, L. Magill, S. Valenti, D. R. Young, S. Gezari, F. Bresolin, R. Kudritzki, D. A. Howell, A. Rest, N. Metcalfe, S. Mattila, E. Kankare, K. Y. Huang, Y. Urata, W. S. Burgett, K. C. Chambers, T. Dombeck, H. Flewelling, T. Grav, J. N. Heasley, K. W. Hodapp, N. Kaiser, G. A. Luppino, R. H. Lupton, E. A. Magnier, D. G. Monet, J. S. Morgan, P. M. Onaka, P. A. Price, P. H. Rhoads, W. A. Siegmund, C. W. Stubbs, W. E. Sweeney, J. L. Tonry, R. J. Wainscoat, M. F. Waterson, C. Waters and C. G. Wynn-Williams. *Ultra-bright Optical Transients are Linked with Type Ic Supernovae.* The Astrophysical Journal Letters, vol. 724, page L16, November 2010.

[Pastorello et al. 2013] A. Pastorello, E. Cappellaro, C. Inserra, S. J. Smartt, G. Pignata, S. Benetti, S. Valenti, M. Fraser, K. Takáts, S. Benitez, M. T. Botticella, J. Brimacombe, F. Bufano, F. Cellier-Holzem, M. T. Costado, G. Cupani, I. Curtis, N. Elias-Rosa, M. Ergon, J. P. U. Fynbo, F.-J. Hambsch, M. Hamuy, A. Harutyunyan, K. M.

Ivarson, E. Kankare, J. C. Martin, R. Kotak, A. P. LaCluyze, K. Maguire, S. Mattila, J. Maza, M. McCrum, M. Miluzio, H. U. Norgaard-Nielsen, M. C. Nysewander, P. Ochner, Y.-C. Pan, M. L. Pumo, D. E. Reichart, T. G. Tan, S. Taubenberger, L. Tomasella, M. Turatto and D. Wright. *Interacting Supernovae and Supernova Impostors: SN 2009ip, is this the End?* The Astrophysical Journal, vol. 767, page 1, April 2013.

[Patat et al. 2011] F. Patat, S. Taubenberger, S. Benetti, A. Pastorello and A. Harutyunyan. *Asymmetries in the type IIn SN 2010jl.* Astronomy & Astrophysics, vol. 527, page L6, March 2011.

[Paxton et al. 2013] B. Paxton, M. Cantiello, P. Arras, L. Bildsten, E. F. Brown, A. Dotter, C. Mankovich, M. H. Montgomery, D. Stello, F. X. Timmes and R. Townsend. *Modules for Experiments in Stellar Astrophysics (MESA): Giant Planets, Oscillations, Rotation, and Massive Stars.* ArXiv e-prints, January 2013.

[Perlmutter et al. 1999] S. Perlmutter, G. Aldering, G. Goldhaber, R. A. Knop, P. Nugent, P. G. Castro, S. Deustua, S. Fabbro, A. Goobar, D. E. Groom, I. M. Hook, A. G. Kim, M. Y. Kim, J. C. Lee, N. J. Nunes, R. Pain, C. R. Pennypacker, R. Quimby, C. Lidman, R. S. Ellis, M. Irwin, R. G. McMahon, P. Ruiz-Lapuente, N. Walton, B. Schaefer, B. J. Boyle, A. V. Filippenko, T. Matheson, A. S. Fruchter, N. Panagia, H. J. M. Newberg, W. J. Couch and The Supernova Cosmology Project. *Measurements of Omega and Lambda from 42 High-Redshift Supernovae.* The Astrophysical Journal, vol. 517, page 565, June 1999.

[Poelarends et al. 2008] A. J. T. Poelarends, F. Herwig, N. Langer and A. Heger. *The Supernova Channel of Super-AGB Stars.* The Astrophysical Journal, vol. 675, page 614, March 2008.

[Portegies Zwart & van den Heuvel 2007] S. F. Portegies Zwart and E. P. J. van den Heuvel. *A runaway collision in a young star cluster as the origin of the brightest supernova.* Nature, vol. 450, page 388, November 2007.

[Potashov et al. 2013] M. Potashov, S. Blinnikov, P. Baklanov and A. Dolgov. *Direct distance measurements to SN 2009ip.* Monthly Notices of the Royal Astronomical Society, vol. 431, page L98, April 2013.

[Pozzo et al. 2004] M. Pozzo, W. P. S. Meikle, A. Fassia, T. Geballe, P. Lundqvist, N. N. Chugai and J. Sollerman. *On the source of the late-time infrared luminosity of SN 1998S and other Type II supernovae.* Monthly Notices of the Royal Astronomical Society, vol. 352, page 457, August 2004.

[Prieto et al. 2008] J. L. Prieto, M. D. Kistler, T. A. Thompson, H. Yüksel, C. S. Kochanek, K. Z. Stanek, J. F. Beacom, P. Martini, A. Pasquali and J. Bechtold. *Discovery of the Dust-Enshrouded Progenitor of SN 2008S with Spitzer.* The Astrophysical Journal Letters, vol. 681, page L9, July 2008.

[Prieto et al. 2013] J. L. Prieto, J. Brimacombe, A. J. Drake and S. Howerton. *The 2012 Rise of the Remarkable Type IIn SN 2009ip.* The Astrophysical Journal Letters, vol. 763, page L27, February 2013.

[Pumo et al. 2009] M. L. Pumo, M. Turatto, M. T. Botticella, A. Pastorello, S. Valenti, L. Zampieri, S. Benetti, E. Cappellaro and F. Patat. *EC-SNe from Super-Asymptotic Giant Branch Progenitors: Theoretical Models Versus Observations.* The Astrophysical Journal Letters, vol. 705, page L138, November 2009.

[Quataert & Shiode 2012] E. Quataert and J. Shiode. *Wave-driven mass loss in the last year of stellar evolution: setting the stage for the most luminous core-collapse supernovae.* Monthly Notices of the Royal Astronomical Society, vol. 423, page L92, June 2012.

[Quimby et al. 2011] R. M. Quimby, S. R. Kulkarni, M. M. Kasliwal, A. Gal-Yam, I. Arcavi, M. Sullivan, P. Nugent, R. Thomas, D. A. Howell, E. Nakar, L. Bildsten, C. Theissen, N. M. Law, R. Dekany, G. Rahmer, D. Hale, R. Smith, E. O. Ofek, J. Zolkower, V. Velur, R. Walters, J. Henning, K. Bui, D. McKenna, D. Poznanski, S. B. Cenko and D. Levitan. *Hydrogen-poor superluminous stellar explosions.* Nature, vol. 474, page 487, June 2011.

[Quimby et al. 2013a] R. M. Quimby, M. C. Werner, M. Oguri, S. More, A. More, M. Tanaka, K. Nomoto, T. J. Moriya, G. Folatelli, K. Maeda and M. Bersten. *Extraordinary Magnification of the Ordinary Type Ia Supernova PS1-10afx.* The Astrophysical Journal Letters, vol. 768, page L20, May 2013.

[Quimby et al. 2013b] R. M. Quimby, F. Yuan, C. Akerlof and J. C. Wheeler. *Rates of superluminous supernovae at $z \sim 0.2$.* Monthly Notices of the Royal Astronomical Society, vol. 431, page 912, May 2013.

[Quimby 2006] R. Quimby. *Supernova 2006gy in NGC 1260.* Central Bureau Electronic Telegrams, vol. 644, page 1, September 2006.

[Rakavy et al. 1967] G. Rakavy, G. Shaviv and Z. Zinamon. - *and Oxygen-Burning Stars and Pre-Supernova Models.* The Astrophysical Journal, vol. 150, page 131, October 1967.

[Rest et al. 2011] A. Rest, R. J. Foley, S. Gezari, G. Narayan, B. Draine, K. Olsen, M. E. Huber, T. Matheson, A. Garg, D. L. Welch, A. C. Becker, P. Challis, A. Clocchiatti, K. H. Cook, G. Damke, M. Meixner, G. Miknaitis, D. Minniti, L. Morelli, S. Nikolaev, G. Pignata, J. L. Prieto, R. C. Smith, C. Stubbs, N. B. Suntzeff, A. R. Walker, W. M. Wood-Vasey, A. Zenteno, L. Wyrzykowski, A. Udalski, M. K. Szymański, M. Kubiak, G. Pietrzyński, I. Soszyński, O. Szewczyk, K. Ulaczyk and R. Poleski. *Pushing the Boundaries of Conventional Core-collapse Supernovae: The Extremely Energetic Supernova SN 2003ma.* The Astrophysical Journal, vol. 729, page 88, March 2011.

[Richardson et al. 2002] D. Richardson, D. Branch, D. Casebeer, J. Millard, R. C. Thomas and E. Baron. *A Comparative Study of the Absolute Magnitude Distributions of Supernovae.* The Astronomical Journal, vol. 123, page 745, February 2002.

[Riess et al. 1998] A. G. Riess, A. V. Filippenko, P. Challis, A. Clocchiatti, A. Diercks, P. M. Garnavich, R. L. Gilliland, C. J. Hogan, S. Jha, R. P. Kirshner, B. Leibundgut, M. M. Phillips, D. Reiss, B. P. Schmidt, R. A. Schommer, R. C. Smith, J. Spyromilio, C. Stubbs, N. B. Suntzeff and J. Tonry. *Observational Evidence from Supernovae for an Accelerating Universe and a Cosmological Constant.* The Astronomical Journal, vol. 116, page 1009, September 1998.

[Riess et al. 2004] A. G. Riess, L.-G. Strolger, J. Tonry, Z. Tsvetanov, S. Casertano, H. C. Ferguson, B. Mobasher, P. Challis, N. Panagia, A. V. Filippenko, W. Li, R. Chornock, R. P. Kirshner, B. Leibundgut, M. Dickinson, A. Koekemoer, N. A. Grogin and M. Giavalisco. *Identification of Type Ia Supernovae at Redshift 1.3 and Beyond with the Advanced Camera for Surveys on the Hubble Space Telescope.* The Astrophysical Journal Letters, vol. 600, page L163, January 2004.

[Roming et al. 2009] P. W. A. Roming, T. A. Pritchard, P. J. Brown, S. T. Holland, S. Immler, C. J. Stockdale, K. W. Weiler, N. Panagia, S. D. Van Dyk, E. A. Hoversten, P. A. Milne, S. R. Oates, B. Russell and C. Vandrevala. *Multi-Wavelength Properties of the Type IIb SN 2008ax.* The Astrophysical Journal Letters, vol. 704, page L118, October 2009.

[Rybicki & Lightman 1986] G. B. Rybicki and A. P. Lightman. Radiative Processes in Astrophysics. June 1986.

[Ryder et al. 2004] S. D. Ryder, E. M. Sadler, R. Subrahmanyan, K. W. Weiler, N. Panagia and C. Stockdale. *Modulations in the radio light curve of the Type IIb supernova 2001ig: evidence for a Wolf-Rayet binary progenitor?* Monthly Notices of the Royal Astronomical Society, vol. 349, page 1093, April 2004.

[Sakurai 1960] A. Sakurai. *On the problem of a shock wave arriving at the edge of a gas.* Communications on Pure and Applied Mathematics, vol. 13, page 353, August 1960.

[Salpeter 1955] E. E. Salpeter. *The Luminosity Function and Stellar Evolution.* The Astrophysical Journal, vol. 121, page 161, January 1955.

[Sana et al. 2012] H. Sana, S. E. de Mink, A. de Koter, N. Langer, C. J. Evans, M. Gieles, E. Gosset, R. G. Izzard, J.-B. Le Bouquin and F. R. N. Schneider. *Binary Interaction Dominates the Evolution of Massive Stars.* Science, vol. 337, page 444, July 2012.

[Sanders et al. 2012] N. E. Sanders, A. M. Soderberg, E. M. Levesque, R. J. Foley, R. Chornock, D. Milisavljevic, R. Margutti, E. Berger, M. R. Drout, I. Czekala and J. A. Dittmann. *A Spectroscopic Study of Type Ibc Supernova Host Galaxies from Untargeted Surveys.* The Astrophysical Journal, vol. 758, page 132, October 2012.

[Sawada & Koyama 2012] M. Sawada and K. Koyama. *X-Ray Observations of the Supernova Remnant W28 with Suzaku. I. Spectral Study of the Recombining Plasma.* Publications of the Astronomical Society of Japan, vol. 64, page 81, August 2012.

[Scannapieco et al. 2005] E. Scannapieco, P. Madau, S. Woosley, A. Heger and A. Ferrara. *The Detectability of Pair-Production Supernovae at $z \lesssim 6$.* The Astrophysical Journal, vol. 633, page 1031, November 2005.

[Schaefer & Pagnotta 2012] B. E. Schaefer and A. Pagnotta. *An absence of ex-companion stars in the type Ia supernova remnant SNR 0509-67.5.* Nature, vol. 481, page 164, January 2012.

[Schawinski et al. 2008] K. Schawinski, S. Justham, C. Wolf, P. Podsiadlowski, M. Sullivan, K. C. Steenbrugge, T. Bell, H.-J. Röser, E. S. Walker, P. Astier, D. Balam, C. Balland, R. Carlberg, A. Conley, D. Fouchez, J. Guy, D. Hardin, I. Hook, D. A. Howell, R. Pain, K. Perrett, C. Pritchet, N. Regnault and S. K. Yi. *Supernova Shock Breakout from a Red Supergiant.* Science, vol. 321, page 223, July 2008.

[Schlegel & Kirshner 1998] E. M. Schlegel and R. P. Kirshner. *SN1987C in MRK 90 = UGC 4438: Evolution of a Type "IIn" to a Type IIP?* New Astronomy, vol. 3, page 125, March 1998.

[Schlegel et al. 1998] D. J. Schlegel, D. P. Finkbeiner and M. Davis. *Maps of Dust Infrared Emission for Use in Estimation of Reddening and Cosmic Microwave Background Radiation Foregrounds.* The Astrophysical Journal, vol. 500, page 525, June 1998.

[Schlegel 1990] E. M. Schlegel. *A new subclass of Type II supernovae?* Monthly Notices of the Royal Astronomical Society, vol. 244, page 269, May 1990.

[Shimizu et al. 2012] T. Shimizu, K. Masai and K. Koyama. *Evolution of Supernova Remnants Expanding out of the Dense Circumstellar Matter into the Rarefied Interstellar Medium.* Publications of the Astronomical Society of Japan, vol. 64, page 24, April 2012.

[Shu 1991] F. H. Shu. The physics of astrophysics. Volume 1: Radiation. 1991.

[Siess 2007] L. Siess. *Evolution of massive AGB stars. II. model properties at non-solar metallicity and the fate of Super-AGB stars.* Astronomy & Astrophysics, vol. 476, page 893, December 2007.

[Silverman et al. 2013] J. M. Silverman, P. E. Nugent, A. Gal-Yam, M. Sullivan, D. A. Howell, A. V. Filippenko, I. Arcavi, S. Ben-Ami, J. S. Bloom, S. B. Cenko, Y. Cao, R. Chornock, K. I. Clubb, A. L. Coil, R. J. Foley, M. L. Graham, C. V. Griffith, A. Horesh, M. M. Kasliwal, S. R. Kulkarni, D. C. Leonard, W. Li, T. Matheson, A. A. Miller, M. Modjaz, E. O. Ofek, Y.-C. Pan, D. A. Perley, D. Poznanski, R. M. Quimby, T. N. Steele, A. Sternberg, D. Xu and O. Yaron. *Type Ia Supernovae Strongly Interacting with Their Circumstellar Medium.* ArXiv e-prints, April 2013.

[Smartt et al. 2009] S. J. Smartt, J. J. Eldridge, R. M. Crockett and J. R. Maund. *The death of massive stars - I. Observational constraints on the progenitors of Type II-P supernovae.* Monthly Notices of the Royal Astronomical Society, vol. 395, page 1409, May 2009.

[Smartt 2009] S. J. Smartt. *Progenitors of Core-Collapse Supernovae.* Annual Review of Astronomy and Astrophysics, vol. 47, page 63, September 2009.

[Smith & Hughes 2010] R. K. Smith and J. P. Hughes. *Ionization Equilibrium Timescales in Collisional Plasmas.* The Astrophysical Journal, vol. 718, page 583, July 2010.

[Smith & McCray 2007] N. Smith and R. McCray. *Shell-shocked Diffusion Model for the Light Curve of SN 2006gy.* The Astrophysical Journal Letters, vol. 671, page L17, December 2007.

[Smith & Owocki 2006] N. Smith and S. P. Owocki. *On the Role of Continuum-driven Eruptions in the Evolution of Very Massive Stars and Population III Stars.* The Astrophysical Journal Letters, vol. 645, page L45, July 2006.

[Smith et al. 2004] N. Smith, J. S. Vink and A. de Koter. *The Missing Luminous Blue Variables and the Bistability Jump.* The Astrophysical Journal, vol. 615, page 475, November 2004.

[Smith et al. 2007] N. Smith, W. Li, R. J. Foley, J. C. Wheeler, D. Pooley, R. Chornock, A. V. Filippenko, J. M. Silverman, R. Quimby, J. S. Bloom and C. Hansen. *SN 2006gy: Discovery of the Most Luminous Supernova Ever Recorded, Powered by the Death of an Extremely Massive Star like η Carinae.* The Astrophysical Journal, vol. 666, page 1116, September 2007.

[Smith et al. 2008] N. Smith, R. J. Foley, J. S. Bloom, W. Li, A. V. Filippenko, R. Gavazzi, A. Ghez, Q. Konopacky, M. A. Malkan, P. J. Marshall, D. Pooley, T. Treu and J.-H. Woo. *Late-Time Observations of SN 2006gy: Still Going Strong.* The Astrophysical Journal, vol. 686, page 485, October 2008.

[Smith et al. 2009a] N. Smith, K. H. Hinkle and N. Ryde. *Red Supergiants as Potential Type IIn Supernova Progenitors: Spatially Resolved 4.6 μm CO Emission Around VY CMa and Betelgeuse.* The Astronomical Journal, vol. 137, page 3558, March 2009.

[Smith et al. 2009b] N. Smith, J. M. Silverman, R. Chornock, A. V. Filippenko, X. Wang, W. Li, M. Ganeshalingam, R. J. Foley, J. Rex and T. N. Steele. *Coronal Lines and Dust Formation in SN 2005ip: Not the Brightest, but the Hottest Type IIn Supernova.* The Astrophysical Journal, vol. 695, page 1334, April 2009.

[Smith et al. 2010a] N. Smith, R. Chornock, J. M. Silverman, A. V. Filippenko and R. J. Foley. *Spectral Evolution of the Extraordinary Type IIn Supernova 2006gy.* The Astrophysical Journal, vol. 709, page 856, February 2010.

[Smith et al. 2010b] N. Smith, A. Miller, W. Li, A. V. Filippenko, J. M. Silverman, A. W. Howard, P. Nugent, G. W. Marcy, J. S. Bloom, A. M. Ghez, J. Lu, S. Yelda, R. A. Bernstein and J. E. Colucci. *Discovery of Precursor Luminous Blue Variable Outbursts in Two Recent Optical Transients: The Fitfully Variable Missing Links UGC 2773-OT and SN 2009ip.* The Astronomical Journal, vol. 139, page 1451, April 2010.

[Smith et al. 2011] N. Smith, W. Li, A. A. Miller, J. M. Silverman, A. V. Filippenko, J.-C. Cuillandre, M. C. Cooper, T. Matheson and S. D. Van Dyk. *A Massive Progenitor of the Luminous Type IIn Supernova 2010jl.* The Astrophysical Journal, vol. 732, page 63, May 2011.

[Smith et al. 2012] N. Smith, J. M. Silverman, A. V. Filippenko, M. C. Cooper, T. Matheson, F. Bian, B. J. Weiner and J. M. Comerford. *Systematic Blueshift of Line Profiles in the Type IIn Supernova 2010jl: Evidence for Post-shock Dust Formation?* The Astronomical Journal, vol. 143, page 17, January 2012.

[Smith 2006] N. Smith. *The Structure of the Homunculus. I. Shape and Latitude Dependence from H_2 and [Fe II] Velocity Maps of η Carinae.* The Astrophysical Journal, vol. 644, page 1151, June 2006.

[Smith 2013] N. Smith. *The Crab Nebula and the class of Type IIn-P supernovae caused by sub-energetic electron capture explosions.* ArXiv e-prints, April 2013.

[Soderberg et al. 2006] A. M. Soderberg, R. A. Chevalier, S. R. Kulkarni and D. A. Frail. *The Radio and X-Ray Luminous SN 2003bg and the Circumstellar Density Variations around Radio Supernovae.* The Astrophysical Journal, vol. 651, page 1005, November 2006.

[Soderberg et al. 2008] A. M. Soderberg, E. Berger, K. L. Page, P. Schady, J. Parrent, D. Pooley, X.-Y. Wang, E. O. Ofek, A. Cucchiara, A. Rau, E. Waxman, J. D. Simon, D. C.-J. Bock, P. A. Milne, M. J. Page, J. C. Barentine, S. D. Barthelmy, A. P. Beardmore, M. F. Bietenholz, P. Brown, A. Burrows, D. N. Burrows, G. Byrngelson, S. B. Cenko, P. Chandra, J. R. Cummings, D. B. Fox, A. Gal-Yam, N. Gehrels, S. Immler, M. Kasliwal, A. K. H. Kong, H. A. Krimm, S. R. Kulkarni, T. J. Maccarone, P. Mészáros, E. Nakar, P. T. O'Brien, R. A. Overzier, M. de Pasquale, J. Racusin, N. Rea and D. G. York. *An extremely luminous X-ray outburst at the birth of a supernova.* Nature, vol. 453, page 469, May 2008.

[Soker 2013] N. Soker. *Merger by migration at the final phase of common envelope evolution.* New Astronomy, vol. 18, page 18, January 2013.

[Sollerman et al. 2000] J. Sollerman, P. Lundqvist, D. Lindler, R. A. Chevalier, C. Fransson, T. R. Gull, C. S. J. Pun and G. Sonneborn. *Observations of the Crab Nebula and Its Pulsar in the Far-Ultraviolet and in the Optical.* The Astrophysical Journal, vol. 537, page 861, July 2000.

[Stephenson & Green 2002] F. R. Stephenson and D. A. Green. *Historical supernovae and their remnants.* Historical supernovae and their remnants, by F. Richard Stephenson and David A. Green. International series in astronomy and astrophysics, vol. 5. Oxford: Clarendon Press, 2002, ISBN 0198507666, vol. 5, 2002.

[Stoll et al. 2011] R. Stoll, J. L. Prieto, K. Z. Stanek, R. W. Pogge, D. M. Szczygieł, G. Pojmański, J. Antognini and H. Yan. *SN 2010jl in UGC 5189: Yet Another Luminous*

Type IIn Supernova in a Metal-poor Galaxy. The Astrophysical Journal, vol. 730, page 34, March 2011.

[Stritzinger et al. 2012] M. Stritzinger, F. Taddia, C. Fransson, O. D. Fox, N. Morrell, M. M. Phillips, J. Sollerman, J. P. Anderson, L. Boldt, P. J. Brown, A. Campillay, S. Castellon, C. Contreras, G. Folatelli, S. M. Habergham, M. Hamuy, J. Hjorth, P. A. James, W. Krzeminski, S. Mattila, S. E. Persson and M. Roth. *Multi-wavelength Observations of the Enduring Type IIn Supernovae 2005ip and 2006jd.* The Astrophysical Journal, vol. 756, page 173, September 2012.

[Susa 2013] H. Susa. *The mass of first stars.* ArXiv e-prints, April 2013.

[Suwa et al. 2010] Y. Suwa, K. Kotake, T. Takiwaki, S. C. Whitehouse, M. Liebendörfer and K. Sato. *Explosion Geometry of a Rotating $13M_{\odot}$ Star Driven by the SASI-Aided Neutrino-Heating Supernova Mechanism.* Publications of the Astronomical Society of Japan, vol. 62, page L49, December 2010.

[Suzuki & Nomoto 1995] T. Suzuki and K. Nomoto. *X-Rays from SN 1993J and Structures of Ejecta and Circumstellar Medium.* The Astrophysical Journal, vol. 455, page 658, December 1995.

[Svirski et al. 2012] G. Svirski, E. Nakar and R. Sari. *Optical to X-Ray Supernova Light Curves Following Shock Breakout through a Thick Wind.* The Astrophysical Journal, vol. 759, page 108, November 2012.

[Swartz et al. 1991] D. A. Swartz, J. C. Wheeler and R. P. Harkness. *Model light curves of linear Type II supernovae.* The Astrophysical Journal, vol. 374, page 266, June 1991.

[Swartz et al. 1995] D. A. Swartz, P. G. Sutherland and R. P. Harkness. *Gamma-Ray Transfer and Energy Deposition in Supernovae.* The Astrophysical Journal, vol. 446, page 766, June 1995.

[Taddia et al. 2013] F. Taddia, M. D. Stritzinger, J. Sollerman, M. M. Phillips, J. P. Anderson, L. Boldt, A. Campillay, S. Castellón, C. Contreras, G. Folatelli, M. Hamuy, E. Heinrich-Josties, W. Krzeminski, N. Morrell, C. R. Burns, W. L. Freedman, B. F. Madore, S. E. Persson and N. B. Suntzeff. *Carnegie Supernova Project: Observations of Type IIn Supernovae.* ArXiv e-prints, April 2013.

[Takahara & Sato 1986] M. Takahara and K. Sato. *The phase transitions of superdense matter and supernova explosions.* Astrophysics and Space Science, vol. 119, page 45, February 1986.

[Takahashi et al. 2013] K. Takahashi, T. Yoshida and H. Umeda. *Evolution of progenitors for electron capture supernovae.* ArXiv e-prints, February 2013.

[Takiwaki et al. 2012] T. Takiwaki, K. Kotake and Y. Suwa. *Three-dimensional Hydrodynamic Core-collapse Supernova Simulations for an 11.2 $M_{\odot}$ Star with Spectral Neutrino Transport.* The Astrophysical Journal, vol. 749, page 98, April 2012.

[Tanaka et al. 2012] M. Tanaka, T. J. Moriya, N. Yoshida and K. Nomoto. *Detectability of high-redshift superluminous supernovae with upcoming optical and near-infrared surveys.* Monthly Notices of the Royal Astronomical Society, vol. 422, page 2675, May 2012.

[Thompson et al. 2009] T. A. Thompson, J. L. Prieto, K. Z. Stanek, M. D. Kistler, J. F. Beacom and C. S. Kochanek. *A New Class of Luminous Transients and a First Census of their Massive Stellar Progenitors.* The Astrophysical Journal, vol. 705, page 1364, November 2009.

[Tominaga et al. 2008] N. Tominaga, M. Limongi, T. Suzuki, M. Tanaka, K. Nomoto, K. Maeda, A. Chieffi, A. Tornambe, T. Minezaki, Y. Yoshii, I. Sakon, T. Wada, Y. Ohyama, T. Tanabé, H. Kaneda, T. Onaka, T. Nozawa, T. Kozasa, K. S. Kawabata, G. C. Anupama, D. K. Sahu, U. K. Gurugubelli, T. P. Prabhu and J. Deng. *The Peculiar Type Ib Supernova 2006jc: A WCO Wolf-Rayet Star Explosion.* The Astrophysical Journal, vol. 687, page 1208, November 2008.

[Tominaga et al. 2009] N. Tominaga, S. Blinnikov, P. Baklanov, T. Morokuma, K. Nomoto and T. Suzuki. *Properties of Type II Plateau Supernova SNLS-04D2dc: Multicolor Light Curves of Shock Breakout and Plateau.* The Astrophysical Journal Letters, vol. 705, page L10, November 2009.

[Tominaga et al. 2011] N. Tominaga, T. Morokuma, S. I. Blinnikov, P. Baklanov, E. I. Sorokina and K. Nomoto. *Shock Breakout in Type II Plateau Supernovae: Prospects for High-Redshift Supernova Surveys.* The Astrophysical Journal Supplement Series, vol. 193, page 20, March 2011.

[Tominaga 2009] N. Tominaga. *Aspherical Properties of Hydrodynamics and Nucleosynthesis in Jet-Induced Supernovae.* The Astrophysical Journal, vol. 690, page 526, January 2009.

[Totani et al. 2008] T. Totani, T. Morokuma, T. Oda, M. Doi and N. Yasuda. *Delay Time Distribution Measurement of Type Ia Supernovae by the Subaru/XMM-Newton Deep Survey and Implications for the Progenitor.* Publications of the Astronomical Society of Japan, vol. 60, page 1327, December 2008.

[Trundle et al. 2008] C. Trundle, R. Kotak, J. S. Vink and W. P. S. Meikle. *SN 2005 gj: evidence for LBV supernovae progenitors?* Astronomy & Astrophysics, vol. 483, page L47, June 2008.

[Turatto et al. 1993] M. Turatto, E. Cappellaro, I. J. Danziger, S. Benetti, C. Gouiffes and M. della Valle. *The Type II supernova 1988Z in MCG + 03-28-022 - Increasing evidence of interaction of supernova ejecta with a circumstellar wind.* Monthly Notices of the Royal Astronomical Society, vol. 262, page 128, May 1993.

[Umeda & Nomoto 2002] H. Umeda and K. Nomoto. *Nucleosynthesis of Zinc and Iron Peak Elements in Population III Type II Supernovae: Comparison with Abundances of Very Metal Poor Halo Stars.* The Astrophysical Journal, vol. 565, page 385, January 2002.

[Umeda & Nomoto 2008] H. Umeda and K. Nomoto. *How Much ^{56}Ni Can Be Produced in Core-Collapse Supernovae? Evolution and Explosions of 30-100 M_{solar} Stars.* The Astrophysical Journal, vol. 673, page 1014, February 2008.

[Uno et al. 2002] S. Uno, K. Mitsuda, H. Inoue, T. Takahashi, F. Makino, K. Makishima, Y. Ishisaki, Y. Kohmura, M. Itoh and W. H. G. Lewin. *X-Ray Spectrum of Supernova 1993J Observed with ASCA and Its Evolution 8-572 Days after the Explosion.* The Astrophysical Journal, vol. 565, page 419, January 2002.

[Utrobin & Chugai 2009] V. P. Utrobin and N. N. Chugai. *High mass of the type IIP supernova 2004et inferred from hydrodynamic modeling.* Astronomy & Astrophysics, vol. 506, page 829, November 2009.

[Utrobin et al. 2010] V. P. Utrobin, N. N. Chugai and M. T. Botticella. *Type IIP Supernova 2009kf: Explosion Driven by Black Hole Accretion?* The Astrophysical Journal Letters, vol. 723, page L89, November 2010.

[van Loon et al. 2005] J. T. van Loon, M.-R. L. Cioni, A. A. Zijlstra and C. Loup. *An empirical formula for the mass-loss rates of dust-enshrouded red supergiants and oxygen-rich Asymptotic Giant Branch stars.* Astronomy & Astrophysics, vol. 438, page 273, July 2005.

[van Marle et al. 2010] A. J. van Marle, N. Smith, S. P. Owocki and B. van Veelen. *Numerical models of collisions between core-collapse supernovae and circumstellar shells.* Monthly Notices of the Royal Astronomical Society, vol. 407, page 2305, October 2010.

[van Veelen 2010] B. van Veelen. *Supernovae Interacting with their Circumstellar Medium.* PhD thesis, Utrecht University, 2010.

[Vanbeveren et al. 2007] D. Vanbeveren, J. Van Bever and H. Belkus. *The Wolf-Rayet Population Predicted by Massive Single Star and Massive Binary Evolution.* The Astrophysical Journal Letters, vol. 662, page L107, June 2007.

[Verner & Yakovlev 1995] D. A. Verner and D. G. Yakovlev. *Analytic FITS for partial photoionization cross sections.* Astronomy & Astrophysics Supplement Series, vol. 109, page 125, January 1995.

[Vink & de Koter 2002] J. S. Vink and A. de Koter. *Predictions of variable mass loss for Luminous Blue Variables.* Astronomy & Astrophysics, vol. 393, page 543, October 2002.

[Vink et al. 1999] J. S. Vink, A. de Koter and H. J. G. L. M. Lamers. *On the nature of the bi-stability jump in the winds of early-type supergiants.* Astronomy & Astrophysics, vol. 350, page 181, October 1999.

[Vink et al. 2001] J. S. Vink, A. de Koter and H. J. G. L. M. Lamers. *Mass-loss predictions for O and B stars as a function of metallicity.* Astronomy & Astrophysics, vol. 369, page 574, April 2001.

[von Neumann & Richtmyer 1950] J. von Neumann and R. D. Richtmyer. *A Method for the Numerical Calculation of Hydrodynamic Shocks.* Journal of Applied Physics, vol. 21, page 232, March 1950.

[Wanajo et al. 2009] S. Wanajo, K. Nomoto, H.-T. Janka, F. S. Kitaura and B. Müller. *Nucleosynthesis in Electron Capture Supernovae of Asymptotic Giant Branch Stars.* The Astrophysical Journal, vol. 695, page 208, April 2009.

[Wang et al. 2009] X. Wang, W. Li, A. V. Filippenko, R. J. Foley, R. P. Kirshner, M. Modjaz, J. Bloom, P. J. Brown, D. Carter, A. S. Friedman, A. Gal-Yam, M. Ganeshalingam, M. Hicken, K. Krisciunas, P. Milne, J. M. Silverman, N. B. Suntzeff, W. M. Wood-Vasey, S. B. Cenko, P. Challis, D. B. Fox, D. Kirkman, J. Z. Li, T. P. Li, M. A. Malkan, M. R. Moore, D. B. Reitzel, R. M. Rich, F. J. D. Serduke, R. C. Shang, T. N. Steele, B. J. Swift, C. Tao, D. S. Wong and S. N. Zhang. *The Golden Standard Type Ia Supernova 2005cf: Observations from the Ultraviolet to the Near-Infrared Wavebands.* The Astrophysical Journal, vol. 697, page 380, May 2009.

[Weaver & Woosley 1979] T. A. Weaver and S. E. Woosley. *Evolution and Final Fate of 10 $M_{\odot}$ Stars.* In Bulletin of the American Astronomical Society, volume 11 of *Bulletin of the American Astronomical Society*, page 724, June 1979.

[Weaver 1976] T. A. Weaver. *The structure of supernova shock waves.* The Astrophysical Journal Supplement Series, vol. 32, page 233, October 1976.

[Weiler et al. 1992] K. W. Weiler, S. D. van Dyk, J. E. Pringle and N. Panagia. *Evidence for periodic modulation of presupernova mass loss from the progenitor of SN 1979 C.* The Astrophysical Journal, vol. 399, page 672, November 1992.

[Weiler et al. 2002] K. W. Weiler, N. Panagia, M. J. Montes and R. A. Sramek. *Radio Emission from Supernovae and Gamma-Ray Bursters.* Annual Review of Astronomy and Astrophysics, vol. 40, page 387, 2002.

[Wellons et al. 2012] S. Wellons, A. M. Soderberg and R. A. Chevalier. *Radio Observations Reveal Unusual Circumstellar Environments for Some Type Ibc Supernova Progenitors.* The Astrophysical Journal, vol. 752, page 17, June 2012.

[Whalen et al. 2012] D. J. Whalen, W. Even, L. H. Frey, J. L. Johnson, C. C. Lovekin, C. L. Fryer, M. Stiavelli, D. E. Holz, A. Heger, S. E. Woosley and A. L. Hungerford. *Finding the First Cosmic Explosions I: Pair-Instability Supernovae.* ArXiv e-prints, November 2012.

[Wilms et al. 2000] J. Wilms, A. Allen and R. McCray. *On the Absorption of X-Rays in the Interstellar Medium.* The Astrophysical Journal, vol. 542, page 914, October 2000.

[Wood-Vasey et al. 2004] W. M. Wood-Vasey, L. Wang and G. Aldering. *Photometry of SN 2002ic and Implications for the Progenitor Mass-Loss History.* The Astrophysical Journal, vol. 616, page 339, November 2004.

[Woosley & Weaver 1994] S. E. Woosley and T. A. Weaver. *Sub-Chandrasekhar mass models for Type IA supernovae.* The Astrophysical Journal, vol. 423, page 371, March 1994.

[Woosley et al. 2002] S. E. Woosley, A. Heger and T. A. Weaver. *The evolution and explosion of massive stars.* Reviews of Modern Physics, vol. 74, page 1015, November 2002.

[Woosley et al. 2007] S. E. Woosley, S. Blinnikov and A. Heger. *Pulsational pair instability as an explanation for the most luminous supernovae.* Nature, vol. 450, page 390, November 2007.

[Woosley 2010] S. E. Woosley. *Bright Supernovae from Magnetar Birth.* The Astrophysical Journal Letters, vol. 719, page L204, August 2010.

[Yamaguchi et al. 2009] H. Yamaguchi, M. Ozawa, K. Koyama, K. Masai, J. S. Hiraga, M. Ozaki and D. Yonetoku. *Discovery of Strong Radiative Recombination Continua from the Supernova Remnant IC 443 with Suzaku.* The Astrophysical Journal Letters, vol. 705, page L6, November 2009.

[Yamaguchi et al. 2012] H. Yamaguchi, M. Ozawa and T. Ohnishi. *New insights into SNR evolution revealed by the discovery of recombining plasmas.* Advances in Space Research, vol. 49, page 451, February 2012.

[Yoon & Cantiello 2010] S.-C. Yoon and M. Cantiello. *Evolution of Massive Stars with Pulsation-driven Superwinds During the Red Supergiant Phase.* The Astrophysical Journal Letters, vol. 717, page L62, July 2010.

[Yoon et al. 2010] S.-C. Yoon, S. E. Woosley and N. Langer. *Type Ib/c Supernovae in Binary Systems. I. Evolution and Properties of the Progenitor Stars.* The Astrophysical Journal, vol. 725, page 940, December 2010.

[Yoshida & Umeda 2011] T. Yoshida and H. Umeda. *A progenitor for the extremely luminous Type Ic supernova 2007bi.* Monthly Notices of the Royal Astronomical Society, vol. 412, page L78, March 2011.

[Yoshida et al. 2008] N. Yoshida, K. Omukai and L. Hernquist. *Protostar Formation in the Early Universe.* Science, vol. 321, page 669, August 2008.

[Young et al. 2010] D. R. Young, S. J. Smartt, S. Valenti, A. Pastorello, S. Benetti, C. R. Benn, D. Bersier, M. T. Botticella, R. L. M. Corradi, A. H. Harutyunyan, M. Hrudkova, I. Hunter, S. Mattila, E. J. W. de Mooij, H. Navasardyan, I. A. G. Snellen, N. R. Tanvir and L. Zampieri. *Two type Ic supernovae in low-metallicity, dwarf galaxies: diversity of explosions.* Astronomy & Astrophysics, vol. 512, page A70, March 2010.

[Zhang et al. 2012] T. Zhang, X. Wang, C. Wu, J. Chen, J. Chen, Q. Liu, F. Huang, J. Liang, X. Zhao, L. Lin, M. Wang, M. Dennefeld, J. Zhang, M. Zhai, H. Wu, Z. Fan, H. Zou, X. Zhou and J. Ma. *Type IIn Supernova SN 2010jl: Optical Observations for over 500 Days after Explosion.* The Astronomical Journal, vol. 144, page 131, November 2012.

[Zhou et al. 2011] X. Zhou, M. Miceli, F. Bocchino, S. Orlando and Y. Chen. *Unveiling the spatial structure of the overionized plasma in the supernova remnant W49B*. Monthly Notices of the Royal Astronomical Society, vol. 415, page 244, July 2011.